FISCHER-TROPSCH SYNTHESIS USING CO_2-CONTAINING SYNGAS MIXTURES OVER COBALT AND IRON BASED CATALYSTS

Yali Yao

A thesis submitted to the Faculty of Engineering and the Built Environment, University of the Witwatersrand, Johannesburg, in fulfillment of the requirements for the Degree of Doctor of Philosophy.

Johannesburg, 2011

DECLARATION

I declare that this thesis is my own, unaided work. It is being submitted to the Degree of Doctor of Philosophy to the University of the Witwatersrand, Johannesburg. It has not been submitted before for any degree or examination to any other University.

_____

Yali Yao

_____ Day of _____ 2011

ABSTRACT

Recently, engineers have devoted a great deal of research to developing a Fischer–Tropsch synthesis (FTS) process with high carbon utilization efficiency and low CO_2 emissions. This is desirable not only to improve the process and make it more economical, but also to promote its industrial sustainability. Because CO_2 is produced in both syngas preparation and the FTS step, it may be a significant component in the syngas or in the FT tailgas that may be recycled back to the FT reactor. With the aim of providing new insights into the process that would help engineers to design FT plants with high overall carbon utilization efficiency, we investigated FTS using CO_2-containing syngas mixtures over cobalt- and iron-based catalysts.

During the course of our research, we conducted a large number of experiments on CO/H_2, CO_2/H_2 and $CO/CO_2/H_2$ syngas mixtures for FTS under different reaction conditions over both cobalt- and iron-based catalysts. The results elicited the following information:

- No apparent catalyst deactivation was observed when we co-fed CO_2 into the feeds during FTS over both cobalt- and iron-based catalysts under the reaction conditions we conducted.
- The rate of hydrocarbon production was maximized at an intermediate composition of the $CO/CO_2/H_2$ mixtures for a cobalt-based catalyst. The hydrocarbon product formation rate reached a maximum and then maintained this value, even at a high concentration of CO_2 in the $H_2/CO/CO_2$ feed, over an iron-based catalyst.
- Most of the products for CO_2-rich syngas were short chain paraffins with high CH_4 selectivity and high molar paraffin to olefin (P/O) ratios. The product distribution followed a typical one-alpha Anderson–Schulz–Flory (ASF)

distribution with low alpha values with carbon number n>2. C_2 selectivity lay on or close to the ASF distribution line. However, CH_4 selectivity was far above the line.

- For CO-rich feeds, the product composition shifted to an FT-type product (mainly long chain hydrocarbons) with a low P/O ratio, and followed a two-alpha ASF distribution with high alpha values for carbon number n>3. Furthermore the composition of C_2 was plotted below the ASF distribution line, while for CH_4 was above it.
- The growth factor for paraffins was always higher than that for olefins under the same reaction conditions.
- Although the product selectivity and P/O ratio for FTS were strongly dependent on the operating conditions, the experimental evidence showed that a linear relationship between $P_{(n+1)}/O_{(n+1)}$ and $P_{(n)}/O_{(n)}$ holds for a large number of experiments, independent of the type of the reactor, the composition of the syngas, the reaction conditions and the kind of catalyst.

We used a number of simple models to analyze the experimental data. First we introduced quasi thermodynamic equilibrium assumptions to explain the olefin and paraffin distribution of each of three adjacent olefins ($O_{(n-1)}$, $O_{(n)}$, and $O_{(n+1)}$) and paraffins ($P_{r,(n-1)}$, $P_{r,(n)}$ and $P_{r,(n+1)}$). These were found to describe the deviations from ASF distribution in the C_1 and C_2 components successfully.

We then developed a simple means, called “the combined paraffin and olefin growth factors distribution model”, to explain the two-alpha ASF distribution. This model indicated that a two-alpha product distribution may be the result of the combination of different product spectrums. Another aspect of product distribution that we considered and discussed was the effect of vapour–liquid equilibrium (VLE). This led to our proposing that the deviations from the ASF

distribution we had observed could be explained as the co-action of the different product spectrums (for olefin and paraffin) and the VLE on product distribution during FTS.

In an attempt to explain the linear relationship between $P_{(n+1)}/O_{(n+1)}$ and $P_{(n)}/O_{(n)}$we had encountered in the experiments, we considered an equilibrium hypothesis. Using a simple VLE model, we found that the ratio of $P_{(n+1)}/O_{(n+1)}$ to $P_{(n)}/O_{(n)}$ changes in a range of (1, 1/β), where β is the variation of the vapour pressure coefficient. Our experimental results supported the expression when the chain length was n>2, but with a chain length of n=2, we discovered that it was unable to explain the relationship between P_3/O_3 and P_2/O_2. Another model, based on quasi reaction equilibrium, was developed to explain the linear relationship between $P_{(n+1)}/O_{(n+1)}$ and $P_{(n)}/O_{(n)}$. We assumed that the reaction of $C_{(n+1)}H_{(2n+2)} + C_{(n)}H_{(2n+2)} = C_{(n+1)}H_{(2n+4)} + C_{(n)}H_{(2n)}$ reaches quasi-equilibrium. Because a comparison between the experimental results and the calculations arising from the equilibrium model showed fairly good agreement, we postulate that the product distribution might be determined by the reaction equilibrium.

Although we could not explain all the questions raised by our experimental results, we must emphasize that the long term effect of the CO_2 on the deactivation of both cobalt- and iron-based catalysts was very small under the reaction conditions we selected. It is thus possible to use CO_2-containing syngases for FT synthesis with both cobalt- and iron-based catalysts. Therefore, it may not be necessary to remove CO_2 from the raw syngas for FTS. The results could have implications for the design of FT processes using cobalt and iron catalysts.

ACKNOWLEDGEMENTS

I would like to express my sincere gratitude to the following people and institutions for assisting me and making this thesis possible.

- My supervisors, Professor Diane Hildebrandt and Professor David Glasser, for their invaluable inspiration, guidance and support. When I was feeling that there was no doorway of escape out of the black research box, they always opened a window for me. It has been a privilege working with two such talented researchers.
- Dr Xinying Liu, Dr Bilal Patel, Dr Kalala Jalama and Dr Michaela Very for their guidance, assistance and co-supervision.
- Our research group members: Mr Xiaojun Lu, Mr Cornelius Mduduzi Masuku, Mrs Xiaowei Zhu, Mr Thierry Musanda and Mr Kalala Mbuyi, for all the discussions, good company and friendship.
- The editors, Mrs Philippa Lange and Ms Eldene Eyssell, for their great help in editing my thesis and papers.
- Mr Basil Chassoulas for technical support in the laboratory.
- The staff and post graduate students at COMPS for providing a stimulating and fun environment in which to learn and grow.
- The University of the Witwatersrand, Johannesburg; Golden Nest International (Pty) Ltd; the National Research Foundation (NRF); the South African Research Chairs Initiative (SARChI); the Technology and Human Resources for Industry Programme (THRIP); and the South African National Energy Research Institute (SANERI), for their financial support.

Finally, I dedicate this work to my family (my parents, my husband, my daughter and my brother) who have always helped, supported, taught and encouraged me in hard or good times. I would especially like to thank my daughter, who is my angel and gives me power.

LIST OF PUBLICATIONS AND PRESENTATIONS

Publications:

1. Yao, Y., Liu, X., Hildebrandt, D. and Glasser, D., Fischer-Tropsch Synthesis Using $H_2/CO/CO_2$ Syngas Mixtures over an Iron Catalyst, Industrial and Engineering Chemistry Research, 2011, 50, 11002-11012.
2. Yao, Y., Hildebrandt, D., Glasser, D. and Liu X., Fischer−Tropsch Synthesis Using $H_2/CO/CO_2$ Syngas Mixtures over a Cobalt Catalyst, Industrial and Engineering Chemistry Research, 2010, 49, 11061-11066.
3. Yao, Y., Hildebrandt, D., Liu, X. and Glasser, D. Fischer-Tropsch synthesis using $H_2/CO/CO_2$ syngas mixtures: A comparison of paraffin to olefin ratios for iron and cobalt based catalysts, Submitted for Publication in Applied Catalysis A: Genernal, 2011.
4. Yao, Y., Hildebrandt, D., Liu, X. and Glasser, D., A Study of Low Temperature Fischer-Tropsch Synthesis by Switching between $H_2/CO_2/N_2$ and $H_2/CO/N_2$ Syngases over a Cobalt-based Catalyst. (In preparation)
5. Yao, Y., Hildebrandt, D., Glasser, D., Liu, X., Fischer-Tropsch Synthesis using $H_2/CO/CO_2$ Syngas Mixtures over Cobalt and Iron based Catalysts: Quasi-Equilibrium Consideration. (In preparation)
6. Yao, Y., Hildebrandt, D., Liu, X. and Glasser, D., Fischer-Tropsch Synthesis Using $H_2/CO/CO_2$ Syngas Mixtures: A Comparison of Product Distribution for Iron- and Cobalt-based Catalysts. (In preparation)

International conference proceedings:

1. Yao, Y., Hildebrandt, D., Liu, X. and Glasser, D., Low Temperature Fischer-Tropsch Synthesis by Switching between $CO_2/H_2/N_2$ and $CO/H_2/N_2$ Syngases over a Cobalt based Catalyst, American Institute of Chemical Engineers (AIChE) 2011 Spring Meeting, Chicago, UAS, March 13-17, 2011. (Oral Presentation)
2. Yao, Y., Hildebrandt, D., Liu, X. and Glasser, D., Fischer-Tropsch Synthesis over a Cobalt based Catalyst: Switching between $CO_2/H_2/N_2$ and $CO/H_2/N_2$

Syngases, 40th South African Chemical Institute (SACI) National Convention and Federation of African Chemical Societies (FACS) meeting, Johannesburg, South Africa, January 16-21, 2011. (Oral Presentation)

3. Yao, Y., Hildebrandt, D., Glasser, D. and Liu, X., Carbon Dioxide Fixation in Two Plug Flow Reactors in Series Over a Copper Based Methanol Synthesis Catalyst in the First Reactor and a Cobalt Based Fischer-Tropsch Synthesis Catalyst in the Second Reactor, American Institute of Chemical Engineers (AIChE) 2010 Annual Meeting, Salt Lake City, UAS, November 7-12, 2010. (Oral Presentation)

4. Yao, Y., Hildebrandt, D. and Glasser, D., Fischer−Tropsch Synthesis Using $H_2/CO/CO_2$ Syngas Mixtures over a Cobalt Catalyst, 21st International Symposium on Chemical Reaction Engineering (ISCRE), Philadelphia, USA, June 13-16, 2010. (Oral Presentation)

5. Yao, Y., Hildebrandt, D. and Glasser, D., Fischer-Tropsch Synthesis Using $H_2/CO/CO_2$ Syngas Mixtures over Iron and Cobalt Based Catalysts: Insight into Reaction Pathways, American Institute of Chemical Engineers (AIChE) 2010 Spring Meeting, San Antonio, UAS, March 21-25, 2010. (Oral Presentation)

6. Yao, Y., Hildebrandt, D. and Glasser, D., CO and CO_2 Hydrogenation on an Iron Catalyst, 8th World Congress of Chemical Engineering (WCCE), Montreal, Canada, August 23-27, 2009. (Poster Presentation)

Local conference proceedings:

1. Yao, Y., Hildebrandt, D. and Glasser, D., Fischer-Tropsch Synthesis Using $H_2/CO/CO_2$ Syngas Mixtures over an Iron Catalyst: Insights into Reaction Pathways, Catalysis Society of South Africa (CATSA) 2009 Conference, Rawsonville, South Africa, November 8-11, 2009. (Poster Presentation)

2. Yao, Y., Hildebrandt, D. and Glasser, D., Comparison of CO and CO_2 Hydrogenation on an Iron Fischer Tropsch Synthesis Catalyst, South Africa Chemical Engineering Conference (SACEC) 2009, Cape Town, South Africa, September 20-23, 2009. (Oral Presentation)

TABLE OF CONTENTS

LIST OF FIGURES

LIST OF TABLES

LIST OF ABBREVIATION AND SYMBOLS

ASF	Anderson-Schulz-Flory	---
BET	Brunauer-Emmet-Teller	---
C	Carbon	---
C_{2+}	Hydrocarbons except methane	---
C_n	Hydrocarbon with carbon number n	---
C_{O_n}	The liquid phase concentration of olefin with chain length n	mol/m^3
CPODM	The combined paraffin and olefin growth factors distribution model	---
$F_{G,tot}$	The total flow of vapour phase	mol/min
F_{in}	The total molar flow rate of the inlet gas feed	mol/min
F_{out}	The total molar flow rate of the reactor outlet gas stream	mol/min
FBR	Fixed bed reactor	---
FID	Flame Ionization Detector	---
FT	Fischer-Tropsch	---
FTS	Fischer-Tropsch Synthesis	---
g	Gram	---
GC	Gas Chromatography	---
H	Hydrogen	---
i	Carbon number	---
iN_{θ_i}	The moles of carbon contained in the product of θ_i	mol
j	Carbon numer	---
k	Constant	---
K	Equilibrium constant	---

k_1	Constant	---
k_2	Constant	---
k_3	Constant	---
k_{hydr}	Constant	---
$k_{n=2}$	Constant when carbon number equal to 2	---
$k_{n>2}$	Constant when carbon number is greater than 2	---
$k_{O_{(i)}}$	Constant for olefin with carbon number *i*	---
$k_{P_{r,(j)}}$	Constant for paraffin with carbon number *j*	---
k_{prim}	Constant	---
k_{sec}	Constant	---
m_{cat}	The mass of the catalyst used in this reaction	g
m_n	The mole fraction of all the species having n carbon atoms	---
m_{O_n}	The mole fraction of olefin with carbon number n	---
$m_{O_{(i)}}$	The mole fraction of olefin with carbon number i	---
$m_{P_{r,(j)}}$	The mole fraction of paraffin with carbon number i	---
m_{P_n}	The mole fraction of paraffin with carbon number n	---
MTG	Methanol to gasoline	---
n	Carbon number or chain length	---
$N_{L,tot}$	The total number of moles in the liquid layer	mol
N_n	The moles of hydrocarbon with carbon number n	mol
$N_{O,n}$	The moles of olefin with carbon number n	mol
$N_{O,t}$	Total moles of the overall olefins	mol
$N_{P,n}$	The moles of paraffin with carbon number n	mol
$N_{P,t}$	Total moles of the overall paraffins	mol
N_t	Total moles of the overall products	mol
NTP	Normal Temperature and Pressure	---

O	Olefins	---
O_n	The yield of Olefin at carbon number n	mol
O/P	Molar olefin to paraffin ratio	---
O_n^{net}	The amount of primary α-olefin with chain length *n* effectively produced	mol/(min gcat)
O_n^{prim}	The amount of primary α-olefin with chain length *n*	mol/(min gcat)
O_n^{sec}	The amount of the secondary reaction rate of α-olefin with chain length *n*	mol/(min gcat)
P	Paraffins	---
P	Pressure	bar
P/O	Molar paraffin to olefin ratio	---
P_{CO}	Patial pressure of carbon monoxide	bar
P_{H_2}	Patial pressure of hydrogen	bar
P_n	The yield of Paraffin at carbon number n	mol
P_n^{net}	The amount of n-paraffins with chain length *n* effectively produced	mol/(min gcat)
P_n^{prim}	The amount of primary n-paraffin with chain length *n*	mol/(min gcat)
P_n^{sec}	The amount of the secondary n-paraffin with chain length *n*	mol/(min gcat)
$P_{O_{(i)}}$	The partial pressure of olefin at carbon number i	bar
p_{O_n}	The partial pressure of olefin with chain length *n*	bar
$P_{P_{r,(j)}}$	The partial pressure of paraffin at carbon number j	bar
P_{tot}	The total pressure	bar
P_{vap,O_n}	The vapour pressure of olefin with chain length *n*	bar
PFR	Plug Flow Reactor	---
QPDM	Quasi-equilibrium product distribution model	---
r_{θ_i}	The rate of formation of a gas product of θ_i	mol/(min gcat)
r_{CO}	Rate of CO consumption	mol/(min gcat)
r_{CO_2}	Rate of CO_2 consumption	mol/(min gcat)

Re-WGS	Reverse Water Gas Shift	---
r_{FT}	The FT reaction rate	mol/(min gcat)
r_{P_n}	The rate of the paraffin with carbon number n	mol/(min gcat)
S_{θ_i}	The selectivity of formation of a gas product of θ_i	---
Syngas	Synthesis gas (CO + H_2)	---
T	Temperature	℃
TCD	Thermal Conductivity Detector	---
TPR	Temperature Programmed Reduction	---
$V_{L,tot}$	The total molar volume of the liquid layer in the catalyst surface	m^3
VLE	Vapour-Liquid Equilibrium	---
vol.%	Percentage by volume	---
WGS	Water Gas Shift	---
W_n	Weight fraction of all the species having n carbon atoms	---
wt.%	Percentage by weight	---
X	Constant	---
$X_{\theta_i,out}$	The molar fraction of θ_i in the reactor outlet gas stream	---
X_A	The nonmaterial mole fraction of A	---
X_B	The nonmaterial mole fraction of B	---
X_C	The nonmaterial mole fraction of C	---
$X_{CO,in}$	The molar fraction of CO in the inlet gas feed	---
$X_{CO_2,in}$	The molar fraction of CO_2 in the inlet gas feed	---
$X_{CO_2,out}$	The molar fraction of CO_2 in the reactor outlet gas stream	---
$X_{N_2,in}$	The molar fraction of N_2 in the inlet gas feed	---
$X_{N_2,out}$	The molar fraction of N_2 in the reactor outlet gas stream	---
$X_{O_{(i)}}$	The mole fraction of olefin with carbon number i	---

X_{O_n}	The mole fraction of the olefin at carbon number n in liquid phase	---
$X_{P_{r,(j)}}$	The mole fraction of paraffin with carbon number j	---
XRD	X-Ray Diffraction	---
XTL	Anything–to–liquids is a process that converts carbon and energy containing feedstock to high quality fuels and products, such as coal–to–liquids, biomass–to–liquids and gas–to–liquids	---
Y_{O_n}	The mole fraction of the olefin at carbon number n in gas phase	---
ΔG	Change in Gibbs Free Energy	J/mol
ΔG^o	Standard-state Gibbs Free Energy of reaction	J/mol
ΔH	Change in Enthalpy	J/mol
ΔH^o	Standard-state Enthalpy of reaction	J/mol

Greek symbols

α	Chain growth probability factor	---
α_1	Chain growth probability factor for the short chain hydrocarbons	---
α_2	Chain growth probability factor for the long chain hydrocarbons	---
α_c	A critical chain growth factor	---
α_O	Chain growth factor of olefin product	---
α_P	Chain growth factor of paraffin product	---
β	Variation of the vapour pressure coefficient	---
θ_i	A gas product	---
∞	Infinite	---

1

INTRODUCTION

1.1 Motivation

With the depleting resource of crude oil all over the world, the Fischer-Tropsch Synthesis (FTS) process, in which syngas is converted into a complex multi-component mixture consisting of linear and branched hydrocarbons and oxygenated products, has become a promising route to meet the continuously increasing demand for liquid fuels and chemical feed stocks [1-3].

However, many challenges face the FTS process industries. One of these is to meet the need to improve carbon utilization efficiency, which is required not only by the economy of the process itself, but by the international drive towards sustainable development [4–5]. An investigation into FTS using CO_2-containing syngas mixtures over cobalt- and iron-based catalysts could provide valuable new information for the design of FT plants with high overall carbon utilization efficiency. The main reasons for seeking to improve the efficiency of FTS processes are listed below.

- In some cases, CO_2 may be a significant component in the syngas obtained from biomass and coal (~30%) [4, 6], and thus require expensive purification measures that increase the cost of the process significantly [7]. However, recent process development studies discuss a potential cost advantage if CO_2 is not removed before the synthesis takes place [8].
- In an iron-based FT process, the formation of CO_2 via the water–gas shift (WGS) reaction limits carbon utilization efficiency. Both H_2O and CO_2 are normally produced in substantial amounts by the FT and WGS reactions, both of which provide important routes for oxygen removal [9–11]. They may also cause oxidation and structural changes in the iron catalyst [12–14].

- The effect of CO_2 (as an oxidizing agent) on cobalt-based catalysts during FTS is still controversial. Some researchers [15–17] believe that CO_2 behaves like an inert diluent in syngas feed for cobalt-based FTS catalysts. However, Kim *et al.* [18] concluded that the presence of CO_2 acts as a mild oxidizing agent on reduced Co/γ-Al_2O_3.
- CO_2 emission control and utilization are now recognized as strategies that are urgently needed to counter the harmful effect of greenhouse gases, chief among them carbon dioxide, on the global climate. It is believed that unchecked carbon emissions will ultimately threaten the survival of humankind [19–20]. Fixation of CO_2 has received a great deal of attention, and one of its most promising forms is the conversion of CO_2 or CO_2-rich syngas into fuels and chemicals by using FTS process over iron- or cobalt-based catalysts [4, 21–22].

1.2 Objective

The major aim of this thesis is to investigate the effect of CO_2 on cobalt- and iron-based catalysts in FTS. This entails detailed research into the influence of CO_2 on catalyst activity, product selectivity and product distribution.

The results of this investigation are intended to provide valuable information, such as whether CO_2 can change the catalyst's properties and/or deactivate its activities under typical FT reaction conditions, and whether or not it is necessary to remove CO_2 from the raw syngas before the FTS takes place.

A comparison of the product distributions obtained by the CO/H_2, CO_2/H_2 and $CO/CO_2/H_2$ mixtures might explain the deviations from the Anderson-Schulz-Flory (ASF) model observed experimentally and reveal possible mechanisms of the FT reaction.

Developing a novel and generic rule to describe the paraffin to olefin ratio, which is reliable for CO, CO_2 and CO/CO_2 hydrogenation under an FTS system is the final objective of this thesis.

1.3 Approach

We conducted a large number of experimental runs for FTS using a range of CO/H_2, CO_2/H_2 and $CO/CO_2/H_2$ mixtures under different reaction conditions over both cobalt- and iron-based catalysts with both steady state and unsteady steady operations. Thereafter we analyzed, calculated, compared and simulated the experimental results before applying various theoretical models to find explanations for the data we obtained.

1.4 Thesis outline

The thesis is composed of nine chapters. Most of these have been prepared or submitted as papers for future publication, or have already been published in journals. Therefore, there is a degree of repetition in the experimental section in each of the chapters, where the same experimental work is described. However, this should serve to strengthen the reader's understanding. This chapter covers the introduction and preliminary material.

Chapter 2 describes the general experimental procedures and the equipment used. The actual work performed to evaluate the effect of CO_2 on FTS is set out in detail in subsequent chapters (3–8).

Chapter 3 deals with an attempt to study the CO_2 effect on a cobalt-based catalyst by repeatedly switching between the CO feed ($CO:H_2:N_2$=30%:60%:10%) and CO_2 feed ($CO_2/H_2/N_2$ = 23%:67%:10%) into a fixed bed reactor (FBR) under low-temperature FTS conditions. In this way we could be sure that any changes

we observed were due to the syngas itself, and not to permanent or long-term alterations in the surface properties of the catalyst.

Chapter 4 concerns a series of low-temperature FTS experiments using a wide range of $H_2/CO/CO_2$ syngas mixtures over a cobalt-based catalyst, which provided further insight into the effect of the CO_2 on a cobalt-based catalyst during FTS and involved measuring and comparing the resultant catalyst activity, product selectivity, distribution, and olefin to paraffin ratios.

Chapter 5 involves two groups of low-temperature FTS experiments carried out over an iron-based catalyst. In each of the groups we used a wide range of $H_2/CO/CO_2$ syngas mixtures: in group one, the feed gas ratio of $H_2/(2CO+3CO_2)$ equalled to 1; in group two, the ratio of $H_2/(CO+CO_2)$ equalled to 1. The catalyst activity, product selectivity, and olefin to paraffin ratios of the two groups of experiments were measured and compared, as were the interactions between the FT and WGS reactions.

Chapter 6 presents the relationships among each of the three adjacent olefins ($O_{(n-1)}$, $O_{(n)}$ and $O_{(n+1)}$) and paraffins ($P_{r,(n-1)}$, $P_{r,(n)}$ and $P_{r,(n+1)}$) that were produced by FTS using $H_2/CO/CO_2$ syngas mixtures over both cobalt- and iron-based catalysts. We introduced quasi thermodynamic equilibrium assumptions to explain these experimental findings.

Chapter 7 entails a comparison of the different product distributions we obtained for FTS using a wide range of $H_2/CO/CO_2$ syngas mixtures over cobalt- and iron-based catalysts. We develop and test a new "combined paraffin and olefin growth factors distribution model" to explain the deviations from the ASF distribution that we observed in the experimental results, and also discuss the effect of vapour liquid equilibrium (VLE) on the FT product distribution.

Chapter 8 involves a comparison between the paraffin/olefin ratios we achieved through FTS experiments using a wide range of $H_2/CO/CO_2$ syngas mixtures over cobalt- and iron-based catalysts. We suggest a new explanation based on a generic relationship between the paraffin to olefin ratios achieved with carbon number *n* and those obtained with carbon number *(n+1)*, which is independent of the type of the reactor, the composition of the syngas, the reaction conditions and the kind of catalyst.

References

[1] Dry, M. E. (2002), The Fischer-Tropsch process: 1950–2000, Catalysis Today, 71, 227−241.

[2] Ngwenya, T., Glasser, D., Hildebrandt, D., Coville, N. and Mukoma, P. (2005), Fischer-Tropsch results and their analysis for reactor synthesis, Industrial and Engineering Chemistry Research, 44, 5987−5994.

[3] Teng, B., Chang, J., Yang, J., Wang, G., Zhang, C., Xu, Y., Xiang, H. and Li, Y. (2005), Water gas shift reaction kinetics in Fischer-Tropsch synthesis over an industrial Fe-Mn catalyst, Fuel, 84, 917−926.

[4] James, O. O., Mesubi, A. M., Ako, T. C. and Maity, S. (2010), Increasing carbon utilization in Fischer-Tropsch synthesis using H_2-deficient or CO_2-rich syngas feeds, Fuel Processing Technology, 91, 136−144.

[5] Unruh, D., Rohde, M. and Schaub, G. (2004), Improving carbon utilization in biomass conversion to synthetic hydrocarbons via Fischer-Tropsch Synthesis, Studies in Surface Science and Catalysis, 153, 91−96.

[6] Higman, C. and Burgt. M. (2003), Gasification, Guif Professional Publishing: Burlington.

[7] Herranz, T., Rojas, S., Perez-Alonso, F. J., Ojeda, M., Terreros, P. and Fierro, J. L. G. (2006), Hydrogenation of carbon oxides over promoted Fe-Mn catalysts prepared by the microemulsion methodology, Applied Catalysis A: General, 311, 66−75

[8] Riedel, T and Schaub, G. (2003), Low-temperature Fischer-Tropsch synthesis on cobalt catalysts-effects of CO_2, Topics in Catalysis, 26, 145−156.

[9] van der Laan, G. P. and Beenackers, A. A. C. M. (1999), Kinetics and selectivity of the Fischer-Tropsch synthesis: a literature review, Catalysis Reviews, Science and Engineering, 41, 255−318.

[10] Liu, Y., Zhang, C., Wang, Y., Li, Y., Hao, X., Bai, L., Xiang, H., Xu, Y., Zhong, B. and Li, Y. (2008), Effect of co-feeding carbon dioxide on Fischer–Tropsch synthesis over an iron-manganese catalyst in a spinning basket reactor, fuel processing technology, 89, 234−241.

[11] Krishnamoorthy, S., Li, A. and Iglesia, E. (2002), Pathways for CO_2 formation and conversion during Fischer-Tropsch synthesis on iron-based catalysts, Catalysis letters, 80, 77−86.

[12] Dry M. E. (1981), in: J.R. Anderson, M. Boudart (Eds.), Catalysis Science and Technology, Vol. 1, Springer, Berlin, 159−255.

[13] Dry, M. E. (1990), Fischer-Tropsch synthesis over iron catalysts. Catalysis Letters, 7, 241−252.

[14] Botes, F. G. (2008), The effects of water and CO_2 on the reaction kinetics in the iron-based low-temperature Fischer-Tropsch synthesis: A literature review, Catalysis Reviews, 50, 471−491.

[15] Visconti, C. G., Lietti, L., Tronconi, E., Forzatti, P., Zennaro, R. and Finocchio, E. (2009), Fischer–Tropsch synthesis on a Co/Al_2O_3 catalyst with CO_2 containing syngas, Applied Catalysis A: General, 355, 61−68.

[16] Gnanamani, M. K., Shafer, W. D., Sparks, D. E. and Davis, B. H. (2011), Fischer-Tropsch synthesis: Effect of CO_2 containing syngas over Pt promoted Co/γ-Al_2O_3 and K-promoted Fe catalysts, Catalysis Communications, 12, 936−939.

[17] Zhang, Y., Jacobs, G., Sparks, D. E., Dry, M. E. and Davis, B. H. (2002), CO and CO_2 hydrogenation study on supported cobalt Fischer-Tropsch synthesis catalysts, Catalysis Today, 71, 411–418.

[18] Kim, S. M., Bae, J. W., Lee, Y. J. and Jun, K. W. (2008), Effect of CO_2 in the feed stream on the deactivation of Co/γ-Al_2O_3 Fischer-Tropsch catalyst, Catalysis Communications, 9, 2269–2273.

[19] Zhang, K., Kogelschatz, U. and Eliasson, B. (2001), Conversion of greenhouse gases to synthesis gas and higher hydrocarbons, Energy & Fuels, 15, 395–402.

[20] Halmann, M. M. (1993), Chemical fixation of carbon dioxide: Methods for recycling CO_2 into useful products, CRC Press: Boca Raton, Florida.

[21] Ning, W., Koizumi, N and Yamada, M. (2009), Researching Fe catalyst suitable for CO_2-containing syngas for Fischer-Tropsch synthesis, Energy Fuels, 23, 4696–4700.

[22] Mignard, D. and Pritchard, C. (2006), Processes for the synthesis of liquid fuels from CO_2 and marine energy, Chemical Engineering Research and Design, 84, 828–836.

2

EXPERIMENTAL

2.1 Introduction

With the aim of investigating FTS using CO_2-containing syngas mixtures, we carried out a large body of experimental work. This involved using a wide range of CO/H_2, CO_2/H_2 and $CO/CO_2/H_2$ feed gas mixtures for FTS conducted under various reaction conditions over both cobalt- and iron-based catalysts. The results were intended to elicit technical information that could make a valuable contribution to the design of FT processes in the future.

The product spectrum of the FTS is difficult to interpret, because it represents a complex system that forms a large number of different products which are usually distributed in the gas, liquid and solid phases. The performance of the FT reaction at the laboratory scale demands a cautious handling of various parameters that are likely to affect the final outcome of the experiment. Thus, special attention is required to ensure that the experimental procedure does not contribute any systematic errors to the analysis of the results.

In this section, we describe the general experimental procedures used and the nature of the equipment. Detailed accounts of the actual work performed to evaluate FTS using CO_2-containing syngas mixtures are presented in the chapters that follow. As Chapters 3–8 have been prepared for submission as papers for future publication or have been published as journal articles, there is a degree of repetition in the experimental section in each of the chapters.

2.2 Materials and chemicals used

2.2.1 Gases

All the gases used in this study were supplied by AFROX (African Oxygen) Ltd. Each of the gas cylinders we used was accompanied by a certificate that indicated the purity of the components used for that particular gas mixture. The carrier gases that were used in all the gas chromatographs (GC) were ultra high purity (UHP) grades (>99.997). More detailed information is given below.

(1) Four kinds of syngas mixture were used in the experiments. These consisted of UHP H_2/CO (or CO_2)/N_2. The ratios of the mixtures are listed as follows:

- Syngas 1: a mixture of $H_2/CO/N_2$ with H_2:CO= 2:1 and 10 vol.% N_2
- Syngas 2: a mixture of $H_2/CO_2/N_2$ with $H_2:CO_2$ =3:1 and 10 vol.% N_2
- Syngas 3: a mixture of $H_2/CO/N_2$ with H_2:CO= 1:1 and 10 vol.% N_2
- Syngas 4: a mixture of $H_2/CO_2/N_2$ with $H_2:CO_2$ =1:1 and 10 vol.% N_2

(2) The calibration gas consisted of UHP
$H_2/CO/CO_2/N_2/CH_4/C_2H_4/C_2H_6$=53.0/29.1/5.1/9.6/2.5/0.2/0.5

(3) UHP N_2 was used to purge or isolate the experimental system.

(4) The gases used by the GC system were:

- two kinds of carrier gas, UHP He and UHP Ar, for the thermal conductivity detector (TCD);
- the flame gases air and UHP H_2 and the carrier gas UHP Ar for the flame ionization detector (FID).

2.2.2 Metal additives and catalyst support

The two metals that were loaded onto the titania support were cobalt and iron. The

cobalt [$Co(NO_3)_2\ 6H_2O$] and the iron [$Fe(NO_3)_3\ 9H_2O$] were supplied by Sigma-Aldrich; and the support, titania [(TiO_2) P25], was obtained from Degussa.

2.3 Experimental setup

We carried out our research into FTS using syngas mixtures containing CO_2 over cobalt- and iron-based catalysts in several groups of experiments. The equipment we used for the experiments on the gas-solid FTS as well as for the product analysis is described below, together with a general explanation of our experimental procedures.

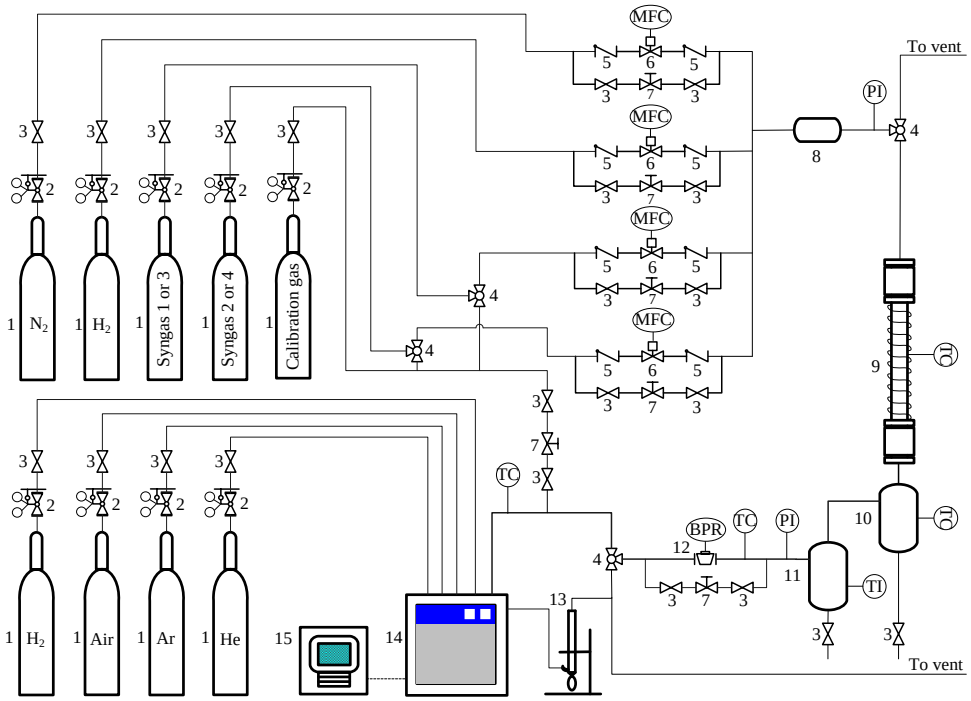

Figure 2.1: Experimental setup:

1: gas cylinders; 2: pressure regulators; 3: shut-off valves; 4: three-way valves; 5: one-way valves; 6: mass flow controllers; 7: needle valves; 8: inlet gas mixer; 9: fixed bed reactor; 10: hot condensable product trap; 11: cold condensable product trap; 12: back pressure regulator; 13: bubble meter; 14: on-line GC; 15: computer for data collection.

All the FT experiments were carried out in two fixed bed reactors (FBR) of the same kind. The experimental setup for one of the two FBRs is shown in Figure 2.1. Information on the gases used is provided in Section 2.2.1.

The syngas mixtures were fed into the reactor, and the flow rate was managed by mass flow controllers (Brooks instrument 5850), which could used to mix two different kinds of syngas mixtures in different proportions to vary the ratios of CO, CO_2, and H_2 in the feed mixtures. The column of the reactor was packed with 10 wt.% Co/TiO_2 and 10 wt.% Fe/TiO_2 catalysts. We prepared these catalysts in our laboratory.

The syngas mixture was preheated by means of the stainless steel ball packed into the top of the reactor (this is discussed in greater detail in Section 2.4, which describes the reactor system). The products and un-reacted materials passed through the bottom of the reactor column to the product traps. To prevent product condensation, the product tubes from the reactor down to the high-pressure hot condensable product trap (maintained at 150 ℃ and reactor pressure) were heated to 200 ℃. The uncondensed stream was then fed into the high-pressure cold condensable product trap (kept at room temperature and reactor pressure) to collect oil and water products. Condensed wax, oil and water products were removed periodically.

The reactor pressure as well as the two traps were controlled by a back pressure regulator (Swagelok). During the tail gas stream passed through the back pressure regulator, the pressure of the stream was reduced from the operating pressure to atmospheric pressure. At this point the stream was fed into the sampling loop of the on-line GC (DANI, GC 1000). To prevent condensation of the light products, we heated the product tubes between the cold condensable product trap and the on-line GC sampling loop to 150 ℃. The gaseous stream leaving the GC was sent to a bubble meter, which was used to indicate the tailgas flow rate, and thereafter

through the vent line to the vent.

2.4 Catalyst preparation and characterization

We used two kinds of catalyst: a supported cobalt catalyst of 10 wt.% Co/TiO_2 and a supported iron catalyst of 10 wt.% Fe/TiO_2. These were prepared by the incipient wetness impregnation method. Details of the catalyst preparation procedures are given in Chapters 3, 4, and 6–8 for the cobalt-based catalyst, and Chapters 5–8 for the iron-based catalyst.

The physicochemical characteristics of these two catalysts were determined by means of the Brunauer-Emmett-Teller (BET), temperature programmed reduction (TPR) and X-ray diffraction (XRD) methods [1, 2]. BET is one of the techniques used in catalysis to determine the surface area and the porosity of the catalyst. For a supported metal catalyst, the BET method yields the total surface area of support and metal. TPR is a powerful tool with which to analyze the reduction kinetics of oxidized catalyst precursors, which permits the researcher to select the most efficient reduction conditions. XRD is used to identify crystalline phases inside catalysts by means of lattice structural parameters, and to obtain an indication of particle size.

Table 2.1: Information related to the catalysts.

	10 wt.% Co/TiO_2	10 wt.% Fe/TiO_2
Catalyst particle size (mm)	0.5−1.0	0.5−1.0
BET surface area (m^2/g)	41.43	38.07
Total Pore volume (cm^3/g)	0.355	0.349
Average pore size (nm)	34	36.6
Reduction temperature (^oC) used in our experiments	350	350

The experimental procedures [3] and results of the catalyst characterization are

given in Appendix A for BET; Appendix B for TPR; and Appendix C for XRD. Part of this information is listed in Table 2.1 above.

2.5 Reactor system

FBR is used for low-temperature (180–250 ℃) FTS with either iron or cobalt catalysts to produce high molecular mass linear waxes, which in turn can be hydro-cracked to produce diesel of an exceptionally high quality [4–5]. The feed gas flows downward through the catalyst bed in a profile approximating that of a plug flow.

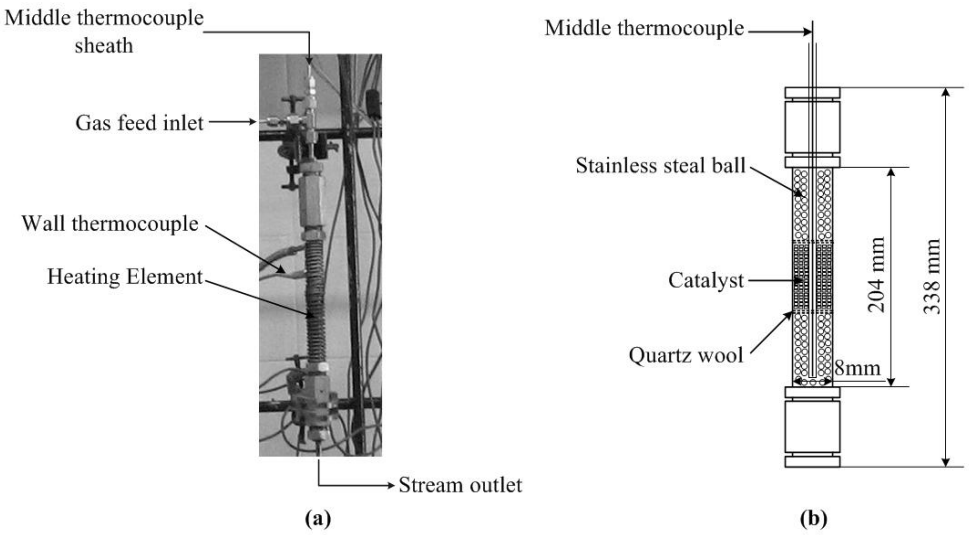

Figure 2.2: An FBR: (a) digital portrait, and (b) sketch portrait.

We used two FBRs of the same kind as shown in Figure 2.2 above for all the experiments described in this thesis. They are stainless steel reactors with an internal diameter of 8 mm and a tube length of 204 mm. The heating element and the wall thermocouple (Figure 2.2 (a)) co-act to control and maintain the operating temperature. The middle thermocouple sheath, a 1/8 inch stainless steel tube (Swagelok), allowed the middle thermocouple to move up and down freely. The middle thermocouple was used to indicate the temperature at different axial

positions in the bed (Figure 2.2 (b)). The stainless steel balls had two functions (preheating the inlet gas and supporting the catalyst bed) when the catalyst was loaded. The quartz wool placed at either the top or the bottom of the catalyst bed was used to rest the catalyst.

2.6 Product Analysis

The analytical equipment was needed to measure the complete product distribution of at least $C_{1–30}$ paraffins and olefins, the inorganic reactants and products of H_2, CO, CO_2 and H_2O as well as the inert gas of N_2, which consist essentially of gas, oil, wax and water.

The tail gas was analyzed every 1.5 hours by means of an online DANI GC. Two TCD detectors were used to analyze H_2, N_2, CO, CO_2 and CH_4, and the gas phase hydrocarbons were analyzed by a FID detector. Wax and oil were both analysed off-line in another FID GC at the end of the mass balance for each run.

2.6.1 On-line GC system

The gas products from the FBR were sent to the GC sampling loop through a heated line (150 ℃). This gas entered the GC through three multiple sampling valves that were heated at 150 ℃, while the TCD and FID detectors were maintained at 220 ℃. The sampling flow scheme for the on-line GC is shown in Figure 2.3. Detailed information concerning the columns, carrier gas and oven temperature programme is given in Table 2.2.

Two TCD detectors were used in the on-line GC: TCD_A was used to analyze CH_4, CO_2, N_2 and CO with UHP He as a carrier gas, while TCD_B was used to analyze H_2 with UHP Ar as a carrier gas (Table 2.2). Each of the TCDs was fitted with a dual filament type detector, connected to an electrometer amplifier. Both

the detectors and the amplifiers provided excellent sensitivity to the concentrations of inorganic components in the range used in our research. A typical chromatogram from the TCDs is given in Figure 2.4 (a), and the information relating to the components of each of the analyzed peaks is set out in Table 2.3.

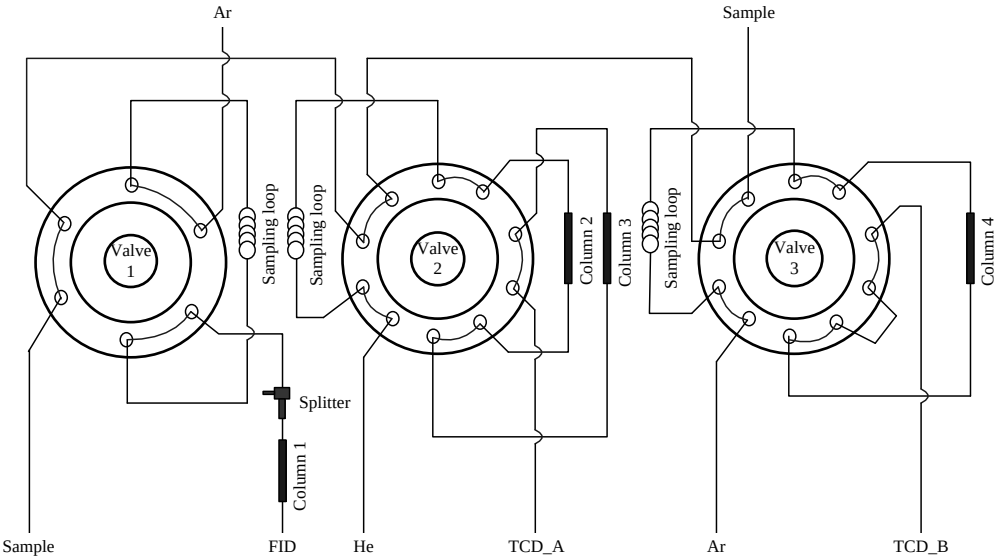

Figure 2.3: The sampling flow scheme for the on-line GC.

The FID detector in the on-line GC was connected to an amplifier. Varian capillary columns were used in this FID system for the analysis of gaseous olefin and paraffin products (C_1–C_9) (the information given in this column is also listed in Table 2.2). UHP Ar was used as a carrier gas in this column. A computer using Clarity software was connected to the on-line GC to record the GC signal. An example of an on-line FID chromatogram is given in Figure 2.4 (b), and the information on the components of each of the analyzed peaks is listed in Table 2.3.

Table 2.2: Characteristics of the GCs employed.

On-line GC	**DANI GC 1000**
Detector 1	FID, T=220 ^{o}C
Column 1	Varian capillary column (Cp-Poraplot Q-HT), 12.5m*0.53mm* 20μm
Sample valve temperature	150 ^{o}C
Carrier gas	UHP Ar with flow rate of 30 ml(NTP)/min
Oven temperature programme	Hold at 50 ^{o}C for 8 min, heat to 200 ^{o}C at 8 ^{o}C/min, hold at 200 ^{o}C for 45 min
Product analysis	C_1-C_9
Detector 2	TCD_A, T=220 ^{o}C
Column 2	Teknokroma, porapack Q (T_{max}: 250 ^{o}C), 80/100 mesh, 2m*1/8"*2.1mm
Column 3	Teknokroma, molecular sieve 13X (T_{max}: 400 ^{o}C), 80/100 mesh, 2m*1/8"
Sample valve temperature	150 ^{o}C
Carrier gas	UHP Ar with flow rate of 30 ml(NTP)/min
Oven temperature programme	Hold at 50 ^{o}C for 8 min, heat to 200 ^{o}C at 8 ^{o}C/min, hold at 200 ^{o}C for 45 min
Product analysis	CH_4, CO_2, N_2, CO
Detector 3	TCD_B, T=220 ^{o}C
Column 4	Teknokroma, molecular sieve 5A (T_{max}: 400 ^{o}C), 80/100 mesh, 1.5m*1/8"
Sample valve temperature	150 ^{o}C
Flame gas	Air with flow rate of 20 ml(NTP)/min and UHP H_2 with flow rate of 200 ml(NTP)/min
Carrier gas	UHP He, 30 ml(NTP)/min
Oven temperature programme	Hold at 50 ^{o}C for 8 min, heat to 200 ^{o}C at 8 ^{o}C/min, hold at 200 ^{o}C for 45 min
Product analysis	H_2
Off-line GC	
Detector	FID, T=350 ^{o}C
Column	Supelcoport column, 80/100 mesh, 3m*1/8"
Sample valve temperature	320 ^{o}C
Flame gas	Air with flow rate of 30 ml(NTP)/min and UHP H_2 with flow rate of 300 ml(NTP)/min
Carrier gas	UHP Ar with flow rate of 30 ml(NTP)/min
Oven temperature programme	Oil: heat to 300 ^{o}C at 3 ^{o}C/min, hold at 300 ^{o}C for 60 min Wax: heat to 300 ^{o}C at 5 ^{o}C/min, hold at 300 ^{o}C for 120 min
Product analysis	C_5-C_{30}

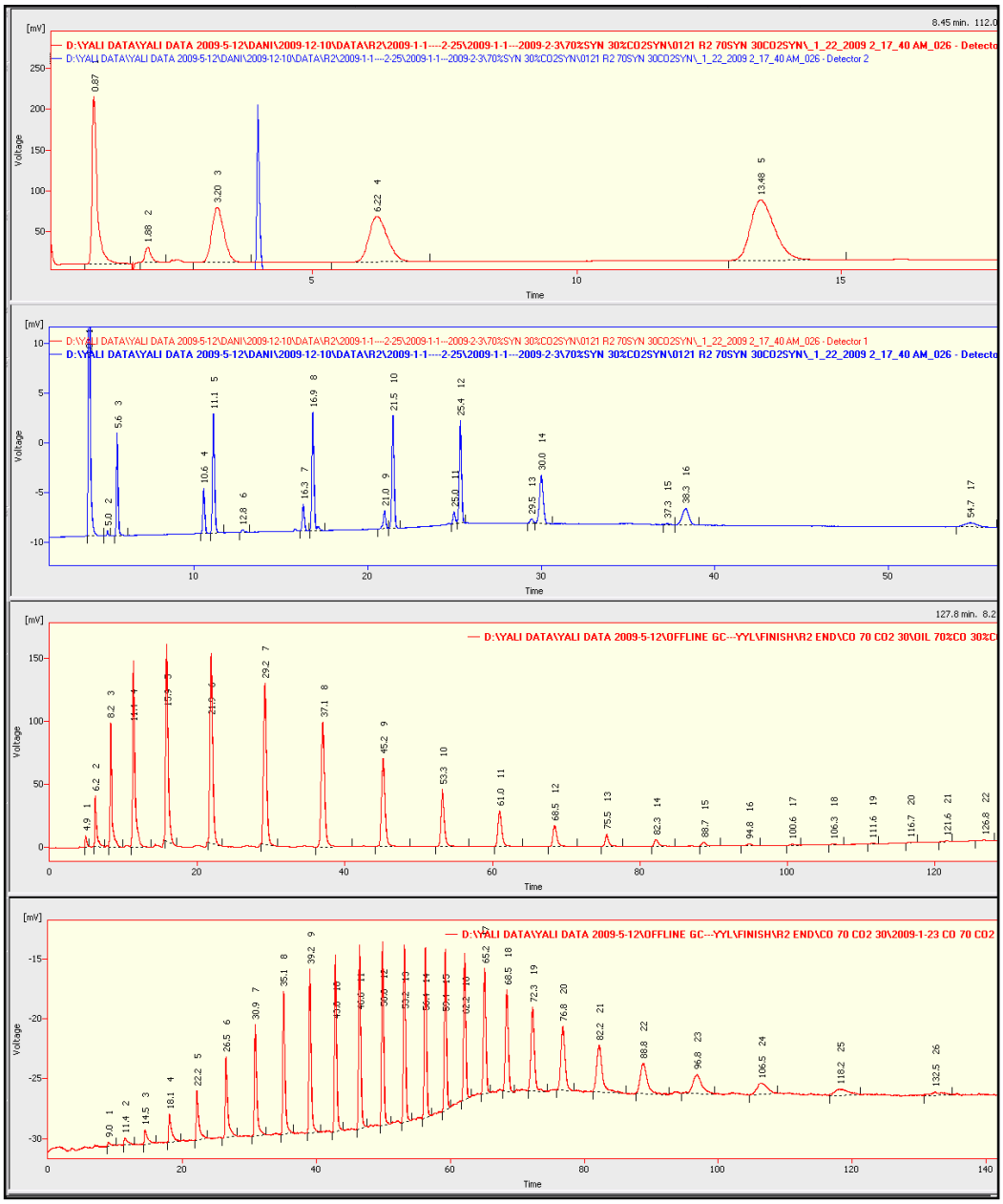

Figure 2.4: Typical on-line analysis and typical off-line analysis: (a) on-line TCD gas phase data; (b) on-line FID gas phase products data; (c) off-line oil products data; and (d) off-line wax products data. The reaction conditions were at 20 bar gauge, 200 ℃, 60 ml(NTP)/(min·gcat) and syngas mixture of $H_2/CO/CO_2/N_2$= 61%/27%/2%/10% over a cobalt based catalyst.

Table 2.3: Summary of the components analyzed by on-line and off-line GCs with different peak numbers as shown in Figure 2.4.

Peak number	On-line TCD gas	On-line FID gas	Off-line FID oil	Off-line FID wax
1	H_2	P_1	C_6	C_8
2	CH_4	O_2	C_7	C_9
3	CO_2	P_2	C_8	C_{10}
4	N_2	O_3	C_9	C_{11}
5	CO	P_3	C_{10}	C_{12}
6		CH_3OH	C_{11}	C_{13}
7		O_4	C_{12}	C_{14}
8		P_4	C_{13}	C_{15}
9		O_5	C_{14}	C_{16}
10		P_5	C_{15}	C_{17}
11		O_6	C_{16}	C_{18}
12		P_6	C_{17}	C_{19}
13		O_7	C_{18}	C_{20}
14		P_7	C_{19}	C_{21}
15		O_8	C_{20}	C_{22}
16		P_8	C_{21}	C_{23}
17		P_9	C_{22}	C_{24}
18			C_{23}	C_{25}
19			C_{24}	C_{26}
20			C_{25}	C_{27}
21			C_{26}	C_{28}
22			C_{27}	C_{29}
23				C_{30}
24				C_{31}
25				C_{32}
26				C_{33}

P = paraffin; O = olefin; and C = hydrocarbon (olefin+paraffin)

2.6.2 Off-line GC system

Analyses of the long chain hydrocarbons (oil and wax) were performed using a off-line FID GC. A three-metre Supelcoport column was used for this purpose. This GC was connected to a computer that recorded the amplified signal from the detector. A 0.2μl sample of each of the oil and wax products was injected into the GC using a syringe. UHP Ar gas was used as a carrier gas in this GC. The temperature programmes used in all the GCs were ramped up to prevent the accumulation of long chain hydrocarbons in the column. Details of the results of the analyses are shown in Figure 2.3 (c) and (d), and the components of each of the analyzed peaks are given in Table 2.3.

2.7 Experimental procedure

2.7.1 Catalyst reduction

In each of the experiments we carried out in a FBR (that is, using both cobalt- and iron-based catalysts), we loaded one gram of catalyst into the reactor. Following the TPR characterization results (Appendix Ⅱ) we had obtained, we set the reduction temperature for both cobalt- and iron-based catalysts at 350 ℃. We used UHP H_2 (AFROX (African Oxygen) Ltd., 99.999%) to reduce the catalysts with a constant flow rate of 60 ml(NTP)/(min gcat), keeping the temperature constant at 350 ℃ for 24 hours. The reactor temperature programme is shown in Figure 2.5.

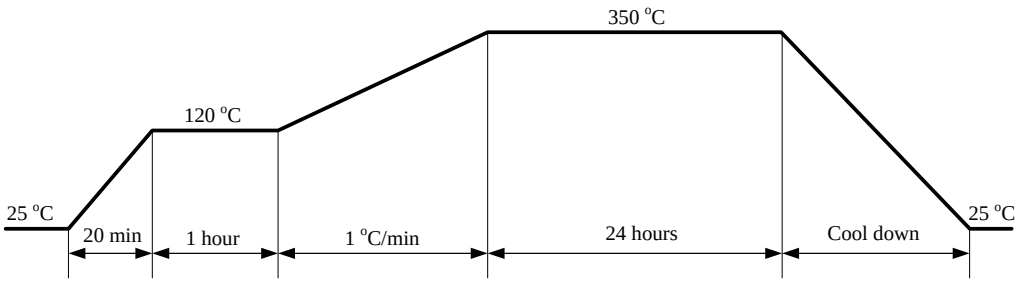

Figure 2.5: The reactor temperature programme during the catalyst reduction.

2.7.2 FT catalytic activity test

We conducted four groups of FTS experiments for a variety of CO/H_2, CO_2/H_2 and $CO/CO_2/H_2$ mixtures under different reaction conditions over both cobalt- and iron-based catalysts. The detailed experimental procedures for the four groups of experiments are given in the corresponding Chapters. The experimental data were analyzed, calculated, compared and simulated both within each group and among different groups. The reaction conditions for each set of experiments were as follows.

- **Group A:** A series of FTS experiments was conducted by repeatedly switching between a CO feed ($CO:H_2:N_2$=30%:60%:10%) and a CO_2 feed ($CO_2/H_2/N_2$ = 23%:67%:10%) into a FBR over a cobalt-based catalyst at 180–220 ℃, 20 bar gauge and 30 ml(NTP)/(min gcat). (This group of experiments forms the subject of Chapter 3.)
- **Group B:** A series of FTS experiments was carried out using a wide range of $H_2/CO/CO_2$ syngas mixtures (with the ratio of $H_2/(2CO+3CO_2)$ equal to 1) over a cobalt-based catalyst at 200 ℃, 20 bar gauge and 60 ml(NTP)/(min gcat). (This group of experiments is discussed in Chapters 4 and 6–8.)
- **Group C:** A series of FTS experiments was conducted with a wide range of $H_2/CO/CO_2$ syngas mixtures (with the ratio of $H_2/(2CO+3CO_2)$ equal to 1) over an iron-based catalyst at 250 ℃, 20 bar gauge and 60 ml(NTP)/(min gcat). (This group provides the material presented in Chapters 5–8.)
- **Group D:** A series of FTS experiments was carried out using a wide range of $H_2/CO/CO_2$ syngas mixtures (with the ratio of $H_2/(CO+CO_2)$ equal to 1) over an iron-based catalyst at 250 ℃, 20 bar gauge and 60 ml(NTP)/(min gcat). (The results obtained for this group are examined in Chapter 5.)

2.8 System mass balance

The CO_2-containing syngas mixtures used as feeds for the FTS experiments comprised CO, CO_2, H_2, and N_2, which had different compositions. CO, CO_2 and H_2 were reactants, while the N_2 was used as an inert tracer for mass balance purposes.

Table 2.4: Molar response factors for hydrocarbon products.

Carbon number	Olefin	Paraffin
2	1	1
3	0.7	0.74
4	0.554	0.554
5	0.47	0.47
6	0.396	0.396
7	0.351	0.351
8	0.316	0.316
9	0.28	0.28
10	0.24	0.24
11	0.224	0.224
12	0.207	0.207
13	0.189	0.189
14	0.179	0.179
15	0.165	0.165
16	0.154	0.154

Using the GC data, we were able to calculate the mole composition of each of the components. The analysis of feed and products by both the TCD and FID detectors obtained an area number for all the individual components in the mixture. Those area numbers were recorded by a computer using Clarity software, and then converted to the mole of each product's composition by using a calibration gas. This gas, a mixture of H_2, CO, CO_2, N_2, CH_4, C_2H_4, and C_2H_6,

which was described in Section 2.2.1, was used to calibrate the FID and TCD data once a day. The hydrocarbon product areas obtained from the FID data were corrected from C_2H_4 (olefin) and C_2H_6 (paraffin) by means of response factors based on those reported by Dietz [6] and Scanlon and Willis [7]. The molar response factors for hydrocarbon products are shown in Table 2.4.

N_2 was used in the reactor feed to serve as an internal standard. As it is inert during the FT reaction, N_2 is only present in the feed stream and in the reactor outlet gas stream. The inlet flow stream was monitored by a mass flow controller. The outlet flow was determined using a N_2 mass balance. The N_2 balance across the reactor is therefore expressed as:

$$F_{in} \times X_{N_2,in} = F_{out} \times X_{N_2,out} \quad (2.1)$$

where F_{in} is the total molar flow rate of the reactor inlet gas feed, mol/min; F_{out} is the total molar flow rate of the reactor outlet gas stream, mol/min; $X_{N_2,in}$ is the molar fraction of N_2 in the reactor inlet gas feed; and $X_{N_2,out}$ is the molar fraction of N_2 in the reactor outlet gas stream.

Because the feed gas mixtures were $CO/CO_2/H_2/N_2$ during FTS in our experiments, CO and CO_2 may convert to hydrocarbons in the reactor at the same time. Therefore, we calculated the CO conversion and the CO_2 conversion using Equations (2.2) and (2.3) following the terms of %CO and $\%CO_2$, respectively:

$$\%CO = \frac{F_{in} X_{co,in} - F_{out} X_{co,out}}{F_{in} X_{co,in}} \quad (2.2)$$

where $X_{co,in}$ is the molar fraction of CO in the reactor inlet gas feed; and $X_{co,out}$ is the molar fraction of CO in the reactor outlet gas stream;

$$\%CO_2 = \frac{F_{in} X_{co\,2,in} - F_{out} X_{co\,2,out}}{F_{in} X_{co\,2,in}} \quad (2.3)$$

where $X_{co_2,in}$ is the molar fraction of CO_2 in the reactor inlet gas feed; and $X_{co_2,out}$ is the molar fraction of CO_2 in the reactor outlet gas stream.

The rate of CO conversion can be calculated as follows:

$$r_{CO} = \frac{F_{out} X_{co,out} - F_{in} X_{co,in}}{m_{cat}} \quad (2.4)$$

where r_{CO} is the rate of CO conversion, mol/(min·gcat); and m_{cat} is the mass of the catalyst used in this reaction, in grams.

The rate of CO_2 conversion can be calculated in terms of:

$$r_{CO_2} = \frac{F_{out} X_{co_2,out} - F_{in} X_{co_2,in}}{m_{cat}} \quad (2.5)$$

where r_{CO_2} is the rate of CO_2 conversion, mol/(min·gcat); and m_{cat} is the mass of the catalyst used in this reaction, in grams.

The rate of formation of a gas product of θ_i, mol/(min·gcat), is calculated as follows:

$$r_{\theta_i} = \frac{F_{out} X_{\theta_i,out}}{m_{cat}} \quad (2.6)$$

where $X_{\theta_i,out}$ is the molar fraction of θ_i in the reactor outlet gas stream.

The FT products may be formed from the conversion of CO, CO_2, or both. Therefore, we calculated the product selectivity of S_{θ_i} (on the basis of moles of carbon) in three of the different reaction conditions, which are:

(1) If the value of $-r_{CO}$ was positive but the value of $-r_{CO_2}$ was negative, which means the FTS was not consuming but forming CO_2, the product selectivity (S_{θ_i}) would be calculated using Equation (2.7):

$$S_{\theta_i} = \frac{iN_{\theta_i}}{m_{cat}\, t\, (-r_{CO})} \tag{2.7}$$

where iN_{θ_i} represents the moles of carbon contained in the product θ_i during the mass balance period of time t, in moles.

(2) If both the values of $-r_{CO}$ and $-r_{CO_2}$ were positive, which means both the CO and CO_2 converted to hydrocarbons during the FTS, the product selectivity (S_{θ_i}) would be expressed by the equation:

$$S_{\theta_i} = \frac{iN_{\theta_i}}{m_{cat}\, t\, (-r_{CO} - r_{CO\,2})} \tag{2.8}$$

(3) If the value of $-r_{CO}$ was negative but the value of $-r_{CO_2}$ was positive, which means the FTS was not consuming but forming CO, the product selectivity (S_{θ_i}) would be calculated according to the formula:

$$S_{\theta_i} = \frac{iN_{\theta_i}}{m_{cat}\, t\, (-r_{CO\,2})} \tag{2.9}$$

When we performed a mass balance on carbon and oxygen, we accepted mass balance data of 100±5% as adequate. The amount of carbon and oxygen entering the reactor equals the amount of carbon and oxygen reacted to form products plus the un-reacted carbon and oxygen leaving the reactor. The % mass balance was calculated using Equation (2.10) below:

$$\%\, mass\ balance = \frac{N_{un-r} + N_r}{N_{in}} \tag{2.10}$$

where N_{un-r} is the mole of un-reacted carbon and oxygen, mol; N_r is the mole of reacted carbon or oxygen, mol; and N_{in} is the mole of carbon or oxygen entering the reactor, mol.

References

[1] Chorkendorff, I. and Niemantsverdriet, J.W. (2007), Concepts of modern catalysis and kinetics, second, revised and enlarged edition, Wiley-VCH, Weinheim.

[2] Niemantsverdriet, J.W. (2007), Spectroscopy in catalysis, An introduction, Third, Completely Revised and Enlarged Edition, Wiley-VCH, Weinheim.

[3] Xiong, H., Moyo, M., Motchelaho, M. A. M., Jewell, L. L. and Coville, N. J. (2010), Fischer-Tropsch synthesis over model iron catalysts supported on carbon spheres: The effect of iron precursor, support pretreatment, catalyst preparation method and promoters, Applied Catalysis A: General, 388, 168–178.

[4] Dry, M. E. (2002), The Fischer-Tropsch process: 1950–2000, Catalysis Today, 71, 227–241.

[5] Dry, M. E. (1981), The Fischer-Tropsch synthesis, catalysis, science and technology, Springer-Verlag, Berlin.

[6] Dietz, W. A. (1967), Response factors for gas chromatographic analysis, Journal of Gas Chromatography, 5, 68–71.

[7] Scanlon, J. T. and Willis, D. E. (1985), Calculation of flame ionization detector relative response factors using the effective carbon number concept, Journal of Chromatographic Science , 23, 333–340.

3

A STUDY OF LOW TEMPERATURE FISCHER-TROPSCH SYNTHESIS WITH SWITCHING BETWEEN $CO_2/H_2/N_2$ AND $CO/H_2/N_2$ SYNGASES OVER A COBALT-BASED CATALYST

This work has been prepared in the form of a paper for future publication. Part of this work was presented at the following conferences:

- *AIChE Spring Meeting, Chicago, UAS, March 13-17, 2011.*
- *SACI conference, Johannesburg, South Africa, January 16-21, 2011.*

Abstract:

A series of Fischer-Tropsch synthesis (FTS) experiments, which entailed repeatedly switching between a CO ($CO/H_2/N_2$) and a CO_2 ($CO_2/H_2/N_2$) feed, were conducted in a fixed bed reactor over a cobalt-based catalyst. It is worth noting that the effect of the CO_2 on the properties of a cobalt-based catalyst was very small under the reaction conditions we chose. There was no apparent catalyst deactivation at reaction temperatures of 180 ℃ and 200 ℃ when we continually alternated between the CO and CO_2 feeds.

We observed dramatic changes in the catalyst activity and product selectivity for CO_2 hydrogenation before and after the initial CO FTS at 180 ℃. In addition, during the initial CO hydrogenation on the cobalt catalyst, both the olefin and paraffin formation rates suddenly changed from one pseudo-stable state to another. These differences may have been caused by liquid products, whether deposited on the catalyst surface or in the catalyst pores during CO FTS.

A mild catalyst deactivation was observed at the operating temperatures of 210 ℃ and 220 ℃, respectively. According to the comparison we made between the conversion of the feed gases and the product formation rates for paraffin and olefin, and our speculations concerning possible side reactions, we conclude that the catalyst deactivation is possibly attributable to the re-oxidation by water.

3.1 Introduction

Fischer-Tropsch synthesis (FTS) is a well-established commercial technology for the conversion of syngas to clean transportation fuels and chemicals. At present there are two modes of operation favoured for commercial FTS processes [1-3]. The first is the high-temperature (300–350 ℃) version employing iron-based catalysts, used for the production of gasoline and linear low molecular mass olefins. The second is the low-temperature (180–250 ℃) process over either iron or cobalt catalysts, producing high molecular mass linear waxes, which in turn can be hydro-cracked to produce diesel of exceptionally high quality. Cobalt is considered the most suitable metal for the low-temperature FTS of long chain hydrocarbons because its activity and selectivity to linear paraffins are high, and its water-gas shift (WGS) activity is low [1, 4−5].

As the cobalt catalysts used in FTS are relatively expensive (compared to the cost of iron), they need to have a high metal dispersion and long life to be able to offer a good balance between cost and performance [6−7]. This is why catalyst deactivation is a major challenge in cobalt-based FTS [6−8]. The oxidation of cobalt metal to cobalt oxide by the product water has long been believed to be a major cause of the deactivation of supported cobalt FTS catalysts [7, 9−11]. This hypothesis arises from the fact that water, the most abundant byproduct of FTS, is an oxidizing agent, and thus may cause surface oxidation of the cobalt nanoparticles [6−7]. Owing to the low activity a cobalt catalyst has for WGS, CO_2

is not the major byproduct. Nevertheless, in some cases CO_2 may be a significant component in the syngas obtained from biomass and coal [3, 12]. It is therefore necessary to investigate the effect of CO_2 (as an oxidizing agent) on cobalt-based low-temperature FTS.

Until recently, the effect of CO_2 on cobalt-based FTS has remained controversial. Some researchers [3, 13–15] believe that CO_2 behaves as an inert diluent in the syngas feed at temperatures below 220 ℃ for FTS over cobalt-based catalysts. Zhang *et al.* [15] claimed that the catalyst deactivates more rapidly for the conversion of CO than for CO_2, even though the H_2O/H_2 ratio is at least two times greater for the conversion of CO_2 in cobalt-based FTS. However, Kim *et al*. [16] concluded that the presence of CO_2 in the feed gas affects the rate of catalytic hydrogenation of CO as well as the product distribution, and that CO_2 acts as a mild oxidizing agent on reduced $Co/\gamma\text{-}Al_2O_3$ at 220 ℃ and 20 bar. Riedel and Schaub [17] also found that CO_2 had a negative effect on both the FT reaction rate and deactivation with a catalyst comprising $Co\text{-}La\text{-}Ru\text{-}SiO_2$. A cobalt catalyst used with a temperature of 220 ℃ for FTS may also cause WGS activity and an increase in methanation rates [3]. The technique most commonly applied when studying the effect of CO_2 is the co-feeding of CO_2 in the feed gas during low-temperature FTS [13–19], but relatively little of the published research [13–21] has dealt with the effect of CO_2 on cobalt-based FTS.

Furthermore, the chemical utilization of CO_2 as a carbon resource is important from both the economic and environmental standpoints [22]. There have been various attempts to transform carbon dioxide into hydrocarbons, mainly by using catalysts that have been proven to be active in FTS, such as Ni, Ru and Co [23]. Although the need for CO_2 separation before the syngas is used in FTS is mentioned in the open literature [17, 24], recent process development studies suggest a potential advantage in not removing the CO_2 before synthesis takes

place. This can be done if the conditions are CO_2 tolerant or if CO_2 is hydrogenated along with CO in the FT reactor. The omission of the separation step is desirable not only to make the process more economical but also to contribute to sustainable development.

In the research described in this chapter, we investigated the effect of CO_2 on cobalt-based low temperature FTS by means of a new experiment, which can be described as cobalt-based catalyst stability testing during CO and CO_2 hydrogenation. The nature of the test was to repeatedly switch between the two feed gases, a CO_2 ($CO_2/H_2/N_2$) and a CO mixture ($CO/H_2/N_2$), which were introduced into a micro fixed bed reactor (FBR) for FTS at 180–220 ℃, 20 bar (gauge) and 30 ml(NTP)/(min gcat) over a Co/TiO_2 catalyst. This provided a means of ensuring that any changes we observed were due to the synthesis gas itself, and not because of permanent or long term changes to the surface or properties of the catalyst.

3.2 Experimental

3.2.1 Catalyst preparation

The Co/TiO_2 catalyst used in this series of experiments was prepared by impregnating TiO_2 with a cobalt nitrate solution. TiO_2 (Degussa P25) was mixed with distilled water in a mass ratio of 1:1, and dried in air at 120 ℃ for 1 hour. The support was then calcined in air at 400 ^{o}C for 16 hours [25]. After calcination the support was crushed and sieved, and the particles with diameters between 0.5 and 1 mm were selected for use. The support was then impregnated with a sufficient quantity of cobalt nitrate ($Co(NO_3)_2 \cdot 6H_2O$) solution to give a cobalt metal loading of 10% by mass. Thereafter the support was dried in air at 120 ℃ for 16 hours, and then calcined in air at 400 ℃ for 6 hours to allow it to decompose and transform from cobalt nitrate to cobalt oxide.

3.2.2 Experimental set-up and procedure

3.2.2.1 Catalyst reduction

We loaded 1 g of catalyst into the FBR, and performed the reduction at atmospheric pressure with H_2 (Afrox (African Oxygen) Ltd., 99.999%) for 24 hours. The reduction temperature and the flow rate were 350 ℃ and 60 ml(NTP)/(min gcat), respectively.

3.2.2.2 Cobalt-based catalyst stability testing during CO and CO_2 hydrogenation

Once the reduction was completed, we allowed the reactor to cool down to room temperature. The CO_2 syngas (hereafter referred to as the CO_2 feed), composed of CO_2:H_2:N_2 = 23%/67%/10% whose N_2 served as an internal standard for mass balance calculations, was introduced into the reactor at a flow rate of 30 ml(NTP)/(min gcat). The reactor pressure was slowly increased to 20 bar (gauge), after which the temperature was gradually raised to 180 ℃. The pressure and temperature were allowed to stabilize, and these operating conditions were maintained in a constant state for 72 hours, during which the composition of the tail gas was monitored. Next, the feed gas was switched from CO_2 feed to the CO syngas (designated as the CO feed), which consisted of CO:H_2:N_2=30%:60%:10%, with N_2 as an internal standard for mass balance calculations. The new reaction conditions retained the same constant pressure, temperature and flow rate as those for the CO_2 feed. These were maintained for 72 hours while the tail gas composition was monitored. After that, the feed gas was switched back to CO_2 feed with the same operating conditions in terms of the constant pressure, temperature and flow rate. Each of the feed gases was interchanged around four to five times, under the same operating conditions. The same sequence was repeated at 200 ℃, 210 ℃ and 220 ℃.

The experimental reaction conditions are shown in Table 3.1, and the simplified flow scheme for the FTS experiments is given in Figure 3.1.

Table 3.1: Summary of experimental conditions for FTS by switching between $CO_2/H_2/N_2$ and $CO/H_2/N_2$ syngases.

Reactor	A micro-FBR
Catalyst	Co (10 wt.%)/TiO_2
Catalyst weight (g)	1
CO_2 feed	$CO_2/H_2/N_2$ 23%/67%/10%
CO feed	$CO/H_2/N_2$ 30%/60%/10%
Total pressure (bar gauge)	20
Flow rate (ml(NTP)/(min gcat))	30
Temperature (^oC)	180-220

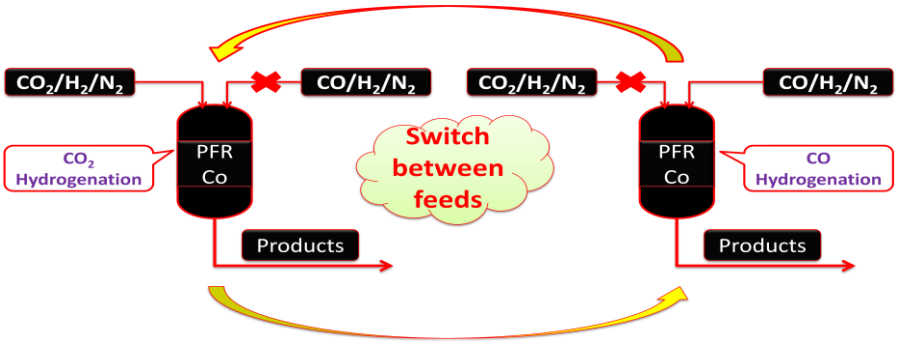

Figure 3.1: Simplified flow scheme for FTS using a micro-FBR by switching between $CO_2/H_2/N_2$ and $CO/H_2/N_2$ syngases over a cobalt-based catalyst (reaction conditions as shown in Table 3.1).

3.2.3 Product analysis

The tail gas was analyzed every 1.5 hours using an online DANI GC. Two thermal conductivity detectors (TCD) were used to analyze H_2, N_2, CO, CO_2 and CH_4, while a flame ionization detector (FID) did the same for the gas phase

hydrocarbons. The wax and liquid products were collected in a hot trap (kept at 150 ℃) and cold trap (maintained at room temperature). The oil and wax products were analysed by an off-line GC at the end of the mass balance for each run.

3.3 Results

3.3.1 Cobalt-based catalyst stability testing during CO and CO_2 hydrogenation for 2700 hours on stream

3.3.1.1 Conversion results

To summarize, we conducted a series of experiments to investigate the effect of CO_2 on cobalt-based low temperature FTS, at 180–220 ℃, 20 bar gauge and 30 ml(NTP)/(min gcat) in which we switched between the CO ($CO/H_2/N_2$) and CO_2 ($CO_2/H_2/N_2$) feeds constantly.

The reaction conversion and product selectivity for both the CO and CO_2 feeds during 2700 hours on-stream are given in Figure 3.2. The data in Figure 3.2 (a) show that the CO and CO_2 are readily hydrogenated on a cobalt-based catalyst, and that in both the conversions improved with an increase in temperature. At the lower temperature of 180 ℃, the catalyst reactivity for CO_2 was close to that of CO. However, when we increased the reaction temperature from 200 to 220 ℃, CO_2 demonstrated a lower reactivity than CO.

It is quite interesting to note that the CO_2 conversion achieved its highest value with the reaction temperature at 180 ℃ (see Figure 3.2 (a)) when the CO_2 feed mixture was first introduced into the reactor. After this, when the repeated switching of the feed gas from CO_2 to CO and then back again was initiated, the conversion of both feed gases remained constant. This indicates that the catalyst was not de-activated under those reaction conditions.

It should be noted that there was no apparent catalyst deactivation during the feed gas switching between CO and CO_2 feeds at the reaction temperature of 200 ℃. However, we found that the CO conversion for the CO feed dropped slightly with time on stream at a reaction temperature of 210 ℃, whereas that of the CO_2 feed did not.

3.3.1.2 Product selectivity results

The CH_4 and C_{2+} selectivity are shown in Figures 3.2 (b) and (c). For the CO feed, the data presented indicate the following.

- The CH_4 selectivity did not change much during the switching between the CO and CO_2 feeds at each operating temperature. Furthermore, it increased slightly from around 8% to 12% when the temperature rose from 180–220 ℃.
- The C_{2+} selectivity showed little change during the period when the operating temperature remained the same, and declined with increasing reaction temperature.

On the other hand, the results for the CO_2 feed follow a different pattern:

- The CH_4 selectivity altered between 87–95% when the temperature was increased from 180 ℃ to 220 ℃. The highest CH_4 selectivity was achieved during the initial run at 180 ℃. The selectively decreased when the temperature was increased from 200 ℃ to 220 ℃.
- The C_{2+} selectivity was only around 5–13%, although it rose in parallel with incremental increases in temperature in the temperature range 200–220 ℃.

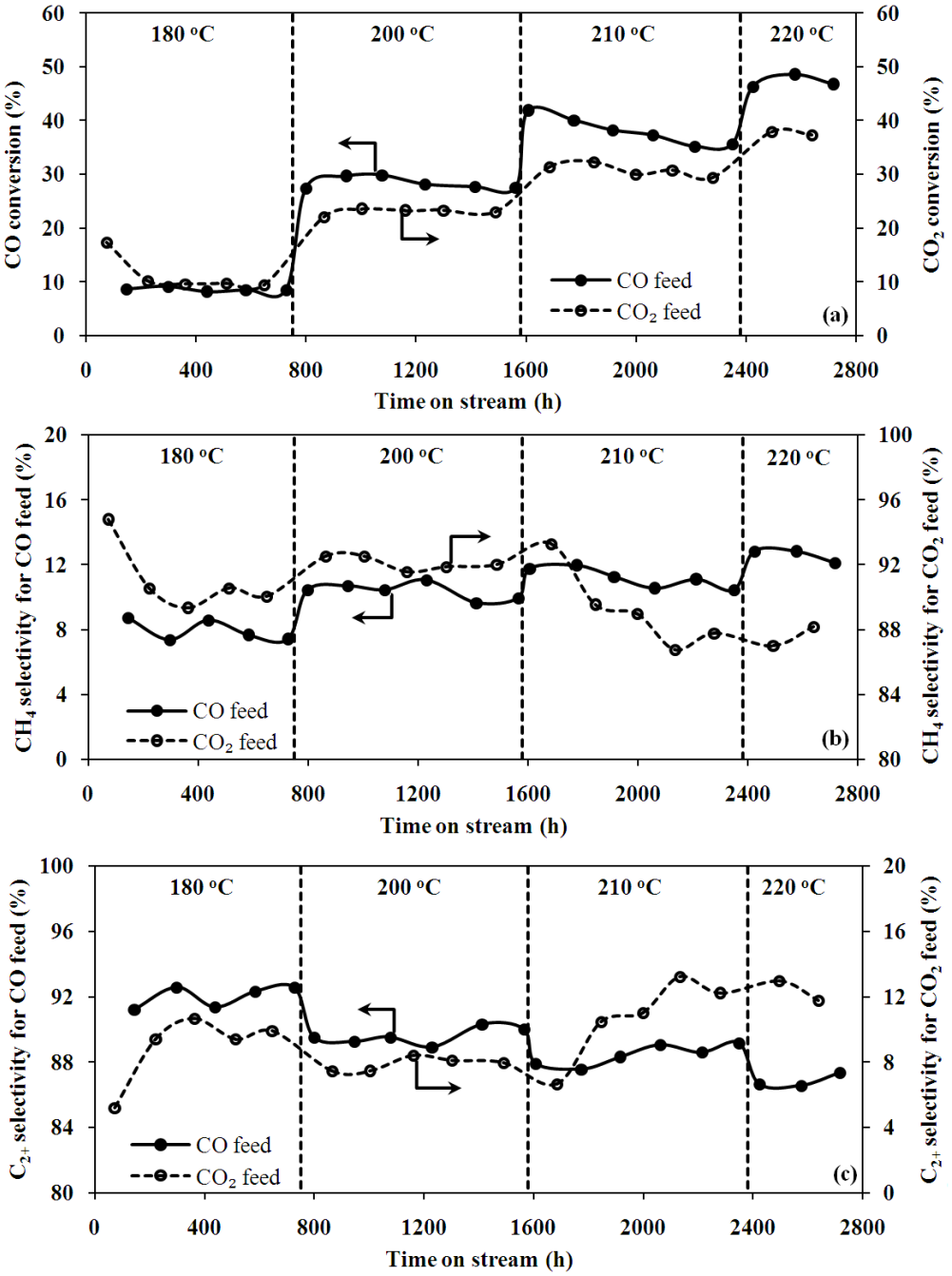

Figure 3.2: CO and CO_2 conversion (a); methane selectivity (b); and C_{2+} selectivity (c), as functions of time on stream over a Co/TiO_2 catalyst (reaction conditions as shown in Table 3.1).

3.3.1.3 Reactant consumption rate

The CO and CO_2 reaction rates for both CO and CO_2 hydrogenation as a function of time on stream are given in Figure 3.3 (a), which show trends similar to those illustrated in Figure 3.2 (a).

- No catalyst deactivation was apparent when the feed gases were switched between CO and CO_2 feeds at the reaction temperatures of 180 ℃ and 200 ℃.
- There was a mild catalyst deactivation when the feed gases alternated between CO and CO_2 feeds at the reaction temperatures 210 ℃ and 220 ℃.
- The highest CO_2 reaction rate was obtained during the first run for the CO_2 feed when compared with the rates for the other four runs at 180 ℃.

Figures 3.3 (b) and (c) plot the CH_4 and C_{2+} formation rates for both CO and CO_2 feeds. The CH_4 formation rate for CO_2 hydrogenation was far higher than that of CO hydrogenation (Figure 3.3 (b)). When the temperature was increased from 180 ℃ to 220 ℃, the CH_4 formation rate rose for both CO and CO_2 hydrogenation. There was a reduction in the CH_4 rate at 210 ℃ for both CO and CO_2. The initial run gave the highest CH_4 reaction rate for CO_2 hydrogenation, which was around two times greater than in the other four runs carried out at 180 ℃.

A point of interest is that although the C_{2+} formation rate for CO_2 feed improved when the temperature rose, the values of the rate were dramatically lower than those obtained with the CO feed (Figure 3.3 (c)). In addition, a drop in the C_{2+} rate with time on stream occurred only in the case of the CO feed when catalyst deactivation took place at 210 ℃ (Figure 3.3 (a)).

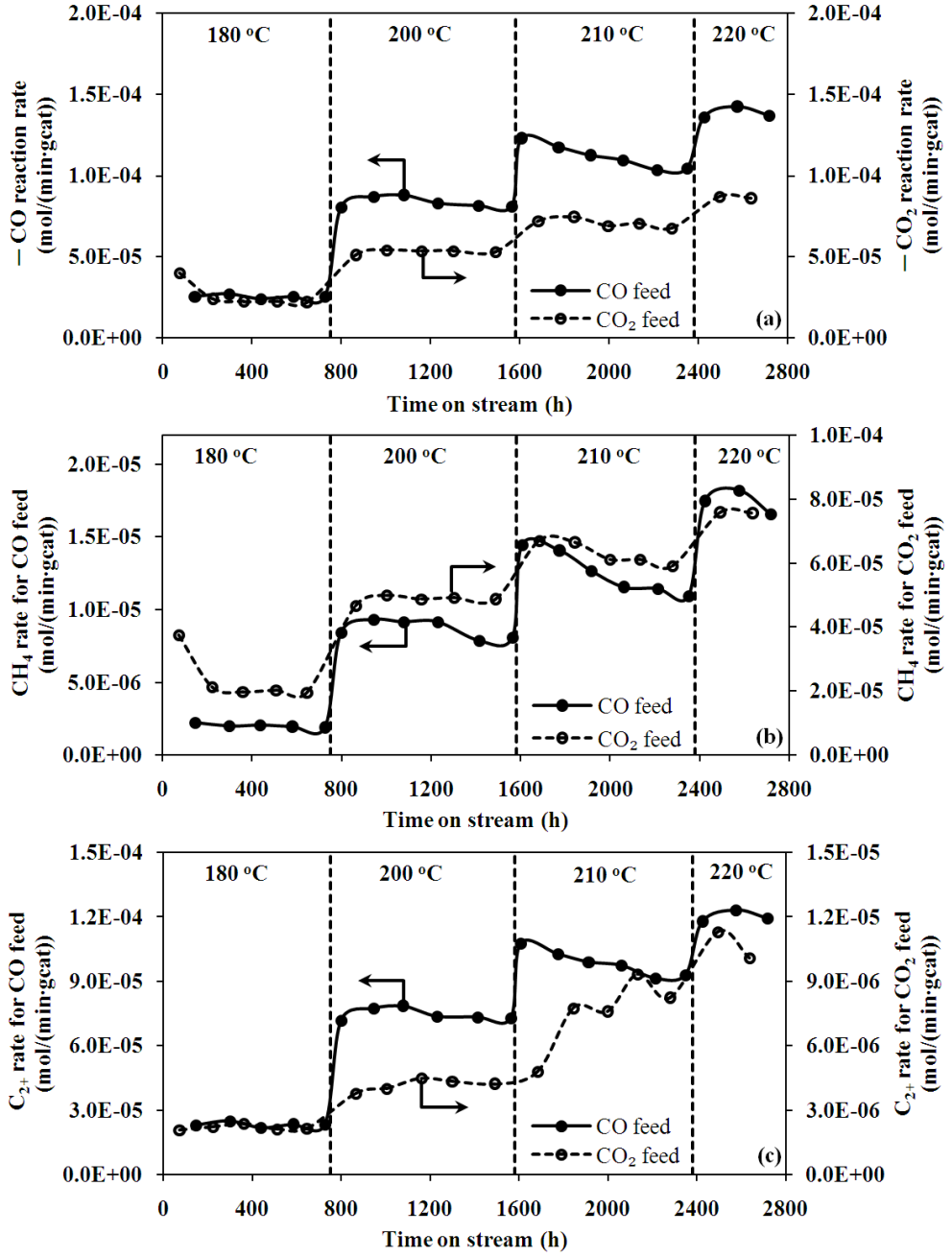

Figure 3.3: Reactant consumption rate (a); CH_4 formation rate (b); and C_{2+} formation rate (c), as functions of time on stream over a Co/TiO_2 catalyst (reaction conditions as shown in Table 3.1).

3.3.1.4 Olefin and paraffin formation rates

The light olefin and paraffin formation rates during the switching between the two feed gases as a function of time on stream are plotted in Figures 3.4 (a–c). The

first of these, (a), shows the olefin formation rate for the CO feed as fairly constant at each of the reaction temperatures, with a rise in the rate corresponding with each upward adjustment to the temperature. The paraffin formation rate for CO feed also rose when the temperature increased, but showed a visible decline with the accumulation of time on stream at 210 ℃ (Figure 3.4 (b)). Comparing the results we obtained for CO hydrogenation with those for CO_2 hydrogenation, we found that no olefin could be detected in the latter, and that all the products were paraffins. The paraffin formation rate for the CO_2 feed was remarkably constant at each of the reaction temperatures, even at the higher temperatures (210 ℃ and 220 ℃), which differed from the case of CO hydrogenation (Figure 3.4 (c)).

In addition, the typical pattern of relatively low yields of ethene and ethane was obtained for the CO feed [26–29], but in contrast the amount of ethane produced by the CO_2 feed was greater than for the other hydrocarbons with a chain length of $n>2$.

3.3.1.5 Olefin to paraffin (O/P) ratios

Because all the products of the CO_2 feed were saturated paraffins, only the O/P ratio derived from the CO feed is given in Figure 3.4 (d). It is generally accepted [30–31] that the O/P ratio changes as a function of carbon number, and that an increment in the carbon number causes a drop in the O/P ratio under each reaction condition excluding O_2/P_2.

It should be noted that the O/P ratio did not change much with time on stream at the lower temperature of 180 ℃, as well as at 200 ℃. However, an increase in the O/P ratio was obtained with time on stream at 210 ℃ and 220 ℃, respectively.

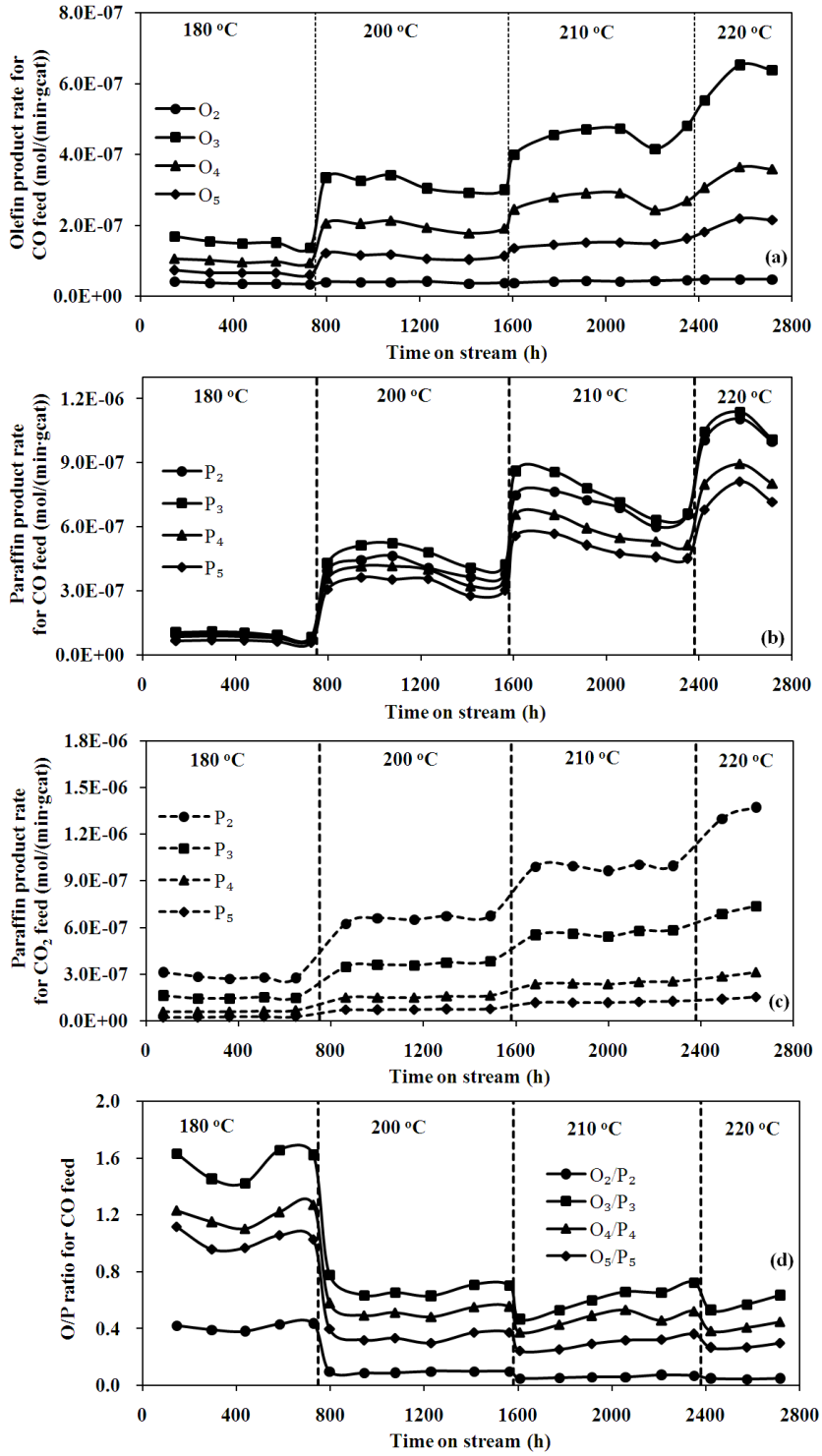

Figure 3.4: The olefin formation rate for CO feed (a); paraffin formation rate for CO feed (b); paraffin formation rate for CO_2 feed (c); and olefin/paraffin (O/P) ratio for CO feed (d), as functions of time on stream for a Co/TiO_2 catalyst (reaction conditions as shown in Table 3.1).

According to the catalyst activity and product selectivity results as shown in Figures 3.2–3.4, we can conclude that:

- both CO and CO_2 are readily hydrogenated over a cobalt-based catalyst;
- in comparison with CO hydrogenation, CO_2 hydrogenation produces methane- rich short chain paraffins, a result in agreement with published research findings [13,15,18,19];
- when the CO and CO_2 feeds were repeatedly alternated, we could observe no catalyst deactivation at the reaction temperatures of 180 ℃ and 200 ℃, although a mild deactivation was observed when the temperatures were increased to 210 ℃ and 220 ℃, respectively;
- when the catalyst was deactivated at 210 ℃, for the CO feed only the paraffin product formation rate showed a significant decline, while the olefin rate did not; but for the CO_2 feed, with the exception of CH_4, the paraffin product formation rate was not affected at that reaction temperature.

In addition, the CO_2 reaction rate achieved its highest rate when the CO_2 feed was initially introduced into the FBR. This was even higher than the CO reaction rate at 180 ℃. However, when the feed gas was subsequently switched from the CO_2 feed to the CO feed and then back again, the CO_2 reaction rate fell to around two times lower than that obtained in the first run. It therefore became necessary to seek more detailed information on what occurred during that period.

3.3.2 Cobalt-based catalyst stability testing during CO and CO_2 hydrogenations at 180 ^oC

Figure 3.2 (a) shows that CO conversion was quite stable when switching occurred between CO and CO_2 feeds in the FBR at a constant temperature of 180 ℃. However, as the data plotted on the Figure 3.2 (a) show the CO_2 conversion was initially changed by the introduction of the CO feed into the reactor, but then

became stable.

Detailed information concerning the product formation rate and O/P ratio is given in Figure 3.5. When we compared the CO_2 hydrogenation data recorded both before and after the initial CO FTS at 180 ℃, we found that

- the CH_4 formation rate decreased from 3.8E-05mol/(min gcat) in the first run of CO_2 hydrogenation to 2.1E-05 mol/(min gcat) in the second (around two times lower than the first);
- the P_2 and P_3 rates decreased slightly, from 3.1E-07 mol/(min gcat) to 2.8 E-07mol/(min gcat) for P_2 and from 1.6E-07 mol/(min gcat) to 1.5E-07 mol/(min gcat) for P_3;
- the P_4 and P_5 rates remained similar to the values obtained in the first run of the CO_2 feed.

With the subsequent repetition of alternation between the two feeds, we found that each of the paraffin formation rates maintained a pseudo-stable state.

When the CO feed was initially introduced into the reactor, the time on stream was 73 hours. Between that point and 144 hours:

- each of the olefin products reached its highest rate and then decreased to a stable state, as shown in Figure 3.5 (b);
- each of the paraffin products achieved its lowest rate, and then increased to a stable state (see Figure 3.5 (c)); and
- each of the O_n/P_n ratios attained its maximum value, and then dropped to a stable state value.

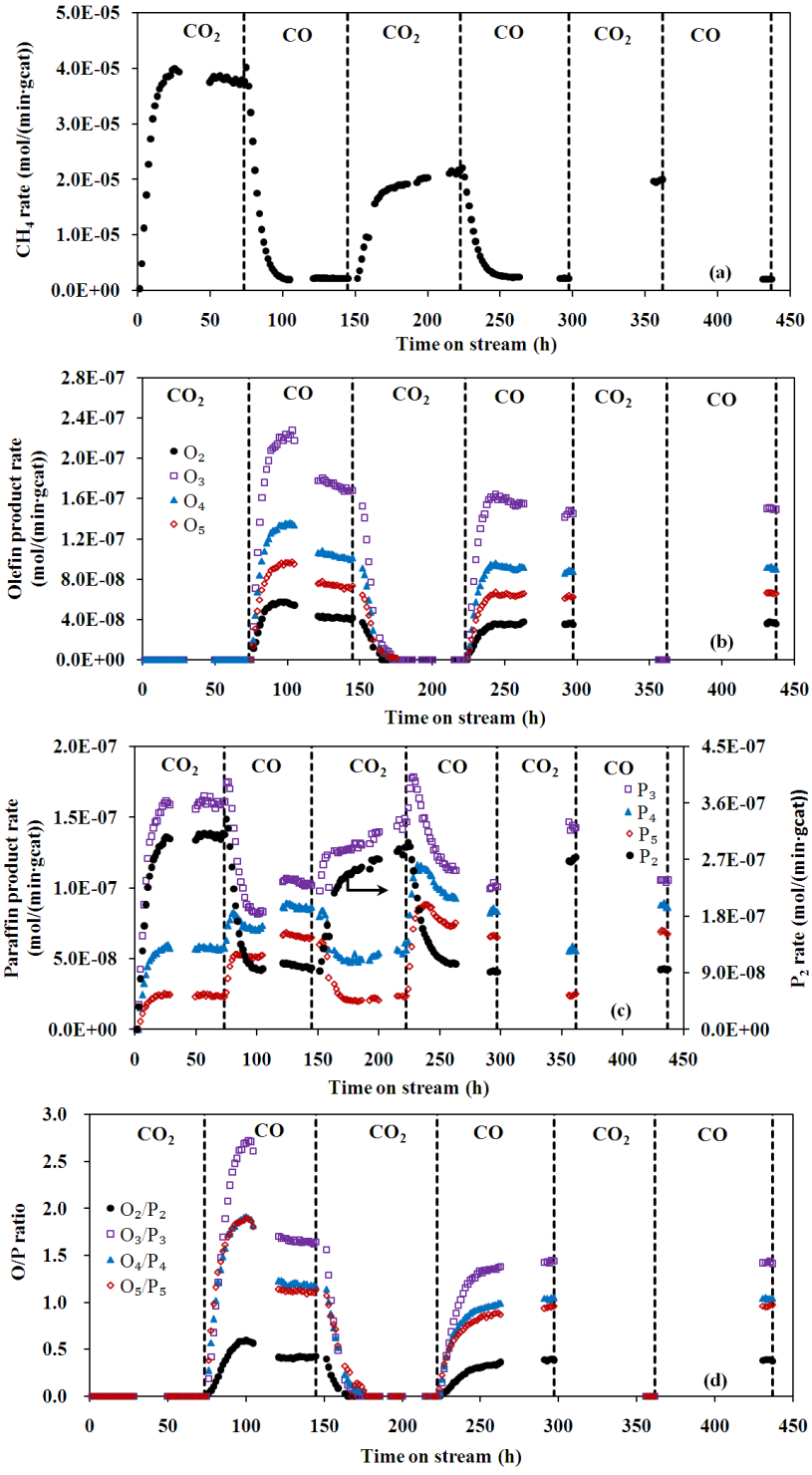

Figure 3.5: The CH_4 formation rate (a); olefin formation rate (b); paraffin formation rate (c); and olefin/paraffin (O/P) ratio for CO feed (d), as functions of time on stream for a Co/TiO_2 catalyst at 180 ℃, 20 bar (gauge) and 30

ml(NTP)/(min gcat): CO_2 represents the CO_2 feed ($CO_2/H_2/N_2$=23%/67%/10%) and CO refers to the CO feed ($CO_2/H_2/N_2$=30%/60%/10%).

The data revealed that both the olefin and paraffin formation rates were suddenly changed from one pseudo-stable state to another during the initial run of CO hydrogenation. With subsequent repeated switching between the two feeds, we found that both the paraffin and olefin product formation rates and O/P ratio for the CO feed reverted to the values obtained with the time on stream from 120–144 hours as shown in Figure 3.5.

3.4 Discussion

3.4.1 Explanation of the experimental results obtained at 180 ℃

The data from Figures 3.2, 3.3 and 3.5 show that the catalyst activity and product selectivity for CO_2 hydrogenation was initially changed by introducing the CO feed into the reactor at the reaction temperature of 180 ℃. During subsequent repeated switching between the two feed gases, catalyst activities for both CO and CO_2 hydrogenations remained constant, indicating that the catalyst was not apparently deactivated under those reaction conditions; thus, deactivation cannot explain the observed phenomenon.

One of the possible reasons for the observed significant changes during the first switching is the formation of the liquid phase either on the catalyst surface or in the catalyst pores. Some researchers [32–33] have reported that under typical reaction conditions the FT products distribute between the vapour and liquid phases within the reactor. The lighter components are carried overhead with the unreacted syngas, while the heavier components form the molten-wax phase within which the catalyst is suspended. Furthermore, the performance of the reactor is strongly dependent on the composition of the wax phase, which affects

both the chemistry [34-35] and the hydrodynamics [36] of the synthesis. Lu *et al.* [37-38] conducted a series of typical FTS experiments followed by flushing experiments in a gas-solid system with a TiO_2-supported cobalt catalyst in a continuously stirred tank reactor. They switched between two kinds of experiment with the time on stream, and compared the results of the FTS reaction rate and product selectivity both before and after flushing. Their conclusions after studying the results they obtained were that the changes they had observed in catalyst activity and product selectivity were caused (either wholly or mainly) by liquid product deposited in the catalyst rather than by the change in the properties of the catalyst surface. Furthermore, by using the deuterium tracer, Liu and co-workers [39] measured that the product accumulation in FTS occurs not only in large continuously stirred tank reactors, but also in small FBR. When we carried out CO FTS experiments in a FBR under reaction conditions similar to those used by Lu *et al.*, we encountered the same trend (dramatic changes in the O/P ratio) for CO hydrogenation (see Figure 3.5 (d) from 73–144 hours) as they had reported [37–38].

It is generally agreed that when CO_2 hydrogenation takes place over a cobalt-based catalyst, the products are methane-rich short chain hydrocarbons, whereas for low-temperature CO based syngases, the FT process is used for the production of high molecular mass linear waxes. Thus, the liquid phase in the reactor can be easily formed by CO FTS, but not by CO_2 FTS. Grounding our reasoning on the research reported in the literature and our own experimental results, we postulate that liquid products may be deposited on the catalyst surface or in the catalyst pores during CO FTS.

When the CO_2 feed was initially introduced into the reactor, the dominant products were methane-rich short chain paraffins, so that only a gas phase occurred. Then, when we switched the feed gas to a CO syngas, which would

gradually replace the CO_2 in the reactor, long chain waxes formed, and accumulated to form a liquid phase on the catalyst surface and in the catalyst pores. These liquid products could therefore change the mass transfer of reactants and products, and, further, affect the catalyst activity and product selectivity. After that, when we switched back to the CO_2 feed, it is possible that a certain amount of liquid remained on the catalyst surface or in the catalyst pores during CO_2 hydrogenation.

Solubility and diffusivity are two factors that are likely to affect the mass transfer of the components. Several researchers [40–42] have investigated the solubility of different gases in the same organic liquid (mostly n-paraffins), and reported the order for the solubility values as: $H_2<CO<CO_2$. When Erkey *et al.* [43] published their findings on the diffusion of the syngas and products in FT wax, they reported the order for the diffusion coefficient values as $CO_2<CO<H_2$. Solubility and diffusivity characteristics should be co-active in the mass transfer of the reactants and products for FTS.

FTS is a surface catalytic reaction. The H/C (hydrogen to carbon) concentration on the catalyst surface can affect the product selectivity of both of the CO and CO_2 hydrogenations [13, 44]. A low H/C ratio leads to reduced selectivity of short chain hydrocarbons, high selectivity of long chain hydrocarbons and olefins, and a low selectivity of paraffins. The absorption of CO, CO_2 and H_2 on the catalyst surface is likely to be different for a gas or a liquid phase in the catalyst pores, which will also affect the H/C surface ratio.

Figures 3.2 and 3.5 show that the catalyst activity and product selectivity for CO_2 hydrogenation are not the same before and after the initial CO FTS at 180 ℃. When we compare the results from the first run with those of the second, we observe that in the latter the CO_2 conversion and methane selectivity dropped and C_{2+} selectivity rose for CO_2 hydrogenation. These data suggest that a lower H/C

ratio is obtained on a liquid-covered catalyst surface than on the dry catalyst surface. This means that the liquid phase is more favourable to the absorption of CO_2 than H_2 for CO_2 hydrogenation. We can deduce that solubility rather than diffusivity may dominate the reactants' mass transfer in the case of CO_2 hydrogenation.

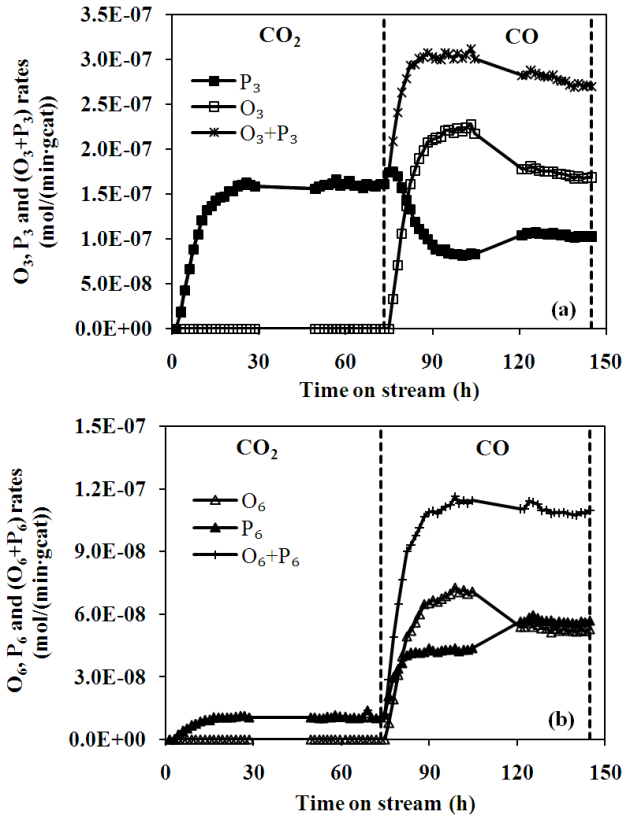

Figure 3.6: Olefin, paraffin and combined olefin+paraffin formation rates for carbon numbers equal to 3 (a) and 6 (b) as functions of time on stream for a Co/TiO_2 catalyst at 180 ℃, 20 bar (gauge) and 30 ml(NTP)/(min gcat). CO_2 represents the CO_2 feed ($CO_2/H_2/N_2$=23%/67%/10%) and CO refers to the CO feed ($CO_2/H_2/N_2$=30%/60%/10%).

When we initially introduced the CO feed into the reactor, both the olefin and paraffin formation rates were suddenly changed from one pseudo-state to another. The O/P ratio obtained in the later pseudo-state (Figure 3.5) was lower, which indicated that in CO hydrogenation a higher H/C ratio is obtained on a

liquid-covered catalyst surface than on a dry catalyst surface. This finding is in agreement with the claim made by Lu *et al.* [38] that the H_2/CO ratio in the liquid-covered catalyst is far higher than in the feed gas.

Figure 3.6 shows the olefin, paraffin and combined olefin+paraffin formation rates with carbon numbers equal to 3 (a) and 6 (b) with time on stream for the first 145 hours. As can be seen, with time on stream the olefin formation rate (O_3 and O_6) decreased between the first pseudo-state and the second, while at the same time the paraffin formation rate (P_3 and P_6) increased, the total (P_3+O_3) rate dropped slightly, and the (P_6+O_6) rate remained constant. These data indicate that the liquid phase may promote a secondary reaction of the primary olefins, especially in the case of olefin hydrogenation (see Reaction (a) below).

$$C_nH_{2n} + H_2 = C_nH_{2n+2} \quad \text{(a)}$$

Because the H/C ratio in the liquid phase is higher than in the gas phase, olefin hydrogenation will more likely occur in the liquid phase with the re-adsorbed olefin products.

3.4.2 Explanation of the experimental results achieved when the catalyst was deactivated at 210–220 ℃

When mild catalyst deactivation was observed at a time on stream of 1600–2700 hours and reaction temperatures of 210 ℃ and 220 ℃ (Figures 3.2 and 3.3), a small amount of CO_2 product was detected in the tailgas for CO hydrogenation (see Figure 3.7). There are two ways to produce CO_2 during CO hydrogenation. These can be expressed in terms of the reaction (b) and (c):

Boudouard reaction: $2CO = CO_2 + C$ (b)

Water gas shift (WGS) reaction: $CO + H_2O = CO_2 + H_2$ (c).

The Boudouard reaction provides atomic carbon, which may be transformed into more stable species (such as bulk cobalt carbide and polymeric carbon), and negatively influences FTS activity [6, 35]. However, Dry [45] reported that little or no carbon was deposited on the catalyst surface at an FT operating temperature below about 240 ℃, regardless of whether Ni, Co, Ru or Fe-based catalysts were being used. The experiments we conducted were in the range 180–220 ℃, which is lower than 240 ℃. Alternatively, if the catalyst deactivation we observed in the experiments was caused by carbon deposition, the catalyst activity for both CO and CO_2 hydrogenations should have decreased. However, the data in both Figure 3.2 (a) and Figure 3.3 (a) show that there was a mild deactivation evident only for the CO feed with the time on stream at an operating temperature of 210 ℃. Thus, we suggest that carbon deposits were unlikely to be the main reason for the deactivation of the catalyst under the reaction conditions we chose.

Therefore, we have to consider whether the production of CO_2 is caused mainly by WGS rather than the Boudouard reaction. It is widely accepted that the WGS reaction is attributable to the transformation of cobalt to oxide forms [6], in other words to re-oxidation of the catalyst, which is the one of the reasons for cobalt catalyst deactivation [6, 8]. When the operating temperature was increased from 200 ℃ to 210 ℃, the feed gas was the CO based syngas. The CO_2 product was the first to be detected (Figure 3.7), which indicates that the catalyst re-oxidation was triggered by the CO feed. Dalai and Davis [8] suggested that the effect of water on a supported cobalt catalyst can be viewed as starting an oxidation process, and that the extent of oxidation is a function of cobalt crystallite size and the ratio of the partial pressures of water and hydrogen (P_{H_2O}/P_{H_2}) in the reactor. Because the amount of water formed depends upon the CO conversion, we found that the CO_2 selectivity curve (Figure 3.7) was similar to that for CO conversion (Figure 3.2 (a)). There was no evidence to show that the catalyst re-oxidation could be attributed to the CO_2 feed in our experimental system.

Based on the discussion above, we suggest that the main cause of the mild catalyst deactivation we observed was catalyst re-oxidation by water. The cobalt oxide forms have activity for both the WGS and reverse WGS reactions (d).

Reverse-WGS: $CO_2 + H_2 = CO + H_2O$ (d)

CO FT reaction: $CO + 2H_2 = CH_2 + H_2O$ (e)

CO_2 FT reaction: $CO_2 + 3H_2 = CH_2 + 2H_2O$ (f)

We postulate that once the CO_2 feed was switched back into the reactor again after the cobalt catalyst re-oxidized, the reverse-WGS reaction could develop, and produce CO. The CO produced would subsequently react in the CO FT reaction (e) to form organic products, which could in turn increase the conversion of CO_2 to CO. Although the CO_2 FT reaction (f) rate will be affected by catalyst re-oxidation, it explains why the total CO_2 conversion for the CO_2 feed was not markedly reduced when the catalyst was deactivated with the time on stream (Figure 3.2 (a)).

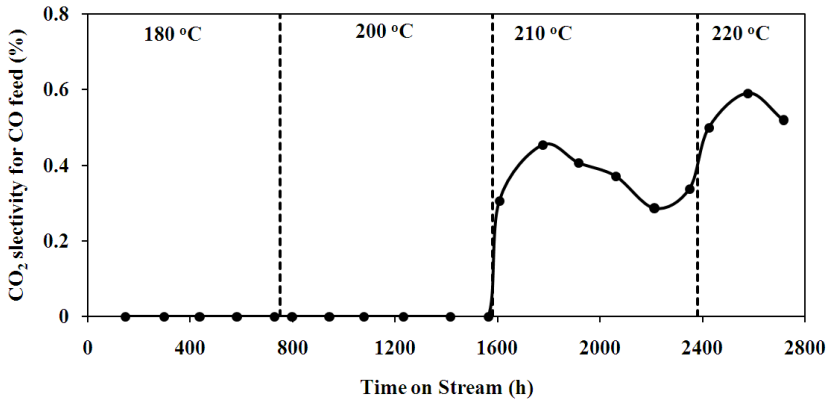

Figure 3.7: CO_2 selectivity for CO hydrogenation as a function of time on stream for a Co/TiO_2 catalyst (reaction conditions as shown in Table 3.1).

In Section 3.4.1, we discussed the postulate that the liquid phase on the catalyst surface and in the catalyst pores may affect the catalyst activity and product selectivity. For instance, secondary olefin hydrogenation can be fostered by the

liquid phase. Any of the factors that alter the amount of liquid accumulated on the catalyst surface or in the catalyst pores will affect the FT product composition as well. The catalyst deactivation observed in our experiments reduced the CO conversion, and could then decrease the amount of the liquid that accumulated in the reactor. Therefore, the extent of the secondary reaction could be restricted by catalyst deactivation, which means the rate of reaction (a) (olefin hydrogenation) would be decreased with a reduced CO conversion during FTS. The restriction of the secondary reaction (owing to the amount of the liquid accumulated in the reactor) may answer the phenomenons observed in Figure 3.4 (a-c): (1) when there was no apparent catalyst deactivation at the lower temperature of 180 ^oC, as well as at 200 ^oC, a stable secondary reaction rate could be achieved, so that the fairly constant olefin and paraffin product formation rates with a constant O/P ratio with time on stream were observed. (2) whereas, when the deactivation of the catalyst was observed, the secondary olefin reaction could be restricted, thus, it is found that the olefin product formation rate did not decrease, but the paraffin product formation rate did with an increase of the O/P ratio with time on stream at the temperature of 210 ^oC and 220 ^oC, respectively. These phenomenons also support the hypothesis of the presence of a liquid phase in the reactor.

3.5 Conclusions

For the experimental work described in this chapter, we prepared 10 wt.% Co/TiO_2 catalyst by impregnating TiO_2 with a cobalt nitrate solution. The new series of experiments, named "cobalt-based catalyst stability testing during CO and CO_2 hydrogenation", entailed switching repeatedly between a CO feed ($CO/H_2/N_2$=30%/60%/10%) and a CO_2 feed ($CO_2/H_2/N_2$=23%/67%/10%) in a FBR at 180–220 ℃, 20 bar (gauge) and 30 ml(NTP)/(min gcat).

We have shown that both CO and CO_2 are readily hydrogenated over a

cobalt-based catalyst, and that, unlike CO hydrogenation, CO_2 hydrogenation produced methane-rich short chain saturated hydrocarbons. When we continually alternated the CO and CO_2 feeds, we were unable to find any signs of catalyst deactivation at reaction temperatures of 180 ℃ and 200 ℃.

The data show that dramatic changes occurred in the catalyst activity and product selectivity for CO_2 hydrogenation between the initial CO FTS at 180 ℃ and the succeeding run. In addition, during the initial CO hydrogenation on the cobalt catalyst, both the olefin and paraffin formation rates suddenly changed from one pseudo-stable state to another, with a higher O/P ratio obtained initially. According to our own data and the findings published in the relevant scientific literature review, we concluded that these changes could be attributed to liquid products deposited on the catalyst surface or in the catalyst pores during CO FTS.

A mild catalyst deactivation was observed at the operating temperatures of 210 ℃ and 220 ℃, respectively. During the period when the catalyst was deactivated, we found that: (1) the reaction rate decreased for CO hydrogenation rather than for CO_2 hydrogenation; (2) only the paraffin product formation rate dropped significantly, while there was no decline in the yield of olefin for CO hydrogenation; (3) except for CH_4, the paraffin product formation rate for the CO_2 feed was not reduced; (4) and CO_2 product was detected for CO hydrogenation. These suggest that the catalyst deactivation was caused by the re-oxidation of the cobalt catalyst by water.

Although we could not explain the experimental phenomena fully, we must emphasize that the long term effect of CO_2 on the properties of a cobalt-based catalyst was very small under the given reaction conditions. We also confirmed that it may not be necessary to remove CO_2 from the raw syngas for cobalt-based FTS. These results provide some guidance on how to design FTS processes and FT catalysts to improve product selectivity.

References

[1] Dry, M. E. (2002), The Fischer-Tropsch process: 1950–2000, Catalysis Today, 71, 227–241.

[2] Schulz, H. (1999), Short history and present trends of Fischer-Tropsch synthesis, Applied Catalysis A: General, 186, 3–12.

[3] James, O. O., Mesubi, A. M., Ako, T. C. and Maity, S. (2010), Increasing carbon utilization in Fischer-Tropsch synthesis using H2-deficient or CO_2-rich syngas feeds, Fuel Processing Technology, 91, 136–144.

[4] Arzamendi, G., Dieguez, P.M., Montes, M., Odriozola, J.A., Sousa-Aguiar, E. F. and Gandia, L.M. (2010), Computational fluid dynamics study of heat transfer in a microchannel reactor for low-temperature Fischer-Tropsch synthesis, Chemical Engineering Journal, 160, 915–922.

[5] Espinoza, R. L., Steynberg, A. P., Jager, B. and Vosloo, A. C. (1999), Low temperature Fischer-Tropsch synthesis from a Sasol perspective, Applied Catalysis A: General, 186, 13–26.

[6] Tsakoumis, N. E., Ronning, M., Borg, O., Rytter, E. and Holmen, A. (2010), Deactivation of cobalt based Fischer-Tropsch catalysts: A review, Catalysis Today, 154, 162–182.

[7] van de Loosdrecht, J., Balzhinimaev, B., Dalmon, J. -A., Niemantsverdriet, J. W., Tsybulya, S. V., Saib, A. M., van Berge, P. J. and Visagie, J. L. (2007), Cobalt Fischer-Tropsch synthesis: Deactivation by oxidation?, Catalysis Today, 123, 293–302.

[8] Dalai, A.K. and Davis, B. H. (2008), Fischer-Tropsch synthesis: A review of

water effects on the performances of unsupported and supported Co catalysts, Applied Catalysis A: General, 348, 1–15.

[9] van Steen, E., Claeys, M., Dry, M. E., van de Loosdrecht, J., Viljoen, E.L. and Visagie, J. L. (2005), Stability of nanocrystals: Thermodynamic analysis of oxidation and re-reduction of cobalt in water/hydrogen mixtures, Journal of Physical Chemistry B, 109, 3575–3577.

[10] Iglesia, E. (1997), Design, synthesis, and use of cobalt-based Fischer-Tropsch synthesis catalysts, Applied Catalysis A: General, 161, 59–78.

[11] Li, J., Jacobs, G., Das, T. and Davis, B. H. (2002), Fischer-Tropsch synthesis: effect of water on the catalytic properties of a ruthenium promoted Co/TiO_2 catalyst, Applied Catalysis A: General, 233, 255–262.

[12] Higman, C. and Burgt. M. (2003), *Gasification*, Guif Professional Publishing, Burlington.

[13] Visconti, C. G., Lietti, L., Tronconi, E., Forzatti, P., Zennaro, R. and Finocchio, E. (2009), Fischer-Tropsch synthesis on a Co/Al_2O_3 catalyst with CO_2 containing syngas, Applied Catalysis A: General, 355, 61–68.

[14] Gnanamani, M. K., Shafer, W. D., Sparks, D. E. and Davis, B. H. (2011), Fischer-Tropsch synthesis: Effect of CO_2 containing syngas over Pt promoted $Co/\gamma\text{-}Al_2O_3$ and K-promoted Fe catalysts, Catalysis Communications, 12, 936–939.

[15] Zhang, Y., Jacobs, G., Sparks, D. E., Dry, M. E. and Davis, B. H. (2002), CO and CO_2 hydrogenation study on supported cobalt Fischer-Tropsch synthesis catalysts, Catalysis Today, 71, 411–418.

[16] Kim, S. M., Bae, J. W., Lee, Y. J. and Jun, K. W. (2008), Effect of CO_2 in the

feed stream on the deactivation of Co/γ-Al_2O_3 Fischer-Tropsch catalyst, Catalysis Communications, 9, 2269–2273.

[17] Riedel, T. and Schaub, G. (2003), Low-temperature Fischer-Tropsch synthesis on cobalt catalysts-effects of CO_2, Topics in Catalysis, 26, 145–156.

[18] Riedel, T., Claeys, M., Schulz, H., Schaub, G., Nam, S. S., Jun, K.W., Choi, M. J., Kishan, G. and Lee, K. W. (1999), Comparative study of Fischer-Tropsch synthesis with H_2/CO and H_2/CO_2 syngas using Fe- and Co-based catalysts, Applied Catalysis A: General, 186, 201–213.

[19] Yao, Y., Hildebrandt, D., Glasser, D. and Liu, X. (2010), Fischer-Tropsch synthesis using $H_2/CO/CO_2$ syngas mixtures over a cobalt catalyst, Industrial and Engineering Chemistry Research, 49, 11061–11066.

[20] Russell, W. W. and Miller, G. H. (1949), Catalytic hydrogenation of carbon dioxide to higher hydrocarbons, Journal of the American Ceramic Society, 72, 2446–2454.

[21] Akin, A. N., Ataman, M., Aksoylu, Z. E. and Onsana, Z. I. (2002), CO_2 Fixation by hydrogenation over coprecipitated Co/Al_2O_3, Reaction Kinetics and Catalysis Letters, 76, 265–270.

[22] Bai, R., Tan Y. and Han, Y. (2004), Study on the carbon dioxide hydrogenation to iso-alkanes over Fe-Zn-M/zeolite composite catalysts, Fuel Processing Technology, 86, 293–301.

[23] Herranz, T., Rojas, S., Perez-Alonso, F. J., Ojeda, M., Terreros, P. and Fierro, J. L. G. (2006), Hydrogenation of carbon oxides over promoted Fe-Mn catalysts prepared by the microemulsion methodology, Applied Catalysis A: General, 311, 66–75.

[24] Dry, M. E. (1981), The Fischer-Tropsch Synthesis, Catalysis Science and Technology, Anderson J. R. and Boudart, M. E. Eds., Springer, New York, 1, 159–255.

[25] Li, J. (1999), The preparation, characterization and evaluation of boronmodified Co/TiO_2 Fischer-Tropsch catalysts, PhD thesis, University of the Witwatersrand, Johannesburg, South Africa.

[26] Wojciechowski, B. W. (1988), The kinetics of the Fischer-Tropsch synthesis, Catalysis Reviews, Science and Engineering, 30, 629−702.

[27] Komaya, T. and Bell, A. T. (1994), Estimates of rate coefficients for elementary processes occurring during Fischer-Tropsch synthesis over Ru/TiO_2, Journal of Catalysis, 146, 237–248.

[28] Cheng, J., Hu, P., Ellis, P., French, S., Kelly, G. and Lok, C. M. (2008), A DFT study of the chain growth probability in Fischer-Tropsch synthesis, Journal of Catalysis, 257, 221–228.

[29] Novak, S., Madon, R. J. and Suhl, H. (1981), Models of hydrocarbon product distributions in Fischer-Tropsch synthesis, Journal of Chemical Physics, 74, 6083–6091.

[30] Kuipers, E. W., Vinkenburg, I. H. and Oosterbeek, H. (1995), Chain length dependence of a-olefin re-adsorption in Fischer-Tropsch synthesis, Journal of Catalysis, 152, 137–146.

[31] Shi, B. and Davis, B. H. (2005), Fischer-Tropsch synthesis: The paraffin to olefin ratio as a function of carbon number, Catalysis Today, 106, 129–131.

[32] Marano, J. J. and Holder, G. D. (2007), Characterization of Fischer-Tropsch

liquids for vapor-liquid equilibria calculations, Fluid Phase Equilibria, 138, 1–21.

[33] Caldwell, L. and van Vuuren, D. S. (1986), On the formation and composition of the liquid phase in Fischer-Tropsch reactors, Chemical Engineering Science, 41, 89–96.

[34] Satterfield, C. N. and Stenger, Jr. H. G. (1985), Effect of liquid composition on the slurry Fischer-Tropsch synthesis: 1. Rate of reaction, Industrial and Engineering Chemistry Process Design and Development, 24, 407–411.

[35] Satterfield, C. N. and Stenger, Jr. H. G. (1985), Effect of liquid composition on the slurry Fischer-Tropsch synthesis: 2. Product selectivity, Industrial and Engineering Chemistry Process Design and Development, 24, 411–415.

[36] Quicker, G. and Deckwer, W. D. (1981), Gas hold-up and interfacial area in aerated hydrocarbons, German Chemical Engineering, 4, 363–370.

[37] Lu, X., Hildebrandt, D., Liu, X. and Glasser, D. (2010), Making sense of the Fischer-Tropsch synthesis reaction: Start-Up, Industrial and Engineering Chemistry Research, 49, 9753–9758.

[38] Lu, X., Zhu, X., Hildebrandt, D., Liu, X. and Glasser, D. (2011), New way to look at Fischer-Tropsch synthesis using flushing, Engineering Chemistry Research, Industrial and Engineering Chemistry Research, 50, 4359−4365.

[39] Liu, Y., Zheng, S., Shi, B. and Li, J. (2007), Deuterium tracer study of Fischer–Tropsch synthesis:A method to eliminate accumulation problems, Journal of Molecular Catalysis A: Chemical, 276, 110–115.

[40] Chou, J. S. and Chao, K. C. (1992), Solubility of Synthesis and Product Gases in a Fischer-Tropsch SASOL Wax, Engineering Chemistry Research, 31, 621–623.

[41] Campanella, E. A. (1997), Correlation and prediction of synthesis gas solubility in n-paraffin systems, Chemical Engineering and Technology, 20, 371–377.

[42] Chou, J. S. and Chao, K. C. (1989), Correlation of synthesis gas solubility in n-paraffin solvents and Fischer-Tropsch waxes, Fluid Phase Equilibria, 46, 179–195.

[43] Erkey, C., Rodden, J. B. and Akgerman, A. (1990), Diffusivities of synthesis gas and n-Alkanes in Fischer-Tropsch wax, Energy & Fuels, 4, 275–276.

[44] Zagli, E. and Falconer, J. L. (1981), Carbon dioxide adsorption and methanation on ruthenium. Journal of Catalysis, 69, 1–8.

[45] Dry, M.E. (2004), chapter 7: FT catalysts, Studies in Surface Science and Catalysis, Steynberg, A. and Dry, M. E. (editors), 152, 533–600.

4

FISCHER-TROPSCH SYNTHESIS USING $H_2/CO/CO_2$ SYNGAS MIXTURES OVER A COBALT CATALYST

This work was has been published in the Ind. Eng. Chem. Res., 2010, 49, 11061-11066. Part of this work was presented at the following conference:

- *ISCRE, Philadelphia, USA, June 13-16, 2010.*

Abstract:

The effect of CO_2 on Fischer-Tropsch synthesis (FTS) over a cobalt based catalyst had been investigated in a fixed bed micro reactor. Two feed gases, H_2:CO:CO_2=2:1:0 and H_2:CO:CO_2=3:0:1, were mixed in various proportions thus varying the ratio of CO, CO_2, and H_2 stoichiometrically. The results show that CO and CO_2 mixtures can be used as feed to a cobalt catalyst. Comparison of the FTS using different syngas mixtures (CO_2/H_2, CO_2/CO/H_2, and CO/H_2) shows that: (1) CO_2 can be hydrogenated along with CO in the FT reactor over cobalt catalyst, especially in the case of high content of CO_2. (2) Hydrogenation of CO_2 or CO/CO_2 mixture leads to a typical Anderson–Schulz–Flory (ASF) distribution. These could support the hypothesis that CO_2 hydrogenation processes might occur with the formation of CO as intermediate. (3) CO feed exhibit the typical two–alpha distribution while CO_2 and CO_2 rich feeds only exhibit a single–alpha distribution. This may also help us to understand the mechanisms that lead to product distributions in FT with single- and dual-alpha distributions. In spite of the fact that cobalt catalysts are not water gas shift active, it is shown the rate of hydrocarbon production is maximized at an intermediate composition of the CO/CO_2/H_2 mixture. The results could have implications for the design of XTL (anything-to-liquids is a process that converts carbon and energy containing

feedstock to high quality fuels and products, such as coal-to-liquids, biomass-to-liquids and gas-to-liquids) using cobalt catalysts in that it might be advantageous to keep some carbon dioxide in the syngas feed to the FTS process.

4.1 Introduction

Fischer-Tropsch synthesis (FTS) is a catalyzed chemical reaction in which syngas is converted into liquid hydrocarbons [1]. Due to their good activity and selectivity, supported cobalt catalysts are often the choice for CO hydrogenation to hydrocarbons in low temperature FTS [2]. The raw syngas from coal or biomass gasification is a mixture of CO, CO_2, H_2, and CH_4 [3, 4]. The composition of CO_2 in the raw syngas varies from around 1% to 30% when using different feed stocks, type of gasifiers, and reaction conditions [4]. Rao et al. [5] report that some gasifiers for coal gasification, such as the conventional Lurgi process, give a CO_2 rich syngas (17% CO, 38% H_2, 32% CO_2, rest others). Although the need for CO_2 separation before using the syngas in FTS is mentioned in the patent literature for some cases, recent process development studies discuss a potential cost advantage if CO_2 is not removed before the synthesis step [6]. Furthermore, if CO_2 is hydrogenated along with CO or tolerated in the FT reactor, the expensive CO_2 removal step may be eliminated. It is therefore interesting to investigate the effect of carbon dioxide on a cobalt catalyst under low temperature FTS conditions.

Similar catalytic activities were obtained for feeds of either CO/H_2 or CO_2/H_2 with a cobalt-based catalyst, but the selectivities were very different. For CO hydrogenation, normal FTS product distributions were observed; in contrast, the CO_2 hydrogenation products contained about 70% or more methane [2, 7]. Cobalt catalysts do not exhibit significant WGS activity [6, 8], and CO_2 is neither formed nor produced during FTS with cobalt catalysts and CO/H_2 feed. Some researchers

propose that CO_2 is neither strongly adsorbed nor hydrogenated, and it plays the role of a diluting gas [6, 9]. However, comparing the reactivity of a 36 wt % Co/Al_2O_3 catalyst with CO/H_2 and CO_2/H_2 mixtures under the same process conditions, Akin et al. [10] observed a three times higher conversion with a CO_2/H_2 feed mixture when compared to the CO/H_2 feed.

Zhang et al. [7] proposed that the conversion of CO and CO_2 occurs by different reaction pathways, the former involving mainly C–H and O–H species as products from the hydrogenation, while the latter involves H–C–O and O–H species. The H–O–C species will be subsequently hydrogenated to the adsorbed intermediate of methanol and then to methane. Other researchers [2, 11, 12] suggest that the CO and CO_2 hydrogenation processes follow the same reaction path, with the formation of adsorbed CO as the intermediate. Indeed CO formation and coordination over reduced cobalt centers has been observed by FT–IR from CO_2/H_2 reaction over a reduced cobalt based catalyst [2].

In addition, fixation of CO_2 has become of greater interest in recent years, primarily because of its impact on the environment through the greenhouse gas effect. There have been various attempts to transform carbon dioxide into hydrocarbons, mainly using those catalysts that have been proved active in the FTS, such as Co, Fe, Ni, and Ru [13].

The mechanism of CO_2 hydrogenation remains controversial. Moreover, much of the literature reports results over small ranges of $H_2/CO/CO_2$ ratios. In this work, the effect of CO_2 on FTS on a cobalt catalyst has been investigated in a fixed bed micro reactor. Two feed gases, $H_2:CO:CO_2=2:1:0$ and $H_2:CO:CO_2=3:0:1$, were mixed in various proportions thus varying the ratio of CO, CO_2, and H_2 stoichiometrically. The catalyst activity and selectivity, product distribution, and olefin/paraffin were measured and compared.

4.2 Experimental Method

4.2.1 Catalyst Preparation

The Co/TiO_2 catalyst used in this study was prepared by impregnation of TiO_2 with a cobalt nitrate solution. TiO_2 (Degussa P25) was mixed with distilled water in a mass ratio of 1:1 and dried in air at 120 ℃ for 1 hour. The support was then calcined in air at 400 ℃ for 16 hours [14]. After calcination, the support was crushed and sieved and the particles with diameters between 0.5 and 1 mm were used. The support was then impregnated with a cobalt nitrate ($Co(NO_3)_2$ $6H_2O$) solution, the quantity added being such as to give a cobalt metal loading of 10% by mass. After the impregnation step, the support was dried in air at 120 ℃ for 16 hours and then calcined in air at 400 ℃ for 6 hours to decompose and transform the cobalt nitrate to cobalt oxide.

4.2.2 Experimental Setup and Procedure

4.2.2.1 Catalyst reduction

One gram of catalyst was loaded in the fixed bed reactor. The reduction was performed at atmospheric pressure with H_2 (AFROX (African Oxygen) Ltd., 99.999%) for 24 hours. The reduction temperature and the flow rate were 350 ℃ and 60 mL/min, respectively.

4.2.2.2 FT catalytic activity tests

Once the reduction was completed, the reactor was allowed to cool down to room temperature. The CO_2 syngas (which we will refer to as the CO_2 feed, and which has composition H_2:CO:CO_2=3:0:1, 10% N_2 as internal standard for mass balance calculations) was introduced into the reactor first at a flow rate of 60 mL(NTP)/(min gcat). The reactor pressure was slowly increased to 20 bar (gauge)

and thereafter the temperature was increased gradually to 200 ℃. The pressure and temperature were allowed to stabilize, and the operating conditions were maintained constant for 72 hours while the tail gas composition was monitored. Thereafter, the flow rate of the CO_2 syngas was decreased by 10%, that is 6 mL(NTP)/(min gcat), and the CO syngas (which we will refer to as the CO feed and which has a composition of H_2:CO:CO_2=2:1:0, 10% N_2 as internal standard for mass balance calculations) was introduced into the reactor (flow rate of 6 mL(NTP)/(min gcat)) so as to keep the total flow rate constant at 60 mL(NTP)/(min gcat). The new reaction conditions were maintained for 72 hours while the tail gas composition was monitored. After that the flow rate of the CO_2 mixture was again decreased while that of the CO mixture was increased so as to keep the total flow rate of gas to the reactor at 60 mL(NTP)/(min gcat). The feed and reaction conditions for the 11 experiments are shown in Table 4.1.

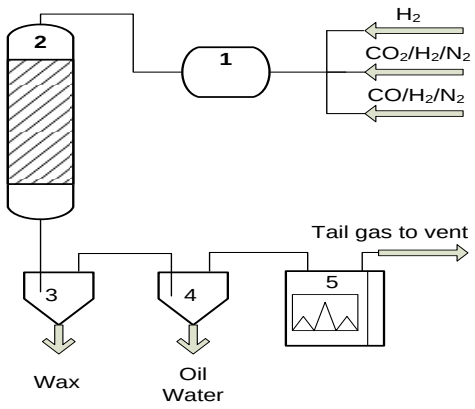

Figure 4.1: Simplified flow scheme of fixed bed reactor used in the experiments. (1) inlet gas mixer; (2) fixed bed reactor; (3) hot condensable product trap; (4) cold condensable product trap; (5) online GC.

4.2.3 Product analysis

The tail gas was analyzed every 1.5 hours using an online DANI gas chromatograph (GC). Two thermal conductivity detectors (TCD) were used to

analyze H_2, N_2, CO, CO_2, and CH_4, and a flame ionization detector (FID) was used for the analysis of gas phase hydrocarbons. The wax and liquid products were collected in a hot trap (kept at 150 ℃) and cold trap (kept at room temperature) (Figure 4.1). Offline analysis of oil and wax products was performed at the end of the mass balance for each run using an offline GC.

Table 4.1: Reaction and feed conditions for the FTS experiments over a cobalt based catalyst.

No.	T (℃)	Flow rate (ml(NTP)/(min gcat)	Total P (bar gauge)	Fraction of the CO and CO_2 mixtures in the feed to the FT reactor		Partial pressure at entrance (bar)			
				CO_2 syngas $H_2/CO/CO_2$ =3:0:1	CO syngas $H_2/CO/CO_2$ =2:1:0	P_{H_2}	P_{CO}	P_{CO_2}	P_{N_2}
1	200	60	20	100%	0%	14.2	0.0	4.8	2.1
2	200	60	20	90%	10%	13.9	0.5	4.2	2.0
3	200	60	20	80%	20%	13.8	1.3	3.9	2.0
4	200	60	20	70%	30%	13.7	1.9	3.3	2.1
5	200	60	20	60%	40%	13.3	2.4	2.8	2.0
6	200	60	20	50%	50%	13.2	3.2	2.3	2.1
7	200	60	20	40%	60%	13.1	3.8	1.9	2.1
8	200	60	20	30%	70%	13.0	4.3	1.5	2.1
9	200	60	20	20%	80%	12.9	4.9	0.9	2.1
10	200	60	20	10%	90%	12.7	5.6	0.4	2.1
11	200	60	20	0%	100%	12.5	6.3	0.0	2.2

4.3 Results and Discussion

4.3.1 Reactant Conversion and Product Selectivity

Figure 4.2 shows the feed gas conversion as a function of syngas composition for the 11 reaction conditions described in Table 4.1. Both the CO and CO_2

conversions increased with increased ratio of $CO_2/(CO+CO_2)$ for all reaction conditions. The data shows that both CO and CO_2 are readily hydrogenated when the feeds are either CO syngas (corresponding to $CO_2/(CO+CO_2)=0$) or CO_2 syngas (corresponding to $CO_2/(CO+CO_2)=1$). Furthermore, the conversion is higher for the CO_2 feed than for the CO feed, indicating a higher reactivity for CO_2 on the cobalt based catalyst. Similar results were reported by Akin et al. [10] and Visconti et al. [2]. Other researchers report similar [12] or lower CO_2 [9] conversion for a CO_2 feed compared to the CO conversion for a CO feed. For the mixtures of the CO syngas and CO_2 syngas, it can be seen in Figure 4.2 that CO_2 can be hydrogenated along with CO in the FT reactor over cobalt catalyst, especially in the case of high content of CO_2. However, CO is converted faster than CO_2 in the FT reaction when both CO and CO_2 are present.

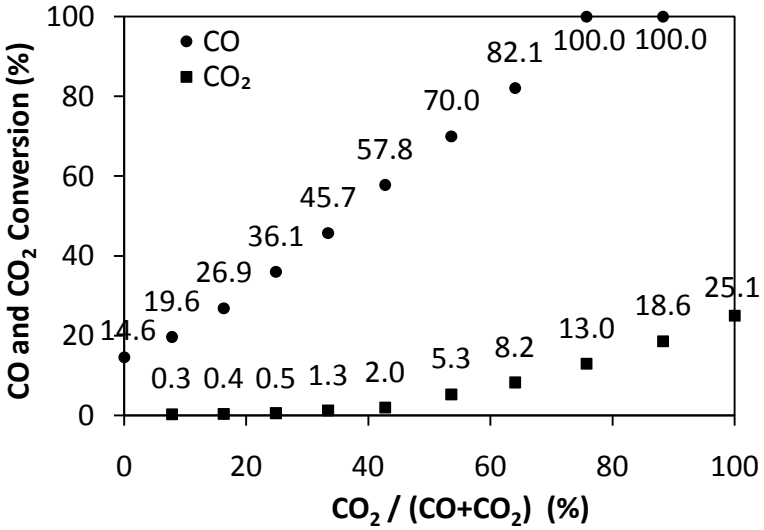

Figure 4.2: Conversion of CO and CO_2 as a function of syngas composition (reaction conditions as in Table 4.1).

The product selectivity as a function of syngas composition for the 11 data points (as shown in Table 4.1) is shown in Figure 4.3. The selectivity of the products is strongly dependent on the syngas composition. CO_2 rich feeds produce products that are mainly methane while CO rich feeds shift the product composition to a

Fischer–Tropsch type (mainly higher hydrocarbons) product; similar results were reported by Visconti et al. [2].

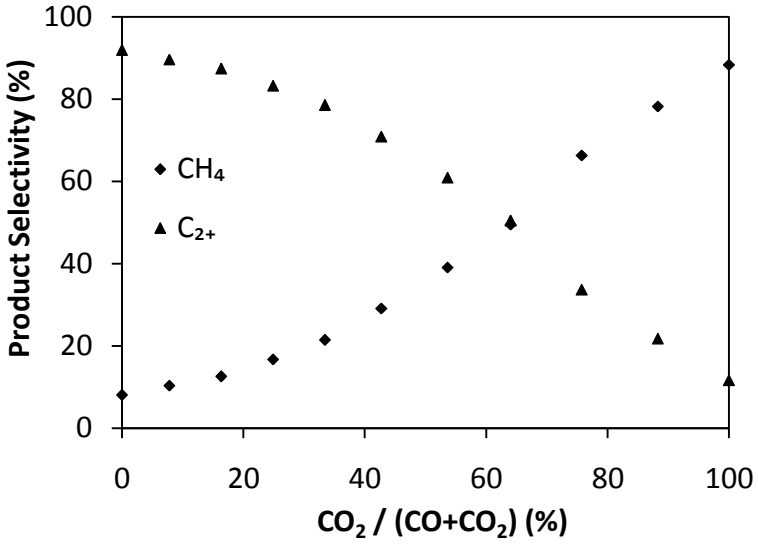

Figure 4.3: Product selectivity as a function of syngas composition (reaction conditions as in Table 4.1).

On the basis of Figures 4.2 and 4.3, we can conclude the following: (1) At a high content of CO_2 ($CO_2/(CO+CO_2) > 50\%$), CO_2 is not functioning as a diluted (inert) gas, but is converted to hydrocarbon products in the FT reactor, which can affect the total FTS product selectivity. This is inconsistent with the literature findings [6, 9]. (2) For feeds with lower CO_2 content ($CO_2/(CO+CO_2) < 50\%$), the conversion of CO_2 is less than 5%, so that most of the hydrocarbon products are from CO hydrogenation. In general, the selectivity changes observed can be explained in terms of a change in the average partial pressure of CO [15], since the H_2 partial pressure does not change much, methane selectivity increases with decreasing partial pressure of CO.

4.3.2 Reactant and Product Reaction Rates and Olefin/Paraffin Ratios

The CO, CO_2, and H_2 reaction rates as a function of the syngas composition are shown in Figure 4.4. It is found that the CO_2 reaction rate has the same trend as the CO_2 conversion in Figure 4.2. However, both the H_2 and CO rates increase, reach a maximum, and then decrease with an increasing ratio of $CO_2/(CO+CO_2)$. When the ratio of $CO_2/(CO+CO_2)$ is between 75% and 80%, the H_2 rate achieves a maximum, whereas the CO reaction rate is a maximum when the ratio is between 40% and 45%. The hydrogen partial pressure for feeds with the ratio of $CO_2/(CO+CO_2)$ between 0% to 40% does not change much (Table 4.1), and it is seen that the CO reaction rate increases with decreasing partial pressure of CO (the same result was reported by Schulz et al. [15]). In addition, because CO is converted faster than CO_2 with $CO/CO_2/H_2$ mixtures, it indicates that the strength of adsorption of CO_2 on the surface of cobalt catalyst might be lower than the strength of adsorption of CO.

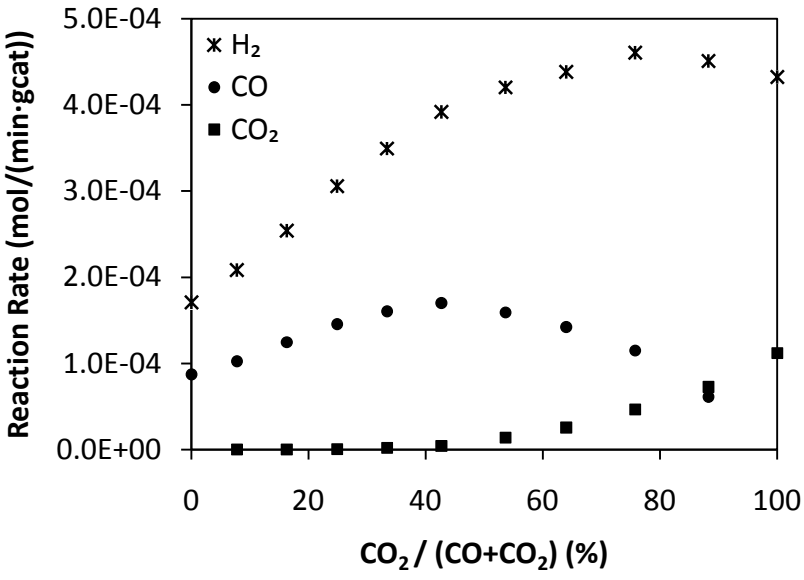

Figure 4.4: The reaction rates of CO, CO_2 and H_2 as a function of syngas composition (reaction conditions as in Table 4.1).

It is also quite interesting to note that the reaction rate of CH_4 as well as that of the

other hydrocarbons (denoted C_{2+}) and the total hydrocarbon products can be maximized by controlling the feed gas composition (Figure 4.5). In this case, the CH_4 rate is maximized at a feed gas composition of $CO_2/(CO+CO_2)$ between 75% and 80%; the C_{2+} rate is maximized at a feed gas composition of $CO_2/(CO+CO_2)$ between 35% and 40%; and the total hydrocarbons rate is maximized at a feed gas composition between 45% and 55%. Thus, there are opportunities to first optimize the FT reaction rate as well as to consume CO_2 in the FTS reaction.

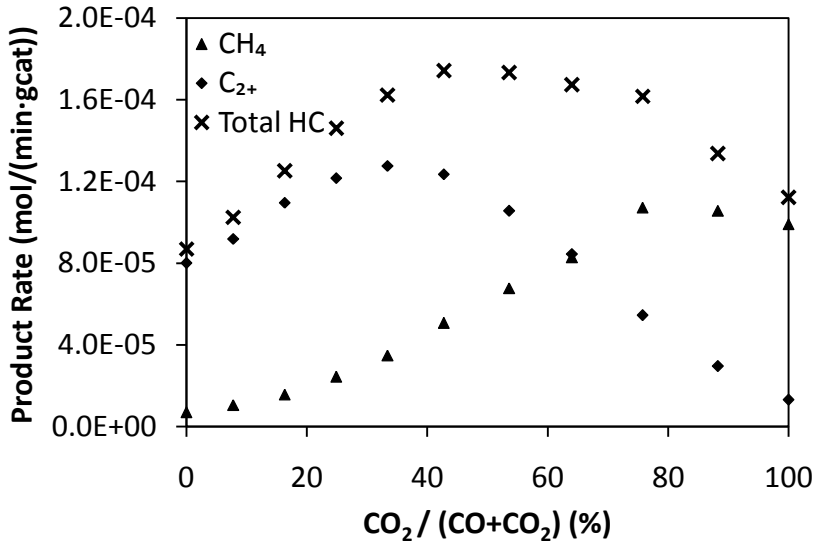

Figure 4.5: The rates of products of CH_4, C_{2+} hydrocarbons and total hydrocarbons (HC) as a function of syngas composition (reaction conditions as in Table 4.1).

According to Visconti et al. [2], they speculated that the different selectivity observed in their experiments during CO and CO_2 hydrogenation was due to the different H/C ratios at the catalyst surface resulting from the CO/H_2 and CO_2/H_2 reaction. In particular, in agreement with Falconer and Zagli [11], it is expected that during CO_2 hydrogenation, a high H/C surface concentration is attained due to the slow CO_2 adsorption. Comparing the rate of formation of CH_4 for the CO syngas (CO/H_2) with those obtained with mixtures of CO and CO_2 as shown in Figure 4.5, the undesired CH_4 rate is higher for feeds that are mixtures, which could be due to a higher H/C concentration on the catalyst surface when the CO

feed is replaced by the CO_2 feed. Although the CH_4 selectivity is quite high when the total hydrocarbon rate achieves a maximum, the data shows important implications for developing a CO_2-to-fuel process by using the $CO/CO_2/H_2$ mixtures as a feed to the reactor. In addition, the hydrogenation reactions of CO and CO_2 to energy carriers such as methane or long chain hydrocarbons are particularly promising [12]. This is more useful if H_2 can be produced without considerable CO_2 emissions, using hydro, solar, or nuclear energy [9]. On the other hand, more work should be done to improve the desired product activity and selectivity, such as finding new better catalysts, changing the operation conditions, or varying the ratio of feed gas.

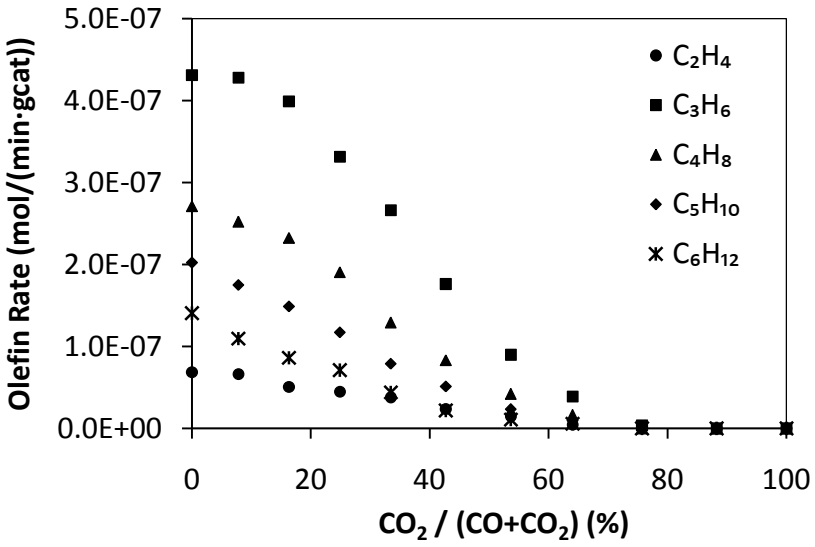

Figure 4.6: The rate of formation of olefins as a function of syngas composition (reaction conditions as in Table 4.1).

In view of the effect of the partial pressures of CO, CO_2, and H_2 on the catalyst activity, the rates of formation of the light olefins and paraffins are plotted in Figures 4.6 and 4.7. The olefin rate decreases with increasing ratios of $CO_2/(CO+CO_2)$. When the ratio of $CO_2/(CO+CO_2)$ is greater than 70%, no olefin can be detected in the product (Figure 4.6). However, a different trend is observed for the rates of formation of the paraffins (Figure 4.7) and the rates go through a

maximum. The paraffin rates are fairly constant when the ratio of $CO_2/(CO+CO_2)$ is in the range of 40–75% (excluding C_2H_6). The results show that the effect of the partial pressures of CO, H_2, and CO_2 on the formations of paraffins and olefins are different.

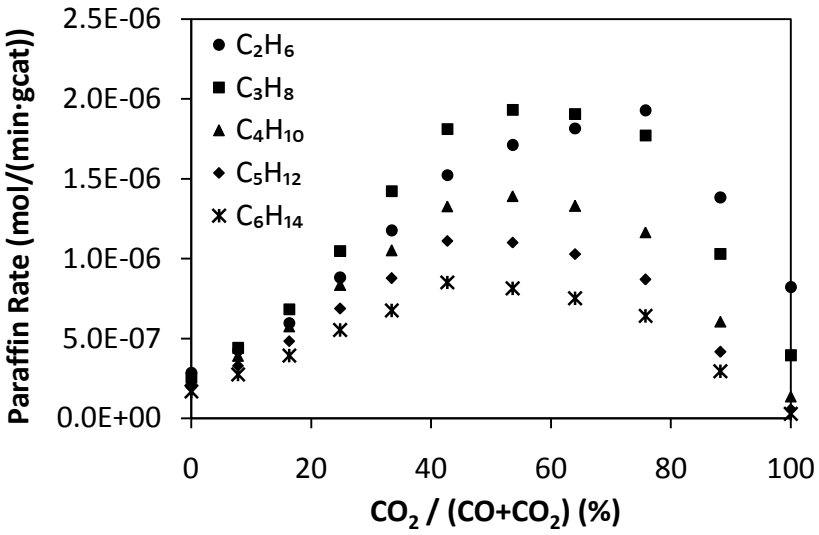

Figure 4.7: The rate of formation of paraffins as a function of syngas composition (reaction conditions as in Table 4.1).

Figure 4.8 shows the olefin to paraffin ratio (O/P) as a function of syngas composition. We find similar results to those found in the literature [16–18] in that the olefin to paraffin ratio changes as a function of carbon number. Increasing the carbon number decreases the olefin to paraffin ratio (excluding O_2/P_2) at each reaction condition. As the amount of CO_2 in the feed gas is reduced and the quantity of CO is increased (as indicated in Table 4.1), the O/P ratio for a particular carbon number increases. CO_2 rich feeds produce products with high paraffin selectivity while CO rich feeds shift the product composition to a Fischer-Tropsch type (mainly higher hydrocarbons) product with both high paraffin and olefin selectivities.

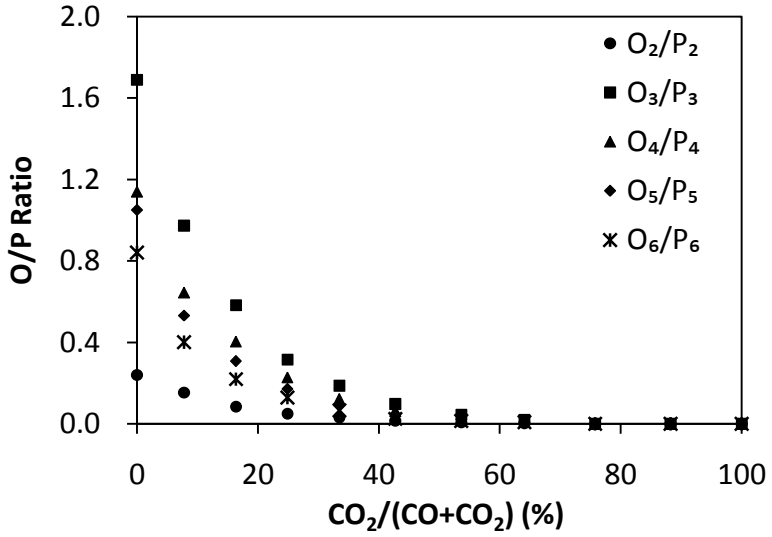

Figure 4.8: The molar olefin to paraffin ratio (O/P) as a function of syngas composition (reaction conditions as in Table 4.1).

The data from Figures 4.4–4.8 might suggest the following. Note that the H_2 partial pressure in the feed does not change much (Table 4.1): (1) With CO rich feeds, the products are both paraffins and olefins with low methane selectivity. This might be as a result of a lower H/C surface concentration caused by the high adsorption strength of CO. (2) Conversely with CO_2 rich feeds, most of the products are paraffins with high methane selectivity. We postulate that this may be a result of a higher H/C surface ratio caused by the low adsorption strength of CO_2 on the catalyst surface.

The mechanism for CO_2 hydrogenation still remains controversial. Zhang et al. [7] proposed that the conversion of CO and CO_2 occurs by different reaction pathways. Other researchers [2, 11, 12] however have suggested that the CO and CO_2 hydrogenation processes follow the same reaction path, with the formation of adsorbed CO as an intermediate. We tried to simulate the system by adding a small amount of CO into the CO_2/H_2 mixtures (reaction condition 2 and 3 in Table 4.1). Our experimental results show that when the CO content in the feed gas is low as occurs at reaction conditions 2 and 3 (the feed is predominately

stoichiometric quantities of CO_2 and H_2), the CO conversion is 100% (Figure 4.2), and no CO can be detected in the tail gas. In these experiments with small quantities of CO in the CO_2 rich feed, the products are as similar to those that are found for CO_2/H_2 feed with high short chain paraffin selectivity. We suggest that CO_2 hydrogenation might proceed via a CO intermediate: the adsorbed CO might be very quickly reduced to hydrocarbon products and it is not be detected in the tail gas as happens when there is a small amount of CO in the feed ($CO_2/(CO+CO_2)$ > 76% in Figure 4.2).

4.3.3 The Product Distribution

According to Anderson [19], the product distribution of hydrocarbons in FTS can be described by the Anderson-Schulz-Flory (ASF) equation:

$$\frac{W_n}{n} = (1-\alpha)^2 \alpha^{(n-1)}$$

Where W_n is the mass fraction of a hydrocarbon (HC) with chain length n and the growth probability factor α is assumed to be constant. α determines the total carbon number distribution of the FT products. Thus, a plot of the logarithm of W_n/n versus n would produce a straight line plot whose slope is related to α. However, for most iron and cobalt catalysts, marked deviations from this ideal distribution are observed. The significant deviations from the ASF distribution for CO hydrogenation are:

(1) relatively high yield of methane [20–23]

(2) relatively low yield of ethylene [20, 21, 24]

(3) a “break” in the distribution has occasionally been observed at a carbon number near nine [25]. In such cases, instead of a single distribution, the products exhibit two linear ASF distributions which cross, resulting in a “break”, always in

a concave direction.

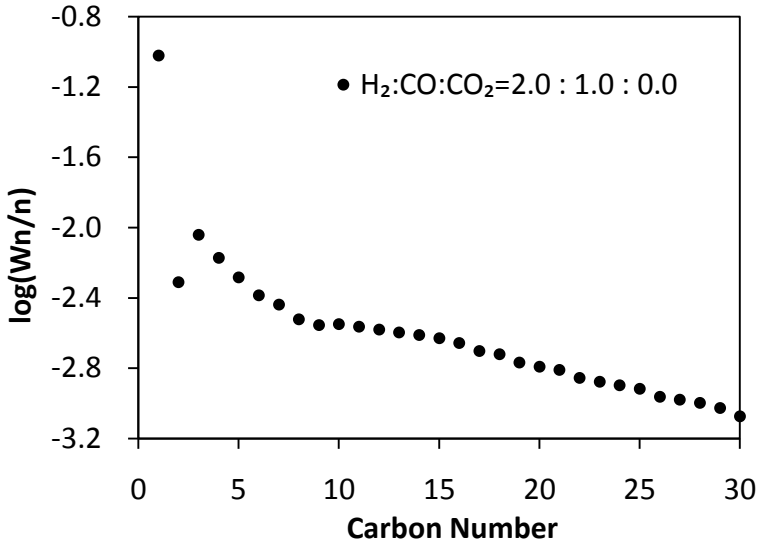

Figure 4.9: Product distribution for CO hydrogenation (reaction condition 11 in Table 4.1).

The product distributions for reaction condition numbers 1, 2, and 11 of Table 4.1 are shown in Figures 4.9–4.11. For CO hydrogenation on the cobalt catalyst, two normal α product distributions are observed in Figure 4.9 with α_1=0.78 and α_2 =0.93. Furthermore, there is a relatively low yield of C_2 (hydrocarbon n=2) products which is fairly typical [20–23]. For CO_2 hydrogenation, methane is the dominant product with a small quantity of short chain paraffins being formed. Figure 4.10 shows that the hydrogenation of CO_2 leads to a typical ASF distribution with a low α value of 0.41. It is also interesting to note that C_2 lies on the ASF distribution in this case.

Condition 2 of Table 4.1 corresponds to 10% of CO_2 feed being replaced by CO feed. Similar reaction rates are observed for CO and CO_2 at this condition (Figure 4.4), which thus implies that both CO and CO_2 are contributing to the product distribution. It appears that the product distribution for this condition follows a typical one-α ASF distribution with an α value of 0.65. Note that C_2 also lies on

the ASF distribution line. Furthermore, these results indicate that even small amounts of CO in the CO_2 rich feed changes the product distribution dramatically (Figures 4.10 and 4.11).

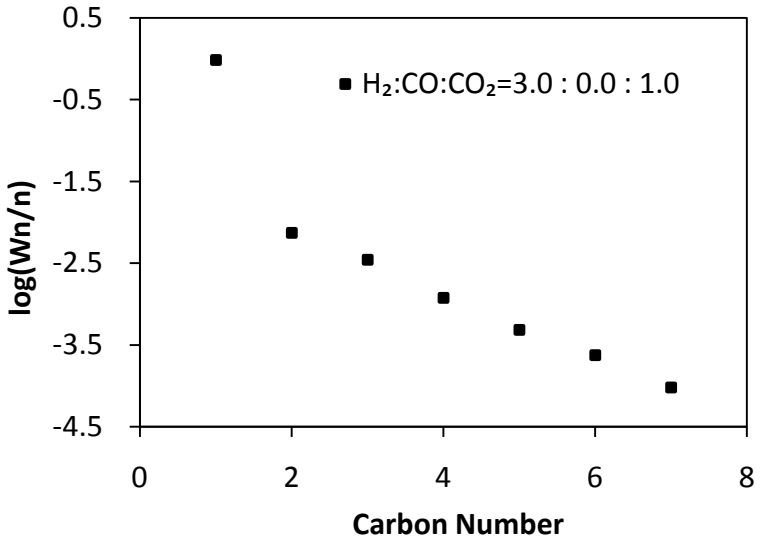

Figure 4.10: Product distribution for CO_2 hydrogenation (reaction condition 1 in Table 4.1).

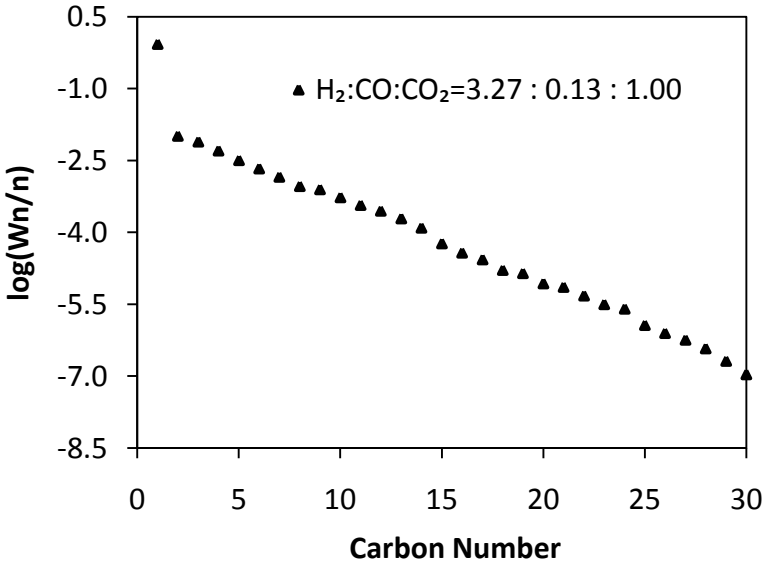

Figure 4.11: Product distribution for a combined feed of CO and CO_2 (reaction condition 2 in Table 4.1).

If we consider the O/P ratio (Figure 4.8), we see that the FTS products are all paraffins for both the CO_2 feed as well as the CO_2 rich feeds. Furthermore, the C_2 product is ethane only. On the other hand, the products of both CO feed and CO rich feeds are both olefins and paraffins. In this case, the C_2 product is the sum of ethane and ethylene. Snel and Espinoza [25] report that, under normal synthesis conditions, a substantial fraction of the primary product ethylene will readsorb on growth sites of the catalyst surface and continue to grow via propagation with monomer or terminate as hydrocarbon product. Therefore, we suggest that, due to the secondary reaction of ethylene, C_2 is below the ASF distribution line when C_2 represents both ethane and ethylene (Figure 4.9) as in CO rich feeds. Moreover, if there is only ethane as the C_2 product, as in CO_2 rich feeds, the C_2 lies on the ASF distribution line (Figures 4.10 and 4.11) as there is no readsorbing and reaction of the ethane.

It is remarkable, that for a CO feed, the product distribution follows a two-α ASF distribution (Figure 4.9). However, for a CO_2 feed and even small quantities of CO in a CO_2 rich feed, a single-α ASF distribution is obtained (Figures 4.10 and 4.11). This may help us understand the mechanisms that lead to product distribution in FT with single and dual-α distribution. Further work should be done which focuses on the products distributions of the 11 experiments in Table 4.1.

Various mechanisms of CO_2 hydrogenation are suggested in the literature:

(1) Some researchers believe that CO_2 hydrogenation occurs with methanol as an intermediate [7, 26]. Fujlwara et al. [26] believe that methanol seems to be an important intermediate for CO_2 hydrogenation and the two reaction pathways are

(a) $CO_2 \rightarrow MeOH \rightarrow MeOMe \rightarrow Olefin \rightarrow Parafin$

(b) $CO_2 \rightarrow \mathrm{MeOH} \rightarrow \mathrm{CO} \rightarrow \mathrm{Hydrocarbons}$

(2) Other researchers believe that CO_2 hydrogenation occurs with CO as intermediate [2, 11, 12].

(c) $CO_2 + H_2 \rightarrow Hydrocarbons$

Thus, it would appear that the reaction mechanisms of CO_2 hydrogenation may be very complicated. Pathway (a) is the typical methanol to gasoline (MTG) reaction. However, MTG is able to produce unsaturated hydrocarbons [26, 27] with non–ASF distributions [26]. On the basis of the comparison of the FTS product distributions using different syngas mixtures (CO_2/H_2, $CO_2/CO/H_2$, and CO/H_2), we find that the products of CO_2 hydrogenation over cobalt catalyst are methane rich saturated products with an ASF distribution (Figure 4.10) and the product distribution of $CO_2/CO/H_2$ mixtures also follows an ASF distribution (Figure 4.11). This might suggest that the CO_2 hydrogenation occurs with the formation of CO as an intermediate.

4.4 Conclusions

FTS experiments over the Co/TiO_2 catalyst with syngas of varying proportions of CO, CO_2, and H_2 have been carried out in a fixed bed micro reactor with a constant total synthesis pressure of 20 bar gauge, flow rate of 60 mL(NTP)/(min gcat), and temperature of 200 ℃. It has been shown that CO_2 and CO mixtures can be used as a feed to the cobalt catalyst. When the feed gas is CO_2 rich and correspondingly CO lean, ($CO_2/(CO+CO_2)$ > 50%), CO_2 is not an inert or diluent gas, but can be converted to hydrocarbon products.

On the basis of the comparison of the FTS products using different syngas mixtures (CO_2/H_2, $CO_2/CO/H_2$, and CO/H_2), we find that the products of CO_2

hydrogenation over cobalt catalyst are methane rich short chain paraffins with a typical low alpha ASF distribution and the product distribution for small quantities of CO in CO_2 rich feed also follow a typical one alpha ASF distribution with high methane selectivity. This might suggest that the CO_2 hydrogenation occurs with the formation of CO as intermediate. Furthermore, it is apparent that even small amounts of CO in the CO_2 rich feed change the product distribution dramatically. This may provide important information for developing a process for conversion of CO_2-to-fuel with $CO_2/CO/H_2$ mixtures. Any mechanism that is proposed for FTS must be able to account for both the typical two–alpha ASF distribution found with CO feed as well as the single–alpha ASF distribution found with CO_2 and CO_2 rich feeds.

In spite of the fact that cobalt catalysts are not water gas shift active, it is shown the rate of hydrocarbon product is maximized at an intermediate composition of CO and CO_2. This result could have implications for the design of XTL (anything–to–liquids is a process that converts carbon and energy containing feedstock to high quality fuels and products, such as coal–to–liquids, biomass–to–liquids and gas–to–liquids) and in particular for the need to remove carbon dioxide from feed gas to the FTS process.

References

[1] Anderson, R. B. (1984), The Fischer-Tropsch Synthesis, Academic Press, Orlando, Florida.

[2] Visconti, C. G., Lietti, L.,Tronconi, E., Forzatti, P., Zennaro, R. and Finocchio, E. (2009), Fischer-Tropsch synthesis on a Co/Al_2O_3 catalyst with CO_2 containing syngas, Applied Catalysis A: General, 355, 61–68.

[3] Wilhelm, D. J., Simbeck, D. R., Karp, A. D. and Dickenson, R. L. (2001), Syngas production for gas-to-liquids applications: technologies, issues and outlook, Fuel Process Technology, 71, 139–148.

[4] Higman, C. and Burgt. M. G. (2003), Gasification, Guif Professional Publishing, Burlington.

[5] Rao, V. U. S., Stiegel, G. J., Cinguegrane, G. J. and Srivastava, R. D. (1992), Iron-based catalysts for slurry phase FTS: technology review, Fuel Processing Technology, 30, 83–107.

[6] Riedel, T. and Schaub, G. (2003), Low-temperature Fischer-Tropsch synthesis on cobalt catalysts-effects of CO_2, Topics in Catalysis, 26, 145–156.

[7] Zhang, Y., Jacobs, G., Sparks, D. E., Dry, M. E. and Davis, B. H. (2002), CO and CO_2 hydrogenation study on supported cobalt Fischer-Tropsch synthesis catalysts, Catalysis Today, 71, 411–418.

[8] Dalai, A. K. and Davis, B. H. (2008), Fischer-Tropsch synthesis: A review of water effects on the performances of unsupported and supported Co catalysts, Applied Catalysis A: Gen., 348, 1–15.

[9] Riedel, T., Claeys, M., Schulz, H., Schaub, G., Nam, S., Jun, K., Choi, M., Kishan, G. and Lee, K. (1999), Comparative study of Fischer-Tropsch synthesis with H_2/CO and H_2/CO_2 syngas using Fe- and Co-based catalysts, Applied catalysis A: General, 186, 201–213.

[10] Akin, A. N., Ataman, M., Aksoylu, A. E. and Onsan, Z. I. (2002), CO_2 fixation by hydrogenation over coprecipitated Co/Al_2O_3, Reaction Kinetics and Catalysis Letters, 76, 265–270.

[11] Zagli, E. and Falconer, J. L. (1981), Carbon dioxide adsorption and methanation on ruthenium. Journal of Catalysis, 69, 1–8.

[12] Weatherbee, G. D. and Bartholomew, C.H. (1984), Hydrogenation of CO_2 on group VIII metals, Catalysis, 87, 352–362.

[13] Herranz, T., Pojas, S., Perez-Alonso, F.J., Ojeda, M., Terrors, P. and Fierro, J. L. G. (2006), Hydrogenation of carbon dioxide over promoted Fe-Mn catalysts prepared by the microemulsion methodology, Applied Catalysis A, 311, 66–75.

[14] Li J, (1999), The preparation, characterization and evaluation of boron modified Co/TiO_2 Fischer-Tropsch catalysts, PhD thesis, University of the Witwatersrand, Johannesburg, South Africa.

[15] Schulz, H., van Steen, E. and Claeys, M. (1994), Selectivity and mechanism of Fischer-Tropsch Synthesis with iron and cobalt catalysts, Studies in Surface Science and Catalysis, 81, 455–460.

[16] van Der Laan, G. P. and Beenachers, A. A. C. M. (1999), Kinetics and selectivity of the Fischer-Tropsch synthesis: A literature review, Catalysis Reviews, Science and Engineering, 4, 255–318.

[17] Kuipers, E. W., Vinkenburg, I. H. and Oosterbeek, H. (1995), Chain length dependence of α-olefin readsorption in Fischer-Tropsch synthesis, Journal of Catalysis, 152, 137–146.

[18] Shi, B. and H. Davis, B. H. (2005), Fischer-Tropsch synthesis: The paraffin to olefin ratio as a function of carbon number, Catalysis Today, 106, 129–131.

[19] Anderson, J. R. and Boudart, M. (1982), Catalyst: science and technology, Springer, Berlin.

[20] Snel, R. (1989), The nature of hydrocarbon synthesis by means of hydrogenation of carbon monoxide on iron based catalysts. Part II. Dynamic adsorption/desorption equilibria, Journal of Molecular Catalysis, 53, 143–154.

[21] Komaya, T. and Bell, A. T. (1994), Estimates of rate coefficients for elementary processes occurring during Fischer-Tropsch synthesis over Ru/TiO_2, Journal of Cataysis, 146, 237–248.

[22] Schulz, H. and Claeys, M. (1999), Kinetic modeling of Fischer-Tropsch product distributions, Applied Catalysis A: General, 186, 91–101.

[23] Kuipers, E. W., Scheper, C., Wilson, J. H. and Oosterbeek, H. (1996), Non-ASF product distributions due to secondary reactions during Fischer-Tropsch synthesis, Journal Catalysis, 158, 288–300.

[24] Novak, S., Madon, R. J. and Suhl, H. (1982), Secondary effects in the Fischer-Tropsch synthesis, Journal Catalysis, 77, 141–151.

[25] Snel, R. and Espinoza, R. (1987), Secondary reactions of primary products of the Fischer-Tropsch Synthesis. Part 1. The role of ethane, Journal of Molecular Catalysis, 43, 237–247.

[26] Fujlwara, M., Kieffer, R., Ando, H., Xu, Q. and Souma, Y. (1997), Change of catalytic properties of Fe-ZnO/zeolite composite catalyst in the hydrogenation of carbon dioxide, Applied Catalysis A: General, 154, 87–101.

[27] Zaidi, H. A. and Pant, K. K. (2004), Catalytic conversion of methanol to gasoline range hydrocarbons, Catalysis Today, 96, 155–160.

5

FISCHER-TROPSCH SYNTHESIS USING $H_2/CO/CO_2$ SYNGAS MIXTURES OVER AN IRON CATALYST

This work has been published in the Ind. Eng. Chem. Res. 2011, 50, 11002-11012.
Part of this work was presented at the following conferences:

- *CATSA, Rawsonville, South Africa, November 8-11, 2009.*

Abstract:

A series of low-temperature Fischer-Tropsch synthesis (FTS) experiments using a wide range of $H_2/CO/CO_2$ syngas mixtures have been performed to provide further insight into the effect of the CO_2 on an iron based catalyst during FTS. In comparison with CO hydrogenation, the reactivity for CO_2 hydrogenation was lower and produced more CH_4-rich short chain paraffins. Based on the correlation between the experimental results and the thermodynamic equilibrium calculations for the water gas shift (WGS) reaction, although the WGS reaction is far from the thermodynamic equilibrium under low-temperature FTS conditions, its equilibrium constraints determine whether CO can converted to CO_2 or CO_2 to CO. It is possible for CO_2 to convert to hydrocarbons only when the composition of co-fed CO_2 has a value higher than that set by the equilibrium constraints.

A remarkable feature of our experimental results was that when the FTS system was not consuming but forming CO_2, the reaction rates of both the FT and the WGS reactions were independent of the partial pressures of CO and CO_2. Furthermore, with a decrease in the ratio of $CO_2/(CO+CO_2)$ in the feed gas, it was observed that the hydrocarbon product formation rate reached a maximum and then maintained this value, even at a very high concentration of CO_2 in the

$H_2/CO/CO_2$ feed mixture. These results could justify the inclusion of CO_2 in the syngas feed to the iron-based catalyst FTS processes.

5.1 Introduction

Fischer-Tropsch synthesis (FTS) is a well-established commercial technology for the conversion of synthesis gas into "clean" transportation fuels and chemicals [1-6]. The raw synthesis gas or syngas, which can be derived from coal, natural gas or biomass, is a mixture of H_2, CO, CO_2 and CH_4 [7]. Because the composition of syngas is dependent on many factors such as gasifier type, operational conditions and gasifying agents, the composition of CO_2 in the raw syngas varies from around 1–30% [7-8]. Although the need in some cases for CO_2 separation before using the syngas in FTS is mentioned in the patent literature, recent process development studies suggest there is a potential cost advantage if CO_2 is not removed before the synthesis takes place [9].

The use of iron-based catalysts in industrial FTS processes has attracted much attention recently. Not only is the cost of iron catalysts low, but they also demonstrate high activity for both FT and water-gas shift (WGS) reactions, which makes it feasible to use them with syngases with low H_2/CO ratios [10-12]. A typical iron-based FTS process can be described in simplified terms as a combination of the FT and the WGS reactions (see Figure 5.1). The latter is thought to be a reversible parallel-consecutive reaction with respect to CO to form CO_2 [13-14]. Both H_2O and CO_2 are normally produced in substantial amounts by the two reactions, which provide two important routes for oxygen removal. They may also cause oxidation and structural changes in the iron catalyst [15-17]. It is therefore of scientific interest to investigate the effect of CO_2 on an iron-based catalyst under low-temperature FTS conditions.

Emission control and utilization of CO_2 has received much attention from scholars

because of its large-scale availability and the deleterious effect of carbon dioxide on the environment [18-19]. Many methods have been proposed to maintain the concentration of atmospheric CO_2 or to reduce and recycle it. Among these, the hydrogenation of CO_2 has traditionally been carried out on catalysts that are considered to be active and selective for the FT reaction, which hydrogenates CO [11, 12, 16, 20, 21]. Considerable work on the use of ^{14}C labeled CO and CO_2 has suggested that, while both CO and CO_2 serve as initiators, CO is the major propagator [22]. The mechanism of FT CO_2 hydrogenation is thought to proceed in two steps: first, the reverse WGS (Re-WGS) reaction takes place to produce CO, which is subsequently consumed in the FT conversion (see Figure 5.1) [22-25]. Whereas, the direct hydrogenation of CO_2 has also been proposed as an additional reaction [16]. However, irrespective of whether the conversion of CO_2 to hydrocarbons occurs in one or many steps, the overall effect is that CO_2 is hydrogenated and we refer to the overall reaction as CO_2 hydrogenation. In principle, iron-based catalysts, which are active in both WGS and Re-WGS reactions, should be ideal candidates for use in FTS for CO_2-containing syngas feeds [16, 25-28]. Using an alkalized iron catalyst, Riedel et al. discovered that H_2/CO_2 could be converted into hydrocarbon products of a structure and composition similar to those obtained with CO/H_2 [16]. Nevertheless, other researchers have found that a comparison of the product selectivity between CO and CO_2 hydrogenation on iron-based catalysts shows that CO_2 hydrogenation has a higher selectivity for light hydrocarbon products with a low alpha distribution [27, 29].

As the WGS reaction is an equilibrium-controlled reaction, the CO_2 formed during this reaction can be minimized by increasing the rate of the Re-WGS reaction, with the possible addition of CO_2 [27]. In an early study, Soled *et al.* [28] observed that CO_2 formation could be significantly decreased on Fe-Zn catalysts when CO_2 was added to the syngas. Research results obtained by Liu and

co-workers [27] showed that co-feeding CO_2 to syngas did not reduce the activity of the catalyst, and that when the partial pressure of CO_2 in the feed gas was increased, the rate of CO_2 formation on the catalyst only dropped slightly. As suggested previously [28], the presence of CO_2 inhibits the net rate of WGS during FTS on iron-based catalysts. The addition or recycling of CO_2 decreases the net rate of CO_2 formation, and increases the fraction of the oxygen atoms in CO that is removed as H_2O. This is an important practical issue when iron-based catalysts are used for H_2/CO mixtures derived from natural gas [30].

Most of the scientific literature on this subject focuses on high-temperature FTS with cofeeding of CO_2 or CO_2 hydrogenation over iron-based catalysts, under which conditions the WGS reaction achieves equilibrium [22, 25, 27, 28, 31, 32]. Yet surprisingly little attention has been paid by researchers to the aspect of adding or recycling CO_2 over an iron catalyst in low-temperature FTS with nonequilibrium WGS.

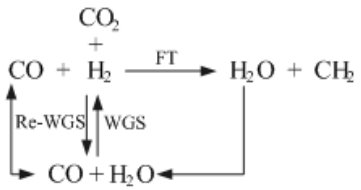

Figure 5.1: Reaction scheme proposed for CO/H_2 or CO_2/H_2 feed gas on an iron-based catalyst. FT: Fischer-Tropsch reaction; WGS: Water-Gas-Shift reaction; and Re-WGS: Reverse Water-Gas-Shift reaction.

At present, the scientific explanations of the mechanism of CO_2 formation and the role of CO_2 in chain growth remain controversial. Moreover, most of the research into cofeeding CO_2 to syngas has been conducted within narrow ranges of $H_2/CO/CO_2$ ratios. Our investigation aims to provide greater insight into the effect of CO_2 on an iron catalyst under low-temperature FTS. To do this, we tested the reactivity of large ranges of $H_2/CO/CO_2$ syngas mixtures over an iron catalyst in

low-temperature FTS experiments using two fixed bed micro reactors of the same kind. In the first group of experiments, designated A, two feed gases, H_2:CO:CO_2 = 2:1:0 and H_2: CO:CO_2 = 3:0:1, were mixed in different proportions, thus varying the ratios of CO, CO_2, and H_2 stoichiometrically with the ratio of $H_2/(2CO+3CO_2)$ equal to 1. In the second group of experiments (B), we combined a further two feed gases, H_2:CO:CO_2 = 1:1:0 and H_2: CO:CO_2 = 1:0:1, in a range of proportions, in this way varying the partial pressure of CO and CO_2 only, leaving the H_2 partial pressure fixed with the ratio of $H_2/(CO+CO_2)$ equaling 1. The catalyst activity, product selectivity and olefin/paraffin ratios in each of the sets of experiments were measured and compared.

5.2 Experimental Method

5.2.1 Catalyst Preparation

The Fe/TiO_2 catalyst was prepared by impregnating TiO_2 with an iron nitrate solution. TiO_2 (Degussa P25) was mixed with distilled water in a mass ratio of 1:1 and dried in air at 120 ℃ for 1 hour. The support was then calcined in air at 400 ℃ for 16 hours [33]. After calcination the support was crushed and sieved and the particles with diameters between 0.5–1 mm were used. The support was then impregnated with a quantity of iron nitrate ($Fe(NO_3)_3$ $9H_2O$) solution sufficient to give an iron metal loading of 10% by mass. The support was next dried in air at 120 ℃ for 16 hours and then calcined in air at 400 ℃ for 6 hours to allow the iron nitrate to decompose and transform to iron oxide.

5.2.2 Experimental Setup and Procedure

5.2.2.1 Catalyst reduction

Two fixed bed micro reactors of the same kind were used for the experiments.

One gram of catalyst was loaded into each of them. The same reduction procedure was carried out in each reactor at atmospheric pressure with H_2 (AFROX (African Oxygen) Ltd., 99.999%) for 24 hours. The reduction temperature and the flow rate were 350 ℃ and 60 ml(NTP)/(min gcat), respectively. Once the reduction was completed, the two reactors were allowed to cool down to room temperature, and the catalyst was isolated by N_2.

5.2.2.2 FT catalytic activity test

Four cylinders of syngas mixture were used in the experiments.

- In cylinder 1, the syngas named "CO-feed-1" is a mixture of $H_2/CO/N_2$ with H_2:CO= 2:1.
- In cylinder 2, the syngas named "CO_2-feed-1" is a mixture of $H_2/CO_2/N_2$ with H_2:CO_2 =3:1.
- In cylinder 3, the syngas named "CO-feed-2" is a mixture of $H_2/CO/N_2$ with H_2:CO= 1:1.
- In cylinder 4, the syngas named "CO_2-feed-2" is a mixture of $H_2/CO_2/N_2$ with H_2:CO_2 =1:1.

All four cylinders contained 10 vol.% N_2, to provide an internal standard for mass balance calculations (More detail is given in Table 5.1.).

Table 5.1: Summary of the syngas composition in the four cylinders.

Cylinder No.	Name	The molar composition of the syngas			
		H_2	CO	CO_2	N_2
1	CO-feed-1	60%	30%	0%	10%
2	CO_2-feed-1	67%	0%	23%	10%
3	CO-feed-2	45%	45%	0%	10%
4	CO_2-feed-2	0%	45%	45%	10%

In order to evaluate the effect of CO_2 on the low-temperature FTS over an iron based catalyst, we conducted two groups of experiments in two fixed bed reactors with operating conditions of T = 250 ℃, P = 20 bar gauge and a flow rate = 60 ml(NTP)/(min gcat).

5.2.2.2.1 Procedure for Group A experiments in the first fixed-bed micro reactor, for reaction conditions 1–11:

The "CO_2-feed-1" syngas (H_2:CO:CO_2 = 3:0:1) was initially introduced into the reactor at a flow rate of 60 ml(NTP)/(min gcat). The reactor pressure was slowly increased to 20 bar (gauge), and thereafter, the temperature was gradually raised to 250 ℃. The pressure and temperature were allowed to stabilize, and these operating conditions were maintained at a constant level for 72 hours, during which the tail gas composition was monitored. Thereafter, the flow rate of the "CO_2-feed-1" syngas was decreased by 10%, that was by 6 ml (NTP)/(min gcat), and the "CO-feed-1" syngas (H_2:CO:CO_2=2:1:0) was introduced into the reactor at a flow rate of 6 ml(NTP)/(min gcat) so as to keep the total flow rate constant at 60 ml(NTP)/(min gcat). The new reaction conditions were maintained for 72 hours, and the composition of the tail gas was continually checked. After that the flow rate of the CO_2 mixture was again decreased, while that of the "CO-feed-1" syngas was increased in order to keep the total flow rate of gas into the reactor at 60 ml(NTP)/(min gcat). The detailed results for the $H_2/CO/CO_2$ mixtures in Group A are shown in Figure 5.2 under reaction conditions 1–11.

Each of the reaction conditions, as shown in Figure 5.2 was maintained at a constant state for 72 hours to stabilize the reactor. Figure 5.3 plots the CO_2 conversion as a function of time on stream for reaction condition 1 as shown in Figure 5.2. The CO_2 conversion reached steady state after 36 hours, which indicated that 72 hours was enough time to stabilize the reactor. The monitored

results for the other reaction conditions also showed that the reactions in the reactor reached steady state after around 40 hours.

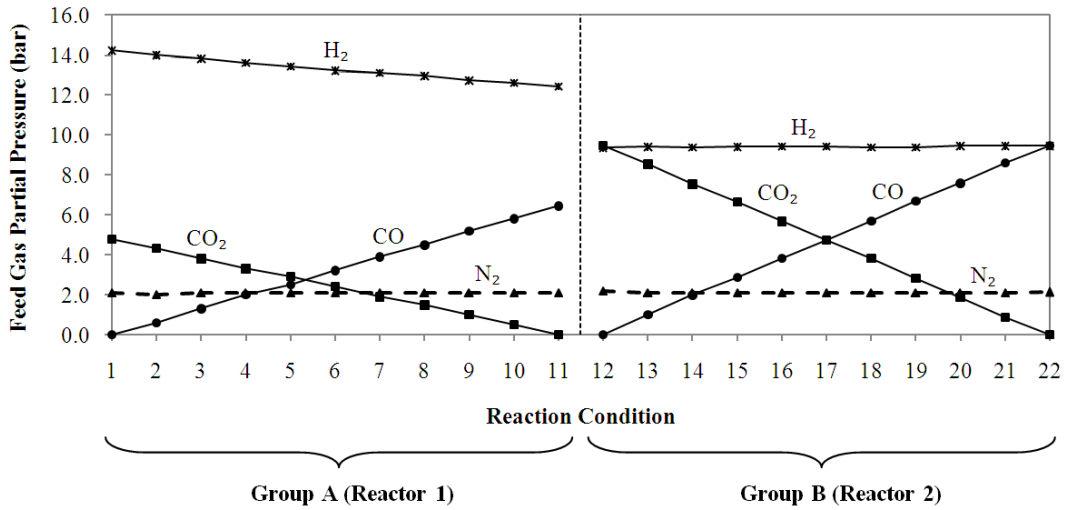

Figure 5.2: Summary of the partial pressures of H_2, CO, CO_2 and N_2 in feed gas on an iron catalyst FTS at 250 ℃, 20 bar gauge and 60 ml(NTP)/(min gcat).

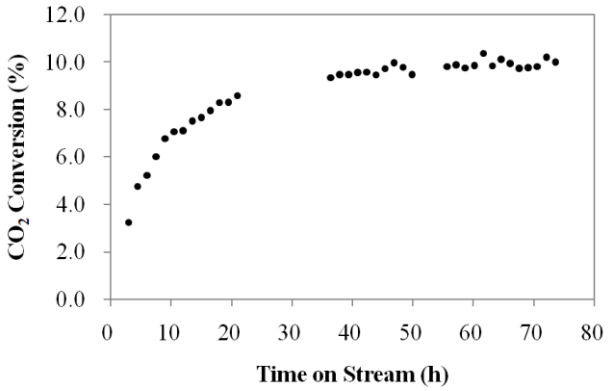

Figure 5.3: CO_2 conversion as a function of time on stream over an iron FTS catalyst at 250 ^oC, 20bar gauge and 60 ml(NTP)/(min gcat) for reaction condition 1 as shown in Figure 5.2.

5.2.2.2.2 Procedure for Group B experiments in the second fixed bed micro reactor, for reaction conditions 12–22:

Two feed gases (different from those used in Group A) named "CO_2-feed-2" syngas (H_2:CO:CO_2=1:0:1) and "CO-feed-2" syngas (H_2:CO:CO_2=1:1:0), were prepared in a range of proportions to vary the partial pressure of CO and CO_2. The same procedure as that outlined for the first group of experiments was followed, and details of the information we obtained from this group are given in Figure 5.2 under reaction conditions 12–22.

5.2.3 Product analysis

The tail gas was analyzed every 1.5 hours by means of an online DANI GC. Two thermal conductivity detectors (TCDs) were used to analyze H_2, N_2, CO, CO_2 and CH_4, and the gas phase hydrocarbons were analyzed by a flame ionization detector (FID). The wax and liquid products were collected in a hot trap (maintained at 150 ℃) and cold trap (kept at room temperature) (see Figure 5.4). We used an offline GC to analyze the oil and wax products at the end of the mass balance for each run.

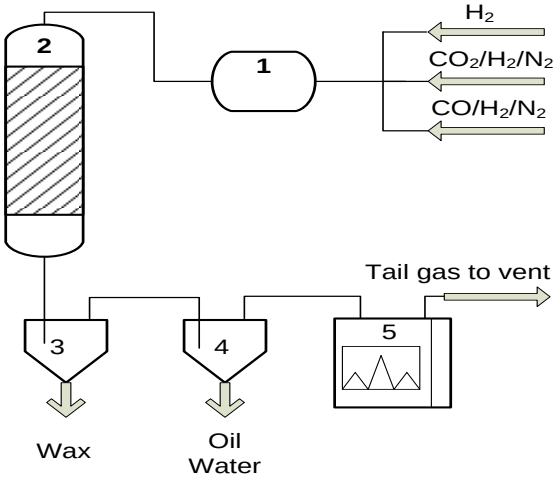

Figure 5.4: Simplified flow scheme of the fixed bed reactor used in the experiments. (1) Inlet gas mixer; (2) fixed bed reactor; (3) hot condensable product trap; (4) cold condensable product trap; (5) online GC

5.3 Results

5.3.1 Definitions

5.3.1.1 Reactant conversion

The CO_2-containing syngas mixtures used as feeds for the FTS experiments comprised CO, CO_2, H_2 and N_2, which had different compositions. H_2, CO and/or CO_2 were reactants, while N_2 was used as an inert tracer for mass balance purposes.

The conversion of reactant i ($Conv_{reactant\ (i)}$) was calculated using the following formula:

$$Conv_{reactant\ (i)}(\%) = \left(\frac{F_{in}X_{reactant\ \ (i),in} - F_{out}X_{reactant\ \ (i),out}}{F_{in}X_{reactant\ \ (i),in}}\right) \times 100 \qquad (5.1)$$

where F_{in} is the total molar flow rate of the reactor inlet gas, mol/min; F_{out} is the total molar flow rate of the reactor outlet gas, mol/min; $X_{reactant(i),in}$ is the molar fraction of reactant (i) in the reactor inlet gas and $X_{reactant(i),out}$ is the molar fraction of reactant (i) in the reactor outlet gas.

5.3.1.2 Reactant consumption and product formation rate

- Consumption rate of reactant i ($r_{reactant(i)}$, mol/(min gcat)) was calculated as follows:

$$-r_{reactant\ (i)} = \frac{F_{in}X_{reactant\ \ (i),in} - F_{out}X_{reactant\ \ (i),out}}{m_{cat}} \qquad (5.2)$$

  where m_{cat} is the mass if the catalyst used in this reaction, g

- Formation rate of product j ($r_{product(j)}$, mol/(min gcat)) was calculated by

$$-r_{product\ (i)} = \frac{F_{out}\, X_{product\ \ (i),out} - F_{in}\, X_{product\ \ (i),in}}{m_{cat}} \quad (5.3)$$

where $X_{product(j),in}$ is the molar fraction of product (j) in the reactor inlet gas and $X_{product(j),out}$ is the molar fraction of product (j) in the reactor outlet gas.

5.3.1.3 Product selectivity

As mentioned earlier, the feed gas was a mixture of $CO/CO_2/H_2/N_2$; therefore, the products could be formed from CO and/or CO_2 conversion. Thus, we calculated the product selectivity of $S_{product(j)}$ (on the basis of moles of carbon) in three different situations as follows:

- When the CO conversion was positive but the CO_2 conversion was negative, which means hydrocarbons, water and CO_2 were the products in the FT reactor, the product selectivity ($S_{product(j)}$) was calculated as follows:

$$S_{product\ (j)}(\%) = \frac{n_j r_{roduct\ (j)}}{-r_{reaction\ \ (CO)}} \times 100 \quad (5.4)$$

where n_j represents the number of carbon atoms contained in product j.

- When both the conversions of CO and CO_2 were positive, which means both CO and CO_2 were converted to hydrocarbons during the FTS, the product selectivity ($S_{product(j)}$) would be expressed as follows:

$$S_{product\ (j)}(\%) = \frac{n_j r_{roduct\ (j)}}{-r_{reaction\ \ (CO)} - r_{reaction\ \ (CO_2)}} \times 100 \quad (5.5)$$

- When the conversion of CO was negative but the conversion of CO_2 was positive, which means hydrocarbons, water and CO as the products in the FT reactor, the product selectivity ($S_{product(j)}$) would be calculated as follows:

$$S_{product\ (j)}(\%) = \frac{n_j r_{roduct\ (j)}}{-r_{reaction\ \ (CO_2)}} \times 100 \quad (5.6)$$

5.3.1.3 Rates of FTS, WGS and Re-WGS reactions

In our experimental system, CO can convert either into hydrocarbon products (FTS) and water or into CO_2 and hydrogen (WGS). Alternatively, CO_2 may also be one of the reactants, and can be converted either into hydrocarbon products (FTS) and water or into CO and hydrogen (Re-WGS). It is thus interesting to compare the rates of these three reactions. Similarly to the product selectivity calculations, the three reaction rates can be calculated in three different situations, which are the following:

- When the CO conversion was positive while the CO_2 conversion was negative, which means CO_2 is one of the products, then both the FTS and WGS reaction occur. These two reaction rates can be calculated as follows:

$$r_{WGS} = r_{product\ (CO_2)} \tag{5.7}$$

$$r_{FT} = -r_{reactant\ (CO)} - r_{product\ (CO_2)} \tag{5.8}$$

  When both the conversions of CO and CO_2 were positive, which means both CO and CO_2 are converted to hydrocarbons during the FTS, the FT reaction rate could be calculated in the system from

$$r_{FT} = -r_{reactant\ (CO)} - r_{reactant\ (CO_2)} \tag{5.9}$$

- When the conversion of CO was negative but the conversion of CO_2 was positive, which means CO was one of the products, then the FTS and Re-WGS reaction happened in the reactor. These two reactions rates can be calculated as follows:

$$r_{Re-WGS} = r_{product\ (CO)} \tag{5.10}$$

$$r_{FT} = -r_{reactant\ (CO_2)} - r_{prodcut\ (CO)} \quad (5.11)$$

5.3.2 Comparison between CO and CO_2 hydrogenation

The reaction conditions 11 and 22 in Figure 5.2 represent CO hydrogenation with different H_2/CO ratios; whereas reaction conditions 1 and 12 show CO_2 hydrogenations with different H_2/CO_2 ratios.

The results for CO and CO_2 hydrogenations are shown in Tables 5.2 and 5.3. For CO hydrogenation (Table 5.2), as the H_2/CO ratio decreased from 2:1 to 1:1, the CO conversion dropped from 21.0% to 12.2%, and CH_4 selectivity decreased from 13.2% to 6.8% (results that are in agreement with those in the published literature [27]). It seems that reducing H_2/CO ratio had little influence on the CO_2 selectivity, which was found to rise only slightly, from 5.4% to 6.0%. The olefin to paraffin (O/P) ratios with chain lengths of 2 and 3 increased with a decline in the H_2/CO ratio, which means the lower the H_2/CO ratio, the higher the olefin product selectivity (van der Laan et al. [10] and Liu et al. [27] have reported similar results.). With a rise in the H_2/CO ratio, both the FT and WGS reaction rates dipped a little, from 1.2×10^{-4} mol/(min·gcat) to 1.0×10^{-4} mol/(min·gcat) in the case of the FT reaction, and from 6.8×10^{-4} mol/(min·gcat) to 6.4×10^{-4} mol/(min·gcat) for the WGS reaction. It is remarkable, as shown in Table 5.2, that the FT reaction rate was far higher than that of the WGS reaction under the same reaction conditions on an iron catalyst.

For the case of CO_2 hydrogenation, as the H_2/CO_2 ratio dropped from 3:1 to 1:1 (Table 5.3), the CO_2 conversion fell from 10.0% to 4.8% and the CH_4 selectivity decreased from 43.7% to 30.1%. However, the CO selectivity climbed from 16.1% to 28.6% with the decline in the H_2/CO_2 ratio. With regard to the O/P ratios, the CO_2 hydrogenation results showed a trend similar to that of CO hydrogenation in that in the case of the former the O/P ratios with chain lengths of 2 and 3 rose with

a falling H_2/CO_2 ratio. However, the value of the O/P ratio was dramatically lower for CO_2 than for CO hydrogenation. As the H_2/CO_2 ratio in the feeds decreased, the FT reaction rate fell from 3.8×10^{-5} mol/(min·gcat) to 3.0×10^{-5} mol/(min·gcat). In contrast, the Re-WGS reaction rate rose from 7.3×10^{-6} mol/(min·gcat) to1.2×10^{-5} mol/(min·gcat) with the declining H_2/CO_2 ratio. The FT reaction rate was higher than the Re-WGS reaction rate under the same reaction conditions.

Table 5.2: The catalytic performance of the iron catalyst for CO hydrogenation at 250 ^oC, 20 bar gauge and 60ml (NTP)/(min gcat).

	CO hydrogenation	
Condition Number	11#	22#
CO/H_2	2:1	1:1
CO Conversion (%)	21.0	12.2
CO_2 Selectivity (%)	5.4	6.0
CH_4 Selectivity (%)	13.2	6.8
O_2/P_2[a]	0.129	0.443
O_3/P_3[b]	0.785	2.423
Rate of FT (mol/(min·gcat))	1.2E-04	1.0E-04
Rate of WGS (mol/(min·gcat))	6.8E-06	6.4E-06

[a] Olefin to Paraffin ratio with chain length 2

[b] Olefin to Paraffin ratio with chain length 3

The activity and selectivity of the catalyst from the first run in Group 1 were compared to that of the repeat experiment when returning to the starting conditions at the end of the 11 experiments in Group 1 (Figure 5.2), as shown in Table 5.3. It is surprising to note that when the reaction operating parameters were adjusted to the initial experimental conditions after around 800 hours of time on line with different feed gas mixtures of $H_2/CO/CO_2$ during this time, the feed gas conversions, product selectivity and reaction rates were quite similar to that of the initial run, which indicates that there was no catalyst deactivation.

Table 5.3: The catalytic performance of the iron catalyst for CO_2 hydrogenation at 250 ^oC, 20 bar gauge and 60 ml(NTP)/(min gcat).

	CO_2 hydrogenation		
Condition Number	1#	12#	Return to 1# [c]
CO_2/H_2	3:1	1:1	3:1
CO_2 conversion (%)	10.0	4.8	9.4
CO Selectivity (%)	16.1	28.6	16.4
CH_4 Selectivity (%)	43.7	30.1	47.9
O_2/P_2 [a]	0.007	0.010	0.007
O_3/P_3 [b]	0.023	0.043	0.029
Rate of FT (mol/(min·gcat))	3.8E-05	3.0E-05	3.6E-05
Rate of Re-WGS (mol/(min·gcat))	7.3E-06	1.2E-05	7.0E-06

[a] Olefin to Paraffin ratio with chain length 2

[b] Olefin to Paraffin ratio with chain length 3

[c] returning to the starting condition 1# at the end of the experimental series

When we compared CO and CO_2 hydrogenation using the same ratios of hydrogen with the oxides of carbon in the feed gases (H_2:CO=1:1 and H_2:CO_2=1:1) as shown in Tables 5.2 and 5.3, we found experimentally the following. (1) Although both the CO and CO_2 were readily hydrogenated, the reactivity for CO_2 is around 2.5 times lower than that of CO. Similar results were reported by Riedel et al. [16]); (2) The methane selectivity was 5 times higher for CO_2 hydrogenation than for CO hydrogenation, which was in agreement with the results obtained by Perez-Alonso et al. [20] and Ando et al. [29]; And (3) the olefin selectivity was far lower for CO_2 than CO hydrogenation, indicating that the CO_2 hydrogenation produced mainly saturated light hydrocarbons.

5.3.3 Catalytic performance for various $H_2/CO/CO_2$ syngas mixtures during FTS

5.3.3.1 Conversion results

Figure 5.5 shows the reaction conversion (a) and product selectivity (b) as functions of the syngas composition for the two groups of experiments, A and B, as shown in Figure 5.2.

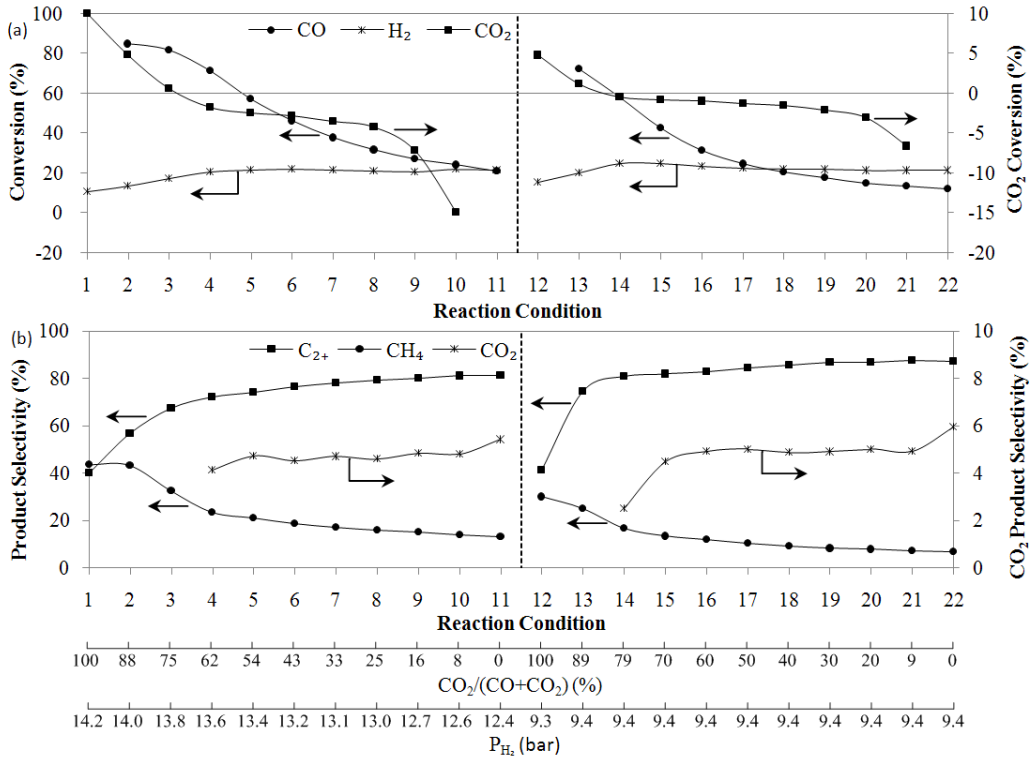

Figure 5.5: The reaction conversion (a) and product selectivity (b) as functions of the syngas composition (reaction conditions as shown in Figure 5.2).

In the Group A experiments, the H_2 conversion increased, reached a maximum value, and then held steady at that value while the ratio of $CO_2/(CO+CO_2)$ was decreased. However, decreasing the ratio $CO_2/(CO+CO_2)$ caused both the CO and CO_2 conversions to decline, and the CO_2 conversion changed from positive to negative values. The positive values of CO_2 conversion indicate the CO_2 is

consumed to form products with CO_2-rich feed gases, while the negative values of CO_2 conversion correspond to the net formation of CO_2 during the FTS processes rather than its net consumption. The data showed that when the ratio of $CO_2/(CO+CO_2)$ was below 75%, the CO_2 conversion became negative in Group A experiments.

The results for the Group B experiments, shown in Figure 5.2 as reaction conditions 12–22, show that the H_2, CO and CO_2 conversions generally have the same trends as were observed in the Group A experiments. It is interesting to note that negative conversions of CO_2 were obtained with ratios of $CO_2/(CO+CO_2)$ below 79% in the second group.

5.3.3.2 Product selectivity results

Figure 5.5 (b) shows the product selectivity as a function of the composition of the syngas. In the Group A experiments, covering reaction conditions 1–11, the CH_4 selectivity dropped from 43.7% to 13.2% as the $CO_2/(CO+CO_2)$ ratio decreased. On the other hand, the C_{2+} product selectivity rose dramatically, from 40.3% to 72.3%, when the ratio of $CO_2/(CO+CO_2)$ declined from 100% to 62%. However, as the $CO_2/(CO+CO_2)$ ratio continued to fall, the C_{2+} product selectivity showed a tapering off from 72.3% to 81.4%. As mentioned above, we found that when the ratio of $CO_2/(CO+CO_2)$ dropped lower than a certain value, CO_2 was formed from CO. (See Figure 5.5 (a)). The selectivity of CO_2, as shown in Figure 5.5 (b) for reaction conditions 4–11, changed over quite a small range, from 4.1% to 5.4%, in response to a wide range of syngas compositions, as shown in Figure 5.2.

The same trends for the CH_4 and C_{2+} product selectivity were to be seen in both groups of experiments (see Figure 5.5 (b)). However, in the Group B results, as compared with those for Group A, a lower CH_4 selectivity and a higher C_{2+}

selectivity were obtained with the same ratio of $CO_2/(CO+CO_2)$. The only point at which CO_2 selectivity dropped to 2.5% occurred when the ratio of $CO_2/(CO+CO_2)$ was 79%. When the ratio of $CO_2/(CO+CO_2)$ fell from 70% to 21%, the CO_2 selectivity was fairly constant at around 5%. For the CO hydrogenation of reaction condition 22, the CO_2 selectivity was 6.0%. It is worth noting that although the $H_2/CO/CO_2$ ratios are totally different in the two groups, the changes in CO_2 selectivity occurred in a relatively small range.

5.3.3.3 Reactant consumption rate

The CO, CO_2, and H_2 reaction rates as a function of the syngas composition are shown in Figure 5.6 (a). When the results for groups A and B were compared, we observe the same trends in the H_2, CO and CO_2 reaction rates as the ratio of $CO_2/(CO+CO_2)$ declines. The CO_2 reaction rate followed a curve similar to that of the CO_2 conversion in Figure 5.5 (a). The rate of consumption of H_2 rose gradually, reached a maximum, and then dipped slightly as the ratio of $CO_2/(CO+CO_2)$ decreased, while in response to an increase in the ratio, the CO consumption rate climbed until it arrived at a maximum, after which it maintained the rate at that value. The reaction rates for both CO and H_2 were higher in the Group A experiments than in Group B.

5.3.3.4 Product formation rate

The product formation rate is shown in Figure 5.6 (b). The reaction rate of CH_4 can be maximized at the feed gas composition of $CO_2/(CO+CO_2)$ around 75% in Group A and round 89% in Group B. It is worth noting that in both groups of experiments, the C_{2+} rate initially increased, reached a maximum, and then held that value as the ratio of $CO_2/(CO+CO_2)$ diminished.

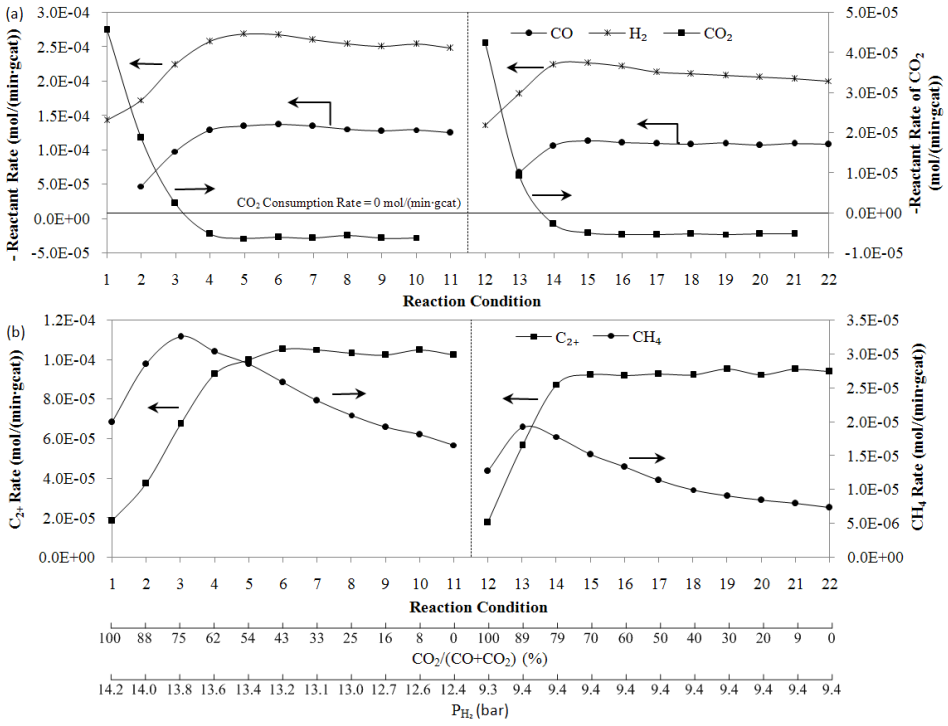

Figure 5.6: The reactant consumption rate (a) and the product formation rate (b) as a function of syngas composition (reaction condition as shown in Figure 5.2).

5.3.3.5 Olefin and paraffin formation rates

In view of the effect of the partial pressures of CO, CO_2, and H_2 on the activity and selectivity of the catalyst, we plotted the rates of formation of the light olefins and paraffins in Figure 5.7 (a) and (b). The olefin rate rose with falling ratios of $CO_2/(CO+CO_2)$ in both groups of experiments, and the values of the olefin reaction rates in both gourps at the same $CO_2/(CO+CO_2)$ ratios were similar. However, a different trend could be observed in the rates of formation for the paraffins and the points at which they reached their maximum (Figure 5.7 (b)). When we compared the data for the two groups, it was clear that higher paraffin formation rates had been obtained in the Group A experiments, which had higher H_2 partial pressures in the inlet gases. These results show that the effects of the partial pressure of CO, H_2, and CO_2 on the formation of paraffins and olefins are not the same.

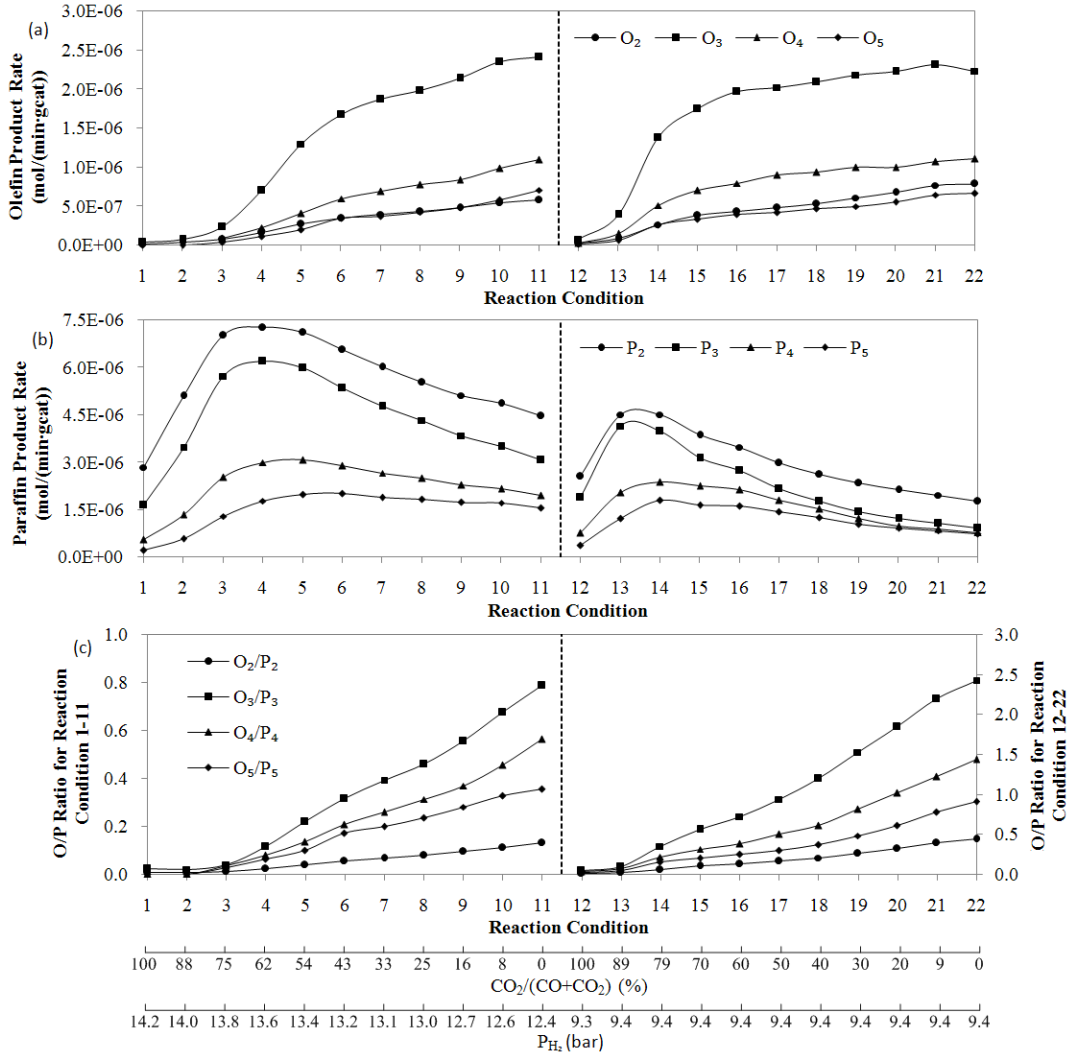

Figure 5.7: The olefin formation rate (a), paraffin formation rate (b) and olefin/paraffin (O/P) ratio (c) as a function of syngas composition (reaction conditions as shown in Figure 5.2) (O represents olefin and P represents paraffin).

5.3.3.6 O/P ratio

Figure 5.7 (c) shows the O/P ratio as a function of syngas composition. The experimental results we obtained are similar to those recorded in the literature on the subject [10, 37–38] in that the O/P ratio changes as a function of carbon number. In general (excluding O_2/P_2) an increment in carbon number causes a drop in the O/P ratio under each reaction condition. As the amount of CO_2 in the feed gas was reduced and the quantity of CO augmented in both group

experiments (see Figure 5.2), the O/P ratio for a particular carbon number increased. Note that CO_2-rich feeds resulted in products with high paraffin selectivity, while CO-rich feeds shifted the product composition to an FT type of product with high selectivities for both paraffin and olefin. Because the Group B experiments were carried out at a lower H_2 partial pressure than was used for Group A, the O/P for Group B was far higher.

5.3.4 Comparison between the FT reaction rate and the WGS (or Re-WGS) reaction rate

Figure 5.1 gives a simplified graphical representation of the range of reactions possible for CO and CO_2 hydrogenations over iron-based catalysts. During the FTS experiments, conducted using $H_2/CO/CO_2$ mixtures with a very high mole fraction of CO_2 in the feed gas, we found that CO_2 could transform to hydrocarbon products with positive CO_2 conversions, as shown in Figure 5.5 (a) for reaction conditions 2, 3 and 13. However, when the ratio of $CO_2/(CO+CO_2)$ was lower than 75% in the first group and 79% in the second group, CO_2 was formed from CO (see Figure 5.5). This made it interesting to compare the rates of the WGS or Re-WGS and FT reactions.

The FT, WGS and Re-WGS reaction rates, as functions of syngas composition, are shown in Figure 5.8 (b). The trend for the FT reaction rates in both groups of experiments was similar in that they first increased, arrived at a maximum value, and maintained it. The WGS reaction rate was equal to the CO_2 formation rate in that the trend of the WGS reaction rate was the same as the CO_2 formation selectivity, as can be seen in Figure 5.5 (b). Although the $H_2/CO/CO_2$ ratios underwent considerable changes with conditions 5-10 in Group A and 15-21 in Group B (see Figure 5.2), the WGS reaction rate altered over quite a small range. Both the FT and WGS reaction rates in the Group A experiments were higher than those in Group B. Furthermore, the WGS reaction rate was lower than the FT

reaction rate under the same value of $CO_2/(CO+CO_2)$ ratio. Figure 5.8 (a) plots the H_2O formation rate for the two groups of experiments, which will be discussed in Section 5.4.

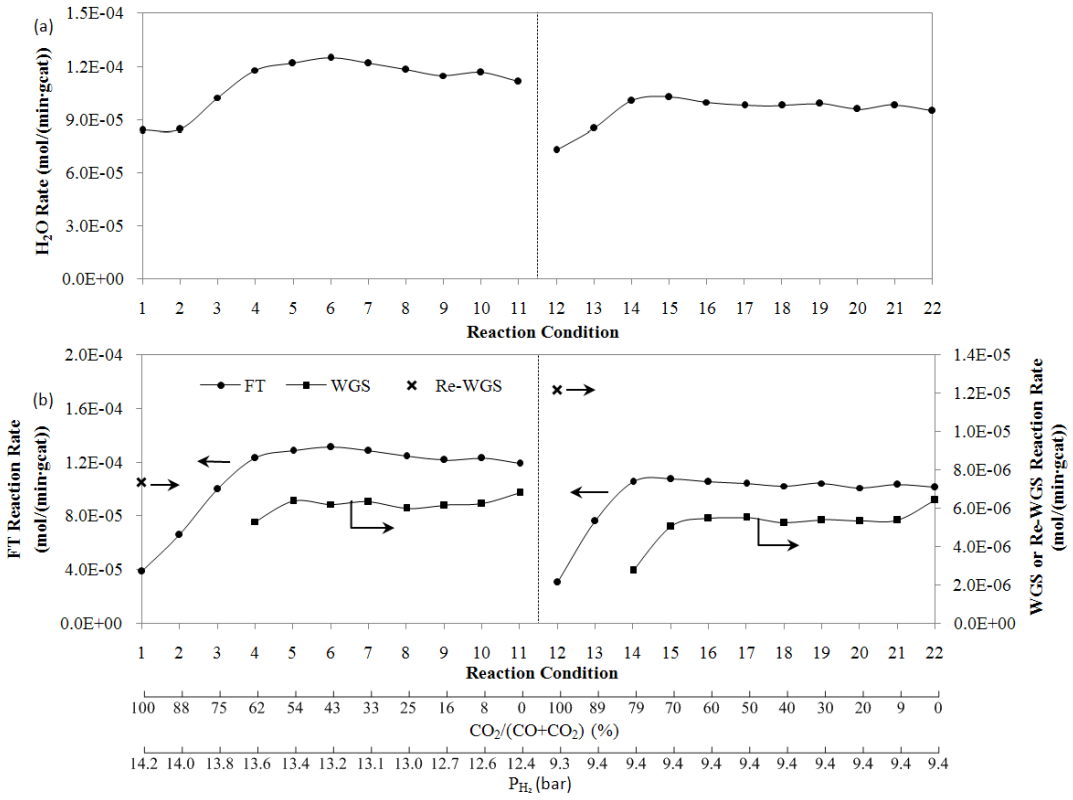

Figure 5.8: The calculated H_2O formation rate (a), FT reaction rate, WGS reaction rate and Re-WGS reaction rate (b) as a function of syngas composition (reaction condition as shown in Figure 5.2).

5.4 Discussion

The two groups of experiments we carried out aimed to investigate the reactivity of large ranges of $H_2/CO/CO_2$ syngas mixtures for low-temperature FTS over an iron catalyst. In both groups of experiments, the ratios of the feed gases [of $H_2/(2CO+3CO_2)$ for Group A, and $H_2/(CO+CO_2)$ for Group B] for each reaction condition equaled 1. Both groups of experiments were carried out at a constant total synthesis pressure of 20bar in gauge, a temperature of 250 ^oC and a flow rate

of 60 ml(NTP)/(min gcat).

A comparison between the results obtained for the two groups of experiments led us to conclude that both CO and CO_2 are readily hydrogenated when the feeds are based on either H_2/CO or H_2/CO_2 (see Tables 5.2 and 5.3). Considering the conversion of CO and CO_2 separately, we could see that CO was converted rapidly during the FT reaction, and that CO_2 was converted to hydrocarbons only when it was present in a high concentration, with a commensurately low concentration of CO in the feed gas (see Figure 5.5 (a)). In addition, CO_2 hydrogenation produced more CH_4-rich short chain paraffin products than CO (see Figure 5.5 (b)).

Visconti et al.[34] speculated that the different selectivity behavior of CO and CO_2 hydrogenation that they observed in their experiments was attributable to the different H/C ratios on the catalyst surface resulting from the H_2/CO and H_2/CO_2 reactions. In particular, and in agreement with Zagli and Falconer [35], we expect that a high H/C surface concentration is attained during CO_2 hydrogenation because of low CO_2 adsorption. The data in Figure 5.7 (c) show that in the two groups of experiments the O/P ratios increased gradually when the CO_2/H_2 syngas was replaced stepwise by CO/H_2 syngas. Furthermore, the O/P ratio in the Group B experiments is significantly higher than in Group A at the same ratio of $CO_2/(CO+CO_2)$, possibly because of the lower partial pressure of H_2 in Group B.

In general, the mechanism of FT CO_2 hydrogenation is thought to proceed in two steps: first the Re-WGS reaction takes place to produce CO, which is subsequently consumed in the FT conversion (Figure 5.1). Therefore, the H/C ratio on the catalyst surface is proportional to the ratio of the partial pressure of CO to the partial pressure of H_2 (P_{CO}/P_{H_2}) in the reactor for both CO and CO_2 hydrogenation. If the CO_2 hydrogenation via Re-WGS produces CO as an intermediate, the partial pressure of the CO is limited by the WGS reaction

equilibrium, so that we found that the olefin selectivity for CO_2 hydrogenation was markedly lower than for CO hydrogenation, as shown in Tables 5.2 and 5.3.

The O/P ratios with different chain lengths [n (n=2, 3 and 4)] as a function of the ratios of P_{CO}/P_{H_2} in the tailgas of the two groups of the experiments are given in Figure 5.9. The results from both groups of experiments indicated that the ratio of O/P rises significantly with an increase in the ratio of P_{CO}/P_{H_2} in the tailgas. Furthermore, at the same value of the ratio of P_{CO}/P_{H_2} in the tailgas, the O/P ratios in the two sets of experimental data are very similar, particularly at a chain length of n=4. Based on our experimental data, we found that the effect of the partial pressure of CO, H_2, and CO_2 on the formation of paraffins and olefins was not the same (Figure 5.7). For CO rich feeds, all the hydrocarbon products were produced by CO, rather than CO_2, so that O/P ratio may due to the surface coverage of CO and H_2. For CO_2 rich feeds, when the conversion of CO_2 was positive, which means that part of the products came from CO_2, the effect of CO_2 on the product selectivity must be accounted for. However, if the FT hydrocarbons are produced from CO_2 hydrogenation via CO as an intermediate, the surface coverage of CO_2 for FT CO_2 hydrogenation may be a function of the surface coverage of CO. This is nicely illustrated by Figure 5.9, which shows the O/P ratio was as a function of P_{CO}/P_{H_2} in the reactor for FTS using $H_2/CO/CO_2$ mixtures.

It is clearly demonstrated in Figure 5.6 that in both sets of experiments, the C_{2+} formation rate initially increased, reached a maximum, and then holding that value at a near-constant level while the ratio of $CO_2/(CO+CO_2)$ decreases. When the rate of formation of hydrocarbon products achieved a fairly constant maximum value, the concentration of CO_2 in the feed gas was at a high concentration (Figure 5.6), which might be of interest to engineers designing XTL systems (XTL, anything-to-liquids is a process that converts carbon and energy

containing feedstock to high quality fuels and products, such as coal-to-liquids, biomass to-liquids and gas-to-liquids) using iron based catalysts.

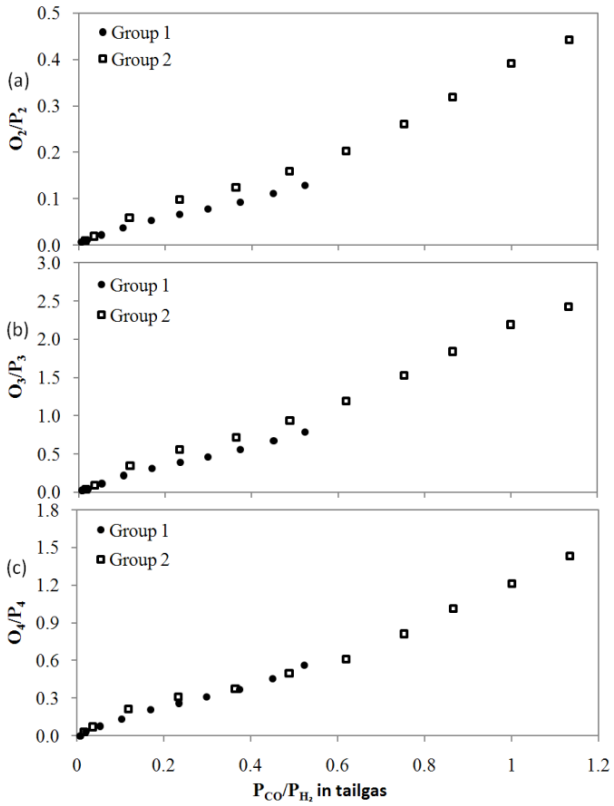

Figure 5.9: O/P ratio as a function of the ratio of P_{CO}/P_{H_2} in tailgas (reaction conditions as shown in Figure 5.2): (a) O_2/P_2, (b) O_3/P_3 and (c) O_4/P_4 (O represents olefin and P represents paraffin or pressure).

It is worth noting that when the conversion of CO_2 becomes negative, both the FT and the WGS reaction rates are fairly constant in both groups of experiments, independent of the ratio of $CO_2/(CO+CO_2)$ (see Figure 5.8). In the research undertaken into FT reactions by Dry [36], he found that for a reduced Fe catalyst at 225–265 ^oC at low conversion and a low partial pressure of H_2O, the rate of the FT reaction is proportional to the partial pressure of H_2, which can be expressed as Equation (5.12):

$$r_{FT} = kP_{H_2} \qquad (5.12)$$

where *k* is a constant and P_{H_2} is the partial pressure of H_2. In our analysis of the results of the research described in this paper, we made the following observations:

- The concentration of the products and water in the reactors was very low in both groups of experiments, because the H_2 conversions shown in Figure 5.5 were below 22%.
- In Group A, when the H_2 partial pressure in the feed gas did not vary much, from 13.6 bar under condition 4 to 12.4 bar in condition 11 (Figure 5.2), the changes brought about by the FT reaction rate were restricted to a small range (Figure 5.8). However, marked variation were seen in the CO and CO_2 partial pressures in the feed gas over the range of reaction conditions shown in Figure 5.2.
- The H_2 partial pressure in the feed gas in Group B was fixed at 9.4 bar, and the FT reaction rates for runs 14–22 were fairly constant (Figure 5.8) even over wide ranges of CO and CO_2 partial pressures in the feed gas as shown in Figure 5.2.
- As the partial pressure of H_2 in the feed gas of Group A was higher than in Group B (see Figure 5.2), with the same ratio of $CO_2/(CO+CO_2)$, a higher FT reaction rate was obtained in Group A (Figure 5.8).
- As the partial pressure of H_2 in the feed gas of Group A was higher than in Group B, with the same ratio of $CO_2/(CO+CO_2)$, a higher FT reaction rate was obtained in Group A (Figure 5.8).
- The conversion levels of CO_2 from reaction conditions 4-11 in Group A and runs 14-22 in Group B were negative (Figure 5.5).

Since the partial pressure of H_2 is nearly constant in our experiments, we would expect, acording to equation (12), that the FT rate is also nearly constant.

The equilibrium of the WGS reaction is very important, and determines the limit

to which either CO can be converted to CO_2 or CO_2 to CO. Figure 5.10 allows the comparison to be made between the equilibrium constant values calculated from thermodynamics ($K_{WGS,equilibrium}$) and value of the equilibrium constant calculated from the experimental data ($K_{WGS,experimental}$) as a function of syngas composition (reaction conditions as shown in Figure 5.2). $K_{WGS,equilibrium}$ is determined from the Van't Hoff expression of ($K_{equilibrium} = exp[-\Delta_r G(T)/(RT)]$), and the value of $K_{WGS,equilibrium}$ at the reaction temperature of 250 ^{o}C is 80.42. Here we define the experimental value of $((P_{CO_2}P_{H_2})/(P_{CO}P_{H_2O}))$ as $K_{WGS,experimental}$, which declines with a decreasing CO_2/(CO+CO_2) ratio in both groups of experiments. Only under the reaction conditions 3, 4 and 14 is the value of $K_{WGS,experimental}$ close to $K_{WGS,equilibrium}$; in contrast, the values of $K_{WGS,experimental}$ are far from the $K_{WGS,equilibrium}$ under the other reaction conditions, which indicates that the WGS reaction has not reached equilibrium. When the values of $K_{WGS,experimental}$ are higher than $K_{WGS,equilibrium}$ under reaction numbers 2 and 3 in Group A and 13 in Group B, positive CO_2 conversions are achieved. In contrast, when the values of $K_{WGS,experimental}$ are lower than $K_{WGS,equilibrium}$ (from conditions 4–11 in Group A and 14–22 in Group B), negative CO_2 conversions are obtained. This phenomenon can be observed in both groups of experiments. We therefore deduce that although the WGS reaction does not achieve equilibrium, the equilibrium constraints determine whether CO can be converted to CO_2, or CO_2 to CO.

Whereas the WGS reaction is far from thermodynamic equilibrium (Figure 5.10), Figure 5.8 shows that the WGS reaction rates are fairly constant when the ratio of CO_2/(CO_2+CO) is lower than 54% in the Group A experiments and 70% in Group B, which indicates that the WGS reaction rate is independent of the partial pressure of CO. Our experimental results in this instance differ from those obtained from the literature [36] which expressed that the WGS reaction rate for iron-based low-temperature FTS is proportional to the partial pressure of CO.

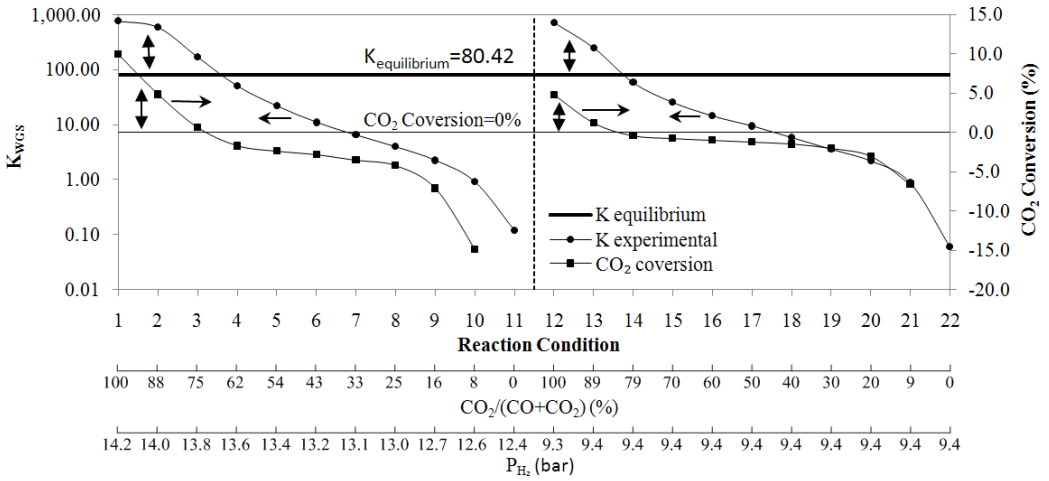

Figure 5.10: A comparison between the equilibrium constant values calculated from thermodynamics ($K_{WGS,equilibrium}$) and the equilibrium constant values calculated from the experimental data ($K_{WGS,experimental}$) as a function of syngas composition (reaction conditions as shown in Figure 5.2).

Figure 5.8 (a) shows the H_2O formation rate for the two groups of experiments, which increases gradually, reaches a maximum, and then levels off with a decreasing $CO_2/(CO+CO_2)$ ratio. The formation rate in Group A is a little higher than in Group B. When we compared the WGS reaction rate with the H_2O formation rate, we find that the trend for the H_2O formation rate is similar to that of the WGS reaction rate in both groups. Since the WGS reaction rate is independent of the partial pressure of CO, and follows a trend similar to that of the H_2O formation rate, we postulate that the WGS reaction rate might be proportional to the concentration of H_2O under the conditions of the iron-based catalysts low-temperature FTS.

5.5 Conclusions

To investigate the effect of CO_2 on an iron-based catalyst under low-temperature FTS conditions, we conducted two groups of experiments, both with the same constant total synthesis pressure of 20 bar gauge, a flow rate of 60

mL(NTP)/(min·gcat), and a temperature of 250 ^oC. In Group A, we mixed two feed gases, H_2:CO:CO_2 = 2:1:0 and H_2: CO:CO_2 = 3:0:1, in different proportions to vary the ratio of CO, CO_2, and H_2 stoichiometrically, with the ratio of $H_2/(2CO+3CO_2)$ equal to 1. In Group B, we used another pair of feed gases, H_2:CO:CO_2 = 1:1:0 and H_2: CO:CO_2 = 1:0:1, in differing proportions to vary the partial pressure of CO and CO_2, with a fixed H_2 partial pressure and a ratio of $H_2/(CO+CO_2)$ that equaled 1.

Using the operation conditions described above, we found that both CO and CO_2 were readily hydrogenated when the feeds contain either H_2/CO or H_2/CO_2. The data showed that, even with a high CO_2 mole fraction in the $H_2/CO/CO_2$ mixture feed, the conversion of CO_2 was negative, which indicated that CO_2 was formed rather than consumed, and that CO_2 could be converted to hydrocarbons only when there was a very high concentration of CO_2 and correspondingly low proportion of CO in the feed gas. However, the reactivity for CO_2 hydrogenation was lower and produced more CH_4-rich short chain paraffins than was the case with CO hydrogenation. The effect of the changes in the partial pressures of CO, H_2, and CO_2 in the feed gas on the formation of paraffins and olefins were different. The O/P ratio increased significantly with an increase in the ratio of P_{CO}/P_{H_2} in the tailgas for $H_2/CO/CO_2$ mixtures during FTS..

The experimental results showed that when the conversion of CO_2 achieved negative values, both, the FT and the WGS reaction rates were fairly constant and independent of the ratio of $CO_2/(CO+CO_2)$.

When we compared the experimental data we obtained from the thermodynamic calculations for the WGS reaction under each of the reaction conditions, we find that that although the WGS reaction is far from the thermodynamic equilibrium under low-temperature FTS with an iron catalyst, its equilibrium limitation determines whether CO can be converted to CO_2 or CO_2 to CO. Since the WGS

reaction rate was independent of the partial pressures of CO_2 and CO, and it followed a trend similar to that of the H_2O formation rate, we postulate that the WGS reaction rate is directly proportional to the concentration of H_2O under the condition of low-temperature FTS over an iron-based catalyst.

In FTS experiments using an iron-based catalyst and wide ranges of $H_2/CO/CO_2$ mixtures for the feed, we found that the hydrocarbon product formation rate achieved fairly constant values that were similar to those for typical FT (i.e., CO hydrogenation). The results could have implications for the design of XTL processes that use iron-based catalysts, in that it might prove advantageous to keep some CO_2 in the syngas feed to the FTS process. With concerns about global warming and problems with disposing CO_2, there is a demand for new ways to hydrogenate CO_2 in order to produce fuels and chemicals by using iron-based FT catalysts.

References

[1] Anderson, R. B. (1984), The Fischer-Tropsch synthesis, Academic Press, Orlando, Florida.

[2] Dry, M. E. (2002), The Fischer-Tropsch process: 1950–2000, Catalysis Today, 71, 227–241.

[3] Schulz, H. (1999), Short history and present trends of Fischer-Tropsch synthesis, Applied Catalysis A: General, 186, 3–12.

[4] Mukoma, P., Hildebrandt, D. and Glasser, D. (2006), A process synthesis approach to investigate the effect of the probability of chain growth on the efficiency of Fischer-Tropsch synthesis, Industrial and Engineering Chemistry Research, 45, 5928–5935.

[5] Davis, B. H. (2007), Fischer-Tropsch Synthesis: Comparison of performances of iron and cobalt catalysts, Industrial and Engineering Chemistry Research, 46, 8938–8945

[6] Williams, R. H., Larson, E. D., Liu, G. and Kreutz, T. G. (2009), Fischer-Tropsch fuels from coal and biomass: Strategic advantages of once-through ("polygeneration") configurations, Energy Procedia, 1, 4379–4386.

[7] Higman, C. and Burgt. M. G. (2003), Gasification, Guif Professional Publishing, Burlington.

[8] Haryanto, A., Fernando, S. D., Pordesimo, L. O. and Adhikari, S. (2009), Upgrading of syngas derived from biomass gasification: A thermodynamic analysis, Biomass and bioenergy, 33, 882–889.

[9] Riedel, T. and Schaub, G. (2003), Low-temperature Fischer-Tropsch synthesis

on cobalt catalysts-effects of CO_2, Topics in Catalysis, 26, 145−156.

[10] van der Laan, G. P. and Beenackers, A. A. C. M. (1999), Kinetics and selectivity of the Fischer-Tropsch synthesis: a literature review, Catalysis Reviews, Science and Engineering, 41, 255–318.

[11] Rao, V. U. S., Stiegel, G. J., Cinquegrane, G. J. and Srivastava, R. D. (1992), Iron-based catalysts for slurry-phase Fischer-Tropsch process: Technology review, Fuel Processing Technology, 30, 83–107.

[12] Luo, M., Hamdeh, H. and Davis, B. H. (2009), Fischer-Tropsch synthesis catalyst activation of low alpha iron catalyst, Catalysis Today, 140, 127–134.

[13] van der Laan, G. P. and Beenackers, A. A. C. M. (2000), Intrinsic kinetics of the gas-solid Fischer-Tropsch and water gas shift reactions over a precipitated iron catalyst, Applied Catalysis A: General, 193, 39–53.

[14] Pour, A. N., Housaindokht, M. R., Tayyari, S. F. and Zarkesh, J. (2010), Kinetics of the water-gas shift reaction in Fischer-Tropsch synthesis over a nano-structured iron catalyst, Journal of Natural Gas Chemistry, 19, 362–368.

[15] Botes, F. G. (2007), Water-gas-shift kinetics in the iron-based low-temperature Fischer-Tropsch synthesis, Applied Catalysis A: General, 328, 237–242.

[16] Riedel, T., Claeys, M., Schulz, H., Schaub, G., Nam, S., Jun, K., Choi, M., Kishan, G. and Lee, K. (1999), Comparative study of Fischer-Tropsch synthesis with H_2/CO and H_2/CO_2 syngas using Fe- and Co-based catalysts, Applied Catalysis A: General, 186, 201–213.

[17] Dry, M. E., in: Anderson, J. R. and Boudart, M. (Eds.), (1981), Catalysis science and technology, Springer, Berlin, 1, 159–255.

[18] Zhang, K., Kogelschatz, U. and Eliasson, B. (2001), Conversion of greenhouse gases to synthesis gas and higher hydrocarbons, Energy & Fuels, 15, 395–402.

[19] Halmann, M. (1993), Chemical fixation of carbon dioxide: Methods for recycling CO_2, CRC Press: Boca Raton, FL.

[20] Perez-Alonso, F. J., Ojeda, M., Herranz, T., Rojas, S., Gonzalez-Carballo, J. M., Terreros, P. and Fierro, J. L. G. (2008), Carbon dioxide hydrogenation over Fe-Ce catalysts, Catalysis Communications, 9 , 1945–1948.

[21] Fiato, R. A., Iglesia, E., Rice G. W. and Soled, S. L. (1998), Iron catalyzed CO_2 hydrogenation to liquid hydrocarbons, Studies in Surface Science and Catalysis, 114, 339–344.

[22] Xu, L., Bao, S., Houpt, D. J., Lambert, S. H., Davis, B. H. (1997), Role of CO_2 in the initiation of chain growth and alcohol formation during the Fischer-Tropsch synthesis, Catalysis Today, 36, 347–355.

[23] Weatherbee, G. D. and Bartholomew, C. H. (1984), Hydrogenation of CO_2 on group VIII metals, Journal of Catalysis, 77, 352–362.

[24] Lee, J. F., Chern, W. S. and Lee, M. D. (1992), Hydrogenation of carbon dioxide on iron catalyst doubly promoted with manganese and potassium, Canadian Journal of Chemical Engineering, 70, 511–515.

[25] Herranz, T., Rojas, S., Perez-Alonso, F. J., Ojeda, M., Terreros, P. and Fierro, J. L. G. (2006), Hydrogenation of carbon oxides over promoted Fe-Mn catalysts prepared by the microemulsion methodology, Applied Catalysis A: General, 311, 66–75.

[26] Dry, M. E. (1996), Practical and theoretical aspects of the catalytic

Fischer-Tropsch process, Applied Catalysis A: General, 138, 319–344.

[27] Liu, Y., Zhang, C., Wang, Y., Li, Y., Hao, X., Bai, L., Xiang, H., Xu, Y., Zhong, B. and Li, Y. (2008), Effect of co-feeding carbon dioxide on Fischer–Tropsch synthesis over an iron-manganese catalyst in a spinning basket reactor, Fuel Processing Technology, 89, 234–241.

[28] Soled, S.L., Iglesia, E., Miseo, S., DeRites, B.A. and Fiato, R. A. (1995), Selective synthesis of a-olefins on Fe-Zn Fischer-Tropsch catalysts, Topics in Catalysis, 2, 193–205.

[29] Ando, H., Matsumura, Y. and Souma, Y. (2000), A comparative study on hydrogenation of carbon dioxide and carbon monoxide over iron catalyst, Journal of Molecular Catalysis A: Chemical, 154, 23–29.

[30] Krishnamoorthy, S., Li, A. and Iglesia, E. (2002), Pathways for CO_2 formation and conversion during Fischer-Tropsch synthesis on iron-based catalyst, Catalysis Letters, 80, 77–86.

[31] Fujlwara, M., Kieffer, R., Ando, H., Qiang X. Q. and Souma, Y. (1997), Change of catalytic properties if Fe-ZnO/zeolite composite catalyst in the hydrogenation of carbon dioxide, Applied Catalysis A: General, 154, 87–101.

[32] Niemela, M. and Nokkosmaki, M. (2005), Activation of carbon dioxide on Fe-catalysts, Catalysis Today, 100, 269–274.

[33] Li, J. (1999), The preparation, characterization and evaluation of boronmodified Co/TiO_2 Fischer-Tropsch catalysts, PhD thesis, University of the Witwatersrand, Johannesburg, South Africa.

[34] Visconti, C. G., Lietti, L., Tronconi, E., Forzatti, P., Zennaro, R. and Finocchio, E. (2009), Fischer-Tropsch synthesis on a Co/Al_2O_3 catalyst with CO_2

containing syngas, Applied Catalysis A: General, 355, 61–68.

[35] Zagli, E. and Falconer, J. L. (1981), Carbon dioxide adsorption and methanation on ruthenium, Journal of Catalysis, 69, 1–8.

[36] Dry, M. E. (1976), Advances in Fischer-Tropsch chemistry, industrial and engineering chemistry product research and development, 15, 282–286.

[37] Kuipers, E. W., Vinkenburg, I. H. and Oosterbeek, H. (1995), Chain length dependence of a-olefin re-adsorption in Fischer-Tropsch synthesis, Journal of Catalysis, 152, 137–146.

[38] Shi, B. and Davis, B. H. (2005), Fischer-Tropsch synthesis: The paraffin to olefin ratio as a function of carbon number, Catalysis Today, 106, 129–131.

6

FISCHER-TROPSCH SYNTHESIS USING $H_2/CO/CO_2$ SYNGAS MIXTURES OVER COBALT AND IRON BASED CATALYSTS: A QUASI-EQUILIBRIUM MODEL TO DESCRIBE OLEFIN AND PARAFFIN PRODUCT DISTRIBUTIONS

This work has been prepared in the form of a paper for future publication.

Abstract

As part of our investigation into Fischer-Tropsch synthesis (FTS) product selectivity, we introduced quasi thermodynamic equilibrium assumptions for each of three adjacent olefins ($O_{(n-1)}$, $O_{(n)}$ and $O_{(n+1)}$) and paraffins ($P_{r,(n-1)}$, $P_{r,(n)}$ and $P_{r,(n+1)}$). In a triangular plot we compared the thermodynamic equilibrium calculations against the results (that is, the products) obtained from FTS experiments using wide ranges of $H_2/CO/CO_2$ mixtures over both cobalt- and iron-based catalysts. This enabled us to show that most of the experimental results were quite close to those arrived at through thermodynamic calculations. We therefore postulated that both paraffin and olefin products may achieve quasi-equilibrium during FTS. Accordingly, we proposed a new simple model, designated "the quasi-equilibrium product distribution model", to predict olefin and paraffin product distributions in FTS. The new model is in many ways consistent with those obtained experimentally, further it can also explain the deviations between C_1 and C_2 components successfully. It is therefore possible to use thermodynamic equilibrium to describe olefin and paraffin product distribution in FTS.

6.1 Introduction

Fischer-Tropsch synthesis (FTS) is a process that produces clean transportation fuels and chemicals from synthesis gas (syngas). The most active metals for FTS are iron, cobalt and ruthenium. Catalysts based on iron or cobalt are those most commonly used for FTS on an industrial scale [1−2]. The syngas, which is produced from coal or biomass gasification, consists of H_2, CO, CO_2 and CH_4 [3−4]. The proportion of CO_2 in the raw syngas varies from 1% to 30%, as the amount required is dependent on many factors such as gasifier type, operating conditions, gasifying agents, and feedstock properties [3−4]. The research described in this thesis investigates the reaction pathways for FTS using H_2/CO/CO_2 syngas mixtures over both iron- and cobalt-based catalysts.

Because the impact of CO_2 on the environment through the greenhouse effect is now a matter of international concern, the utilization of CO_2 as a raw material has become of interest to scientists [5–6]. Various attempts have been made to transform CO_2 into hydrocarbons, mainly using those catalysts that have proven to be active for FTS, but many aspects of this process remain unexplained [7–8]. A number of researchers have studied the hydrogenation of CO, CO_2 and mixtures of the two under FTS reaction conditions [9–13], and the data they have reported indicates that FTS with CO_2 or CO_2 rich feed gas leads to products that consist mainly of methane-rich light saturated hydrocarbons [10–13].

The Anderson-Schulz-Flory (ASF) distribution model has been used with consistent success to describe the product distribution obtained from FTS [14]. This model postulates that the formation of hydrocarbon chains is a stepwise polymerization procedure, and assumes that the chain growth probability (α) is independent of the carbon number [15], which can be expressed as Equation (6.1):

$$m_n = (1-\alpha)\alpha^{n-1} \tag{6.1}$$

where *n* is the number of carbon atoms in the chain, m_n is the mole fraction of all the species having n carbon atoms, and α is the chain growth probability factor. According to the equation, a plot of $log(m_n)$ versus *n* should give a straight line. The value of α is obtained from the slope of the plot. A higher α value indicates that a higher mole fraction of long chain hydrocarbons should be expected.

However, when FTS takes place over most iron and cobalt catalysts, deviations from the ideal ASF distribution can be observed [15–19]. The most significant of these are: (1) a relatively high yield of methane [20–24]; (2) a relatively low yield of ethane [20, 21, 24, 25]; and (3) a distinct change in the slope of the line between carbon numbers 8–12 [26–28].

Some researchers [26, 28, 29] believe that these deviations are predominantly caused by secondary reactions of α-olefins, which may re-adsorb on the growth sites of the catalyst surface, and continue to grow via propagation with monomers or terminate as hydrocarbon products. However, experiments with co-feeding of ethene and 1-alkenes have shown that these deviations are not attributable to α-olefin re-adsorption, but are the consequence of two different mechanisms of chain growth that cause a superposition of two ASF distributions [30–31]. Furthermore, Huyser *et al.* [27] reported that the total product spectrum is a combination of two distinct sets of products formed as a result of either two different mechanisms (for instance, two different reactive intermediates) or two different catalytic surfaces, each producing a different product spectrum. Other researchers have noted similar findings [18, 32]. However, none of these explanations has been sufficiently comprehensive to cover the full range of product distributions that have been obtained experimentally. In particular, the deviations in C_1 and C_2 components have not been accounted for.

Most attempts to describe FT product distributions have a kinetic basis. Relatively few researchers have explained the product distribution in terms of

thermodynamic considerations [33 - 35]. The aim of this chapter is to develop and test a new quasi-equilibrium approach to the FTS product distribution to explain the deviations from the ASF distribution model. It is based on the results obtained from FTS experiments carried out under typical operating conditions, using $H_2/CO/CO_2$ syngas mixtures over cobalt- and iron-based catalysts.

6.2 Methodology

6.2.1 Assumptions

Harvey *et al*. [34] conducted research into the product distribution of FTS in the hope of establishing some connection between the distribution trends and thermodynamic equilibrium. However, their analysis of thermodynamic equilibrium overall predicted a product for the FTS reaction that was predominantly methane. Although the FT product distribution may not be described by thermodynamic equilibrium in any universal sense, there may be aspects of it that can be explained in terms of quasi-equilibrium. Recently Masuku *et al*. [33] have postulated that a quasi-equilibrium is set up among the α-olefins, and the experimental results obtained by Lu *et al.*[35] have suggested that the olefin distribution in FTS might be attributable to thermodynamic equilibrium.

FTS produces hydrocarbons and oxygenates with a broad range of chain lengths and functional groups. The most dominant products are linear hydrocarbons, including paraffins and olefins [36–40]. For simplicity of simulation, we have focused on linear paraffins and olefins in our research. Basing our investigation on work previously published in the scientific literature [33–35] and our own experimental results, we adopted a set of assumptions that would enable us to develop a new quasi-equilibrium approach to explaining the FTS product distribution. These are:

(1) α-olefins and n-paraffins are the hydrocarbon products of FTS;

(2) all the products are in the gas phase;

(3) an equilibrium distribution is set up between the α-olefins, as expressed in Reaction (a):

$$C_{i-1}H_{2(i-1)} + C_{i+1}H_{2(i+1)} = 2C_iH_{2i} \quad \text{(a)}$$

(4) an equilibrium distribution is also set up between the n-paraffins, as described in Reaction (b):

$$C_{j-1}H_{2(j-1)+2} + C_{j+1}H_{2(j+1)+2} = 2C_jH_{2j+2} \quad \text{(b)}$$

where i and j present the number of carbon atoms in the chain (i≥3 and j≥2).

6.2.2 Product distribution as plotted in a triangular area

Assuming that there are three components (A, B and C), which are all in the gas phase and follow the equilibrium Reaction (c) below, we can describe it as:

$$A + C = 2B \quad \text{(c)}$$

The mole fraction of each component is defined as:

- the nonmaterial mole fraction of A in the 3 components is Equation (6.2):

$$X_A = \frac{P_A}{P_A+P_B+P_C} \quad (6.2)$$

where P is the partial pressure of the component

- the nonmaterial mole fraction of B in the 3 components is Equation (6.3):

$$X_B = \frac{P_B}{P_A+P_B+P_C} \quad (6.3)$$

- the nonmaterial mole fraction of C in the 3 components is expressed in Equation (6.4):

$$X_C = \frac{P_C}{P_A + P_B + P_C} \tag{6.4}$$

From Equations (6.2–6.4), we can get Equation (6.5)

$$X_A + X_B + X_C = 1 \tag{6.5}$$

The values of X_A, X_B and X_C can be plotted in a triangular area, which is illustrated in Figure 6.1. Each corner of the triangle assumes that the nonmaterial mole fraction of the component to which it refers is equal to 1.

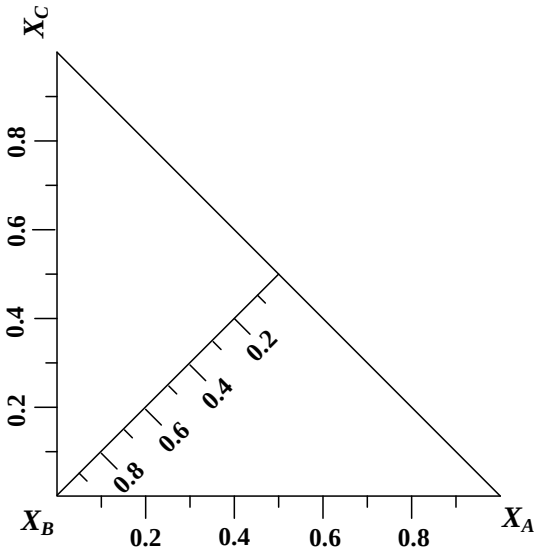

Figure 6.1: Schematic presentation of the triangular area representing the normalized mole fractions of 3 species – A, B, and C.

Because Reaction (c) is assumed to reach equilibrium, the equilibrium constant for this reaction can be calculated by the partial pressure of each of the components in the experimental results as Equation (6.6):

$$K_{experimental,Reaction(c)} = \frac{(P_B)^2}{P_A P_c} \tag{6.6}$$

The equilibrium constant is determined from the Van't Hoff expression given by two equations:

$$K_{equilibrium} = exp[\frac{-\Delta G(T)}{RT}] \quad (6.7)$$

and $$\frac{d\ln[K_{equilibrium}(T)]}{dT} = \frac{\Delta H(T)}{RT^2} \quad (6.8)$$

The Gibbs Free Energy and enthalpy of formation involved in each reaction can be evaluated from the standard energy of formation of each compound using the following two thermodynamic equations:

$$\Delta G(T) = \sum \Delta G^{O}_{products} - \sum \Delta G^{O}_{reactants} \quad (6.9)$$

$$\Delta H(T) = \sum \Delta H^{O}_{products} - \sum \Delta H^{O}_{reactants} \quad (6.10)$$

We can then use Equations (6.7–6.10) to calculate the temperature dependency of the equilibrium constant under each of the reaction conditions.

Assuming that Reaction (c) reaches equilibrium, we obtain:

$$K_{experimental,Reaction(c)} = K_{equilibrium,Reaction\,(c)} \quad (6.11)$$

Substituting Equations (6.2–6.5) and (11) into Equation (6.6), we obtain:

$$K_{equilibrium,Reaction(c)} = \frac{(1 - X_A - X_C)^2}{X_A X_C} \quad (6.12)$$

Since the equilibrium constant is fixed under typical reaction conditions, Equation (6.12) indicates that X_C is a function of X_A under the constraint of (X_A+X_B+X_C=*1*). Because the form of Reactions (a) and (b) are the same as that of Reaction (c), the following expressions can be obtained:

- For Reaction (a):

$$K_{equilibrium,Reaction(a)_{(i)}} = \frac{(1-X_{O_{(i-1)}}-X_{O_{(i+1)}})^2}{X_{O_{(i-1)}}X_{O_{(i+1)}}} \quad (6.13)$$

$$X_{O_{(i-1)}} + X_{O_{(i)}} + X_{O_{(i+1)}} = 1 \quad (6.14)$$

- For Reaction (b):

$$K_{equilibrium,Reaction(b)_{(j)}} = \frac{(1-X_{P_{r,(j-1)}}-X_{P_{r,(j+1)}})^2}{X_{P_{r,(j-1)}}X_{P_{r,(j+1)}}} \quad (6.15)$$

$$X_{P_{r,(j-1)}} + X_{P_{r,(j)}} + X_{P_{r,(j+1)}} = 1 \quad (6.16)$$

where O represents olefin and P_r refers to paraffin. Using Equations (6.13–6.16), we can then plot the relationships among each three of the adjacent olefin or paraffin products of FTS in the triangular area. More detailed information will be provided in Section 6.4 of this chapter.

6.3 Experimental

6.3.1 Cobalt catalyst

6.3.1.1 Catalyst preparation

The Co/TiO_2 catalyst used in this study was prepared by impregnating TiO_2 with a cobalt nitrate solution. TiO_2 (Degussa P25) was mixed with distilled water in a mass ratio of 1:1 and dried in air at 120 ℃ for 1 hour. The support was then calcined in air at 400 ℃ for 16 hours [41]. Thereafter, the support was crushed and sieved, and the particles with diameters between 0.5 and 1 mm were retained for use. The support was then impregnated with sufficient cobalt nitrate ($Co(NO_3)_2{\cdot}6H_2O$) solution to give it a cobalt metal loading of 10% by mass. Next, the support was

dried in air at 120 ℃ for 16 hours and then calcined in air at 400 ℃ for 6 hours to decompose and transform from cobalt nitrate to cobalt oxide.

6.3.1.2 Experimental set-up and procedure

6.3.1.2.1 Catalyst reduction

We loaded 1 g of catalyst into the micro fixed bed reactor (FBR), and performed the reduction with H_2 (Afrox (African Oxygen) Ltd., 99.999%) at atmospheric pressure for 24 hours. The reduction temperature and the flow rate were 350 ℃ and 60 ml(NTP)/(min gcat), respectively.

Table 6.1: Summary of experimental conditions for FTS using H_2/CO/CO_2 mixtures over cobalt- and iron-based catalysts.

	Cobalt-based catalyst				Iron-based catalyst			
Temperature (℃)	200				250			
Total pressure (bar gauge)	20				20			
Flow rate (ml(NTP)/(min gcat)	60				60			
	Partial pressure at entrance (bar)				Partial pressure at entrance (bar)			
Run	P_{H_2}	P_{CO}	P_{CO_2}	P_{N_2}	P_{H_2}	P_{CO}	P_{CO_2}	P_{N_2}
1	14.2	0.0	4.8	2.1	14.2	0.0	4.8	2.1
2	13.9	0.5	4.2	2.0	14.0	0.6	4.3	2.0
3	13.8	1.3	3.9	2.0	13.8	1.3	3.8	2.1
4	13.7	1.9	3.3	2.1	13.6	2.0	3.3	2.1
5	13.3	2.4	2.8	2.0	13.4	2.5	2.9	2.1
6	13.2	3.2	2.3	2.1	13.2	3.2	2.4	2.1
7	13.1	3.8	1.9	2.1	13.1	3.9	1.9	2.1
8	13.0	4.3	1.5	2.1	13.0	4.5	1.5	2.1
9	12.9	4.9	0.9	2.1	12.7	5.2	1.0	2.1
10	12.7	5.6	0.4	2.1	12.6	5.8	0.5	2.1
11	12.5	6.3	0.0	2.2	12.4	6.4	0.0	2.1

6.3.1.2.2 FTS using $H_2/CO/CO_2$ syngas

Once the reduction was completed, we allowed the reactor to cool down to room temperature. We introduced the CO_2 syngas (or CO_2 feed), composed of H_2:CO:CO_2 = 3:0:1, with 10 vol.% of N_2 to act as an internal standard for mass balance calculations, into the reactor, beginning with a flow rate of 60 ml(NTP)/(min gcat). The reactor pressure was slowly increased to 20 bar (gauge) and then the temperature was gradually increased to 200 ℃. The pressure and temperature were allowed to stabilize, and the operating conditions were kept constant for 72 hours while the tail gas composition was monitored. Thereafter, the flow rate of the CO_2 syngas was decreased by 10%, that is 6 ml(NTP)/(min gcat). At this point we introduced the CO syngas (the CO feed), comprising H_2:CO:CO_2 = 2:1:0 with 10 vol.% N_2 as an internal standard for mass balance calculations, into the reactor, maintaining a flow rate of 6 ml(NTP)/(min gcat)) so as to keep it constant at 60 ml(NTP)/(min gcat). The new reaction conditions were maintained for 72 hours, while the tail gas composition was monitored. Afterwards we decreased the flow rate of the CO_2 mixture and raised that of the CO mixture, while keeping the total flowrate of gas to the reactor constant at 60 ml(NTP)/(min gcat). The feed and reaction conditions for the 11 experiments over the cobalt-based catalyst are shown in Table 6.1.

6.3.2 Iron catalyst

6.3.2.1 Catalyst preparation

The Fe/TiO_2 catalyst was prepared by impregnating the support with an iron nitrate ($Fe(NO_3)_3$ $9H_2O$) solution by a single-step incipient wetness process, using the same procedure as that for the cobalt catalyst. For a more detailed description, refer to the Co catalyst preparation described earlier.

6.3.2.2 Experimental set-up and procedure

6.3.2.2.1 Catalyst reduction

A quantity of 1g of catalyst was loaded into the micro FBR. The reduction was performed at atmospheric pressure by H_2 (Afrox (African Oxygen) Ltd., 99.999%) for 24 hours. The reduction temperature and the flow rate were 350 ℃ and 60 ml/min, respectively.

6.3.2.2.2 FTS using $H_2/CO/CO_2$ syngas

FTS experiments over iron based catalysts were carried out in a micro FBR. The operating procedures were those outlined in Section 6.3.1.2.2. The only difference was that the operating temperature for the iron catalyst was set at 250 ℃, whereas for cobalt it was 200 ℃. The process conditions for an iron-based catalyst are shown in Table 6.1.

6.3.3 Product analysis

The tail gas was analyzed every 1.5 hours using an online DANI GC. Two thermal conductivity detectors (TCD) were used for H_2, N_2, CO, CO_2 and CH_4 and a flame ionization detector (FID) for the gas phase hydrocarbons. The wax and liquid products were collected in a hot trap (kept at 150 ℃) and cold trap (maintained at room temperature). The analysis of the oil and wax products was performed at the end of the mass balance for each run, using an off-line GC.

6.4 Results

To calculate the product distribution that would result from quasi-equilibrium under operating conditions typical of the FTS process, we assumed that both paraffin and olefin products approach equilibrium in each of the three adjacent

species. This has already been described in Section 6.2 as Reaction (a) for olefins and Reaction (b) for paraffins. This makes it possible for us to plot the product distribution for each of the three adjacent homologous products in a triangular area, using the results derived from the thermodynamic equilibrium calculations (Equations (6.13–6.16)).

Using the series of low-temperature FTS experiments over cobalt- and iron-based catalysts with a wide range of $H_2/CO/CO_2$ syngas mixtures, under the reaction conditions shown in Table 6.1, we were able to calculate the mole fraction of the products for each of the three adjacent homologous species using Equations (6.2–6.4). The experimental results could also be illustrated in the same triangular area on which the thermodynamic equilibrium calculations were plotted. Having done this, we could compare the thermodynamic equilibrium calculations and the experimental results analysis.

6.4.1 Cobalt catalyst

6.4.1.1 Product formation rate

Eleven experiments were carried out in the FBR over a cobalt-based catalyst with the same constant total synthesis pressure of 20 bar gauge, a flow rate of 60 mL(NTP)/(min·gcat), and a temperature of 200 ℃. The CO_2 feed was gradually replaced by CO feed from Runs 1 to 11 (See Table 6.1). Figures 6.2 and 6.3 show the rates of formation of the light olefins and paraffins under the reaction conditions as shown in Table 6.1 for a cobalt-based catalyst. The olefin rate rose as the run numbers 1 to 11 increased. However, a different trend could be observed in the rates of formation for the paraffins, and the points at which they reached their maxima (Figure 6.3). The data indicate that CO_2-rich feeds produce more saturated paraffin products than CO-rich feeds.

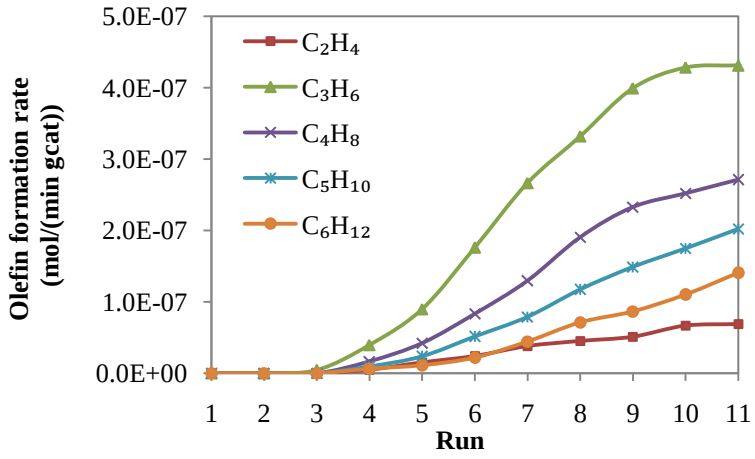

Figure 6.2: The olefin formation rate for 11 runs under the reaction conditions shown in Table 6.1 for FTS over a cobalt-based catalyst.

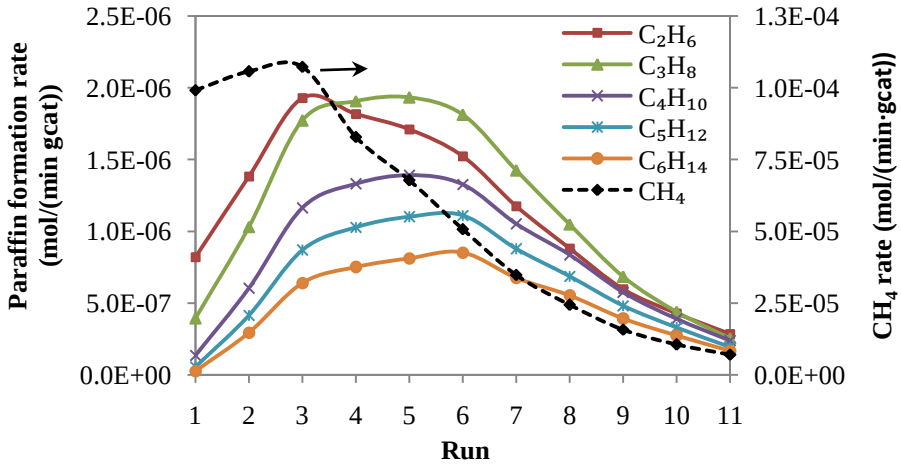

Figure 6.3: The paraffin formation rate for 11 runs under reaction conditions as shown in Table 6.1 for FTS over a cobalt-based catalyst.

6.4.1.2 Comparison between the thermodynamic equilibrium calculations and the experimental results in a triangular area

The triangular area was used to plot both the thermodynamic equilibrium calculations and those relating to the experimental results for each of the three adjacent homogenous products. Figure 6.4 shows the comparison between the two calculations for olefin products (reaction conditions as shown in Table 6.1 over a

cobalt-based catalyst). Figure 6.4 (a) indicates that the experimental results for the relationship of X_{O_2}, X_{O_3} and X_{O_4} is close to the thermodynamic equilibrium curve. It is notable that the results from the group of X_{O_3}, X_{O_4} and X_{O_5} (Figure 6.4 (b)) and the group of X_{O_4}, X_{O_5} and X_{O_6} (Figure 6.4 (c)) reveal a remarkable agreement between the thermodynamic results and the experimental data.

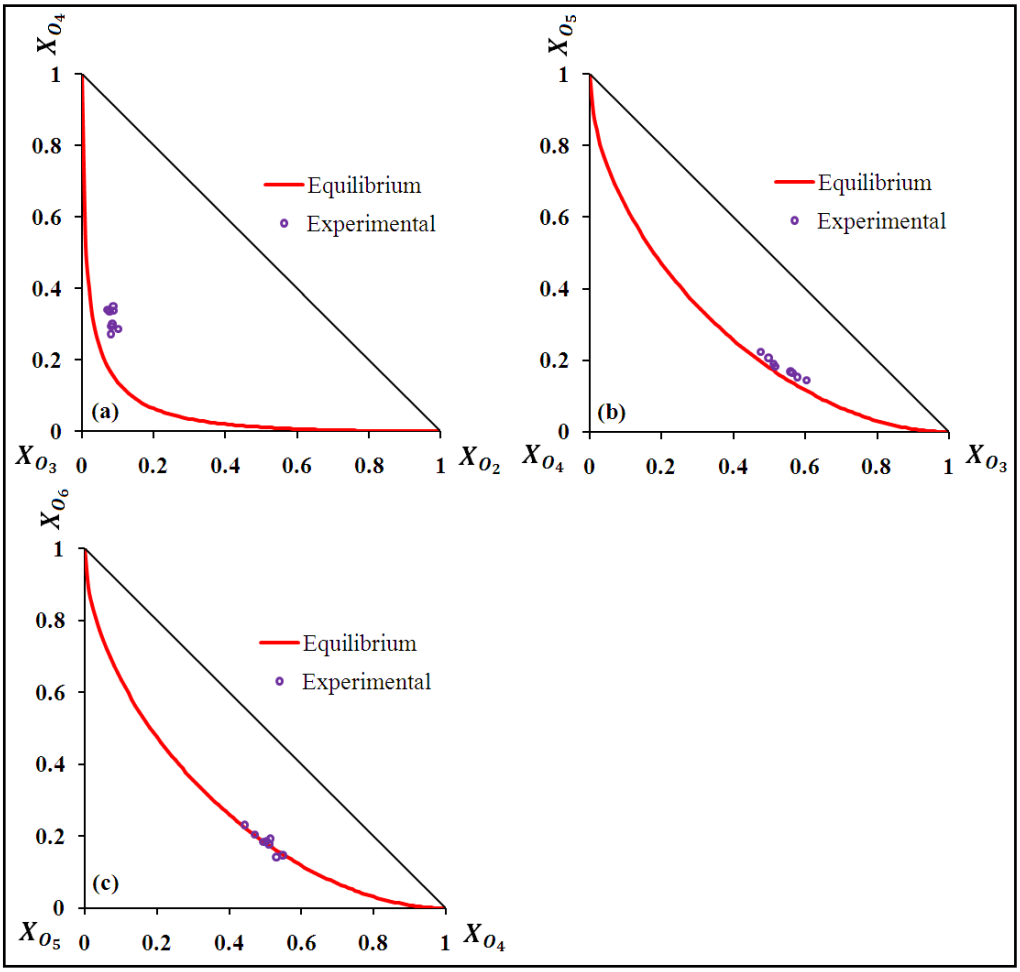

Figure 6.4: Comparison between the thermodynamic equilibrium calculations and the experimental results for olefin products over a cobalt-based FTS (reaction conditions as shown in Table 6.1).

A comparison between the thermodynamic equilibrium calculations and the experimental results for each of the three adjacent paraffins (under reaction

conditions as shown in Table 6.1 for a cobalt-based catalyst) is given in Figure 6.5. Although most of the experimental data from the group of $X_{P_{r,1}}$, $X_{P_{r,2}}$and $X_{P_{r,3}}$ lie above the equilibrium line shown in Figure 6.5 (a) for the 11 runs (Table 6.1), the values are not far from the thermodynamic calculations. It is remarkable that the results from the group of $X_{P_{r,2}}$, $X_{P_{r,3}}$and $X_{P_{r,4}}$ (Figure 6.5 (b)), the group of $X_{P_{r,3}}$, $X_{P_{r,4}}$and $X_{P_{r,5}}$ (Figure 6.5 (c)) and the group of $X_{P_{r,4}}$, $X_{P_{r,5}}$ and $X_{P_{r,6}}$ (Figure 6.5 (c)) illustrate that the experimental data are consistent with the thermodynamic calculations.

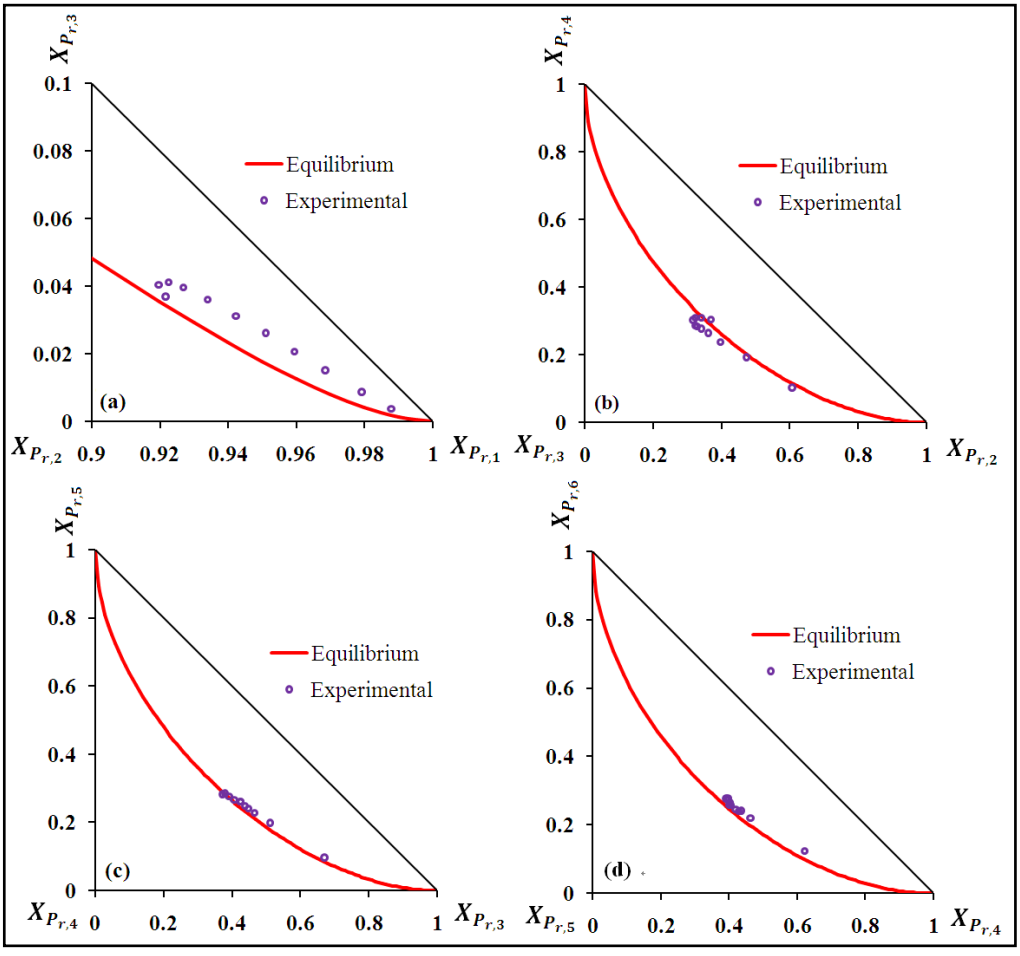

Figure 6.5: Comparison between the thermodynamic equilibrium calculations and the experimental results for paraffin products over a cobalt-based FTS (reaction conditions as shown in Table 6.1).

6.4.2 Iron catalyst

6.4.2.1 Product formation rate

The same kinds of experiments as were conducted over a cobalt-based catalyst were carried out over an iron-based catalyst, with the same constant total synthesis pressure of 20 bar gauge, a flow rate of 60 mL(NTP)/(min·gcat), and a temperature of 250 ℃. Comparing Figures 6.2 and 6.3, we can see that the data of the formation rates of light olefins (Figure 6.6) and paraffins (Figure 6.7) followed the same trend as was observed in the case of the cobalt-based catalyst:

- Olefin rates rose from runs 1 to 11.
- Paraffin rates first increased, and then, having achieved their maximum point, reduced.
- CO_2-rich feeds produced more saturate paraffin products than CO-rich feeds.

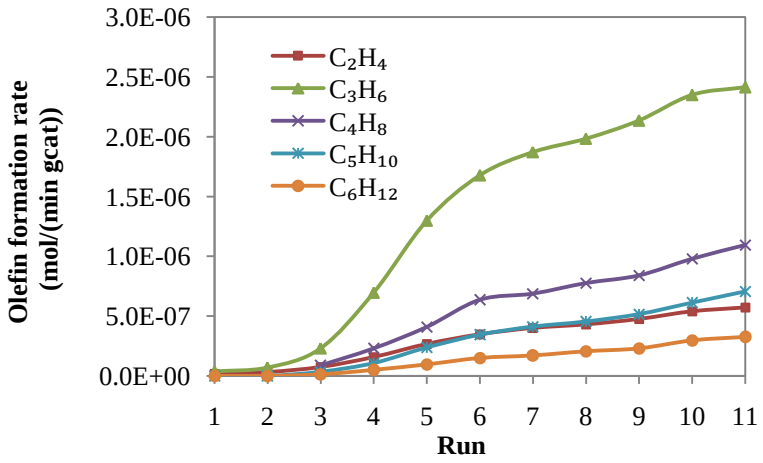

Figure 6.6: The olefin formation rate for 11 runs under the reaction conditions as shown in Table 6.1 over an iron-based catalyst.

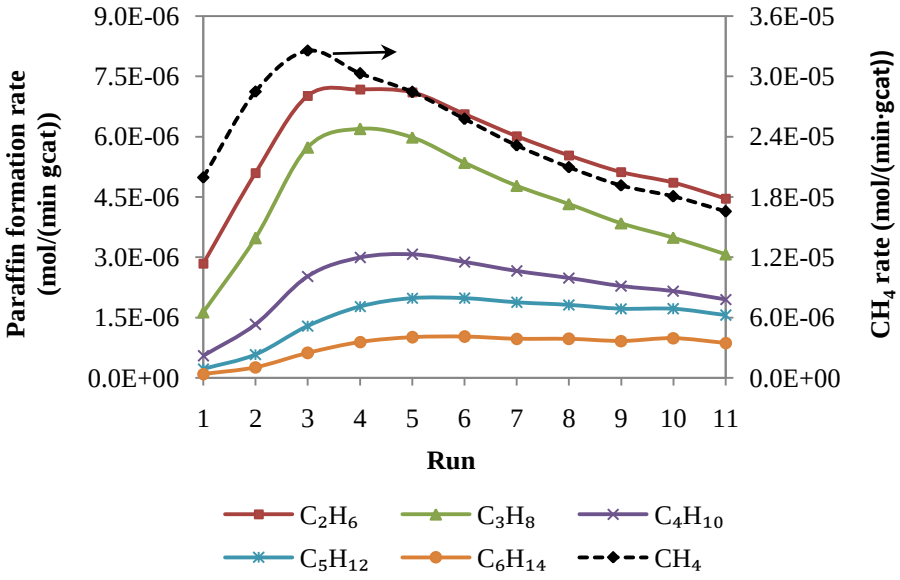

Figure 6.7: The paraffin formation rate for 11 runs under the reaction conditions as shown in Table 6.1 over an iron-based catalyst.

6.4.2.2 Comparisons between the thermodynamic equilibrium calculations and the experimental results in a triangular area

The comparison we made between the thermodynamic equilibrium calculations and the experimental results for olefin products over an iron-based catalyst is shown in Figure 6.8. There the data indicate that although the experimental results failed to reach the thermodynamic calculation curve, the experimental points were not far from the equilibrium line for the mole fraction of the three adjacent olefins (X_{O_2}, X_{O_3} and X_{O_4}), and the trend is similar to that shown in Figure 6.5 (a) for experiments over a cobalt-based catalyst. As the similar results are obtained from the cobalt-based catalyst as shown in Figure 6.4 (b-c), the results from the group of X_{O_3}, X_{O_4} and X_{O_5} (Figure 6.8 (b)) and the group of X_{O_4}, X_{O_5} and X_{O_6} (Figure 6.8 (c)) over an iron-based catalyst indicate that the experimental data for the groups of each of the three adjacent olefins with the chain length higher than 2 were quite close to the thermodynamic calculations.

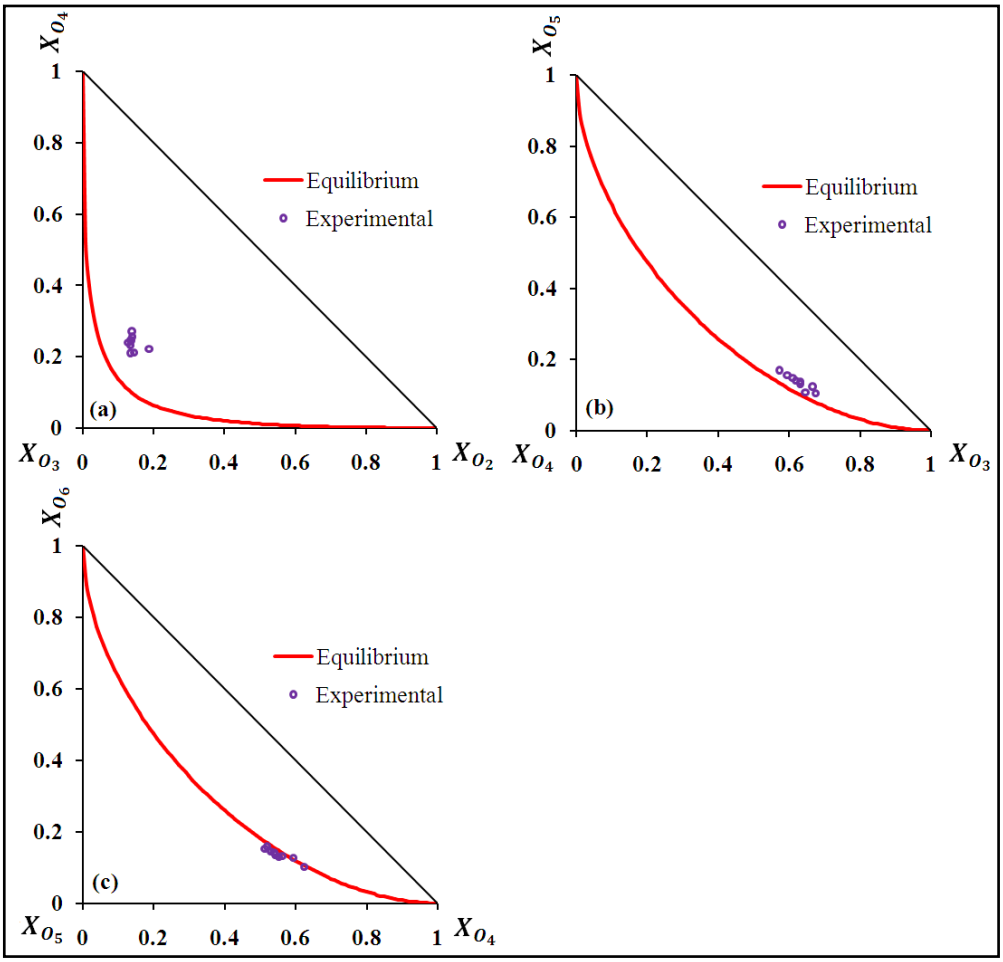

Figure 6.8: Comparison between the thermodynamic equilibrium calculations and the experimental results for olefin products over an iron-based FTS catalyst (reaction conditions as shown in Table 6.1).

Another comparison between the thermodynamic equilibrium calculations and the experimental results for each of the three adjacent paraffins is presented in Figure 6.9, which shows that all of the experimental results from the group of $X_{P_{r,1}}$, $X_{P_{r,2}}$ and $X_{P_{r,3}}$ for the 11 runs (Table 6.1) over an iron-based catalyst were below the equilibrium line. This is contrary to the results obtained from the cobalt-based catalyst, as shown in Figure 6.5 (a). The results from Figure 6.9 (b–d) indicate that the experimental data for the other groups of each of the three adjacent paraffins were quite close to the thermodynamic calculations, and the same phenomenon

was also obtained with the results of FTS over a cobalt-based catalyst (Figure 6.5 (b–d)).

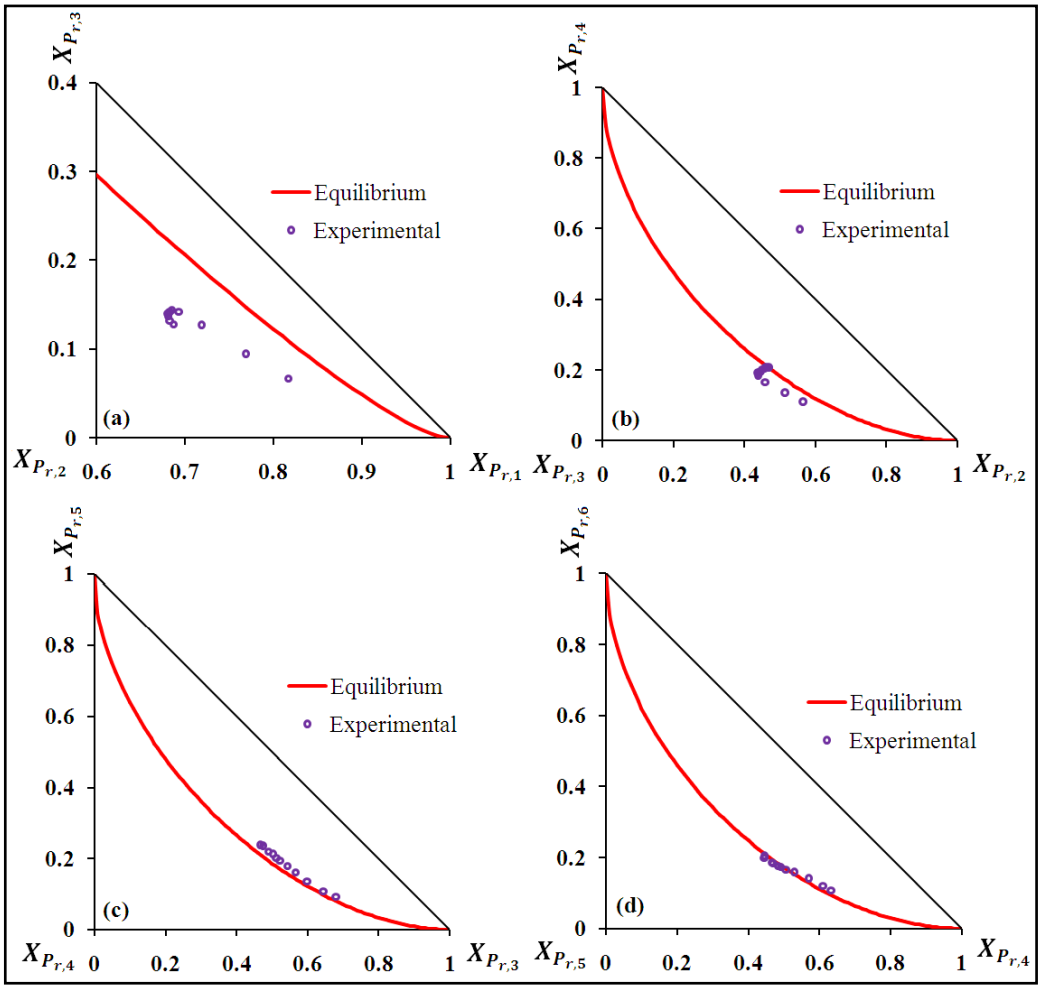

Figure 6.9: Comparison between the thermodynamic equilibrium calculations and the experimental results for paraffin products over an iron-based FTS catalyst (reaction conditions as shown in Table 6.1).

6.5 Discussion

6.5.1 Implications of the triangular area model

Because we conducted the experiments over a cobalt-based and an iron-based catalyst at 200 ℃ and 250 ℃, respectively, we plot the effect of temperature on

the thermodynamic equilibrium calculations for Reactions (a) and (b) with different carbon numbers (i=3, 4, 5 for olefin products and j=2, 3, 4, 5 for paraffin products) in Figure 6.10.

Figure 6.10 (a), which represents the olefin products, shows the following.

- The thermodynamic equilibrium line for carbon number i=3 is far different from those for i=4 and 5.
- The thermodynamic equilibrium line with carbon number i=4 is almost superimposed with that of i=5.
- The thermodynamic equilibrium line for carbon number i=3 is sensitive to temperature, as is shown by the direction of the red arrow in Figure 6.10 (a) which traces an upward trend with increasing temperature from 200 ℃ to 250 ℃.
- The thermodynamic equilibrium lines for carbon numbers i=4 and 5 are not sensitive to temperature.

Figure 6.10 (b) refers to the paraffin products, and indicates the following.

- The thermodynamic equilibrium line for carbon number j=2 is very different from the lines for j=3, 4 and 5.
- The thermodynamic equilibrium lines for carbon numbers j=3, 4 and 5 are almost superimposed.
- The thermodynamic equilibrium line for carbon number j=2 is slightly sensitive to temperature, as can be seen by the movement of the line in the direction of the red arrow in Figure 6.10 (b)) in response to the rise in the temperature from 200 ℃ to 250 ℃. This result is the opposite of that obtained for the direction of olefin products with the carbon number i=3 (See Figure 6.10 (a)).
- The thermodynamic equilibrium lines for carbon number j=3, 4 and 5 are not

sensitive to temperature.

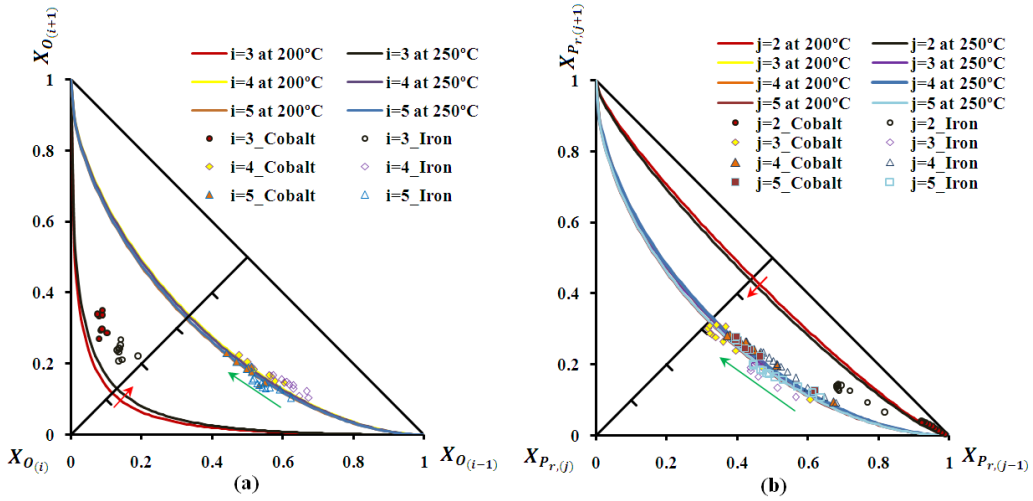

Figure 6.10: Comparison between the thermodynamic equilibrium calculations and the experimental results: (a) for each of the 3 adjacent olefin products with carbon numbers i=3, 4, 5; and (b) for each of the 3 adjacent paraffin products with carbon numbers j=2, 3, 4, 5, respectively. Reaction conditions are as listed in Table 6.1. Lines represent the results derived from the thermodynamic equilibrium calculations and symbols the results obtained from the experimental calculations.

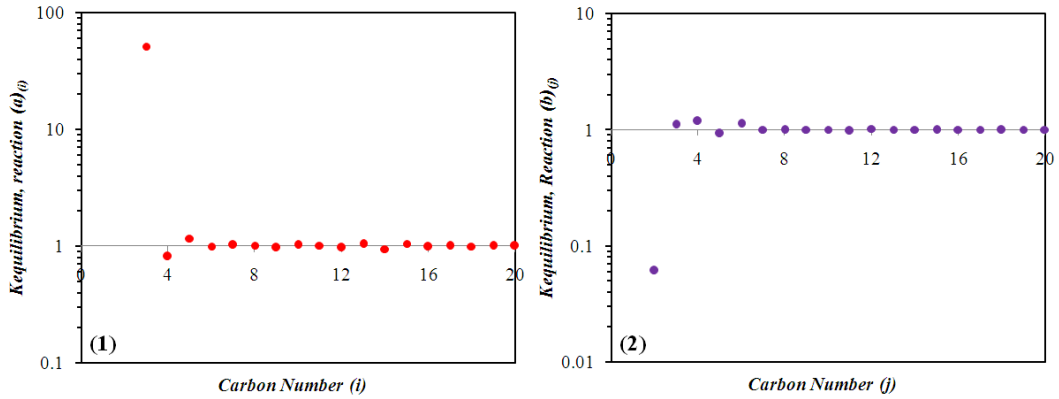

Figure 6.11: $K_{equilibrium}$ as a function of carbon number at 200 ℃: (1) for Reaction (a) with carbon number i (i>2); and (2) for Reaction (b) with carbon number j (j>1).

Figure 6.11 shows the values of the equilibrium constants with different carbon numbers for both Reactions (a) and (b). These demonstrate that: the value of

$K_{equilibrium}$ for Reaction (a) with i=3 is very different for i>3; the value of $K_{equilibrium}$ for Reaction (b) with j=2 is very different from that for j>2; and with i>3 and j>2, the value of $K_{equilibrium}$ with all the different carbon numbers is near 1. The reason for the last of these is that the values of $\Delta G(T)$ for Reactions (a) and (b) are near, or equal to, 0. Because the equilibrium lines as shown in Figure 6.10 were calculated from the equilibrium constants (Equations (6.12) and (6.15)), the results shown in Figure 6.11 can explain the phenomenon observed in Figure 6.10.

We collected all the experimental calculations for the olefin products over both cobalt (Figure 6.4) and iron (Figure 6.8) catalysts together, and put all of them into one triangular area, Figure 6.10 (a). We did the same for the paraffin products in Figure 6.10 (b). A comparison between the thermodynamic equilibrium calculations and the experimental calculations makes it possible to summarize the results as follows.

- For olefin products, the results reveal that: (1) for carbon number i=3, all the experimental results show that $X_{O_3} > X_{O_4} > X_{O_2}$, which indicates the low yield of ethene obtained; (2) for carbon numbers i=4 and 5, all the experimental results follow the direction of the green arrow shown in Figure 6.10 (a) when the CO_2 feed was gradually replaced with CO feed from Run 1 to Run 11, as shown in Table 6.1 for cobalt- and iron-based catalysts. This suggests that there is higher light olefin selectivity for CO_2-rich feeds, and the higher long chain olefin selectivity for CO-rich feeds.
- For paraffin products, the results demonstrate that: (1) for carbon number j=2, the points calculated from the experimental data are below the equilibrium line for the iron-based catalyst, but in contrast are above the equilibrium line for the cobalt-based catalyst; (2) for carbon numbers j=3, 4 and 5, all the experimental results follow the direction of the green arrow (see Figure 6.10 (b)) when the CO_2 feed was being replaced by the CO feed from Runs 1 to

Run 11 (see Table 6.1) over both cobalt- and iron-based catalysts. This indicates that CO_2-rich feeds have a higher light paraffin selectivity and the CO-rich feeds a higher long chain paraffin selectivity.

- The experimental results for both olefin and paraffin products are listed in the triangular region that created between $X_{O_{(i-1)}} > X_{O_{(i+1)}}$ (except i=3) and $X_{P_{r,(j-1)}} > X_{P_{r,(j+1)}}$.
- It is worth noting that most of the experimental results are fairly similar to those based on thermodynamic calculations of the products formed from FTS using $H_2/CO/CO_2$ mixtures over both cobalt- and iron- based catalysts.

Although the experimental data from the group of X_{O_2}, X_{O_3} and X_{O_4} and the group of $X_{P_{r,1}}$, $X_{P_{r,2}}$ and $X_{P_{r,3}}$ were not on the equilibrium line, their values were not far from the line representing the thermodynamic calculations.

6.5.2 Quasi-equilibrium product distribution model

6.5.2.1 Model description and assumptions

Having compared our experimental data and the thermodynamic calculations, we postulated that Reaction (a) for olefin products and Reaction (b) for paraffin products might reach thermodynamic equilibrium during FTS over both cobalt- and iron-based catalysts. We also assumed that all or most of the FTS products are in the gas phase.

- For olefin products:

The mole fraction of olefin products with chain length i ($i \geqslant 2$) is defined by the following Equation:

$$m_{O_{(i)}} = \frac{P_{O_{(i)}}}{\sum_{i=2}^{i=\infty} P_{O_{(i)}}} \tag{6.17}$$

Based on the proposition that Reaction (a) reaches equilibrium, we obtain:

$$K_{equilibrium,Reaction(a)} = \frac{(P_{O_{(i)}})^2}{P_{O_{(i-1)}} P_{O_{(i+1)}}} \tag{6.18}$$

Substituting Equation (6.17) to (6.18), we can arrive at:

$$K_{equilibrium,Reaction(a)} = \frac{(m_{O_{(i)}})^2}{m_{O_{(i-1)}} m_{O_{(i+1)}}} \tag{6.19}$$

and if we define:

$$k_{O_{(i)}} = \frac{P_{O_{(i)}}}{P_{O_{(i-1)}}} = \frac{m_{O_{(i)}}}{m_{O_{(i-1)}}} \tag{6.20}$$

we can easily obtain one of the calculated values of $k_{O_{(i)}}$ with a certain carbon number of i from our experimental data. Then, using Equations (6.19) and (6.20), we can predict the olefin product distribution for the other carbon numbers.

- For paraffin products:

The mole fraction of paraffin products with chain length j ($j \geqslant 2$) is defined by the following Equation:

$$m_{P_{r,(j)}} = \frac{P_{P_{r,(j)}}}{\sum_{j=1}^{j=\infty} P_{P_{r,(j)}}} \tag{6.21}$$

Based on the postulation that Reaction (b) reaches equilibrium, we obtain:

$$K_{equilibrium,Reaction(b)} = \frac{(P_{P_{r,(j)}})^2}{P_{P_{r,(j-1)}} P_{P_{r,(j+1)}}} \tag{6.22}$$

Substituting Equation (6.21) to (6.22), we can deduce:

$$K_{equilibrium,Reaction(b)} = \frac{(m_{P_{r,(j)}})^2}{m_{P_{r,(j-1)}} m_{P_{r,(j+1)}}} \tag{6.23}$$

If we define:

$$k_{P_{r,(j)}} = \frac{P_{P_{r,(j)}}}{P_{P_{r,(j-1)}}} = \frac{m_{P_{r,(j)}}}{m_{P_{r,(j-1)}}} \tag{6.24}$$

we can also easily get one of the calculated values of $k_{P_{r,(j)}}$ with a certain carbon number j from our experimental data, as for the olefin products. After that, we can apply Equations (6.23) and (6.24) to predict paraffin product distribution of the other carbon numbers. We have named the use of Equations (6.19) and (6.20) for olefin products and (23) and (24) for paraffin products for these purposes the "quasi-equilibrium product distribution model" (QPDM).

6.5.2.2 Testing the new model against experimental data

The experiments we carried out entailed FTS using H_2/CO/CO_2 mixtures over a cobalt-based catalyst, under the reaction conditions set out in Table 6.1. More detailed information on the results, such as those concerning conversion and selectivity, can be obtained from an article on our research published in 2010 [11]. Our analysis of the experimental results found that no olefin products could be detected for Runs 1, 2 and 3, and Run 4 showed less than 1% olefin product selectivity (see Figure 6.2). This meant that the product distribution for Runs 1–4 was dominated by paraffin products. Figure 6.12 shows the FTS product distribution for each of the 4 runs. When the model was being developed, we assumed that all the products are in the gas phase. However, various reseachers [44, 45, 46] have reported that under typical reaction conditions, FT products may distribute between the vapour and liquid phases within the reactor. Fortunately, the inlet gases for the four runs we chose were CO_2-rich syngases, and the H_2/CO ratios were far higher than the that for the normal syngas (H_2/CO =2:1) as shown

in Table 6.1, which produced a high selectivity toward short chain hydrocarbons. In addition, even if some liquid products were produced, most of the short chain hydrocarbons should occur in the gas phase. Therefore, we used the experimental data for the short chain hydrocarbons in Figure 6.12.

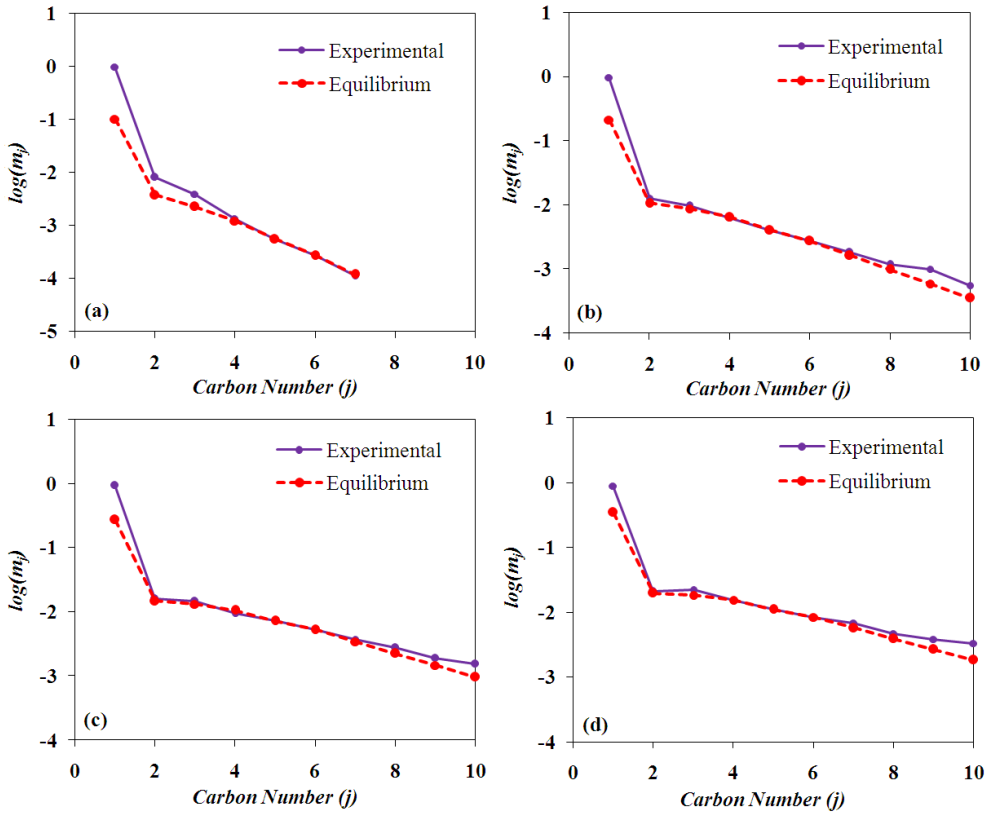

Figure 6.12: The predicted and measured FTS product distribution. Experimental conditions as shown in Table 6.1 over a cobalt-based catalyst: (a) Run 1; (b) Run 2; (c) Run 3 and (d) Run 4. The symbols represent the experimental data, while the lines stand for the predictions obtained by using the QPDM.

The values of $k_{P_{r,(j)}}$ from Equation (6.24) can be obtained by using the experimental data under each of the reaction conditions shown in Table 6.1 over a cobalt-based catalyst. In this case, we substituted the values of $m_{P_{r,(6)}}$ and $k_{P_{r,6}}$ into Equation (6.23) to calculate the mole fractions of the other products so that we could compare the difference in the mole fraction values between the

experimental data and the predicted result for each of the hydrocarbons (except $m_{P_{r,(5)}}$ and $m_{P_{r,(6)}}$). The most important information we elicited from the comparison was the following.

- Although the error margin between the model prediction and the experimental data is not small, a high yield of methane was obtained (in both experimental results and model predictions) under the reaction conditions shown for Runs 1–4.
- The trend of ethane production predicted through the model is quite similar to that obtained from the experimental data. In both cases a low yield of ethane was observed under the reaction conditions for Run 4.

The prediction results matched the experimental data, especially when the carbon number was higher than 1.

6.5.3 Implications of the new model

On the basis of results that have been presented in publications on the subject [29, 42, 43, 47-49], as well as our own experience, we find that the values of $k_{O_{(i)}}$ are normally changed in the range of [0.4, 0.7] and $k_{P_{r,(j)}}$ in the range of [0.4, 0.95] for FTS using cobalt- and iron-based catalysts (except i=2 and j=2 and 3). If we suppose k_{O_6} equals 0.4, 0.5, 0.6 and 0.7 and $k_{P_{r,6}}$ equals 0.4, 0.5, 0.6, 0.7, 0.8 and 0.9, we can use the QPDM to anticipate FTS olefin and paraffin product distributions. Figure 6.13 shows the results of the predicted product distribution at 200 ℃.

(1) For olefin products:

- A low yield of ethene is obtained, which is quite typical.

- A higher k_{O_6} value indicates that higher mole fractions of long chain olefin products should be expected.
- The shapes of the predicted distribution lines are similar to the results published in the literature [29, 42, 43, 45, 46].

(2) For paraffin products:

- A high yield of methane is obtained, which is quite typical.
- A low yield of ethane is obtained when $k_{P_{r,6}} > 0.8$.
- A higher $k_{P_{r,6}}$ value indicates that higher mole fractions of long chain paraffin products should be expected.

In addition, Figure 6.13 clearly shows that the trends of the lines derived from the QPDM are similar to those that follow a typical one-alpha ASF distribution with the carbon number of i⩾3 for olefin products and j⩾3 for paraffin products, respectively. If we rearrange Equations (6.19) and (6.23), we get:

$$K_{equilibrium,Reaction(a)_{(i)}} = \frac{m_{O_{(i)}}/m_{O_{(i-1)}}}{m_{O_{(i+1)}}/m_{O_{(i)}}} \quad (6.25)$$

$$K_{equilibrium,Reaction(b)_{(j)}} = \frac{m_{P_{r,(j)}}/m_{P_{r,(j-1)}}}{m_{P_{r,(j+1)}}/m_{P_{r,(j)}}} \quad (6.26)$$

The ASF product distribution model was presented as Equation (6.1). Substituting this equation into Equations (6.25) and (6.26), we can obtain:

$$K_{equilibrium,Reaction(a)_{(i)}} = 1 \quad (6.27)$$

$$K_{equilibrium,Reaction(b)_{(j)}} = 1 \quad (6.28)$$

Equations (6.27) and (6.28) indicate that if both the paraffin and the olefin product distribution follow the ASF model, the values of $K_{equilibrium}$ for Reaction (a) and

Reaction (b) should be equal to 1. According to the results shown in Figure 6.11, the values of $K_{equilibrium}$ are near or equal to 1, with carbon number i>3 for olefin products and with carbon number j>2 for paraffin products. These results suggest that the empirical ASF product distribution might be attributable to thermodynamic equilibrium.

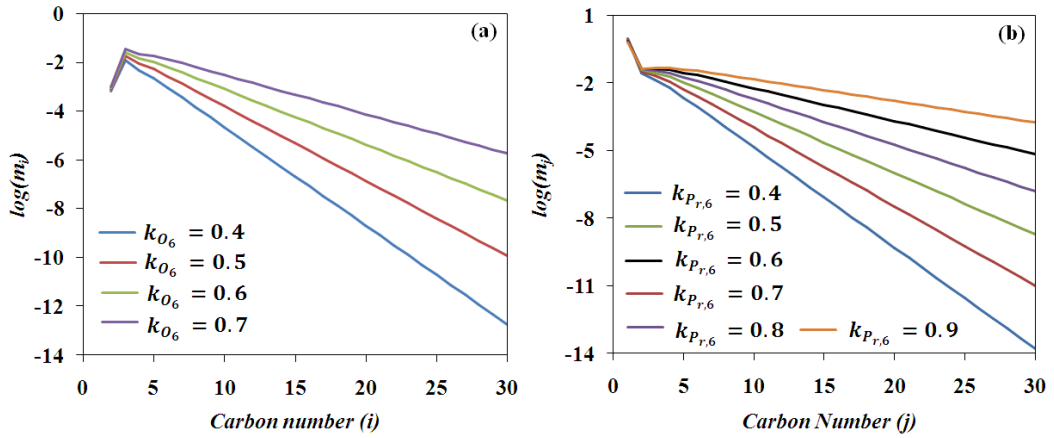

Figure 6.13: The predicted FTS product distribution derived form the QPDM at 200 ℃: (a) for olefin products; (b) for paraffin products.

The drawback of the new model is that we assume all the FT products are in the gas phase. It is generally accepted that FT products may distribute between the vapour and liquid phases under certain reaction conditions. Raje *et al*. [46] have noted that vapour-liquid equilibrium (VLE) can affect product distribution, and more research should be done to investigate the effect of VLE on product distribution.

6.6 Conclusions

With the aim of using thermodynamic considerations to explain the FT product distribution, we assumed that each of three adjacent olefins and paraffins reach a quasi-equilibrium state. Having carried out a series of FTS experiments using a wide range of $H_2/CO/CO_2$ mixtures over both cobalt- and iron-based catalysts, we

made a comparison between the thermodynamic equilibrium calculations of the products and our experimental results, which we plotted in a triangular area for each of the three adjacent homologous products. We found that most of the experimental results were quite close to those arrived at through thermodynamic calculations. Although the experimental data from the group of X_{O_2}, X_{O_3} and X_{O_4} and the group of $X_{P_{r,1}}$, $X_{P_{r,2}}$ and $X_{P_{r,3}}$ were not exactly on the equilibrium line, their values were not far from it. We therefore postulated that both paraffin and olefin products may achieve or approach a quasi-equilibrium during FTS over both cobalt- and iron-based catalysts.

We therefore proposed a new simple model named the "quasi-equilibrium product distribution model" to predict the olefin and the paraffin product distribution. This model was able to predict results that were in many ways consistent with those obtained experimentally. It could successfully describe the deviations in C_1 and C_2 components (a higher methane and a lower C_2 selectivity). Furthermore, the model predicted that the spectrums for both olefin and paraffin products (with a carbon number higher than 3) are similar to those of a typical one-alpha ASF distribution when the FTS products are in the gas phase. We therefore suggest that the olefin and paraffin product distribution in FTS may be described by thermodynamic equilibrium.

Although the thermodynamic distribution calculations do not fully match those observed experimentally, it must be emphasized that the calculations of product distributions are made independent of mechanism and catalyst, and therefore represent a generic distribution.

References

[1] de la Pena O'Shea, V. A., Alvarez-Galvan, M. C., Campos-Martin, J. M. and Fierro, J. L. G. (2007), Fischer-Tropsch synthesis on mono- and bimetallic Co and Fe catalysts in fixed-bed and slurry reactors, Applied Catalysis A: General, 326, 65–73.

[2] van Steen, E. and Claeys, M. (2008), Fischer-Tropsch Catalysts for the Biomass-to-Liquid Process, Chemical Engineering and Technology, 31, 655–666.

[3] Higman, C. and Burgt. M. (2003), Gasification, Guif Professional Publishing, Burlington.

[4] Haryanto, A., Fernandoc, S. D., Pordesimo, L. O. and Adhikari, S. (2009), Upgrading of syngas derived from biomass gasification: A thermodynamic analysis, biomass and bioenergy, 33, 882–889.

[5] Park, S.E., Nam, S.S., Choi, M.J. and Lee, K.W. (1995), Catalytic reduction of carbon dioxide, Energy Conversion and Management, 36, 573–576.

[6] Centi, G. and Perathoner, S. (2009), Opportunities and prospects in the chemical recycling of carbon dioxide to fuels, Catalysis Today, 148, 191–205.

[7] Choi, P. H., Jun, K. W., Lee, S. J., Choi, M. J. and Lee, K. W. (1996), Hydrogenation of carbon dioxide over alumina supported Fe-K catalysts, Catalysis Letters, 40, 115–118.

[8] Zhang, Y., Jacobs, G., Sparks, D. E., Dry, M. E. and Davis, B. H. (2002), CO and CO_2 hydrogenation study on supported cobalt, Catalysis Today, 71, 411–418.

[9] Riedel, T., Claeys, M., Schulz, H., Schaub G., Nam, S. S., Jun, K. W., Choi, M. J., Kishan, G. and Lee, K. W. (1999), Comparative study of Fischer–Tropsch

synthesis with H_2/CO and H_2/CO_2 syngas using Fe- and Co-based catalysts, Applied Catalysis A: General, 186, 201–213.

[10] Visconti, C. G., Lietti, L., Tronconi, E., Forzatti, P., Zennaro, R. and Finocchio, E. (2009), Fischer-Tropsch synthesis on a Co/Al_2O_3 catalyst with CO_2 containing syngas, Applied Catalysis A: General, 355, 61–68.

[11] Yao, Y., Hildebrandt, D., Glasser, D., and Liu, X. (2010), Fischer-Tropsch synthesis using $H_2/CO/CO_2$ syngas mixtures over a cobalt catalyst, Industrial and Engineering Chemistry Research., 49, 11061–11066.

[12] Krishnamoorthy S., Li, A. and Iglesia, E. (2002), Pathways for CO_2 formation and conversion during Fischer-Trosch synthesis on iron-based catalysts, catalysis letters, 80, 77-86.

[13] Liu, Y., Zhang, C., Wang, Y., Li, Y., Hao, X., Bai, L., Xiang, H., Xu, Y., Zhong, B. and Li, Y. (2008), Effect of co-feeding carbon dioxide on Fischer-Tropsch synthesis over an iron-manganese catalyst in a spinning basket reactor, Fuel processing technology, 89, 234–241.

[14] Dry, M. E. (1981), The Fischer-Tropsch Synthesis, Catalysis Science and Technology, Anderson, J. R. and Boudart, M. E., (Editors), Springer, New York, 1, 159–255.

[15] Tavakoli, A., Sohrabi, M. and Kargari, A. (2008), Application of Anderson-Schulz-Flory (ASF) equation in the product distribution of slurry phase FT synthesis with nanosized iron catalysts, Chemical Engineering Journal, 136, 358–363.

[16] Patzlaff, J., Liu, Y., Graffmann, C. and Gaube, J. (1999), Studies on product distributions of iron and cobalt catalyzed Fischer-Tropsch synthesis, Applied

Catalysis A: General, 186, 109–119.

[17] Madodand, R. J. and Taylor, W. F. (1981), Fischer-Tropsch synthesis on a precipitated iron catalyst, Journal of Catalysis, 69, 32–43.

[18] Huff, G. A. JR., and Satterfield, C. N. (1984), Evidence for two chain growth probabilities on iron catalysts in the Fischer-Tropsch synthesis, Journal of Catalysis, 85, 370–379.

[19] Iglesia, E., Reyes, S. C. and Madon, R. J. (1991), Transport-enhanced a-olefin readsorption pathways in Ru-catalyzed hydrocarbon synthesis, Journal of Catalysis, 129, 238–256 .

[20] Wojciechowski, B. W. (1988), The kinetics of the Fischer-Tropsch synthesis, Catalysis Reviews, Science and Engineering, 30, 629–702.

[21] Komaya, T. and Bell, A. T. (1994), Estimates of rate coefficients for elementary processes occurring during Fischer-Tropsch synthesis over Ru/TiO_2. Journal of Catalysis, 146, 237–248.

[22] Schulz, H., van Steen, E. and Claeys, M. (1993), Olefin formation, hydrogenation and isomerization in the kinetic regime of Fischer-Tropsch synthesis, In Selective hydrogenation and dehydrogenation; DGMK: Kassel, Germany.

[23] Kuipers, E. W., Scheper, C., Wilson, J. H. and Oosterbeek, H. (1996), Non-ASF product distributions due to secondary reactions during Fischer-Tropsch synthesis. Journal of Catalysis, 158, 288–300.

[24] Cheng, J., Hua, P., Ellis, P., French, S., Kelly, G. and Lok, C. M. (2008), A DFT study of the chain growth probability in Fischer–Tropsch synthesis, Journal of Catalysis, 257, 221–228.

[25] Novak, S., Madon, R. J. and Suhl, H. (1981), Models of hydrocarbon product distributions in Fischer-Tropsch synthesis. Journal of Chemical Physics, 74, 6083–6091.

[26] Rich, N. M., Hsu, C. C. and Wojciechowshi, B.W. (1988), The effect of catalyst surface heterogeneity on the Fischer-Trosch synthesis, the Canadian Journal of Chemical Engineering, 66, 694–696.

[27] Huyser, J., van Vuuren, M. J. and Kupi, G. (2009), The value of a two alpha model in the elucidation of a full product spectrum for Fe-LTFT, advances in Fischer-Tropsch Synthesis, Catalysts, and Catalysis, CRC Press, Chapter 10, 185–197.

[28] Schulz, H., and Claeys M. (1999), Kinetic modelling of Fischer-Tropsch product distribution, Applied Catalysis A: General, 186, 91–107.

[29] van der Laan, G. P. and Beenackers, A. A. C. M. (1999), Hydrocarbon Selectivity Model for the Gas-Solid Fischer-Tropsch Synthesis on Precipitated Iron Catalysts, Industrial and Engineering Chemistry Research, 38, 1277–1290.

[30] Patzlaff, J., Liu, Y., Graffmann, C. and Gaube, J. (1999), Studies on product distributions of iron and cobalt catalyzed Fischer-Tropsch synthesis, Applied Catalysis A: General, 186, 109–119.

[31] Patzlaff, J., Liu, Y., Graffmann, C. and Gaube, J. (20020, Interpretation and kinetic modeling of product distributions of cobalt catalyzed Fischer-Tropsch synthesis, Catalysis Today, 71, 381–394.

[32] Dictor, R. A. and Bell, A. T. (1986), Fischer-Tropsch Synthesis over Reduced and Unreduced Iron Oxide Catalysts, Journal of Catalysis, 121–136.

[33] Masuku, C. M., Hildebrandt, D. and Glasser, D. (2010), Olefin

Pseudo-Equilibrium in the Fischer-Tropsch Reaction, American Institute of Chemical Engineers (AIChE) 2010 Spring Meeting, San Antonio, UAS, March 21–25.

[34] Stenger, H. G. Jr. and Askonas, C. F. (1986), Thermodynamic Product Distributions for the Fischer-Tropsch Synthesis, Industrial and Engineering Chemistry Research Fundamentals, 25, 410–413.

[35] Lu, X., Hildebrandt, D. and Glasser, D. (2010), A Thermodynamic Approach to the Olefin Products Distribution in Fischer-Tropsch Synthesis, American Institute of Chemical Engineers (AIChE) 2010 Spring Meeting, San Antonio, UAS, March 21–25.

[36] Kuipers, E. W., Vinkenburg, I. H. and Oosterbeek, H. (1995), Chain length dependence of α-olefin readsorption in Fischer-Tropsch synthesis. Journal of Catalysis, 152, 137–146.

[37] Tau, L. M., Dabbagh, H. A. and Davis, B. H. (1990), Fischer-Tropsch synthesis: carbon-14 tracer study of alkene incorporation, Energy Fuels, 4, 94–99.

[38] Zheng, S., Liu, Y., Li, J., and Shi, B. (2007), Deuterium tracer study of pressure effect on product distribution in the cobalt-catalyzed Fischer-Tropsch synthesis, Applied Catalysis A: General, 330, 63–68.

[39] van Dijk, H. A. J., Hoebink, J. H. B. J. and Schouten, J. C. (2001), Steady-state isotopic transient kinetic analysis of the Fischer-Tropsch synthesis reaction over cobalt-based catalysts, Chemical Engineering Science, 56, 1211–1219.

[40] Lox, E. S. and Froment, G. F. (1993), Kinetics of the Fischer-Tropsch reaction on a precipitated promoted iron catalyst. 2. kinetic modeling, Industrial

and Engineering Chemistry Research, 32, 71–82.

[41] Li, J. (1999), The preparation, characterization and evaluation of boron modified Co/TiO2 Fischer-Tropsch catalysts, PhD thesis, University of the Witwatersrand, Johannesburg, South Africa.

[42] Donnelly, T. J. and Satterfield, C. N. (1989), Product Distributions of the Fischer-Tropsch synthesis on Precipitated Iron Catalysts, Applied Catalysis, 52, 93–114.

[43] Charles, N. Satterfle, M. and Harvey, G. (1984), Stenger Fischer-Tropsch Synthesis on a Precipitated Mn/Fe Catalyst in a Well-Mixed Slurry Reactor, Industrial and Engineering Chemistry Process Design and Development, 23, 26–29.

[44] Marano, J. J. and Holder, G. D. (2007), Characterization of Fischer-Tropsch liquids for vapor-liquid equilibria calculations, Fluid Phase Equilibria, 138, 1–21.

[45] Caldwell, L. and van Vuuren, D. S. (1986), On the formation and composition of the liquid phase in Fischer-Tropsch reactors, Chemical Engineering Science, 41, 89–96.

[46] Raje, A. P. and Davis, B. H. (1996), Effect of vapor-liquid equilibrium on Fischer-Tropsch hydrocarbon selectivity for a deactivating catalyst in a slurry reactor, Energy & Fuels, 10, 552–560.

[47] Fernandes, F. A. N. and Sousa, E. M. M. (2006), Fischer-Tropsch synthesis product grade optimization in a fluidized bed reactor, AIChE Journal, 52, 2844–2850.

[48] Kuipers, E. W., Vinkenburg, I. H. and Oosterbeek, H. (1995), Chain length dependence of α-olefin readsorption in Fischer-Tropsch synthesis, Journal of

catalysis, 152, 137–146.

[49] van Dijk, H. A. J., Hoebink, J. H. B. J. and Schouten, J. C. (2001), Steady-state isotopic transient kinetic analysis ofthe Fischer-Tropsch synthesis reaction over cobalt-based catalysts, Chemical Engineering Science, 56, 1211–1219.

7

FISCHER-TROPSCH SYNTHESIS USING $H_2/CO/CO_2$ SYNGAS MIXTURES: A COMPARISON OF PRODUCT DISTRIBUTION FOR IRON- AND COBALT-BASED CATALYSTS

This work has been prepared in the form of a paper for future publication.

Abstract:

Fischer-Tropsch synthesis (FTS) using $H_2/CO/CO_2$ syngas mixtures over cobalt- and iron-based catalysts were carried out in a fixed-bed micro reactor. The data show that: (1) For CO_2-rich feeds, most of the products are short chain paraffins with high methane selectivity, and the product distribution follows a typical one-alpha Anderson-Schulz-Flory (ASF) distribution with low alpha values; (2) For CO-rich feeds, the product composition shifts to an FT type product (mainly long chain hydrocarbons), and follows a two-alpha ASF distribution with high alpha values.

The growth factors for paraffin, olefin and oxygenate produced by means of FTS differ. We therefore introduce a new product distribution model entailing a combination of the paraffin and olefin product growth factors to explain the observed two-alpha ASF distribution of FTS. This model shows the likelihood that two-alpha product distribution may be the result of the combination of different product spectrums. We also considered the effect of the vapour-liquid equilibrium (VLE) on the product distribution, and found that our experimental data support the postulate that the double-alpha type plot often encountered in FT

results is attributable to VLE.

We therefore deduce that the deviations from the ASF distribution can be explained as the co-action of the different product spectrums and the VLE on the product distribution during FTS, which can be summarised as: (1) when a liquid layer is formed on the catalyst surface, a two-alpha distribution will be achieved, no matter what kinds of product are produced; (2) when there is only gas phase adsorbing on the catalyst surface and the products are mixtures of paraffins, olefins and oxygenates, a two-alpha distribution will be obtained because of the combination of the different product spectrums and growth factors; (3) when there is only gas phase adsorbing on the catalyst surface, with only one kind of hydrocarbon product (such as paraffin or olefin), the FTS product distribution will follow a typical one-alpha distribution.

7.1 Introduction

Fischer-Tropsch synthesis (FTS) is a process by means of which synthesis gas (syngas) is converted into long chain hydrocarbons which can be transformed to fuels and chemicals [1-3]. Among the FTS catalysts reported in the scientific literature [6–9], iron and cobalt are used commercially at temperatures between 200–300 ℃, and at 10–60 bar pressure. The syngas produced from coal or biomass gasification consists of H_2, CO, CO_2 and CH_4 [10−12]. The CO_2 composition in the raw syngas varies from around 1–30%, and is dependent on many factors such as gasifier type, operating conditions, gasifying agents and feedstock properties [11−12]. Although the patent literature makes mention in some cases of a need for CO_2 separation before using the syngas for FTS, recent process development studies suggest that there is a potential cost advantage if CO_2 is not removed before FTS is carried out [13]. We therefore set out to investigate

the effect of carbon dioxide on the product distribution derived from low-temperature FTS over iron- and cobalt-based catalysts.

The Anderson-Schulz-Flory (ASF) distribution model has been used consistently to describe the FTS product distribution [14]. If the hydrocarbon chain is formed step-wise by the insertion or addition of CH_2 intermediates with constant growth probability (α), then the ASF model gives the chain length distribution [15]. Assuming that α is independent of the hydrocarbon chain length, an equation may be derived as follows:

$$log\left(\frac{W_n}{n}\right) = nlog(\alpha) + log\left(\frac{(1-\alpha)^2}{\alpha}\right) \quad (7.1)$$

where W_n is the mass fraction of a hydrocarbon with chain length n. According to the equation, a plot of $\log(W_n/n)$ versus n should give a straight line, as shown in Figure 7.1 (a). The value of α is obtained from the slope of the plot, and a higher α value indicates that a heavier hydrocarbon weight percentage should be expected.

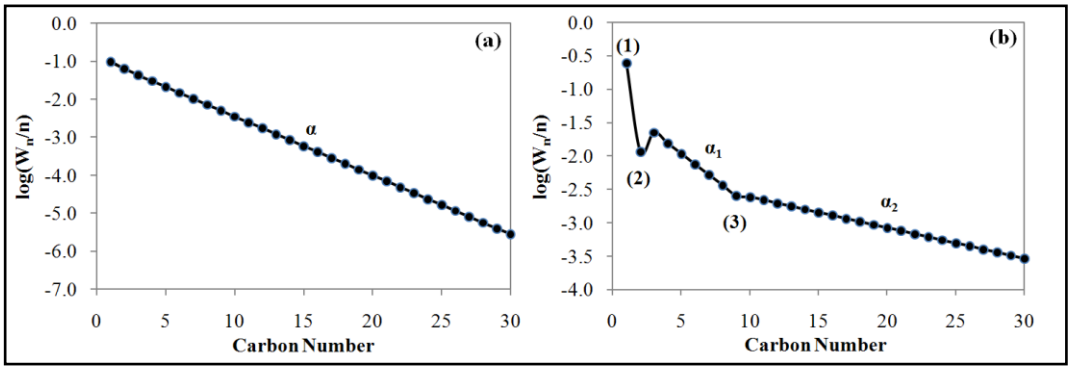

Figure 7.1: Illustrative plot of an ASF distribution: (a) ideal distribution and (b) with deviations from the ideal distribution.

However, the product distribution for most iron and cobalt catalysts show marked deviations from this ideal distribution plot [15-19]. The most noticeable of these deviations (see Figure 7.1 (b)) from the ASF model on CO hydrogenation show:

- a relatively high yield of methane [20–24];
- a relatively low yield of ethene [20, 21,24, 25]; and
- a distinct change in the slope of the line between carbon numbers 8–12 [26-28].

Some researchers [26, 28, 29] believe that these deviations are predominantly caused by secondary reactions of α-olefins, which may re-adsorb on growth sites of the catalyst surface and continue to grow via propagation with monomers, or terminate as hydrocarbon products. However, experiments with co-feeding ethene and 1-alkenes have shown that these deviations are not significantly due to the re-adsorption of α-olefins but are the consequence of two different mechanisms of chain growth that result in a superposition of two ASF distributions [30–31]. Furthermore, Huyser *et al*. [27] reported that the total product spectrum is a combination of two distinct sets of products resulting from either two different mechanisms (for instance, two different reactive intermediates) or two different catalytic sites, each producing a different product spectrum. This explanation has been mentioned by other researchers as well [18, 32]. Nevertheless, the D_2/H_2 switching method has been used to demonstrate that the two-alpha distribution may be as a result of the accumulation of heavier products in the reactor [33-34]. Thus, the deviations may just be an artifact due to the experimental methods employed.

The low-temperature FT process with either iron or cobalt catalysts is used for the production of high molecular mass linear waxes [35]. Under typical reaction conditions, the FT products distribute between the vapour and liquid phases within the reactor [36, 37]. The lighter components are carried overhead with the unreacted syngas, while the heavier components form the molten-wax phase within which the catalyst is suspended. Reactor performance is strongly dependent on the composition of the wax phase, which affects both the synthesis

chemistry [38-39] and the hydrodynamics [40]. Vapour-liquid equilibrium (VLE) places constraints on the composition of the two phases. Raje *et al*. [41] mentioned that the prediction of two-α selectivity plots by the VLE model indicates that VLE phenomena are responsible for the occurrence of the two-α product selectivity in the case of a deactivating catalyst. Masuku *et. al.* [42-43] considered the effects of VLE on the FT product distribution, and developed a mathematical model to describe it. The results derived from applying the model show that the effect of VLE is the most probable reason for the observation of a two-alpha product distribution.

Hydrogenation of carbon dioxide has traditionally been carried out with catalysts that have been demonstrated to be active and selective for the FTS reaction, which hydrogenates CO [13, 44]. Iron-based catalysts are active in both water-gas shift (WGS) and reverse WGS reactions [45], so in principle, they would be ideal candidates to be used in FTS with CO_2-containing syngas feeds [46–50]. Cobalt catalysts with low WGS activity have a high hydrogenation activity, and tend to produce linear alkanes [51–52]. When CO and CO_2 hydrogenation experiments were conducted by various researchers [53–54], the resultant activity data clearly showed that when used alone, both CO and CO_2 are readily hydrogenated over the catalyst under actual low-temperature FTS conditions. A comparison of the product distribution of CO and CO_2 hydrogenation over both iron- and cobalt-based catalysts revealed that CO_2 hydrogenation (in contrast to that for CO) shows [44, 50, 54, 55]:

- a low alpha distribution;
- a higher selectivity to light hydrocarbons; and
- a higher paraffin selectivity in the products.

The mechanism of product distribution remains controversial. In the work described in this paper, we focused on discussing the effect of co-feeding CO_2 on

the product distribution of FTS over iron- and cobalt-based catalysts. Two kinds of feed gases, CO_2 syngas (H_2:CO:CO_2 = 3:0:1) and CO syngas (H_2:CO:CO_2 = 2:1:0), were mixed in different proportions, thus varying the partial pressure of CO, CO_2 and H_2 stoichiometrically with the ratio of $H_2/(2CO+3CO_2)$ equal to 1. The purpose of these experiments was to obtain new and potentially interesting information about the product distribution by researching the FTS using the co-feeding CO_2 feed gases.

7.2 Experimental

7.2.1 Cobalt catalyst

7.2.1.1 Catalyst preparation

The Co/TiO_2 catalyst used in this study was prepared by impregnation of TiO_2 with a cobalt nitrate solution. TiO_2 (Degussa P25) was mixed with distilled water in a mass ratio of 1:1 and dried in air at 120 ℃ for 1 hour. The support was then calcined in air at 400 ℃ for 16 hours [56], after which it was crushed and sieved, and the particles with diameters between 0.5–1 mm reserved for use. The support was then impregnated with a cobalt nitrate ($Co(NO_3)_2 \cdot 6H_2O$) solution, the quantity added being sufficient to give a cobalt metal loading of 10% by mass. Thereafter, the support was dried in air at 120 ℃ for 16 hours, and then calcined in air at 400 ℃ for 6 hours to decompose and transform the cobalt nitrate to cobalt oxide.

7.2.1.2 Experimental setup and procedure

7.2.1.2.1 Catalyst reduction

We loaded 1 g of catalyst into the micro fixed bed reactor (FBR), and performed the reduction at atmospheric pressure with H_2 (AFROX (African Oxygen) Ltd.,

99.999%) for 24 hours. The reduction temperature and the flow rate were 350 ℃ and 60 ml(NTP)/(min gcat), respectively.

Table 7.1: Summary of experimental conditions for FTS using $H_2/CO/CO_2$ mixtures over cobalt- and iron-based catalysts.

	Cobalt-based catalyst				Iron-based catalyst			
Temperature (℃)	200				250			
Total Pressure (Bar gauge)	20				20			
Flow-Rate (ml(NTP)/(min gcat)	60				60			
	Partial pressure at entrance (bar)				Partial pressure at entrance (bar)			
Reaction Condition Number	P_{H_2}	P_{CO}	P_{CO_2}	P_{N_2}	P_{H_2}	P_{CO}	P_{CO_2}	P_{N_2}
1	14.2	0.0	4.8	2.1	14.2	0.0	4.8	2.1
2	13.9	0.5	4.2	2.0	14.0	0.6	4.3	2.0
3	13.8	1.3	3.9	2.0	13.8	1.3	3.8	2.1
4	13.7	1.9	3.3	2.1	13.6	2.0	3.3	2.1
5	13.3	2.4	2.8	2.0	13.4	2.5	2.9	2.1
6	13.2	3.2	2.3	2.1	13.2	3.2	2.4	2.1
7	13.1	3.8	1.9	2.1	13.1	3.9	1.9	2.1
8	13.0	4.3	1.5	2.1	13.0	4.5	1.5	2.1
9	12.9	4.9	0.9	2.1	12.7	5.2	1.0	2.1
10	12.7	5.6	0.4	2.1	12.6	5.8	0.5	2.1
11	12.5	6.3	0.0	2.2	12.4	6.4	0.0	2.1

7.2.1.2.2 FTS using $H_2/CO/CO_2$ syngas

Once the reduction was completed, the reactor was allowed to cool down to room temperature. The CO_2 syngas (hereafter referred to as the CO_2 feed), composed of H_2:CO:CO_2 = 3:0:1, and 10% (by mole) N_2 as an internal standard for mass balance calculations, was introduced into the reactor at a flow rate of 60

ml(NTP)/(min gcat). The reactor pressure was slowly increased to 20 bar (gauge), after which the temperature was gradually raised to 200 ℃. The pressure and temperature were allowed to stabilize, and these operating conditions were maintained constant for 72 hours, during which the composition of the tail gas was monitored. Next, the flow rate of the CO_2 syngas was reduced by 10%, that is by 6 ml(NTP)/(min gcat). The CO syngas (designated as the CO feed), which consisted of H_2:CO:CO_2 = 2:1:0, with 10% (by mole) N_2 as an internal standard for mass balance calculations, was introduced at a flow rate of 6 ml(NTP)/(min gcat)) so as to keep the total flow rate constant at 60 ml(NTP)/(min gcat). The new reaction conditions were maintained for 72 hours while the tail gas composition was monitored. After that the flow rate of the CO_2 feed was dropped again, while that of the CO feed was increased so as to keep the total flowrate of the feed gas to the reactor at 60 ml(NTP)/(min gcat). The feed and reaction conditions for the 11 experiments carried out over the cobalt-based catalyst are shown in Table 1.

7.2.2 Iron catalyst

7.2.2.1 Catalyst preparation

The Fe/TiO_2 catalyst was prepared by a single-step incipient wetness impregnation of the support with an iron nitrate ($Fe(NO_3)_3$ $9H_2O$) solution. In the stages that followed, we used the same procedure as was applied in the case of the cobalt catalyst (see Section 7.2.1.1).

7.2.2.2 Experimental Setup and Procedure

7.2.2.2.1 Catalyst reduction

A quantity of 1g of catalyst was loaded in the micro-FBR. The reduction by H_2 (AFROX (African Oxygen) Ltd., 99.999%) was performed at atmospheric

pressure for 24 hours. The reduction temperature and the flow rate were 350 ℃ and 60 ml/min, respectively.

7.2.2.2.2 FTS using $H_2/CO/CO_2$ syngas

The FTS experiments over iron-based catalysts were carried out in a fixed-bed micro reactor, following the same operating procedures as outlined in Section 7.2.1.2.2. The only difference was that the operating temperature for the iron catalyst was 250 ℃, whereas for cobalt it was 200 ℃. The process conditions are shown in Table 1.

7.2.3 Product analysis

In both groups of experiments the tail gas was analyzed every 1.5 hours by an online DANI GC, using two thermal conductivity detectors (TCD) for H_2, N_2, CO, CO_2 and CH_4, and a flame ionization detector (FID) for gas phase hydrocarbon analysis. The wax and liquid products were collected in a hot trap (kept at 150 ℃) and a cold trap (maintained at room temperature). The analysis of oil and wax products was performed at the end of the mass balance for each run, using an offline GC.

7.3 Results

7.3.1 The product distribution of paraffins and olefins with low chain length

7.3.1.1 Cobalt catalyst

Some researchers have chosen to plot the ASF distribution of olefins and paraffins separately [57–60]. In this Chapter, the short chain paraffin and olefin product distributions under different reaction conditions (described in Table 1 as experiments 1, 5, 7, 9 and 11 over a cobalt catalyst) are shown in Figure 7.2 (a–e).

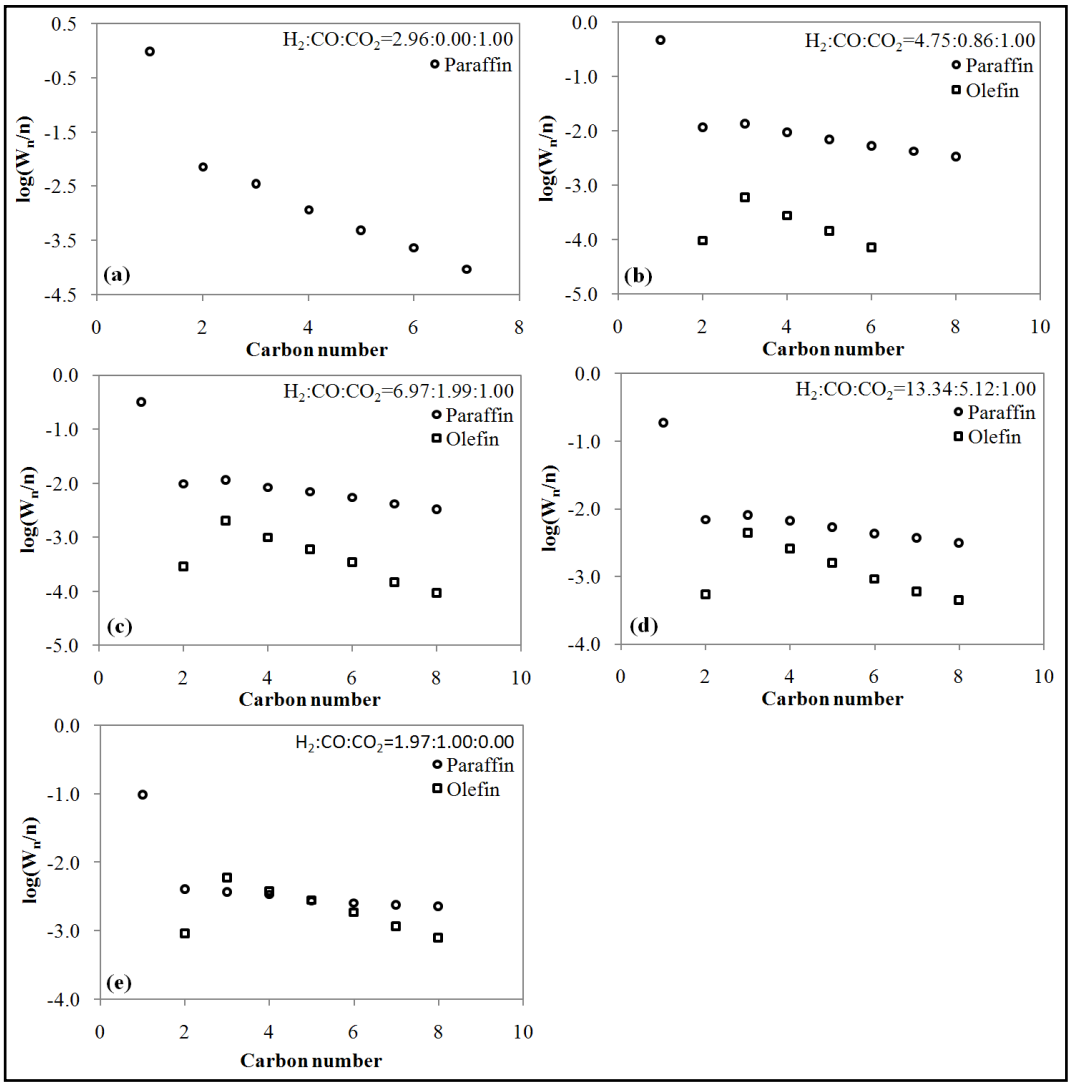

Figure 7.2: The paraffin and olefin product distribution under the reaction conditions described in Table 1 over a cobalt-based catalyst: (a) Experiment 1; (b) Experiment 5; (c) Experiment 7; (d) Experiment 9; and (e) Experiment 11.

Figure 7.2 (a) shows that the hydrogenation of CO_2 leads to a typical ASF distribution with the lowest α value of 0.41 when the feed is only CO_2/H_2 (corresponding to H_2:CO:CO_2 = 2.96:0.00:1.00). Because no olefin products can be detected, all the products are paraffins for CO_2 hydrogenation. It is also interesting to note that C_2 (ethane) lies on the ASF distribution in this case. As the proportions of CO_2 feed are replaced by CO feed, as shown in Figure 7.2 (b–e), more olefin

products are obtained as the CO partial pressure rises. There is a relatively low yield of C_2 (both ethane and ethylene) products, which is a fairly typical result [20–25].

The data show that both the paraffin and olefin product distributions follow the ASF model with the carbon number from 3 to 8 under the reaction conditions given in Table 1 over the cobalt-based catalyst. However, there is a distinct difference between the slope of the line for paraffins and that for olefins with carbon numbers from 3 to 8, which indicates that their growth factors are dissimilar. We calculated the growth factors for the paraffin (α_P) and the olefin (α_O) products under the different reaction conditions given in Table 1 from the slope values of the paraffin and olefin product distribution plots. A comparison between the paraffin and the olefin growth factors is made in Figure 7.3. The results in summary showed that:

- with CO_2-rich feeds, both paraffins and olefins had lower growth factors;
- with CO-rich feeds, both paraffins and olefins had higher growth factors; and
- under the same reaction condition, paraffins had a higher growth factor and olefins a lower one.

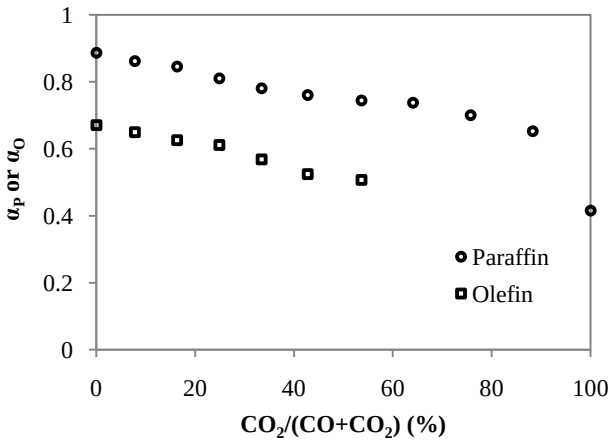

Figure 7.3: The comparison between paraffin growth factors and olefin growth factors under the reaction conditions described in Experiments 1–11 in Table 1 (cobalt-based catalyst).

7.3.1.2 Iron catalyst

Figure 7.4 (a-d) shows the paraffin and olefin product distribution under the reaction conditions described in Experiments 1, 5, 7 and 11 in Table 1 (iron catalyst). The data also indicate that both the paraffin and olefin product distributions follow the ASF model when the carbon number is equal to, or greater than, 3. The comparison between the paraffin and olefin growth factors for FTS with an iron catalyst is drawn in Figure 7.5. For the short chain products, the same trends as were seen in the experiments using a cobalt-based catalyst were obtained (higher growth factors for CO-rich feeds, lower growth factors for CO_2-rich feeds, and a higher growth factor for paraffin than olefin under the same reaction conditions).

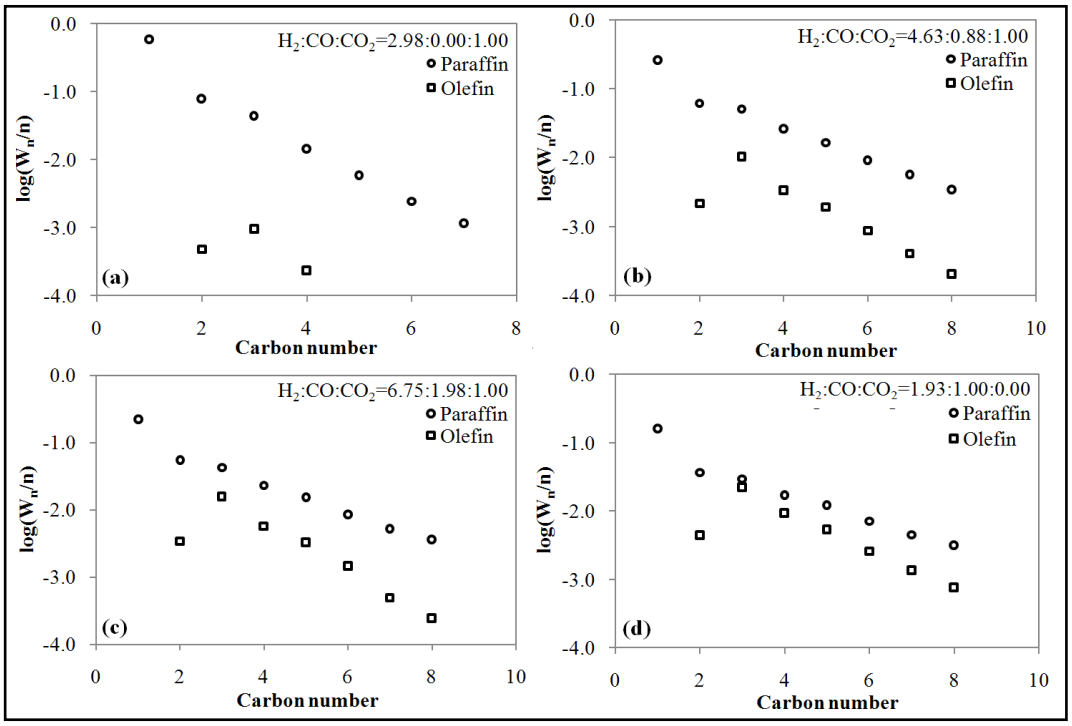

Figure 7.4: The paraffin and olefin product distribution under the reaction conditions described in Table 1 over an iron-based catalyst: (a) Experiment 1; (b) Experiment 5; (c) Experiment 7; and (e) Experiment 11.

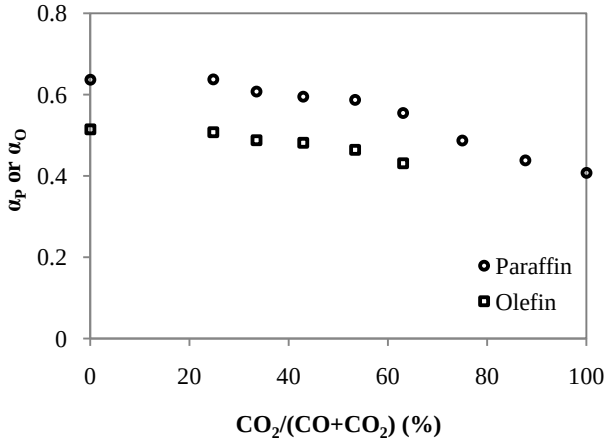

Figure 7.5: The comparison between paraffin and olefin growth factors under the reaction conditions described in Experiments 1–11 in Table 1 (iron-based catalyst).

7.3.2 The product distribution of hydrocarbons (olefins + paraffins)

7.3.2.1 Cobalt catalyst

Figures 7.6–7.8 show the FTS product distribution over the cobalt-based catalyst with the reaction conditions as shown in Table 1. These data indicate that the hydrogenation of CO_2 with a feed of only H_2/CO_2, leads to a typical ASF distribution with a low α value of 0.41, and also that C_2 (ethane) lies on the ASF distribution line in this case. Experiments 2 and 3 in Table 1 correspond to a constant total flow rate of 60 ml(NTP)/(min·gcat) to the reactor and where 10% and 20% of CO_2 syngas was replaced by CO syngas, respectively. It appears that the product distribution for these two conditions follows a typical one-α ASF distribution (Figure 7.6). As the amount of CO_2 in the feed gas is reduced and the quantity of CO is increased (as indicated in Table 1), the product distribution changes from a typical one-alpha to a typical two-alpha ASF distribution (Figures 7.6–7.8). As illustrated in Figures 7.7 and 7.8, there is a distinct change in the slope of the line from carbon numbers 8–12. Furthermore, there is a relatively low yield of C_2 products, which is fairly typical. For CO hydrogenation when the feed

is only CO/H_2 (corresponding to H_2:CO:CO_2=1.97:1.00:0.00), two normal α product distributions can be observed in Figure 7.8 with α_1=0.78 and α_2=0.93.

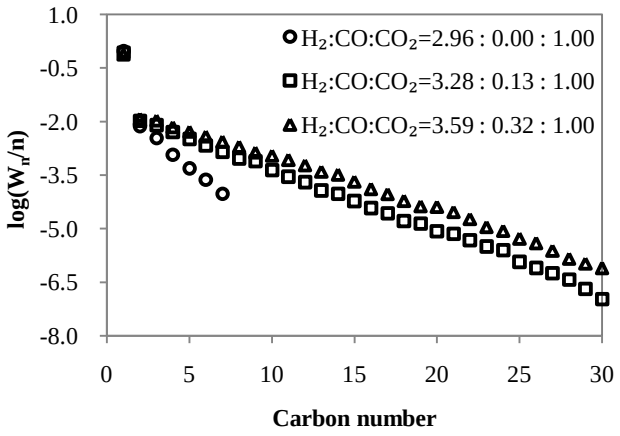

Figure 7.6: The FTS product distribution under the reaction conditions described in Experiments 1, 2 and 3 in Table 1 (cobalt-based catalyst).

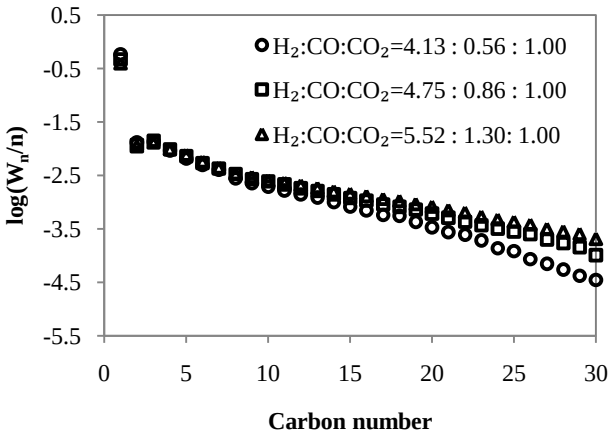

Figure 7.7: The FTS product distribution under the reaction conditions described in Experiments 4, 5 and 6 in Table 1 (cobalt-based catalyst).

Chain growth probabilities α_1 and α_2 (see Figure 7.1 (b)) as a function of synthesis gas composition (reaction conditions as in Table 1) over a cobalt catalyst are shown in Figure 7.9. For the CO_2-rich syngas, the product distribution is based on a typical one-alpha ASF distribution with a low alpha value, while for the CO-rich syngas, the distribution obeys a typical two-alpha ASF distribution with a high

alpha value. When $CO_2/(CO+CO_2)<40\%$, the values of α_1 and α_2 do not change significantly.

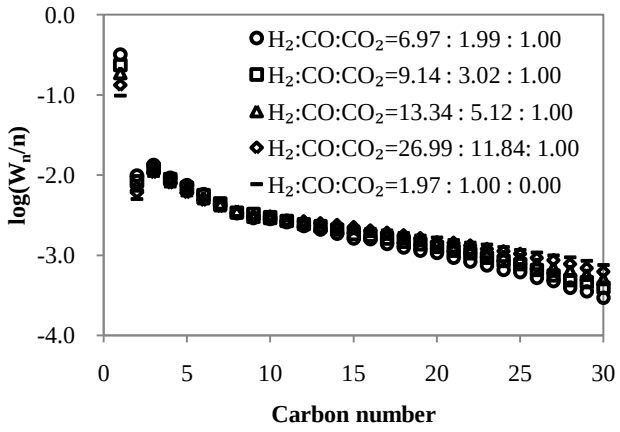

Figure 7.8: The FTS product distribution under the reaction conditions described in Experiments 6, 7, 8, 9 and 10 in Table 1 (cobalt-based catalyst).

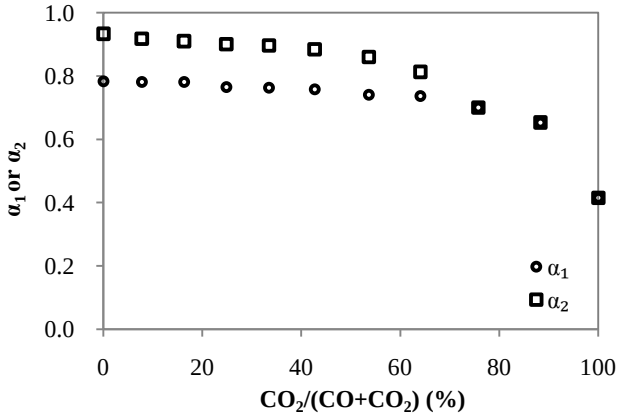

Figure 7.9: Chain growth probabilities α_1 and α_2 as a function of synthesis gas composition (reaction conditions as shown in Table 1) over a cobalt catalyst.

7.3.2.2 Iron catalyst

The product distribution obtained from FTS over an iron-based catalyst under the reaction conditions shown in Table 1 is plotted in Figures 7.10 and 7.11. The data also reveal that the hydrogenation of CO_2 leads to a typical ASF distribution with the lowest α value at 0.41 when the feed is only CO_2/H_2 (corresponding to

H_2:CO:CO_2=2.96:0.00:1.00) (see Figure 7.10). When a small amount of CO_2 syngas was replaced by CO syngas in the cases of Experiments 2 and 3, the selectivity for light hydrocarbons (C_1–C_4) was higher than 77%. Because it was not easy to separate the very small amount of oil from the water collected in the cold trap, the data shown are the result of tail gas analysis, and the alpha values are 0.44 and 0.49, respectively (Figure 7.10). In the case of Experiment 4 in Table 1, where 30% of the CO_2 syngas was replaced with CO syngas, the data in the Figure 7.10 show that the product distribution follows a typical one-alpha ASF distribution.

As the amount of CO_2 in the feed gas is decreased and the quantity of CO is raised (as indicated in Table 1), the product distribution changes from a typical one-alpha ASF distribution (Figure 7.10) to a typical two-alpha ASF distribution (Figure 7.11). There is also a distinct change in the slope of the line from carbon number 8 to 10, as depicted in Figure 7.11.

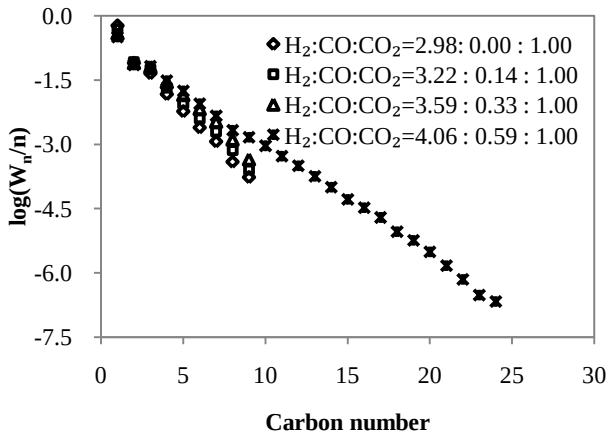

Figure 7.10: The FTS product distribution under the reaction conditions as described in Experiments 1, 2, 3 and 4 in Table 1 (iron-based catalyst).

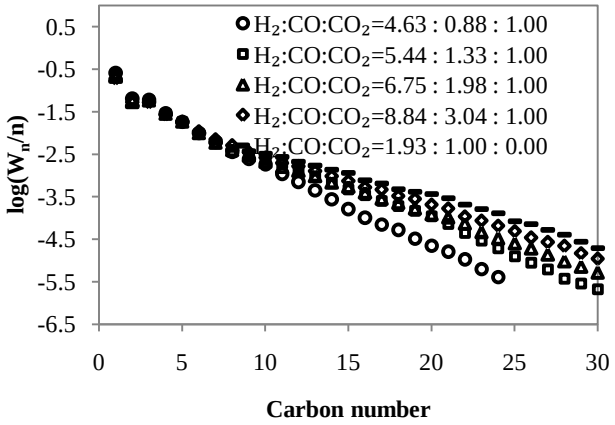

Figure 7.11: The FTS product distribution under the reaction conditions described in Experiments 5, 6, 7, 8 and 11 in Table 1 (iron-based catalyst).

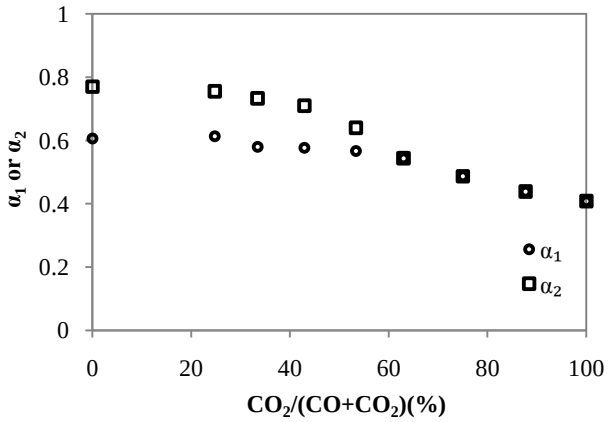

Figure 7.12: Chain growth probabilities α_1 and α_2 as a function of synthesis gas composition (reaction conditions as in Table 1) over an iron catalyst.

The chain growth probabilities α_1 and α_2 as a function of synthesis gas composition (under the reaction conditions given in Table 1) over an iron catalyst are plotted in Figure 7.12. It also appears that for CO_2-rich syngas, the product distribution is based on a typical one-alpha ASF distribution with low alpha value, while for syngas rich in CO, the distribution obeys a typical two-alpha ASF distribution with high alpha value.

We will consider two different models that may describe the observed product

distribution, which are presented in Section 7.4.

7.4 Discussion

7.4.1 The combined paraffin and olefin growth factors distribution model (CPODM)

Many kinetic and reaction route models have been developed to explain the observed deviations from the standard ASF model. Huff and Satterfield [18] suggested a model that accounts for two-catalytic sites with two different growth factors that yield a positive deviation from the standard ASF model. As mentioned in the Introduction to this paper, Huyser *et al.* [27] claimed that the total product spectrum can be explained as a combination of two distinct sets of outcomes derived from either two different mechanisms (such as dissimilar reactive intermediates) or two different catalytic surfaces, each producing a different range of products.

FTS products cover an extremely wide range, and include alkanes, alkenes and oxygenates with carbon numbers extending from C_1 to more than C_{100} [61]. Some researchers [18, 27, 29, 62] have compared the paraffins, olefins and oxygenates product distributions for FTS. Their results show that the growth factors for paraffin, olefin and oxygenates are not the same, which may suggest that different mechanisms are at play in each case. Figures 7.2 and 7.4 also show that the growth factors for paraffin and olefin products are different: with higher growth factors for paraffins and lower for olefins.

Although FTS produces hydrocarbons and oxygenates with a broad spectrum of chain lengths and functional groups, the major products are linear hydrocarbons, including paraffins and olefins [63–64]. The data in Figures 7.2 and 7.4 show that both the paraffin and the olefin product distribution follow the ASF models with

the carbon number from 3 to 8.

According to the previous work from the scientific publications in this field and the results from our experiments, we attempted to explain the FTS two-alpha ASF distribution by constructing a model called "the combined paraffin and olefin growth factors distribution model (CPODM)". For simplicity of modeling only, we assume that:

- Linear paraffins and olefins are the hydrocarbon products of FTS.
- Both the paraffin and olefin product distribution follow a typical one-alpha ASF model (when the carbon number is equal to, or greater than 3) and the growth factors are α_P and α_O, respectively.

The overall molar balance for the products is expressed as:

$$N_t = N_{P,t} + N_{O,t} \tag{7.2}$$

$$N_n = N_{P,n} + N_{O,n} \tag{7.3}$$

$$N_{P,t} = N_{P,1} + N_{P,2} + N_{P,3} + N_{P,4} + N_{P,5} + \cdots + N_{P,\infty} \tag{7.4}$$

$$N_{O,t} = N_{O,2} + N_{O,3} + N_{O,4} + N_{O,5} + \cdots + N_{O,\infty} \tag{7.5}$$

where N_t refers to the total moles of products; $N_{P,t}$ to the total moles of paraffins; $N_{O,t}$ to the total moles of olefins; N_n to the moles of hydrocarbon at chain length n; $N_{P,n}$ to the moles of paraffin at chain length n; and $N_{O,n}$ denotes the moles of olefin at chain length n.

The mole fraction of a hydrocarbon with chain length n is defined as:

$$m_{P,n} = \frac{N_{P,n}}{N_{p,t}} \tag{7.6}$$

$$m_{O,n} = \frac{N_{O,n}}{N_{O,t}} \tag{7.7}$$

$$m_n = \frac{N_n}{N_t} \tag{7.8}$$

where $m_{P,n}$ is the mole fraction of paraffin with chain length n; $m_{O,n}$ is the mole fraction of olefin with chain length n; m_n is the mole fraction of all the species having n carbon atoms.

From the definition, we can get:

$$\sum_{n=1}^{\infty} m_{P,n} = 1 \tag{7.9}$$

$$\sum_{n=2}^{\infty} m_{O,n} = 1 \tag{7.10}$$

$$\sum_{n=1}^{\infty} m_n = 1 \tag{7.11}$$

The ASF distribution Equation (7.1) can also be described as [65]:

$$m_n = (1-\alpha)\alpha^{(n-1)} \tag{7.12}$$

Because the assumption was made that both olefin and paraffin species for carbon numbers greater than 2 follow separate ASF distributions, we can explain α_P and α_O as follows:

$$\alpha_P = \left.\frac{m_{P,n+1}}{m_{P,n}}\right|_{n\geq 3} = \left.\frac{N_{P,n+1}}{N_{P,n}}\right|_{n\geq 3} \tag{7.13}$$

$$\alpha_O = \left.\frac{m_{O,n+1}}{m_{O,n}}\right|_{n\geq 3} = \left.\frac{N_{O,n+1}}{N_{O,n}}\right|_{n\geq 3} \tag{7.14}$$

Substituting Equations (7.13) and (7.14) in Equations (7.4) and (7.5), we get:

$$N_{P,t} = N_{P,1} + N_{P,2} + N_{P,3}\left(\frac{1}{1-\alpha_P}\right) \tag{7.15}$$

and $N_{O,t} = N_{O,2} + N_{O,3}(\frac{1}{1-\alpha_O})$ (7.16)

Then, substituting from Equations (7.13—7.16) in Equations (7.6) and (7.7), we obtain:

$$m_{P,1} = \frac{1}{1+\frac{N_{P,2}}{N_{P,1}}+\frac{N_{P,3}}{N_{P,1}}(\frac{1}{1-\alpha_P})} \quad (7.17)$$

$$m_{P,2} = \frac{1}{\frac{N_{P,1}}{N_{P,2}}+1+\frac{N_{P,3}}{N_{P,2}}(\frac{1}{1-\alpha_P})} \quad (7.18)$$

$$m_{P,3} = \frac{1}{\frac{N_{P,1}}{N_{P,3}}+\frac{N_{P,2}}{N_{P,3}}+(\frac{1}{1-\alpha_P})} \quad (7.19)$$

$$m_{P,n(n\geq 3)} = m_{P,3}\alpha_P^{(n-3)} \quad (7.20)$$

$$m_{O,2} = \frac{1}{1+\frac{N_{O,3}}{N_{O,2}}(\frac{1}{1-\alpha_O})} \quad (7.21)$$

$$m_{O,3} = \frac{1}{\frac{N_{O,2}}{N_{O,3}}+(\frac{1}{1-\alpha_O})} \quad (7.22)$$

$$m_{O,n(n\geq 3)} = m_{O,3}\alpha_O^{(n-3)} \quad (7.23)$$

Equation (7.3) can be modified as:

$$N_n = N_{P,n} + N_{O,n} = N_t \frac{N_{P,t}}{N_t}\frac{N_{P,n}}{N_{p,t}} + N_t \frac{N_{O,t}}{N_t}\frac{N_{O,n}}{N_{O,t}} \quad (7.24)$$

Substituting from Equation (7.24) in Equation (7.8), we gain:

$$m_n = \frac{N_{P,t}}{N_t}\frac{N_{P,n}}{N_{P,t}} + \frac{N_{O,t}}{N_t}\frac{N_{O,n}}{N_{O,t}} \quad (7.25)$$

If we define:

$$X = \frac{N_{P,t}}{N_t} \quad (7.26)$$

substituting from Equations (7.2), (7.6), (7.7) and (7.26) in Equation (7.25), we obtain:

$$m_n = X m_{P,n} + (1 - X) m_{O,n} \tag{7.27}$$

Equations (7.17—7.23) and (7.27) can be used to calculate the product selectivity and this model is named "CPODM". $N_{P,1}$, $N_{P,2}$, $N_{P,3}$, $N_{O,2}$, $N_{O,3}$, α_p and α_O depend on the reaction conditions and the catalyst properties, so the values are not constant, but can be easily determined from the experimental data for the light hydrocarbons. Using our model and data on the light hydrocarbons, we can predict the selectivity of the long chain hydrocarbons.

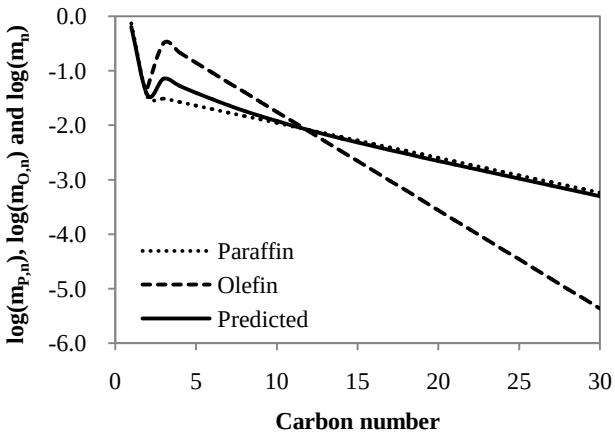

Figure 7.13: The predicted FTS product distribution calculated by using the "CPODM" under the reaction conditions as described in Experiment 11 in Table 1 (cobalt-based catalyst).

We tested the new model by means of our experiments. Figure 7.13 shows the modelling results under the reaction conditions over a cobalt based catalyst as described for Experiment 11 in Table 1. Supposing that the paraffin and olefin products display constant growth factors when the carbon number is equal to, or greater than, 3, we find that the total hydrocarbon product shows a two-alpha distribution with a break between C_8–C_{10} (Figure 7.13):

- For the light hydrocarbons when the carbon number is less than 8, the total hydrocarbon distribution lies between that of the paraffins and olefins;
- For the long chain hydrocarbons when the carbon number is greater than 12, the total hydrocarbon distribution is near that of the paraffin.

The model therefore indicates that the two-alpha ASF distribution may be a combination of different product spectrums.

Equation (7.27) represents the relationship among the mole fractions of all the hydrocarbon species with n carbon atoms, the paraffin mole fraction at carbon number n, and the olefin mole fraction at carbon number n. The value of factor X, which is the function of the reaction conditions and the catalyst properties, changes from 0 to 1. The meaning of the X value in FTS is summarized in Table 2 below.

Table 7.2: Summary of the meaning of the X value in FTS.

Region	Implications
X=0	All the FTS products are olefins. The total hydrocarbon product growth factor is equal to that of the olefin products.
0<X<1	The FTS products are both paraffins and olefins. The total hydrocarbon product growth factor is not constant. The two-alpha ASF distribution will be obtained by the combination of different product spectrums (those for paraffin and olefin).
X=1	All the FTS products are paraffins. The total hydrocarbon product growth factor is equal to that of the paraffin products.

The accuracy of the new model can be demonstrated by comparing the measured against the calculated product distribution. In Figure 7.14, the experimental data for the total distribution of hydrocarbon products are compared with the results of

using the "CPODM". Figure 7.14 shows that there are small discrepancies between the predictions based on the model calculations and the experimental values. The analysis of the results showed that the yield of the paraffin products is around 10 times higher than that of the olefin products under the reaction conditions described in Experiment 5 in Table 1 over an iron-based catalyst, so the total two-alpha ASF product distribution is close to that of the paraffin products. We also can see in Figure 7.14 that the two-alpha values are similar under this reaction condition.

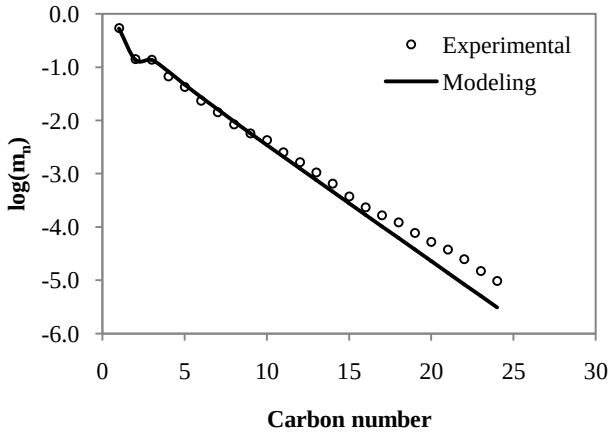

Figure 7.14: The measured and predicted product distributions for FTS. The symbols represent the experimental data, while the line represents the predictions obtained by using the "CPODM" under the reaction conditions described for Experiment 5 in Table 1 (iron-based catalyst).

Figures 7.15 and 7.16 make a comparison between the calculations derived from the model and the experimental values obtained under the reaction conditions described in Experiments 3 and 4 over a cobalt-based catalyst, shown in Table 1. In Figure 7.15, there is good agreement between the model calculations and the experimental values. The results of analysis [66] were that no olefin products could be detected under the reaction conditions for Experiments 1, 2 and 3. Thus, the X value in Equation (7.27) is equal to 1 under the reaction condition defined in Experiment 3 in Table 1 (cobalt based catalyst), and the total hydrocarbon product

growth factor is equal to that of the paraffin products (see Table 2). The experimental data plotted in Figure 7.15 show that the paraffin product distribution follows a one-alpha ASF distribution, with a deviation for the selectivity to C_1.

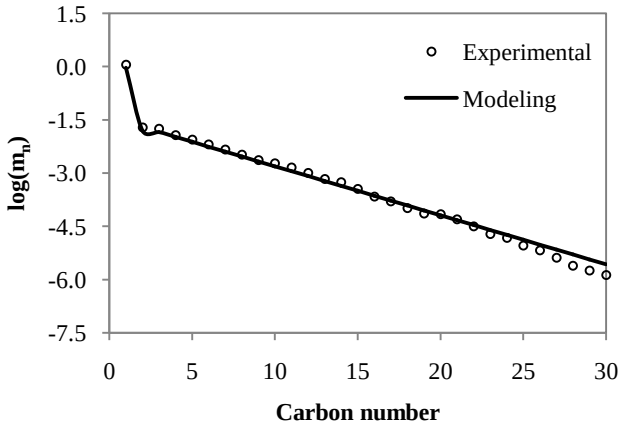

Figure 7.15: The measured and predicted product distributions for FTS. The symbols represent the experimental data, while the line represents the predictions obtained by using the "CPODM" under the reaction conditions described for Experiment 3 in Table 1 (cobalt-based catalyst).

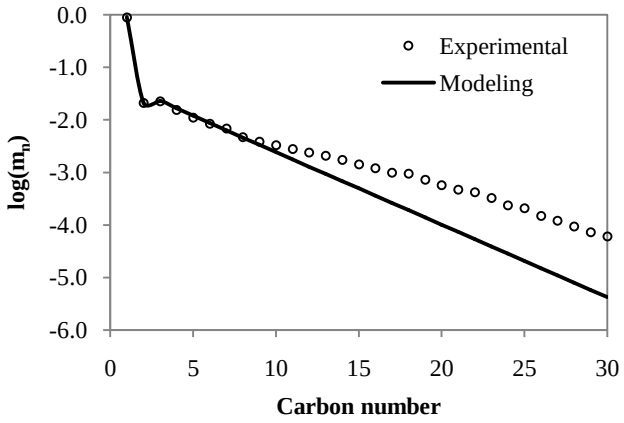

Figure 7.16: The measured and predicted product distributions for FTS. The symbols represent the experimental data, while the line represents the predictions obtained by using the "CPODM" under the reaction conditions described for Experiment 4 in Table 1 (cobalt-based catalyst).

However, in Figure 7.16, large deviations between the prediction based on the model and the experimental data can be observed. The product analysis [66] showed that there was less than 1% of olefin produced, so the X in Equation (7.27) is close to 1 under the reaction conditions in Experiment 4 in Table 1 (cobalt-based catalyst). From the summary given in Table 2, we can postulate that if X approaches unity, most of the FTS products will be paraffins and the total hydrocarbon product distribution will approach the line for the paraffin product distribution. The data shown in Figure 7.16 indicate that the paraffin product distribution follows a typical two-alpha ASF distribution with a deviation for the selectivity to C_1 and C_2.

Because the one-alpha ASF distribution of paraffin product was postulated when the simulation of the "CPODM" was carried out, the model was unable to explain why the paraffin distribution changed from a typical one-alpha to a two-alpha ASF distribution when most of the FTS products were paraffins (Figures 7.15 and 7.16). We therefore suggest that there might be other causes for this phenomenon.

7.4.2 The effects of Vapour-Liquid Equilibrium (VLE) on FT product distribution

Raje *et al*. [41] reported that the prediction of two-alpha selectivity plots using a VLE model indicates that VLE phenomena are responsible for the occurrence of two-alpha ASF distribution in the case of a deactivating catalyst. Masuku *et al.* considered the effects of VLE on FT product distribution [42], and developed a mathematical model to describe it [43]. The results obtained from applying this model show that VLE could describe the observed two-alpha product distribution [43].

Geerlings *et al.* [67] noted that there is a critical chain growth factor, α_c of 0.7, below which the FT reaction is a dry process, and above which heavy wax is

inevitably present. The phenomenon seen in Figures 7.15 and 7.16 indicates that although most of the products under both of the reaction conditions over a cobalt catalyst are paraffins [66], as described in Experiment 3 and 4 in Table 1, the product distributions for these two reaction conditions are totally different: there is a one-alpha (α=0.70) distribution in Experiment 3 and a two-alpha (α_1=0.74>α_c and α_2=0.81>α_c) distribution in Experiment 4. This suggests that there might be a liquid layer on the catalyst surface under the conditions applied in Experiment 4. When feed gas was shifted from CO_2 rich to CO rich, the phase in the reactor could change from one-phase (gas only) to two-phase (gas and liquid), so that the effect of the VLE results in a two-alpha product distribution. Thus the findings of these experiments support the postulate that the double-alpha type plot often observed in FT results could be attributed to VLE.

Table 7.3: Summary of the experimental data for both cobalt- and iron-based catalysts.

Item	CO_2-rich feeds	CO-rich feeds
Product selectivity	Mostly short chain hydrocarbons with methane rich	Mostly long chain hydrocarbons
P/O ratio	High P/O ratio	Low P/O ratio
Product distribution	One-alpha ASF distribution with low alpha value	Two-alpha ASF distribution with high alpha value
The probable phase in the reactor	Gas	Gas and liquid

If we re-examine our experimental data in Table 3, we see that for the CO_2-rich feeds most of the products are short chain paraffins with high methane selectivity, and that the product distribution follows a typical one-alpha distribution with low alpha value. For the CO-rich feeds, the product composition shifts to a typical FT distribution consisting mainly of long chain hydrocarbons, and follows a

two-alpha distribution with high alpha value. The literature [35–37] already published have concurred that under typical reaction conditions, FT products distribute between the vapour and liquid phases within the reactor, so that it is reasonable to conclude that the phase in the reactor changes from gas only to gas and liquid when the feed gas is shifted from CO_2-rich to CO-rich.

7.5 Conclusions

FTS experiments over iron- and cobalt-based catalysts were carried out in a fixed-bed micro reactor. Two feed gases, one comprising H_2:CO:CO_2 = 3:0:1 and the other H_2:CO:CO_2 = 2:1:0, were fed to the reactor and the resultant reactions were monitored. The proportions of the components of the two feed gases were varied to alter the ratio of CO, CO_2 and H_2 stoichiometrically. The experimental data showed that for the CO_2-rich feeds most of the products were short chain paraffins with high methane selectivity, and the product distribution followed a typical one-alpha ASF distribution with low alpha value. In the case of the CO-rich feeds, the product composition shifted to a FT type (mainly long chain hydrocarbons), and a two-alpha distribution with high alpha value.

The combined paraffin and olefin growth factors distribution model was introduced in an attempt to explain the two-alpha ASF distribution, in line with the postulate that both the paraffin and olefin product distribution follow the one-alpha ASF model when the carbon number is equal to, or greater than, 3 and the growth factors are α_P and α_O respectively. The model showed that the two-alpha product distribution may be caused by the combination of different product spectrums. We tested the accuracy of the new model by comparing the predictions derived from the model against our experimental data. While part of the data showed good agreement between the calculations and the experimental values, the model was unable to supply a reason for the change in the paraffin

distribution from a typical one-alpha ASF to a two-alpha distribution.

To explain the phenomenon that when most of the products are paraffins under two different controlled reaction conditions over a cobalt catalyst, the product distribution shifted from a one-alpha ASF pattern under one reaction condition to a two-alpha pathway under the other, we considered the effects of VLE as a probable solution. Masuku *et al*. [42] in their investigation of the effects of VLE on FT product distribution showed that at high alphas, a two-alpha distribution will be measured experimentally when a liquid layer is formed on the catalyst. For CO_2-rich feeds, the alpha value of the product distribution is very low, all the products (short chain) are in the gas phase, and the product follows a single alpha distribution. However, for CO-rich feeds, the alpha value of the product distribution is higher, resulting in products in two phase (gas and liquid), so that the effect of the VLE causes a two-alpha product distribution. These findings support the postulate that the double-alpha type plot often observed in FT results is attributable to VLE.

We therefore conclude that the separate product spectrums and VLE act together to determine the product distribution for FTS. It therefore follows that:

- when a liquid layer is formed on the catalyst surface, a two-alpha distribution will be found, whether the products are olefins or paraffins.
- when there is only gas phase on the catalyst surface, a two-alpha distribution will be observed because of the combination of the different product spectrums whether the products are a mixture of paraffins, olefins and oxygenates, because of their different product growth factors.
- when there is only gas phase on the catalyst surface and only one kind of hydrocarbon product, the FTS product distribution follows a typical one-alpha pathway.

References

[1] Ngwenya, T., Glasser, D., Hildebrandt, D., Coville, N. and Mukoma, P. (2005), Fischer-Tropsch results and their analysis for reactor synthesis, Industrial and Engineering Chemistry Research, 44, 5987–5994.

[2] Mukoma, P., Hildebrandt, D. and Glasser, D. (2006), A process synthesis approach to investigate the effect of the probability of chain growth on the efficiency of Fischer-Tropsch synthesis, Industrial and Engineering Chemistry Research, 45, 5928–5935.

[3] Davis, B. H. (2007), Fischer-Tropsch Synthesis: Comparison of Performances of Iron and Cobalt Catalysts Ind. Eng. Chem. Res., 46, 8938–8945.

[4] Bahome, M. C., Jewell, L. L., Hildebrandt, D., Glasser, D. and Coville, N. J. (2005), Fischer-Tropsch synthesis over iron catalysts supported on carbon nanotubes, Applied Catalysis A: General, 287, 60–67.

[5] Jager, B. and Espinoza, R. (1995), Advances in low temperature Fischer-Tropsch synthesis, Catalysis Today, 23, 17–28.

[6] Jean-Marie, A., Griboval-Constant, A., Khodakov, A. Y. and Diehl, F. (2009), Cobalt supported on alumina and silica-doped alumina: catalyst structure and catalytic performance in Fischer-Tropsch synthesis, Comptes rendus Chimie, 12, 660–667.

[7] de la Pena O'Shea, V. A., Alvarez-Galvan, M. C., Campos-Martin, J.M. and Fierro, J. L. G. (2007), Fischer-Tropsch synthesis on mono- and bimetallic Co and Fe catalysts in fixed-bed and slurry reactors, Applied Catalysis A: General , 326 ,65–73.

[8] Schulz, H. (2007), Comparing Fischer-Tropsch synthesis on iron- and cobalt catalysts: The dynamics of structure and function, Fischer-Tropsch Synthesis, Catalysts and Catalysis, Davis, B. H. and Occelli, M. L. (Editors), Elsevier B.V., Burlington, 163, 177–199.

[9] O'Brien, R. J., Xu, L., Spicer, R. L., Bao, S., Milburn, D. R. and Davis, B. H. (1997), Activity and selectivity of precipitated iron Fischer-Tropsch catalysts, Catalysis Today, 36, 325–334.

[10] Ahmed, I. and Gupta, A.K. (2009), Evolution of syngas from cardboard gasification, Applied Energy, 86, 1732–1740.

[11] Higman, C. and Burgt, M. (2003), Gasification, Guif professional publishing, Burlington.

[12] Haryanto, A., Fernandoc, S. D., Pordesimo, L. O. and Adhikari, S. (2009), Upgrading of syngas derived from biomass gasification: A thermodynamic analysis, biomass and bioenergy, 33, 882–889.

[13] Riedel, T. and Schaub, G. (2003), Low-temperature Fischer-Tropsch synthesis on cobalt catalysts-effects of CO_2, Topics in Catalysis, 26, 145–156.

[14] Dry, M. E. (1981), The Fischer-Tropsch synthesis, catalysis science and technology, Anderson J. R. and Boudart, M. E. (Editors), Springer, New York, 1, 159–255.

[15] Tavakoli, A., Sohrabi, M. and Kargari, A. (2008), Application of Anderson-Schulz-Flory (ASF) equation in the product distribution of slurry phase FT synthesis with nanosized iron catalysts, Chemical Engineering Journal, 136, 358–363.

[16] Patzlaff, J., Liu, Y., Graffmann, C. and Gaube, J. (1999), Studies on product

distributions of iron and cobalt catalyzed Fischer–Tropsch synthesis, Applied Catalysis A: General, 186, 109–119.

[17] Madodand, R. J. and Taylor, W. F. (1981), Fischer-Tropsch synthesis on a precipitated iron catalyst, Journal of Catalysis, 69, 32–43.

[18] Huff JR. G. A. and Satterfield, C. N. (1984), Evidence for two chain growth probabilities on iron catalysts in the Fischer-Tropsch synthesis, Journal of Catalysis, 85, 370–379.

[19] Iglesia, E., Reyes, S. C. and Madon, R. J. (1991), Transport-enhanced a-olefin readsorption pathways in Ru-catalyzed hydrocarbon synthesis, Journal of Catalysis , 129, 238–256.

[20] Wojciechowski, B. W. (1988), The kinetics of the Fischer-Tropsch synthesis, Catalysis Reviews, Science and Engineering, 30, 629–702.

[21] Komaya, T. and Bell, A. T. (1994), Estimates of rate coefficients for elementary processes occurring during Fischer-Tropsch synthesis over Ru/TiO_2. Journal of Catalysis, 146, 237–248.

[22] Schulz, H., van Steen, E. and Claeys, M. (1993), Olefin formation, hydrogenation and isomerization in the kinetic regime of Fischer-Tropsch synthesis, In Selective hydrogenation and dehydrogenation, DGMK, Kassel, Germany.

[23] Kuipers, E. W., Scheper, C., Wilson, J. H. and Oosterbeek, H. (1996), Non-ASF product distributions due to secondary reactions during Fischer-Tropsch synthesis. Journal of Catalysis, 158, 288–300.

[24] Cheng, J., Hu, P., Ellis, P., French, S., Kelly, G. and Lok, C. M. (2008), A DFT study of the chain growth probability in Fischer–Tropsch synthesis, Journal

of Catalysis, 257, 221–228.

[25] Novak, S., Madon, R. J. and Suhl, H. (1981), Models of hydrocarbon product distributions in Fischer-Tropsch synthesis. Journal of Chemical Physics, 74, 6083–6091.

[26] Rich, N. M., Hsu, C. C. and Wojciechowshi, B. W. (1988), The effect of catalyst surface heterogeneity on the Fischer-Trosch synthesis, the Canadian Journal of Chemical Engineering, 66, 694–696.

[27] Huyser, J., van Vuuren, M. J. and Kupi, G. (2010), The value of a two alpha model in the elucidation of a full product spectrum for Fe-LTFT, Advances in Fischer-Tropsch Synthesis, Catalysts, and Catalysis, CRC Press, chapter 10, 185–197.

[28] Schulz, H. and Claeys, M. (1999), Kinetic modelling of Fischer-Tropsch product distributions, Applied Catalysis A: General, 186, 91–107.

[29] van der Laan, G. P. and Beenackers, A. A. C. M. (1999), Hydrocarbon selectivity model for the gas-solid Fischer-Tropsch synthesis on precipitated iron catalysts, Industrial and Engineering Chemistry Research, 38, 1277–1290.

[30] Patzlaff, J., Liu, Y., Graffmann, C. and Gaube, J. (1999), Studies on product distributions of iron and cobalt catalyzed Fischer-Tropsch synthesis, Applied Catalysis A: General, 186, 109–119.

[31] Patzlaff, J., Liu, Y., Graffmann, C. and Gaube, J. (2002), Interpretation and kinetic modeling of product distributions of cobalt catalyzed Fischer–Tropsch synthesis, Catalysis Today, 71, 381–394.

[32] Ronald, A. and Bell, A. T. (1986), Fischer-Tropsch synthesis over reduced and unreduced iron oxide catalysts, Journal of Catalysis, 97, 121–136.

[33] Liu, Y., Zheng, S., Shi, B. and Li, J. (2007), Deuterium tracer study of Fischer–Tropsch synthesis:A method to eliminate accumulation problems, Journal of Molecular Catalysis A: Chemical, 276, 110–115.

[34] Shi, B. and Davis, B. H. (2004), Fischer–Tropsch synthesis: accounting for chain-length related phenomena, Applied Catalysis A: General, 277, 61–69.

[35] Dry, M. E. (2002), The Fischer-Tropsch process: 1950–2000, Catalysis Today, 71, 227–241.

[36] Marano, J. J. and Holder, G. D. (2007), Characterization of Fischer-Tropsch liquids for vapor-liquid equilibria calculations, Fluid Phase Equilibria, 138, 1–21.

[37] Caldwell, L. and van Vuuren, D. S. (1986), On the formation and composition of the liquid phase in Fischer-Tropsch reactors, Chemical Engineering Science, 41, 89–96.

[38] Satterfield, C. N. and Stenger Jr. H. G. (1985), Effect of liquid composition on the slurry Fischer-Tropsch synthesis: 1. Rate of reaction, Industrial and Engineering Chemistry Process Design and Development, 24, 407–411.

[39] Satterfield, C. N. and Stenger Jr. H. G. (1985), Effect of liquid composition on the slurry Fischer-Tropsch synthesis: 2. Product selectivity, Industrial and Engineering Chemistry Process Design and Development, 24, 411–415.

[40] Quicker, G. and Deckwer, W. D. (1981), Gas hold-up and interfacial area in aerated hydrocarbons, German Chemical Engineering, 4, 363–370.

[41] Raje, A. P. and Davis, B. H. (1996), Effect of vapor-liquid equilibrium on Fischer-Tropsch hydrocarbon selectivity for a deactivating catalyst in a slurry reactor, Energy & Fuels, 10, 552–560.

[42] Masuku, C. M., Hildebrandt, D. and Glasser, D. (2007), Thermodynamic prediction of the chain propagation probability (α) for the Fischer-Tropsch reaction, AIChE Spring National Meeting.

[43] Masuku, C. M., Hildebrandt, D. and Glasser, D. (2009), Fischer-Tropsch reactor modelling considering vapour-liquid equilibrium, AIChE Annual Meeting.

[44] Perez-Alonso, F. J., Ojeda, M., Herranz, T., Rojas, S., Gonzalez-Carballo, J. M., Terreros, P. and Fierro, J. L. G. (2008), Carbon dioxide hydrogenation over Fe–Ce catalysts, Catalysis Communications, 9 , 1945–1948 .

[45] Newsome, D. S. (1980), The water-gas shift reaction, Catalysis Reviews, Science and Engineering, 21, 275–318.

[46] Dry, M. E. (1996), Practical and theoretical aspects of the catalytic Fischer-Tropsch process, Applied Catalysis A: General, 138, 319–344.

[47] Riedel, T., Schaub, G., Jun, K. and Lee, K. (2001), Kinetics of CO_2 hydrogenation on a K-promoted Fe catalyst, Industrial and Engineering Chemistry Research, 40, 1355–1363.

[48] Weatherbee, G. D. and Bartholomew, C. H. (1984), Hydrogenation of CO_2 on group VIII metals. Journal of Catalysis, 77, 352–362.

[49] Lee, J. F., Chern, W. S. and Lee, M. D. (1992), Hydrogenation of carbon dioxide on iron catalyst doubly promoted with manganese and potassium. Canadian Journal of Chemical Engineering, 70, 511–515.

[50] Herranz, T., Rojas, S., Perez-Alonso, F. J., Ojeda, M., Terreros, P. and Fierro, J. L. G. (2006), Hydrogenation of carbon oxides over promoted Fe-Mn catalysts prepared by the micro emulsion methodology, Applied Catalysis A: General , 311, 66–75 .

[51] Zhou, W., Chen, J., Fang, K. and Sun, Y. (2006), The deactivation of Co/SiO_2 catalyst for Fischer-Tropsch synthesis at different ratios of H_2 to CO, Fuel Processing Technology, 87, 609–616.

[52] Xiong, H., Zhang, Y., Liew, K. and Li, J. (2005), Catalytic performance of zirconium-modified Co/Al_2O_3 for Fischer-Tropsch synthesis, Journal of Molecular Catalysis A: Chemical, 231, 145–151.

[53] Zhang, Y., Jacobs, G., Sparks, D. E., Dryb, M. E. and Davis, B. H. (2002), CO and CO_2 hydrogenation study on supported cobalt Fischer-Tropsch synthesis catalysts, Catalysis Today, 71, 411–418.

[54] Riedel, T., Claeys, M.m Schulz, H., Schaub, G., Nam, S., Jun, K., Choi, M., Kishan, G. and Lee, K. (1999), Comparative study of Fischer-Tropsch synthesis with H_2/CO and H_2/CO_2 syngas using Fe- and Co-based catalysts, Applied Catalysis A: General, 186, 201–213.

[55] Visconti, C. G., Lietti, L., Tronconi, E., Forzatti, P., Zennaro, R. and Finocchio, E. (2009), Fischer-Tropsch synthesis on a Co/Al_2O_3 catalyst with CO_2 containing syngas, Applied Catalysis A: General, 355, 61–68.

[56] Li, J. (1999), The preparation, characterization and evaluation of boron modified Co/TiO_2 Fischer-Tropsch catalysts. PhD thesis, University of the Witwatersrand, Johannesburg, South Africa.

[57] Botes, F. G. (2007), Proposal of a new product characterization model for the iron-based low temperature Fischer-Tropsch synthesis, Energy & Fuels, 21, 1379–1389.

[58] van Der Laan, G. P. and Beenachers, A. A. C. M. (1999), Hydrocarbon Selectivity Model for the Gas-Solid Fischer-Tropsch Synthesis on Precipitated

Iron Catalysts, Industrial and Engineering Chemistry Research, 38, 1277–1290.

[59] Egiebor, N. O. and Cooper, W. C. (1985), The Polyfunctionality of iron catalysts during CO hydrogenation: I. occurrence of dual chain propagation sites, Applied Catalysis, 14, 323–332.

[60] Satterfield, C. N. and Stenger, H. G. (1984), Fischer-Tropsch synthesis on a precipitated Mn/Fe catalyst in a well-mixed slurry reactor, Industrial and Engineering Chemistry Process Design and Development, 23, 26–29.

[61] Shi, B. and Davis, B. H. (2005), Fischer-Tropsch synthesis: The paraffin to olefin ratio as a function of carbon number. Catalysis Today, 106, 129–131.

[62] van Vuuren, M. J., Huyser, J., Grobler, T. and Kupi, G. (2010), Fe-LTFT selectivity a sasol perspective, advances in Fischer-Tropsch synthesis, Catalysts, and Catalysis, CRC Press, chapter 13, 229–241.

[63] Kuipers, E. W., Vinkenburg, I. H. and Oosterbeek, H. (1995), Chain length dependence of α-olefin readsorption in Fischer-Tropsch synthesis. Journal of Catalysis, 152, 137–146.

[64] Zheng, S., Liu, Y., Li, J. and Shi, B. (2007), Deuterium tracer study of pressure effect on product distribution in the cobalt-catalyzed Fischer–Tropsch synthesis, Applied Catalysis A: General, 330, 63–68.

[65] Stenger, Jr. H. G. and Askonas, C. F. (1986), Thermodynamic product distributions for the Fischer-Tropsch synthesis, Industrial and Engineering Chemistry Research Fundamentals, 25, 410–413.

[66] Yao, Y., Hildebrandt, D., Glasser, D. and Liu, X. (2010), Fischer-Tropsch synthesis using $H_2/CO/CO_2$ syngas mixtures over a cobalt catalyst, Industrial and Engineering Chemistry Research, 49 , 11061–11066.

[67] Geerlings, J. J. C., Wilson, J. H., Kramer, G. J., Kuipers, H. P. C. E., Hoek, A. and Huisman, H. M. (1999), Fischer-Tropsch technology- from active site to commercial process, Applied Catalysis A: General, 186, 27–40.

8

FISCHER-TROPSCH SYNTHESIS USING $H_2/CO/CO_2$ SYNGAS MIXTURES: A COMPARASON OF PARAFFIN TO OLEFIN RATIOS FOR IRON AND COBALT BASED CATALYSTS

This work has been submitted in the form of a paper for future publication in Appl. Catal. A: Gen., 2011. Part of this work was presented at the following conference:

- *AIChE Spring Meeting, San Antonio, UAS, March 21-25, 2010.*

Abstract

Fischer-Tropsch synthesis (FTS) using $H_2/CO/CO_2$ syngas mixtures over cobalt and iron based catalysts was carried out in a fixed-bed micro reactor. CO_2 rich feeds produce products that are mostly light hydrocarbons with a high molar paraffin to olefin (P/O) ratio, whereas CO rich feeds shift the product composition to an FT type (mainly higher hydrocarbons) product with low P/O ratio over both iron and cobalt based catalysts. Although the product selectivity and P/O ratio for FTS are strongly dependent on the operating conditions, the experimental evidence shows that the linear relationship between $P_{(n+1)}/O_{(n+1)}$ and $P_{(n)}/O_{(n)}$ holds for a large number of experiments. It is also shown to be independent of the type of the reactor, the composition of the syngas, reaction conditions and the kind of catalyst. Two features about the ratio of $k=[P_{(n+1)}/O_{(n+1)}]/[P_{(n)}/O_{(n)}]$ for the FT products have been identified: (1) with $n>2$, the experimental values of $k_{n>2}$ is higher than 1, fairly constant and independent of chain length n; (2) with chain length $n=2$, the ratio of P_3/O_3 to P_2/O_2 ($k_{n=2}$) is significantly different, and shows that $k_{n=2} \ll k_{n>2}$. An equilibrium hypothesis is considered in an attempt to explain

this experimental phenomenon.

A simple vapour-liquid equilibrium (VLE) model indicates that the ratio of $P_{(n+1)}/O_{(n+1)}$ to $P_{(n)}/O_{(n)}$ changes in a range of (1, $1/\beta$), where β is the variation of the vapour pressure coefficient. Our experimental results support the expression when the chain length $n>2$. But with chain length $n=2$, this expression is unable to explain the relationship between P_3/O_3 and P_2/O_2. Another model, based on quasi reaction equilibrium, is developed to explain the linear relationship between $P_{(n+1)}/O_{(n+1)}$ and $P_{(n)}/O_{(n)}$. We assume that the reaction of $C_{n+1}H_{2n+2}+C_nH_{2n+2}=C_{n+1}H_{2n+4}+C_nH_{2n}$ reaches quasi-equilibrium. Because the experimental results are quite close to the equilibrium calculations, we postulate that the product distribution might be determined by considering reaction equilibrium.

8.1 Introduction

The conversion of syngas to mainly straight chain hydrocarbons with wide carbon number distribution via Fischer–Tropsch synthesis (FTS), is becoming a promising route to meet the continuously increasing demand for liquid fuels and chemical feed-stocks [1–2]. Among the reported FTS catalysts, only iron and cobalt catalysts appear economically feasible on an industrial scale [3–6]. The high water-gas shift (WGS) activity of iron makes it an ideal catalyst for converting hydrogen-lean syngas derived from coal [7–8]. Cobalt catalysts with low WGS activity have a high activity for hydrogenation and tend to produce linear alkanes [9–12]. The synthesis gas, a mixture of predominantly CO and H_2 with different H_2/CO ratios, can be produced from coal, natural gas or biomass [13]. In some cases, CO_2 may be a significant component in the syngas [14]. It is therefore interesting to gain insight into the reaction pathways for FTS using H_2/CO/CO_2 syngas mixtures over both iron and cobalt based catalysts.

Hydrogenation of CO_2 has been traditionally carried out on catalysts that have been demonstrated to be active and selective for the FT reaction, which hydrogenates CO [7, 8, 15]. Iron based catalysts are active in both WGS and reverse-water-gas shift (R-WGS) reactions [16]. In principle, they would be ideal candidates to be used in the FTS of CO_2-containing syngas feeds [17]. Xu *et al.* [18] discovered that $^{14}CO_2$ added to the syngas serves to initiate chain growth to produce both oxygenates and hydrocarbons for FTS over an iron-based catalyst. The FT reaction utilizing CO_2 is thought to proceed in two stages: first the Reverse-WGS reaction takes place ($CO_2+H_2=CO+H_2O$) and then the CO formed is consumed in the FT reaction ($CO+H_2\rightarrow CH_2+H_2O$) [18–20]. The comparison of the selectivity of the CO and CO_2 hydrogenation on iron catalysts without promoters shows that CO_2 hydrogenation exhibits [15, 21]: (1) a low alpha distribution; (2) a higher selectivity for light hydrocarbons and (3) a higher paraffin selectivity in the products.

Cobalt catalysts with low WGS activity have a high activity for hydrogenation and tend to produce linear alkanes [9–12]. CO and CO_2 hydrogenation on cobalt based catalysts were conducted by various researchers [22–25]. Activity data clearly showed that when used alone, both CO and CO_2 are readily hydrogenated over the catalyst under actual low temperature FTS conditions. The product distribution during the CO and CO_2 hydrogenation process was found to be very different. For CO hydrogenation, a typical FTS product distribution was observed, with a high chain growth probability (α); conversely, the CO_2 hydrogenation leads to mainly light saturated hydrocarbons. In particular, methane accounts for more than 90% of the products in the case of CO_2 hydrogenation and for less than 10% in the case of CO hydrogenation [23–25].

The paraffin to olefin (P/O) ratio in FTS, and what it depends on, remains elusive [26]. Experimentally, various interesting features about P/O have been identified

[26–30]: (1) the P/O ratio generally increases exponentially with chain length *n* (*n*>2), and (2) when the chain length is *n* = 2, the P/O ratio deviates significantly. The P/O ratio increases exponentially with chain length, which is attributed to a chain-length-dependent olefin readsorption mechanism [26–33]. Various models which consider diffusion [32], solubility [27–31, 33], physisorption [27–31, 33] or chemisorption [26] have been obtained to describe the product distribution of FTS, and these models [26, 27, 30, 33] are used to explain why the P/O ratio increases exponentially with chain length. Iglesia and co-workers [32] introduce a transport model that concludes that the rate of diffusion enhances olefin readsorption. They also believe that the diffusion limitation between the catalyst surface and the FT wax layer is the reason for the strong exponential decrease of the P/O ratio. However, experimental evidence [27, 29] has shown that without diffusion limitations on the catalyst surface, the P/O ratio still increases exponentially with chain length, demonstrating that diffusion limitation is not a predominantly influencing factor, compared to solubility and physisorption. In addition, van der Laan [30] developed a model where the rate of olefin readsorption depends on the chain length because of both increasing physisorption strength on the catalyst surface and increasing solubility of long-chain molecules in the liquid medium. Nevertheless, Cheng et al. [26] say that the preferential physisorption may not be the main reason for the chain length-dependent P/O ratio because the transfer processes must be much faster than the surface reactions, and that chemisorption may be the reason. Although much effort has been devoted to this issue, it is still unclear which factors predominately determine α-olefin selectivity. Perhaps more importantly, to date there is very little information about the P/O ratio for FTS with $H_2/CO/CO_2$ syngas mixtures.

In this work, experiments using $H_2/CO/CO_2$ syngas mixtures over iron and cobalt based FTS catalysts were conducted. Two feed gases, $H_2:CO:CO_2$ = 2:1:0 and $H_2:CO:CO_2$ = 3:0:1, were mixed in various proportions, thus varying the ratio of

CO, CO_2 and H_2 stoichiometrically. The product selectivity, reaction rate and P/O ratio for each reaction condition were measured and compared.

8.2 Experimental

8.2.1 Cobalt catalyst

8.2.1.1 Catalyst preparation

The Co/TiO_2 catalyst used in this study was prepared by impregnating TiO_2 with a cobalt nitrate solution. TiO_2 (Degussa P25) was mixed with distilled water in a mass ratio of 1:1 and dried in air at 120 ℃ for 1 hour. The support was then calcined in air at 400 ℃ for 16 hours [12]. After calcination the support was crushed and sieved and the particles with diameters between 0.5 and 1 mm were used. The support was then impregnated with a cobalt nitrate ($Co(NO_3)_2 \cdot 6H_2O$) solution, the quantity added being such as to give a cobalt metal loading of 10% by mass. After the impregnation step, the support was dried in air at 120 ℃ for 16 hours and then calcined in air at 400 ℃ for 6 hours to decompose and transform the cobalt nitrate to cobalt oxide.

8.2.1.2 Experimental set-up and procedure

8.2.1.2.1 Catalyst reduction

One gram of catalyst was loaded in the micro fixed bed reactor (FBR). The reduction was performed at atmospheric pressure with H_2 (Afrox (African Oxygen) Ltd., 99.999%) for 24 hours. The reduction temperature and the flow rate were 350 ℃ and 60 ml(NTP)/(min gcat), respectively.

8.2.1.2.2 FTS using $H_2/CO/CO_2$ syngas

Once the reduction was completed, the reactor was allowed to cool down to room temperature. The CO_2 syngas (which we will refer to as the CO_2 feed, and which has composition H_2:CO:CO_2 = 3:0:1, 10 vol.% N_2 as an internal standard for mass balance calculations) was introduced into the reactor first at a flow rate of 60 ml(NTP)/(min gcat). The reactor pressure was slowly increased to 20 bar (gauge) and thereafter the temperature was increased gradually to 200 ℃. The pressure and temperature were allowed to stabilize, and the operating conditions were maintained constant for 72 hours while the tail gas composition was monitored. Thereafter, the flow rate of the CO_2 syngas was decreased by 10%, that is 6 ml(NTP)/(min gcat), and the CO syngas (which we will refer to as the CO feed, and which has a composition of H_2:CO:CO_2 = 2:1:0, 10% N_2 as an internal standard for mass balance calculations) was introduced into the reactor (flow rate of 6 ml(NTP)/(min gcat)) so as to keep the total flow rate constant at 60 ml(NTP)/(min gcat). The new reaction conditions were maintained for 72 hours while the tail gas composition was monitored. After that the flow rate of the CO_2 mixture was again decreased while that of the CO mixture was increased so as to keep the total flow rate of gas to the reactor at 60 ml(NTP)/(min gcat). The feed and reaction conditions for the 11 experiments over the cobalt based catalyst are shown in Table 8.1.

8.2.2 Iron catalyst

8.2.2.1 Catalyst preparation

The Fe/TiO_2 catalyst was prepared by a single-step incipient wetness impregnation of the support with an iron nitrate ($Fe(NO_3)_3$ $9H_2O$) solution. The same procedure as that of the cobalt catalyst preparation was used. For more detailed information please refer to the Co catalyst preparation mentioned above.

Table 8.1: Summary of experimental conditions for FTS using $H_2/CO/CO_2$ mixtures over cobalt and iron based catalysts.

	Cobalt based catalyst				Iron based catalyst			
Temperature (℃)	200				250			
Total pressure (bar gauge)	20				20			
Flow rate (ml(NTP)/(min gcat)	60				60			
	Partial pressure at entrance (bar)				Partial pressure at entrance (bar)			
Reaction condition number	P_{H_2}	P_{CO}	P_{CO_2}	P_{N_2}	P_{H_2}	P_{CO}	P_{CO_2}	P_{N_2}
1	14.2	0.0	4.8	2.1	14.2	0.0	4.8	2.1
2	13.9	0.5	4.2	2.0	14.0	0.6	4.3	2.0
3	13.8	1.3	3.9	2.0	13.8	1.3	3.8	2.1
4	13.7	1.9	3.3	2.1	13.6	2.0	3.3	2.1
5	13.3	2.4	2.8	2.0	13.4	2.5	2.9	2.1
6	13.2	3.2	2.3	2.1	13.2	3.2	2.4	2.1
7	13.1	3.8	1.9	2.1	13.1	3.9	1.9	2.1
8	13.0	4.3	1.5	2.1	13.0	4.5	1.5	2.1
9	12.9	4.9	0.9	2.1	12.7	5.2	1.0	2.1
10	12.7	5.6	0.4	2.1	12.6	5.8	0.5	2.1
11	12.5	6.3	0.0	2.2	12.4	6.4	0.0	2.1

8.2.2.2 Experimental set-up and procedure

8.2.2.2.1 Catalyst reduction

A quantity of one gram of catalyst was loaded into the micro-FBR. The reduction was performed at atmospheric pressure with H_2 (Afrox (African Oxygen) Ltd.,

99.999%) for 24 hours. The reduction temperature and the flow rate were 350 ℃ and 60 ml(NTP)/min, respectively.

8.2.2.2.2 FTS using $H_2/CO/CO_2$ syngas

FTS experiments over iron based catalysts were carried out in a micro-FBR. The same operating procedures were used as outlined in Section 8.2.1.2.2. The only difference was that the operating temperature for the iron catalyst was 250 ℃, whereas for cobalt it was 200 ℃. The process conditions for an iron based catalyst are shown in Table 8.1.

8.2.3 Product analysis

The tail gas was analyzed every 1.5 hours using an online DANI GC. Two thermal conductivity detectors (TCD) were used to analyze H_2, N_2, CO, CO_2 and CH_4 and a flame ionization detector (FID) was used for the analysis of gas phase hydrocarbons. The wax and liquid products were collected in a hot trap (kept at 150 ℃) and cold trap (kept at room temperature) (Figure 8.1). Off-line analysis of oil and wax products, using an off-line GC, was performed at the end of the mass balance for each run.

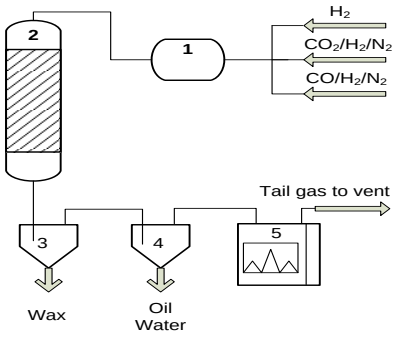

Figure 8.1: Simplified flow scheme of fixed bed reactor used in the experiments: (1) inlet gas mixer; (2) fixed bed reactor; (3) hot condensable products trap; (4) cold condensable products trap; (5) online GC.

8.3 Results

Table 8.1 lists the reaction conditions for both cobalt and iron based catalysts. There were two feed gases, H_2:CO:CO_2 = 2:1:0 and H_2:CO:CO_2 = 3:0:1, which were mixed in various proportions, thereby varying the ratio of CO, CO_2 and H_2 stoichiometrically. The various compositions of CO, CO_2 and H_2 feed gases were introduced into one micro-FBR with the cobalt catalyst, and the other micro-FBR with the iron catalyst.

The results agree with the results of previous researchers [25, 33]. We have presented the results below in graphical form; some of the graphs and the ways of displaying the results have not been used before. The reason for using the graphs and interpretation of the graphs will be discussed in Section 8.4.

8.3.1 Product selectivity and reaction rate

The product selectivity as a function of syngas composition for the 11 data points (Table 8.1) over a cobalt based catalyst is shown in Figure 8.2. The data show that the selectivity of the products is strongly dependent on the syngas composition: the methane selectivity is around 90% when the feed is CO_2/H_2 (corresponding to $CO_2/(CO+CO_2)$ = 1), but it is only 9% when the feed is CO/H_2 (corresponding to $CO_2/(CO+CO_2)$ = 0). CO_2 rich feeds produce products that are mostly light hydrocarbons with methane rich, whereas CO rich feeds shift the product composition to an FT-type (mainly higher hydrocarbons) product; similar results were reported by Visconti et al. [24].

In view of the effect of the partial pressures of CO, CO_2 and H_2 on the catalyst activity, the rates of formation of the light olefins and paraffins over cobalt catalyst are plotted in Figure 8.3. The olefin rate decreases with an increase in the ratio of $CO_2/(CO+CO_2)$. When the ratio of $CO_2/(CO+CO_2)$ is greater than 70%,

no olefin can be detected in the product. However, a different trend is observed for the rates of formation of the paraffins; and, the rates pass through a maximum. The paraffin rates are fairly constant when the ratio of $CO_2/(CO+CO_2)$ is in the range of 40% to 75%. The results show that the effects of the partial pressures of CO, H_2 and CO_2 on the formation of paraffins and olefins are different.

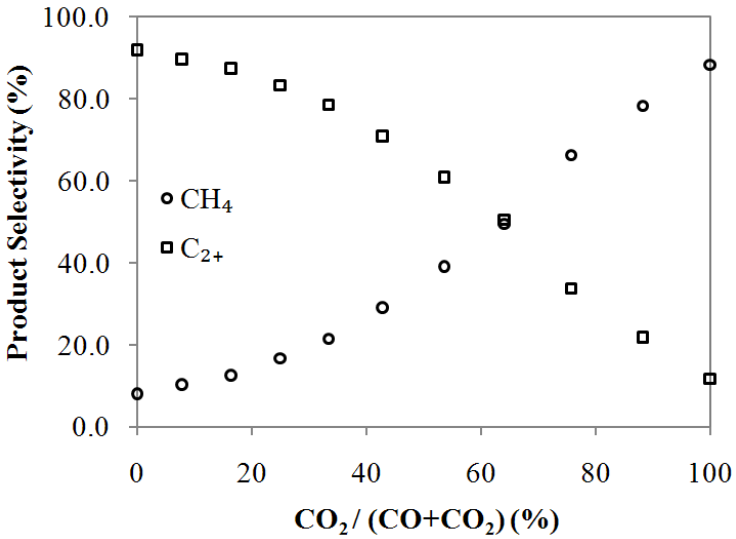

Figure 8.2: Product selectivity as a function of synthesis gas composition (reaction conditions as in Table 8.1) over a cobalt based catalyst.

Figure 8.4 and Figure 8.5 show the product selectivity and reaction rate as a function of syngas composition (as shown in Table 8.1) over the iron based catalyst, which show the same trend as for the cobalt based catalyst shown in Figure 8.2 and Figure 8.3, respectively, in that CO_2 rich feeds produce products that are mostly light hydrocarbons, whereas CO rich feeds shift the product composition to an FT type (mainly higher hydrocarbons) product. The data in Figure 8.5 also show that the olefin rate decreases with an increase in the ratio of $CO_2/(CO+CO_2)$; however, the paraffin rate first increases and then decreases with an increase in the ratio of $CO_2/(CO+CO_2)$.

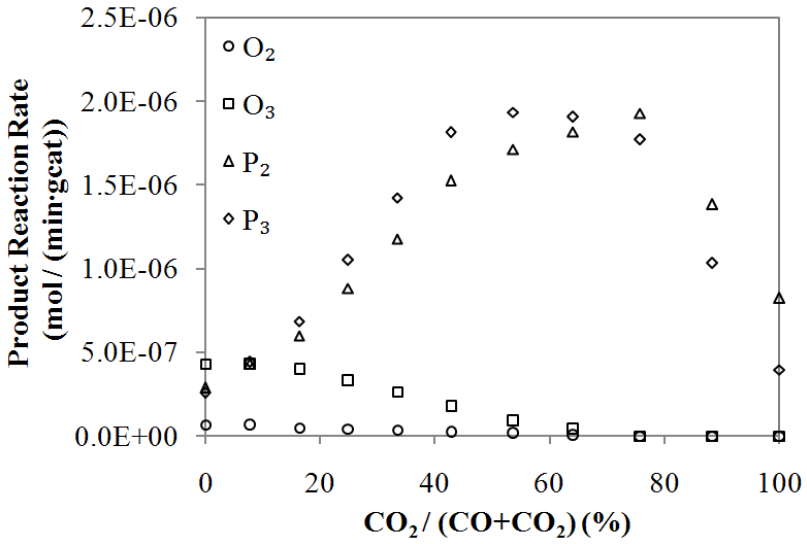

Figure 8.3: Product reaction rate as a function of synthesis gas composition (reaction conditions as in Table 8.1) over a cobalt based catalyst (O represents olefin and P represents paraffin).

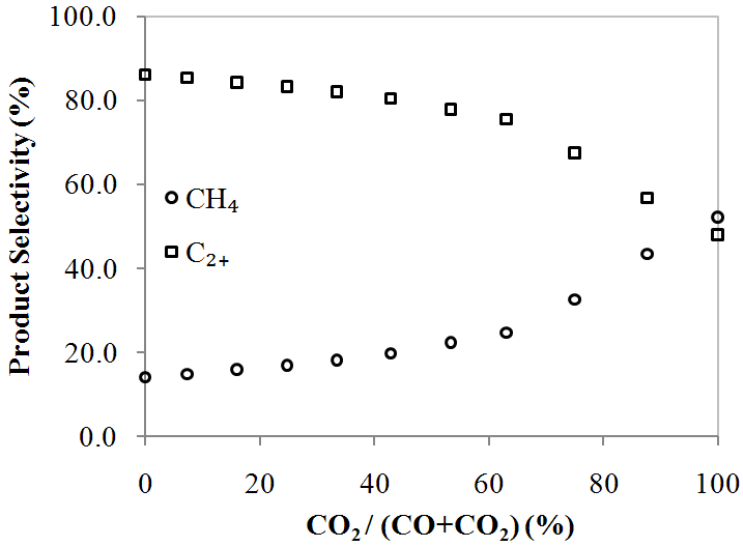

Figure 8.4: Product selectivity as a function of synthesis gas composition (reaction conditions as in Table 8.1) over an iron based catalyst.

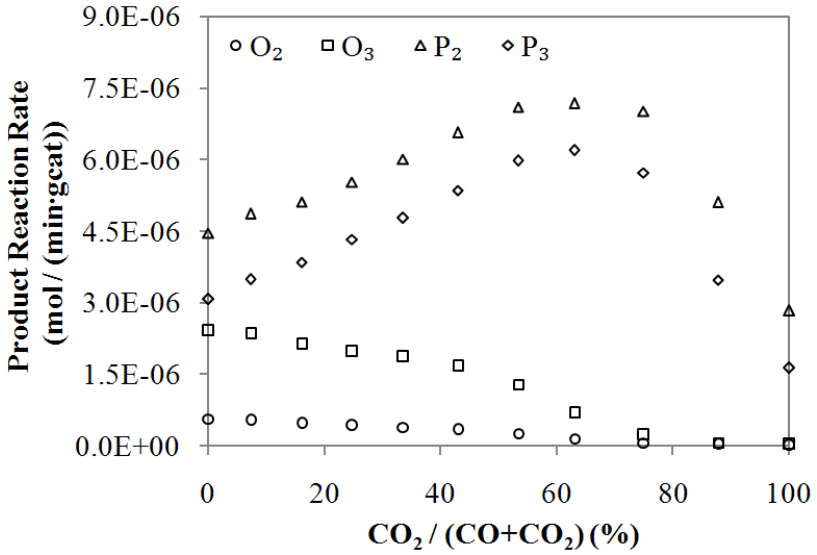

Figure 8.5: Product reaction rate as a function of synthesis gas composition (reaction conditions as in Table 8.1) over an iron based catalyst (O represents olefin and P represents paraffin).

8.3.2 Paraffin to olefin ratio

Figure 8.6 shows the molar paraffin to olefin (P/O) ratio as a function of synthesis gas composition over a cobalt based catalyst. We find results similar to those found in the literature [26-33] in that the paraffin to olefin ratio changes as a function of carbon number. Increasing the carbon number increases the paraffin to olefin ratio at each reaction condition. As the amount of CO_2 in the feed gas is increased and the quantity of CO is reduced (as indicated in Table 8.1), the P/O ratio for a particular carbon number increases. CO_2 rich feeds produce products with high paraffin selectivity, whereas CO rich feeds shift the product composition to an FT type (mainly higher hydrocarbons) product with both high paraffin and olefin selectivities. The same trend is obtained over an iron based catalyst (Figure 8.7).

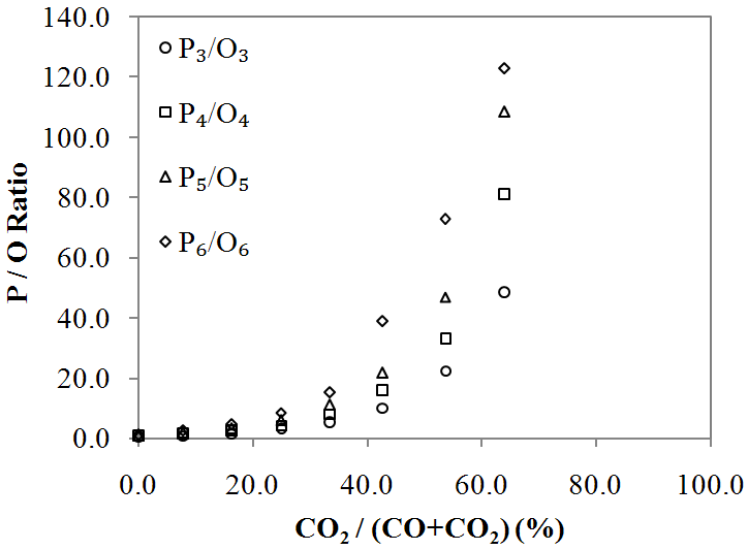

Figure 8.6: The molar paraffin to olefin (P/O) ratio as a function of synthesis gas composition over a cobalt based catalyst (reaction conditions as in Table 8.1).

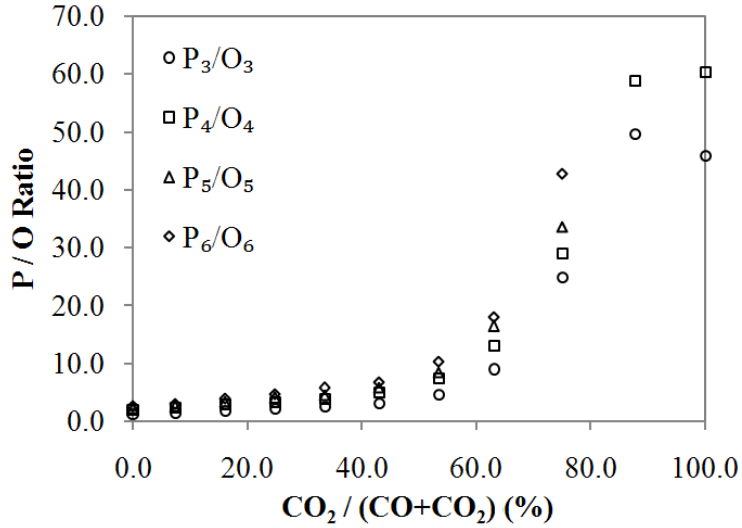

Figure 8.7: The molar paraffin to olefin (P/O) ratio as a function of synthesis gas composition over an iron based catalyst (reaction conditions as in Table 8.1).

8.3.3 The relationship between $P_{(n+1)}/O_{(n+1)}$ and $P_{(n)}/O_{(n)}$

The results from Figure 8.2 to Figure 8.7 show that the product selectivity and the P/O ratio are strongly dependent on the syngas composition. CO_2 rich feeds produce products that are most light hydrocarbons with a high P/O ratio, whereas

CO rich feeds shift the product composition to an FT type (mainly higher hydrocarbons) product with a low P/O ratio.

In this work, the P/O ratio among different carbon numbers over cobalt and iron catalysts was also compared under the reaction conditions as shown in Table 8.1. Figure 8.8 shows the molar ratio of $P_{(n+1)}/O_{(n+1)}$ as a function of the molar ratio of $P_{(n)}/O_{(n)}$ over the cobalt catalyst:

(1) With chain length n>2, $P_{(n+1)}/O_{(n+1)}$ versus $P_{(n)}/O_{(n)}$ follow a good linear relationship, which can be described as follows:

$$\left.\frac{P_{(n+1)}/O_{(n+1)}}{P_{(n)}/O_{(n)}}\right|_{n>2} \approx k_{n>2}^{1} = 1.376 \tag{8.1}$$

(2) With chain length n=2, P_3/O_3 versus P_2/O_2 still form more or less straight line with a lower value of the slope than for n>2, which can be expressed as Equation (8.2). Because of the limitation of the analytical equipment, when P_2/O_2 >90, the data are scattered and are likely inaccurate.

$$\frac{P_3/O_3}{P_2/O_2} \approx k_{n=2}^{1} = 0.150 \tag{8.2}$$

The molar ratio of $P_{(n+1)}/O_{(n+1)}$ as a function of the molar ratio of $P_{(n)}/O_{(n)}$ over the iron based catalyst (reaction conditions in Table 8.1) is shown in Figure 8.9. The same trend as shown in Figure 8.8 can also be described:

(1) with chain length n>2

$$\left.\frac{P_{(n+1)}/O_{(n+1)}}{P_{(n)}/O_{(n)}}\right|_{n>2} \approx k_{n>2}^{2} = 1.244 \tag{8.3}$$

and (2) with chain length n=2

$$\frac{P_3/O_3}{P_2/O_2} \approx k_{n=2}^{2} = 0.181 \tag{8.4}$$

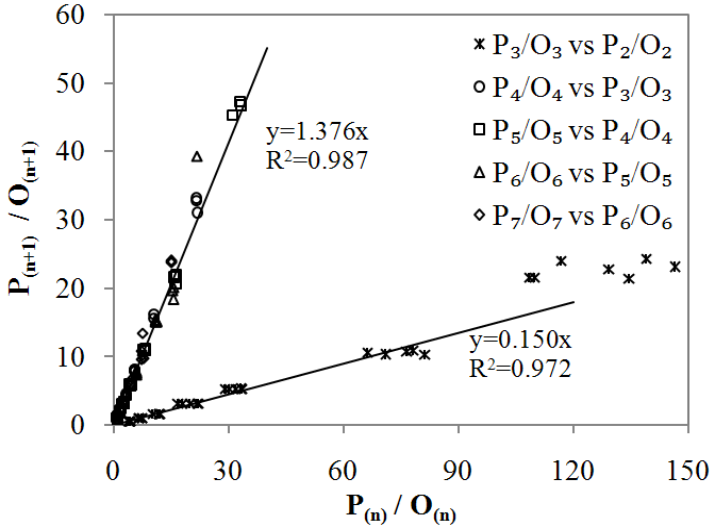

Figure 8.8: The molar ratio of $P_{(n+1)}/O_{(n+1)}$ as a function of the molar ratio of $P_{(n)}/O_{(n)}$ for Fischer-Tropsch synthesis using a fixed bed reactor over a cobalt based catalyst (P represents paraffin, O represents olefin, *n* represents the carbon number), and reaction conditions as shown in Table 8.1.

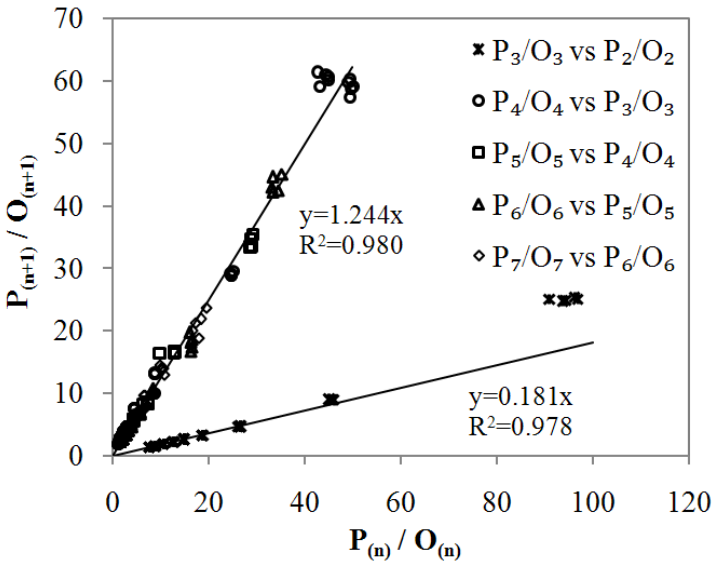

Figure 8.9: The molar ratio of $P_{(n+1)}/O_{(n+1)}$ as a function of the molar ratio of $P_{(n)}/O_{(n)}$ for Fischer-Tropsch synthesis using a fixed bed reactor over an iron based catalyst (P represents paraffin, O represents olefin, *n* represents carbon number), and reaction conditions as shown in Table 8.1.

The linear relationship between $P_{(n+1)}/O_{(n+1)}$ and $P_{(n)}/O_{(n)}$ for FTS, using a fixed

bed reactor with different partial pressures of H_2, CO and CO_2 feed gases over both cobalt based and iron based catalysts, is shown in Figure 8.8 and Figure 8.9. In order to see if the trend is general, we used data from the open literature [34] and plotted similar graphs. For data from the literature [34], FT experiments were carried out in two different types of reactors with various reaction conditions over an iron based catalyst: (1) in a spinning basket reactor (SBR), the reaction conditions were varied: T = 250 ^{o}C, P = 8–40 bar, H_2/CO ratio = 0.25–4.0, and flow rate = 30–120 ml/(min gcat); (2) in a slurry reactor (SR), the reaction conditions were varied: T = 250 ^{o}C, P = 12–40 bar, H_2/CO ratio = 0.25–4.0, and flow rate = 15–30 ml/(min ·gcat). Although the reaction conditions in literature [34] were varied on a large scale in each reactor, the same linear relationship between $P_{(n+1)}/O_{(n+1)}$ and $P_{(n)}/O_{(n)}$ is also shown when using a spinning basket reactor (Figure 8.10) and when using a slurry reactor (Figure 8.11). Although some of the data points in Figure 8.10 and Figure 8.11 are scattered with chain length n=2, the overall data show a linear trend.

When using the spinning basket reactor (Figure 8.10):

(1) with chain length n>2

$$\left.\frac{P_{(n+1)}/O_{(n+1)}}{P_{(n)}/O_{(n)}}\right|_{n>2} \approx k_{n>2}^{3} = 1.31 \tag{8.5}$$

and (2) with chain length n=2

$$\frac{P_3/O_3}{P_2/O_2} \approx k_{n=2}^{3} = 0.104 \tag{8.6}$$

When using the slurry reactor (Figure 8.11):

(1) with chain length n>2

$$\left.\frac{P_{(n+1)}/O_{(n+1)}}{P_{(n)}/O_{(n)}}\right|_{n>2} \approx k_{n>2}^{4} = 1.248 \tag{8.7}$$

and (2) with chain length n=2

$$\frac{P_3/O_3}{P_2/O_2} \approx k_{n=2}^4 = 0.146 \tag{8.8}$$

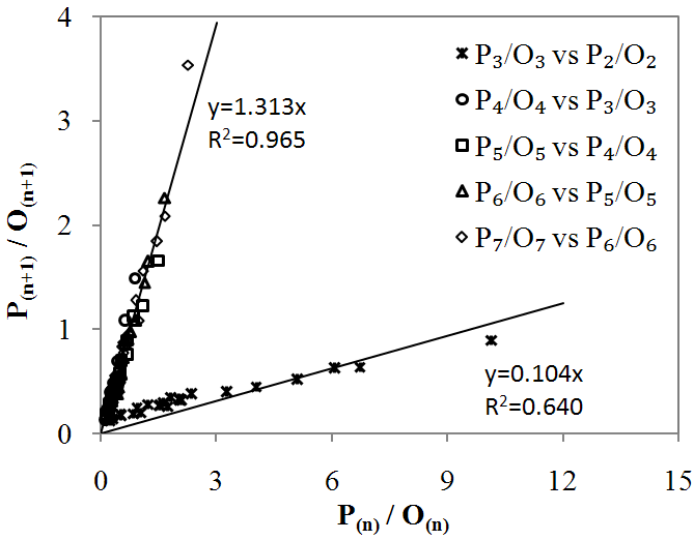

Figure 8.10: The molar ratio of $P_{(n+1)}/O_{(n+1)}$ as a function of the molar ratio of $P_{(n)}/O_{(n)}$ for Fischer-Tropsch synthesis using a spinning basket reactor (P is paraffin, O is olefin, n is the carbon number), data from literature [34].

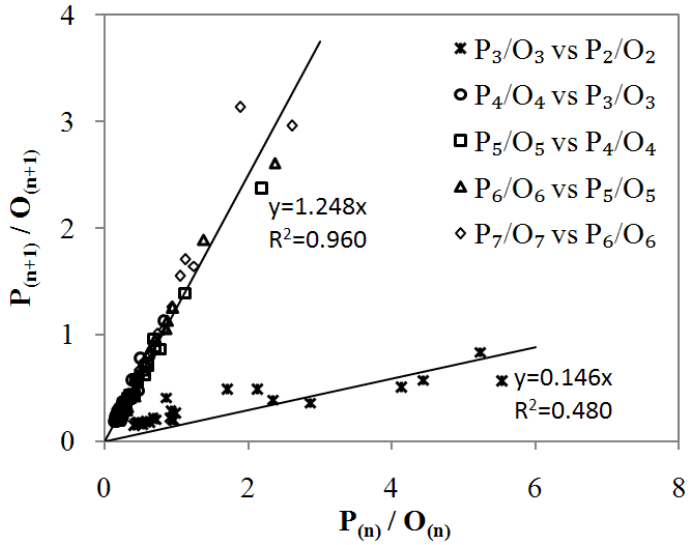

Figure 8.11: The molar ratio of $P_{(n+1)}/O_{(n+1)}$ as a function of the molar ratio of $P_{(n)}/O_{(n)}$ for Fischer-Tropsch synthesis using a slurry reactor (P is paraffin, O is olefin, n is the carbon number), data from literature [34].

Comparing the different *k* values from Equation (8.1) to Equation (8.8), we note:

- With *n*>2, the values of $k^1_{n>2}$, $k^2_{n>2}$, $k^3_{n>2}$ and $k^4_{n>2}$ are 1.376, 1.244, 1.313 and 1.248, respectively. There is little difference among these four values, which show that the value of $k_{n>2}$ is relatively constant over a range of catalysts, reactor types and operating conditions.
- With *n*=2, the values of $k^1_{n=2}$, $k^2_{n=2}$, $k^3_{n=2}$and $k^4_{n=2}$are 0.150, 0.181, 0.104 and 0.146, respectively, which also indicates that the value of $k_{n=2}$ changes over a relatively small range.
- The value of $k_{n=2} \ll k_{n>2}$.

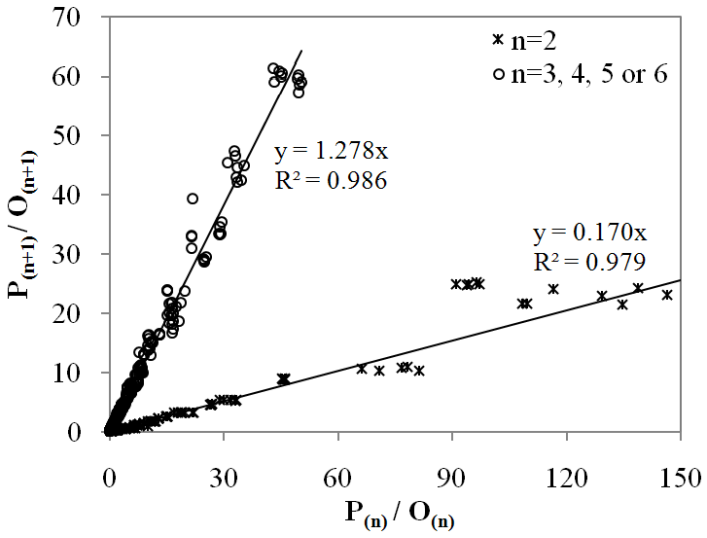

Figure 8.12: The molar ratio of $P_{(n+1)}/O_{(n+1)}$ as a function of the molar ratio of $P_{(n)}/O_{(n)}$ for Fischer-Tropsch synthesis; the data are from Figures 8.8–8.11.

Combining all the data from Figure 8.8 to Figure 8.11, we obtain Figure 8.12, which shows that the linear relationship between $P_{(n+1)}/O_{(n+1)}$ and $P_{(n)}/O_{(n)}$ for FTS is independent of the type of the reactor (plug flow, spinning basket or slurry), the composition of the syngas, reaction conditions and the kind of catalyst (cobalt or iron based). This can be explained as:

(1) with *n*>2,

$$\left.\frac{P_{(n+1)}/O_{(n+1)}}{P_{(n)}/O_{(n)}}\right|_{n>2} \approx k_{n>2} \tag{8.9}$$

and (2) with *n*=2

$$\frac{P_3/O_3}{P_2/O_2} \approx k_{n=2} \tag{8.10}$$

8.4 Discussion

8.4.1 Implications

Based on the comparison between the authors' work and the literature results, the linear relationship between $P_{(n+1)}/O_{(n+1)}$ and $P_{(n)}/O_{(n)}$ for FTS is obtained from a large amount of data; it is furthermore independent of the type of reactor (plug flow, spinning basket or slurry), the composition of the syngas (H_2/CO/CO_2), reaction conditions and the kind of the catalyst (cobalt or iron based) as shown in Figures 8.8–8.12, and explained in Equations (8.9) and (8.10). If Equations (8.9) and (8.10) are rearranged, the following expressions are obtained:

(1) with *n*>2,

$$\left.\frac{P_{(n+1)}}{P_{(n)}}\right|_{n>2} \approx k_{n>2} \left.\frac{O_{(n+1)}}{O_{(n)}}\right|_{n>2} \tag{8.11}$$

and (2) with *n*=2

$$\frac{P_3}{P_2} \approx k_{n=2} \frac{O_3}{O_2} \tag{8.12}$$

Some researchers considered plotting the Anderson-Schulz-Flory (ASF) distribution of olefins and paraffins separately [30, 33, 35, 36]. The chain growth factors of both paraffin and olefin product distribution can be described as Equations (8.13) and (8.14), respectively:

$$\frac{P_{(n+1)}}{P_{(n)}} = \alpha_{P,n} \tag{8.13}$$

$$\frac{O_{(n+1)}}{O_{(n)}} = \alpha_{O,n} \tag{8.14}$$

Substituting Equations (8.13) and (8.14) into Equations (8.11) and (8.12), we obtain:

$$\alpha_{P,n>2} = k_{n>2} \cdot \alpha_{O,n>2} \tag{8.15}$$

$$\alpha_{P,n=2} = k_{n=2} \cdot \alpha_{O,n=2} \tag{8.16}$$

Equations (8.15) and (8.16) indicate that there is a relationship between the paraffin and olefin product distributions:

- If the paraffin chain growth factor is increased the olefin chain growth factor will increase as described by Equations (8.15) and (8.16).
- Any of the factors that can affect the olefin product spectrum and change the olefin chain growth factor will also act on the paraffin spectrum so that the paraffin chain growth factor will change as described in Equations (8.15) and (8.16).

Therefore, the experimental results provide some insights on the limit of the variability of the product distribution in FTS to improve or change the product selectivity for the design of the FTS process and FT catalyst. We will next develop two simple models which may be able to explain the results.

8.4.2 Simple model based on reaction and vapour-liquid equilibrium (VLE) assumptions

For FTS, if the hydrocarbon chain is postulated to be formed stepwise by the insertion or addition of CH_2 intermediates with constant growth probability, then

the chain length distribution is given by the ASF distribution [37]. However, most iron and cobalt catalysts show marked deviations from this ideal distribution [38–41]. Some researchers [26–33, 42, 43] believe that the secondary reactions of α-olefins occur in FTS, which may readsorb on growth sites of the catalyst surface and continue to grow via propagation with monomer, or terminate as hydrocarbon product. This is possibly one of the influences on the product spectrum. Presently, solubility of the hydrocarbons in the wax phase is considered to be one of the possible influences on the chances of escape or readsorption of α-olefin in a catalyst particle [44, 45]. The low-temperature process, with either iron or cobalt catalysts, is used for the production of high molecular mass linear waxes [46]. At typical reaction conditions, the FT products distribute between the vapour and liquid phases within the reactor [47, 48].

In our present work, the low temperature FT reaction conditions over cobalt and iron catalysts are shown in Table 8.1. To obtain a simple expression to describe the relationship between $P_{(n+1)}/O_{(n+1)}$ and $P_{(n)}/O_{(n)}$ (Fig 8-11), we assume that:

- All or the majority of the products leave the reactor in the vapour phase;
- There is a liquid layer on the catalyst surface;
- At the interface, the liquid and vapour are in equilibrium.

Many previous studies claim that α-olefins and to some extent *n*-paraffins are the major primary products of FT synthesis [27, 44, 50-52]. We will assume that paraffins are produced in parallel with olefins (i.e., as primary products), and also from hydrogenation of olefins (i.e., as secondary products). At steady state, the amount of paraffins with carbon number *n* effectively produced (primary + secondary paraffins), P_n^{net}, (mol/(min·gcat)), can be given by:

$$P_n^{net} = P_n^{prim} + P_n^{sec} \tag{8.17}$$

where P_n^{prim} is the amount of primary paraffin with chain length *n* (mol/(min·gcat)); and P_n^{sec} is the amount of the secondary paraffin with chain length *n* (mol/(min·gcat)), produced from the hydrogenation of olefins. The amount of α-olefin with carbon number *n* effectively produced (primary – secondary olefins), O_n^{net}, (mol/(min·gcat)), can be given by:

$$O_n^{net} = O_n^{prim} - O_n^{sec} \tag{8.18}$$

where O_n^{prim} is the amount of primary α-olefin with chain length *n* (mol/(min·gcat)); and O_n^{sec} is the amount of the secondary reaction rate of α-olefin with chain length *n* (mol/(min·gcat)). Since the desorption probability of paraffin or olefin is independent of chain length, the P_n^{prim}/O_n^{prim} ratio for hydrocarbons with different chain lengths should be constant in the absence of further secondary reactions [27, 44, 51], which can be explained as:

$$P_n^{prim} = k_{prim}\, O_n^{prim} \tag{8.19}$$

where k_{prim} is constant, and O_n^{prim} is the amount of primary α-olefin with chain length *n* produced from the dehydrogenation of growing chains (mol/(min·gcat)).

If we suppose that the secondary reaction rate of α-olefins is a function of the concentration of α-olefins on the catalyst surface, then:

$$P_n^{sec} = k_{hydr}\, C_{O_n} \tag{8.20}$$

$$O_n^{sec} = k_{sec}\, C_{O_n} \tag{8.21}$$

where k_{hydr} and k_{sec} are reaction rate constants (note that $k_{hydr} \neq k_{sec}$ since k_{hydr} covers only the hydrogenated fraction of the olefins, whereas k_{sec} covers the reinserted fraction as well), and C_{O_n} is the liquid phase concentration of olefin with chain length *n* (mol/m^3). Combining Equations (8.17–8.21) yields the following expression:

$$P_n^{net} = k_{prim}\left(O_n^{net} + k_{sec}\,C_{O_n}\right) + k_{hydr}\,C_{O_n} \tag{8.22}$$

At the interface, wax and vapour are in equilibrium and thus the mole fraction of an olefin with chain length *n* in the liquid phase, X_{O_n}, is given by Raoult's law:

$$Y_{O_n} P_{tot} = X_{O_n} P_{vap,O_n} \tag{8.23}$$

where Y_{O_n} is the mole fraction of olefin with chain length *n* in the gas phase, P_{tot} is the total pressure (bar), and P_{vap,O_n} is the vapour pressure of olefin with chain length *n* (bar). In our model, we assume that all products leave the reactor in the vapour phase; thus

$$Y_{O_n} = \frac{p_{O_n}}{P_{tot}} = \frac{O_n^{net}}{F_{G,tot}} \tag{8.24}$$

$$X_{O_n} = \frac{V_{L,tot}}{N_{L,tot}} C_{O_n} \tag{8.25}$$

where p_{O_n} is the partial pressure of olefin with chain length *n* (bar), $F_{G,tot}$ is the total flow of vapour phase (mol/(min·gcat)), $V_{L,tot}$ is the total molar volume of the liquid layer on the catalyst surface (m^3), $N_{L,tot}$ is the total number of moles in the liquid layer (mol). Combining Equations (8.22–8.25) yields the following expression:

$$P_n^{net} = k_{prim}\left(O_n^{net} - \frac{k_{sec}\,N_{L,tot}\,P_{tot}}{F_{G,tot}\,V_{L,tot}\,P_{vap,O_n}} O_n^{net}\right) + \frac{k_{hydr}\,N_{L,tot}\,P_{tot}}{F_{G,tot}\,V_{L,tot}\,P_{vap,O_n}} O_n^{net} \tag{8.26}$$

We can rearrange to obtain the following equation to express the P/O ratio:

$$\frac{P_n}{O_n} = \frac{P_n^{net}}{O_n^{net}} = k_1 - \frac{k_2}{P_{vap,O_n}/P_{tot}} + \frac{k_3}{P_{vap,O_n}/P_{tot}} \tag{8.27}$$

where k_1, k_2 and k_3 are constants, defined as:

$$k_1 = k_{prim} \tag{8.28}$$

$$k_2 = \frac{k_{prim}\ k_{sec}\ N_{L,tot}}{F_{G,tot}\ V_{L,tot}} \tag{8.29}$$

$$k_3 = \frac{k_{hydr}\ N_{L,tot}}{F_{G,tot}\ V_{L,tot}} \tag{8.30}$$

At steady state, the following equation can be obtained to express the ratio of $P_{(n+1)}/O_{(n+1)}$ to $P_{(n)}/O_{(n)}$:

$$\frac{P_{(n+1)}/O_{(n+1)}}{P_{(n)}/O_{(n)}} = \left(\frac{k_1\frac{P_{vap,O_{n+1}}}{P_{tot}}+k_2+k_3}{k_1\frac{P_{vap,O_n}}{P_{tot}}+k_2+k_3}\right)\frac{P_{vap,O_n}}{P_{vap,O_{n+1}}} \tag{8.31}$$

Caldwell and van Vuuren [48] report an empirical relation for the vapour pressure of n-alkane as a function of temperature:

$$\beta = \frac{P_{vap,P_{n+1}}}{P_{vap,P_n}} \tag{8.32}$$

$$\beta = e^{[-427.218\left(1/T-1.029807\times10^{-3}\right)]} \tag{8.33}$$

where β is the variation of the vapour pressure coefficient, which is related to the incremental energy of vaporization per CH_2 unit of the hydrocarbon chain. Comparing this to the gas-liquid data of both n-paraffins and α-olefins, we find that Equations (8.32–8.33) can also be used for α-olefins, and the following equation is obtained:

$$\beta = \frac{P_{vap,P_{n+1}}}{P_{vap,P_n}} = \frac{P_{vap,O_{n+1}}}{P_{vap,O_n}} \tag{8.34}$$

Substituting Equation (8.34) into Equation (8.31), we obtain:

$$\frac{P_{(n+1)}/O_{(n+1)}}{P_{(n)}/O_{(n)}} = \frac{k_1\frac{P_{vap,O_n}}{P_{tot}}+\frac{k_2+k_3}{\beta}}{k_1\frac{P_{vap,O_n}}{P_{tot}}+k_2+k_3} \tag{8.35}$$

Based on Equation (8.33), the value of β is less than 1 when the temperature is varied over typical FT reaction conditions (180 ℃–350 ℃). Thus, from Equation

(8.35), the ratio of $P_{(n+1)}/O_{(n+1)}$ to $P_{(n)}/O_{(n)}$ is in the range of:

$$\frac{P_{(n+1)}/O_{(n+1)}}{P_{(n)}/O_{(n)}} \epsilon [1, \frac{1}{\beta}] \quad (8.36)$$

Table 8.2: Summary of the model results for different situations.

Conditions	Model results	Comments
(1) $k_2+k_3=0$ and $k_1\neq0$	$\frac{P_{(n+1)}/O_{(n+1)}}{P_{(n)}/O_{(n)}} = 1$	Both olefins and paraffins are the initial products formed from the surface complexes that represent the FTS pathways from CO and H_2. Paraffins are not formed by hydrogenation of olefins.
(2) $k_1\neq0$, $k_2\neq0$ and $k_3\neq0$	$\frac{P_{(n+1)}/O_{(n+1)}}{P_{(n)}/O_{(n)}} \epsilon (1, \frac{1}{\beta})$	Olefins are initially formed and take part in the secondary reactions. Some of the paraffins are from the initial products and others from the secondary hydrogenation reactions.
(3) $k_1=0$ and $k_2+k_3\neq0$	$\frac{P_{(n+1)}/O_{(n+1)}}{P_{(n)}/O_{(n)}} = \frac{1}{\beta}$	Olefins are the initial products, and paraffins are produced from secondary hydrogenation reactions.

The explanation of the model results from Equation (8.36) is shown in Table 8.2. The meanings of k_1, k_2 and k_3 are defined in Equations (8.28–8.30). Table 8.2 shows that:

- If $k_2+k_3=0$, which means that $k_{sec}=0$ and $k_{hydr}=0$, both olefins and paraffins are the initial products formed from the surface complexes that represent the FTS pathways from CO and H_2. Paraffins are not formed by secondary reactions of olefins;
- If $k_1\neq0$, $k_2\neq0$ and $k_3\neq0$, which means that $k_{prim}\neq0$, $k_{sec}\neq0$ and $k_{hydr}\neq0$, α-olefins

and to some extent n-paraffins are the major primary products of FT synthesis. Paraffins are produced in parallel with olefins (primary products), and also from hydrogenation of olefins (secondary products);

- If $k_1=0$, which means that $k_{prim}=0$, olefins are the initial products and paraffins are produced from secondary hydrogenation reactions of olefins.

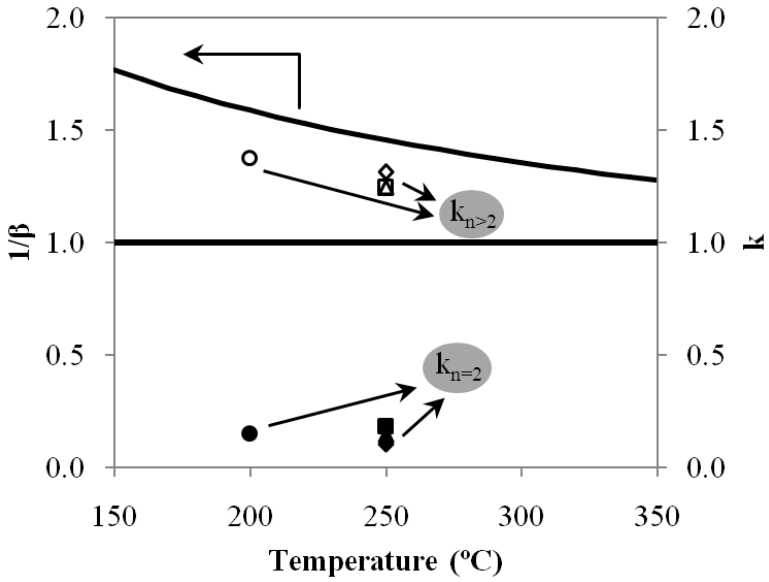

Figure 8.13: Comparison between the values of $1/\beta$ calculated by Equation (8.33) and the experimental results of k (the ratio of $P_{(n+1)}/O_{(n+1)}$ to $P_{(n)}/O_{(n)}$ as shown in Equations (8.1–8.8)). The top line is the value of $1/\beta$; ● and ○ represent the k values from Equations (8.1) and (8.2), respectively; ■ and □ represent the k values from Equations (8.3) and (8.4), respectively; ◆ and ◇ represent the k values from Equations (8.5) and (8.6), respectively; ▲ and △ represent the k values from Equations (8.7) and (8.8), respectively.

Figure 8.13 shows the comparison between the values of $1/\beta$ calculated by Equation (8.33) and the experimental results of k (Equations (8.1–8.8)). The values of $1/\beta$ decreases from 1.65 to 1.29 when the operating temperature for FTS increases from 150 ℃ to 350 ℃, which shows that the rate of change of $1/\beta$ with temperature is quite small. The same trend is observed for the experimental values

of $k_{n>2}$ which decrease slightly with an increase in temperature from 200 ^{o}C to 250 ^{o}C. Moreover, at the same reaction temperature of 250 ^{o}C, the data are quite close to each other with different reaction conditions as shown in Figures 8.9–8.11. Note that in Figure 8.13, the experimental data of $k_{n>2}$ is in between the value of (1, 1/β), which fits the model results as shown in Equation (8.32). The model would suggest that the olefin products are formed initially and may react in secondary reactions; some of the paraffins are from the initial products as well as the secondary hydrogenation (as shown in Table 8.2, condition 2). The model indicates that the reactor performance depends on the secondary reaction rate and VLE considerations. We therefore postulate that the product distribution might be determined by VLE.

The expression of Equation (8.36) indicates that the ratio of $P_{(n+1)}/O_{(n+1)}$ to $P_{(n)}/O_{(n)}$ is higher than 1 and changes over a small range, which may due to the greater solubility of larger hydrocarbons resulting in an increase in the readsorption rates for larger olefins on the catalyst surface. In addition, our experimental results support the expression when the chain length n>2. However, for chain length n=2, this expression falls short of explaining the abnormal relationship between P_3/O_3 and P_2/O_2 as shown in Figure 8.13 ($k_{n=2} \ll 1$).

8.4.3 Simple model based on quasi reaction equilibrium assumption

Based on the data from Figure 8.8 to Figure 8.11, we found that the linear relationship between $P_{(n+1)}/O_{(n+1)}$ to $P_{(n)}/O_{(n)}$ for FTS which is independent of the type of reactor (plug flow, spinning basket or slurry), the composition of the syngas, reaction conditions and the kind of catalyst (cobalt or iron based). Two features about the ratio of $k=[P_{(n+1)}/O_{(n+1)}]/[P_{(n)}/O_{(n)}]$ for the FT products have been identified:

- With n>2, the experimental values of $k_{n>2}$ (Equations (8.1), (8.3), (8.5) and

(8.7)) are higher than 1, fairly constant and independent of chain length *n*;

- With chain length *n*=2, the ratio of P_3/O_3 to P_2/O_2 ($k_{n=2}$ from Equations (8.2), (8.4), (8.6) and (8.8)) is significantly different from $k_{n>2}$, and furthermore, $k_{n=2} << k_{n>2}$.

The VLE based model developed previously can explain only that the ratio of $P_{(n+1)}/O_{(n+1)}$ to $P_{(n)}/O_{(n)}$ changes over a small range for chain length n>2. But it can not explain the different relationship between P_3/O_3 and P_2/O_2 as shown in Figures 8.8–8.11. We therefore need insight into the reaction pathways to find if there is another factor which can limit the product distribution in FTS. One of the main secondary reactions is the hydrogenation of the primary α-olefin product, which can be explained as follows:

$$C_nH_{2n} + H_2 \rightarrow C_nH_{2n+2} \quad \text{(a)}$$

$$C_{n+1}H_{2n+2} + H_2 \rightarrow C_{n+1}H_{2n+4} \quad \text{(b)}$$

If we subtract Reaction (b) from Reaction (a), the following Reaction (c) can be obtained:

$$C_{n+1}H_{2n+2} + C_nH_{2n+2} \rightleftharpoons C_{n+1}H_{2n+4} + C_nH_{2n} \quad \text{(c)}$$

If we assume that this reaction reaches quasi-equilibrium, the equilibrium constant for Reaction (c) can be expressed as:

$$K_{equilibrium} = \frac{[C_{n+1}H_{2n+4}][C_nH_{2n}]}{[C_{n+1}H_{2n+2}][C_nH_{2n+2}]} \quad (8.37)$$

If one compares Equations (8.9–8.10) and Equation (8.37), the following relationship can be obtained:

$$K_{equilibrium} = \frac{P_{(n+1)}/O_{(n+1)}}{P_{(n)}/O_{(n)}} = k \quad (8.38)$$

Equation (8.38) indicates that the ratio of $P_{(n+1)}/O_{(n+1)}$ to $P_{(n)}/O_{(n)}$ equals the value of the equilibrium constant $K_{equilibrium}$ under the assumption that Reaction (c) is in equilibrium. The temperature dependency of the equilibrium constant is determined from the Van't Hoff expression given by:

$$K_{equilibrium} = \exp\left[\frac{-\Delta G(T)}{RT}\right] \tag{8.39}$$

and

$$\frac{d\ln[K(T)]}{dT} = \frac{\Delta H(T)}{RT^2} \tag{8.40}$$

The Gibbs Free Energy and enthalpy of formation involved in each reaction can be evaluated from the standard energy of formation of each compound using the following thermodynamic equations:

$$\Delta G(T) = \sum \Delta G^{\circ}_{products} - \sum \Delta G^{\circ}_{reactants} \tag{8.41}$$

$$\Delta H(T) = \sum \Delta H^{\circ}_{products} - \sum \Delta H^{\circ}_{reactants} \tag{8.42}$$

Based on Equations (8.39–8.42), for the feasible reaction temperature range of 453K–623K, the equilibrium constants ($K_{equilibrium}$ from Equation (8.34)), evaluated with chain length n equal to 2, 3, 4, 5 and 6, of Reaction (c) are illustrated in Figure 8.14. When we calculate the equilibrium constant $K_{equilibrium}$, we find that the equilibrium constant is quite sensitive to small differences in the Gibbs Free Energy and enthalpy data which affect the value of the equilibrium constant. Therefore, the Gibbs Free Energy and enthalpy data from different handbooks are used to calculate the value of the equilibrium constant $K_{equilibrium}$ with chain length n=2 to 6, which is listed in Tables 8.3 and 8.4. The experimental results with chain length n=2 to 6 over cobalt based and iron based catalysts (reaction conditions as shown in Table 8.1) are also listed in Tables 8.3 and 8.4. In order to clearly identify the relationship between the equilibrium constant

calculated from thermodynamics and the equilibrium constant calculated from the experimental results as shown in Tables 8.3 and 8.4, error bars are used to indicate the uncertainties in the $K_{equilibrium}$ values, which are shown in Figure 8.15 and 16. In Figures 8.15 and 8.16, the $K_{equilibrium}$ values are calculated based on the data from ASPEN V7.0, and the positive and negative error values indicate the highest and lowest values calculated from different handbooks [53–58].

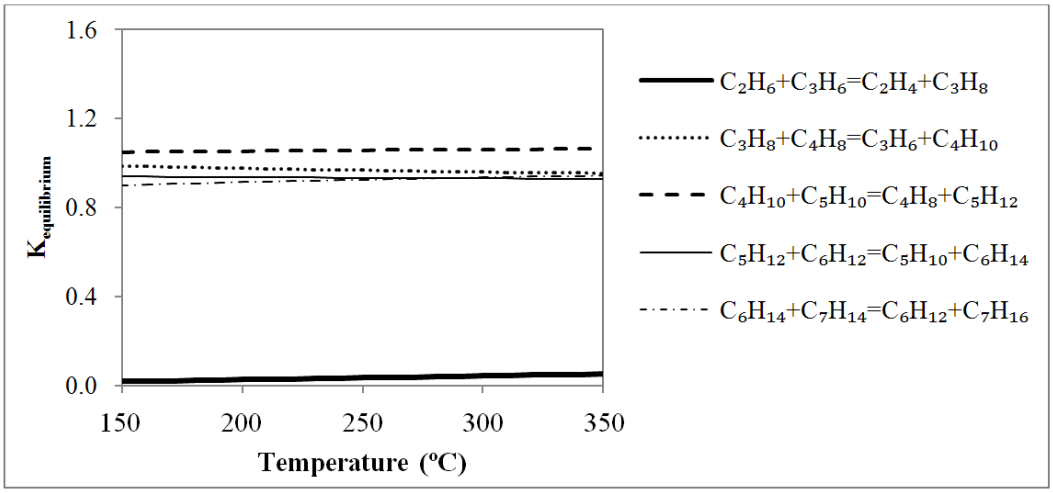

Figure 8.14: Chart of dependency of equilibrium constant (*K*) on temperature, and the data of Gibbs Free Energy and enthalpy are from Aspen V7.0.

Based on Figures 8.14–8.16 and Tables 8.3 and 8.4, we can see that:

- The values of the $K_{equilibrium}$, calculated by using different handbooks' Gibbs Free Energy and enthalpy data, change over a small range, which means that a small error of the components' physical parameters can affect the results of $K_{equilibrium}$.
- With chain length n>2, values of the $K_{equilibrium}$ among different reactions are quite similar and do not change much with an increase in temperature. The experimentally determined values of $k_{experimental}$ with different chain length n are also quite similar to each other (Figures 8.8 and 8.9) and the experimental values are close to the calculated $K_{equilibrium}$ values.

- With chain length n=2, the $K_{equilibrium}$ is also not a strong function of temperature. The experimental data are 8 or 9 times higher than the calculated $K_{equilibrium}$ values.
- It is both predicted from the calculation and found from the experimental data that $K_{equilibrium,(n>2)} > K_{equilibrium,(n=2)}$, as well as $k_{experimental,(n>2)} > k_{experimental,(n=2)}$. Therefore, this indicates that the abnormal P_3/O_3 to P_2/O_2 ratio as shown in Figures 8.8–8.11 might be due to the thermodynamic equilibrium consideration.

Because the equilibrium constant K is quite sensitive to the components' Gibbs Free Energy and enthalpy data and the values of the same hydrocarbon's free energy and enthalpy data from different handbooks are very close but not equal, it is hard to know the accurate value of the equilibrium constant K for a certain chain length. Even then, we can still obtain some important information, since the same trend is observed from the thermodynamic equilibrium values and the equilibrium values from the experimental results. It is both predicted from the calculation and found from the experimental data that $K_{equilibrium,(n>2)} > K_{equilibrium,(n=2)}$, as well as $k_{experimental,(n>2)} > k_{experimental,(n=2)}$.

Because the same trend is achieved from the equilibrium calculations and the experimental data, and the values are close to each other (Tables 8.3 and 8.4), we therefore postulate that the product distribution might be determined by a quasi reaction equilibrium between the olefins and paraffins.

Table 8.3: Comparison between the equilibrium constant values calculated from thermodynamics and the equilibrium constant values calculated from the experimental results over a cobalt based catalyst (reaction conditions as shown in Table 8.1).

	Cobalt based catalyst							
T(℃)	200							
n	$K_{equlibrium}^{1}$	$K_{equlibrium}^{2}$	$K_{equlibrium}^{3}$	$K_{equlibrium}^{4}$	$K_{equlibrium}^{5}$	$K_{equlibrium}^{6}$	$K_{equlibrium}^{7}$	$k_{experimental}$
2	0.025	0.017	0.017	0.022	0.024	0.022	0.017	0.150
3	0.976	1.454	2.067	1.905	0.976	0.797	1.914	1.448
4	1.053	0.726	0.731	0.668	1.098	1.356	0.731	1.364
5	0.936	1.005	1.088	0.442	0.879	0.663	1.088	1.308
6	0.914	0.975	1.000	2.670	1.035		1.059	1.390

Note: $K_{equlibrium}$ are calculated based on different handbooks' free energy and enthalpy data: [1] from Aspen V7.0, [2-7] from literature [53–58]

Table 8.4: Comparison between the equilibrium constant values calculated from thermodynamics and the equilibrium constant values calculated from the experimental results over an iron based catalyst (reaction conditions as shown in Table 8.1)

	Iron based catalyst							
T(℃)	250							
n	$K_{equlibrium}^{1}$	$K_{equlibrium}^{2}$	$K_{equlibrium}^{3}$	$K_{equlibrium}^{4}$	$K_{equlibrium}^{5}$	$K_{equlibrium}^{6}$	$K_{equlibrium}^{7}$	$k_{experimental}$
2	0.034	0.023	0.023	0.029	0.032	0.029	0.023	0.180
3	0.967	1.397	1.981	1.819	0.962	0.748	1.834	1.234
4	1.057	0.732	0.740	0.668	1.093	1.406	0.740	1.270
5	0.933	1.005	1.088	0.465	0.890	0.641	1.088	1.249
6	0.925	0.971	1.000	2.556	1.033		1.060	1.215

Note: $K_{equlibrium}$ are calculated based on different handbooks' free energy and enthalpy data: [1] from Aspen V7.0, [2-7] from literature [53–58]

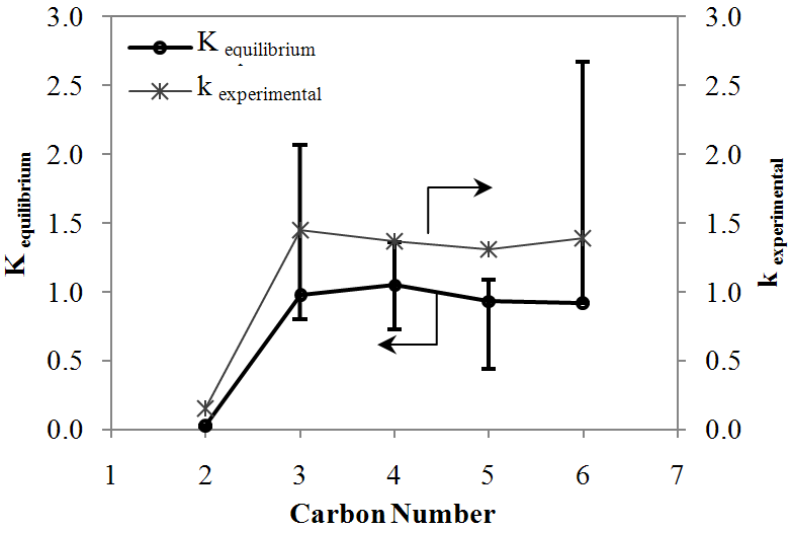

Figure 8.15: Comparison between the equilibrium constant values from thermodynamics using ASPEN and the equilibrium constant values from the experimental results over a cobalt based catalyst (reaction conditions as shown in Table 8.1) at 200 ^{o}C. The error bars show the range of $K_{equilibrium}$ calculated from literature [53–58].

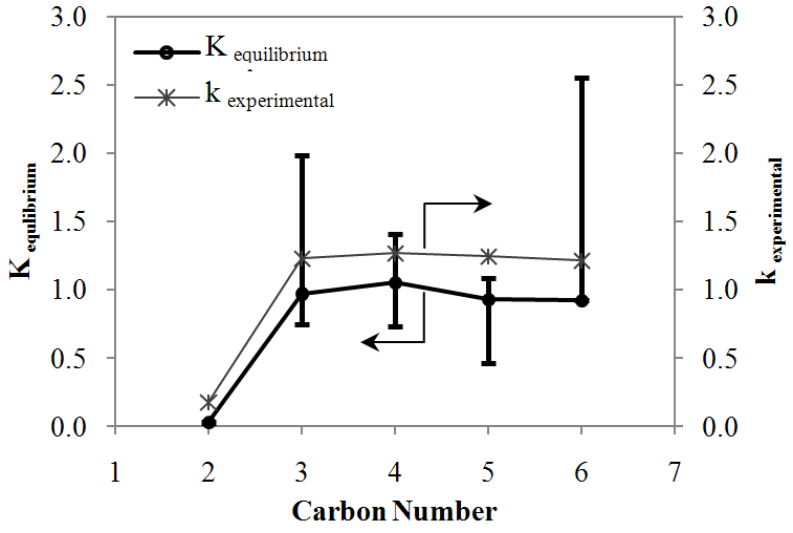

Figure 8.16: Comparison between equilibrium constant values from thermodynamics using ASPEN and the equilibrium constant values from the experimental results over an iron based catalyst (reaction conditions as shown in Table 8.1) at 250 ^{o}C. The error bars show the range of $K_{equilibrium}$ calculated from literature [53–58].

8.5 Conclusions

FTS experiments over iron and cobalt based catalysts were carried out in a fixed-bed micro reactor. Two feed gases, one of composition H_2:CO:CO_2 = 3:0:1 and the other of H_2:CO:CO_2 = 2:1:0 were fed to the reactor and the reactions monitored. Mixtures of various proportions of the two feed gases were fed to the reactor, thus varying the ratio of CO, CO_2 and H_2 stoichiometrically.

The data show that the product selectivity and the P/O ratio are strongly dependent on the syngas composition (Figures 8.6–8.7). CO_2 rich feeds produce products that are mostly light hydrocarbons with a high P/O ratio, whereas CO rich feeds shift the product composition to an FT type (mainly higher hydrocarbons) product with a low P/O ratio over both iron and cobalt based catalysts.

Based on the comparison between the authors' work and the literature results, the linear relationship between $P_{(n+1)}/O_{(n+1)}$ and $P_{(n)}/O_{(n)}$ for FTS is obtained for a large amount of data; it is furthermore independent of the type of reactor (plug flow, spinning basket or slurry), the composition of the syngas (H_2/CO/CO_2), reaction conditions and the kind of the catalyst (cobalt or iron based). Two features of the ratio of $k=[P_{(n+1)}/O_{(n+1)}]/[P_{(n)}/O_{(n)}]$ for the FT products have been identified: (1) with $n>2$, the experimental values of $k_{n>2}$ (Equations (8.1), (8.3), (8.5) and (8.7)) are higher than 1, fairly constant and independent of chain length n; (2) with chain length $n=2$, the ratio of P_3/O_3 to P_2/O_2 ($k_{n=2}$ from Equations (8.2), (8.4), (8.6) and (8.8)) is significantly different and it is shown that $k_{n=2} \ll k_{n>2}$.

By considering a VLE based model, a new expression describing the ratio of $P_{(n+1)}/O_{(n+1)}$ to $P_{(n)}/O_{(n)}$ is obtained. The expression indicates that the ratio of $P_{(n+1)}/O_{(n+1)}$ to $P_{(n)}/O_{(n)}$ varies in a range of $(1,1/\beta)$, where β is the variation of the vapour pressure coefficient, which is related to the incremental energy of

vaporization per CH_2 unit of the hydrocarbon chain. In addition, our experimental results support the expression for the chain length n>2. But with chain length n=2, this expression is unable to explain the abnormal relationship between P_3/O_3 and P_2/O_2 as shown in Figures 8.8–8.11.

A model based on a quasi thermodynamic equilibrium assumption is introduced to explain the linear relationship between $P_{(n+1)}/O_{(n+1)}$ and $P_{(n)}/O_{(n)}$. We assume that the reaction of ($C_{n+1}H_{2n+2}+C_nH_{2n+2} = C_{n+1}H_{2n+4}+C_nH_{2n}$) reaches quasi-equilibrium. It is found that the model predicts the same trend for the equilibrium calculations as found in the experimental data; and the results show that the experimental values of k ($k=[P_{(n+1)}/O_{(n+1)}]/[P_{(n)}/O_{(n)}]$) agree closely with the values of the calculated equilibrium constant K for a given chain length n. Therefore, we postulate that the product distribution might be determined by a quasi reaction equilibrium reaction between the olefins and paraffins.

By focusing on the paraffin to olefin ratio with different chain length n, our work indicates that there is a relationship between the paraffin and the olefin product distribution: any of the factors that can affect the olefin chain growth probability, will also affect the chain growth probability of the paraffins in a simple linear manner. Therefore, the experimental results provide some hints on how much flexibility there is in the design of FTS processes and FT catalysts to improve the target product selectivity.

References

[1] Ngwenya, T., Glasser, D., Hildebrandt, D. Coville, N., and Mukoma, P. (2005), Fischer-Tropsch results and their analysis for reactor synthesis. Industrial and Engineering Chemistry Research, 44, 5987–5994.

[2] Teng, B., Chang, J. and Wang, G. (2005), Water gas shift reaction kinetics in Fischer-Tropsch synthesis over an industrial Fe-Mn catalyst. Fuel, 84, 917–926.

[3] Jean-Marie, A. Griboval-Constant, A., Khodakov, A. Y. and Diehl, F. (2009), Cobalt supported on alumina and silica-doped alumina: catalyst structure and catalytic performance in Fischer-Tropsch synthesis, Comptes Rendus Chimie, 12, 660–667.

[4] De la Peña O'Shea, V. A., Álvarez-Galván, M. C., Campos-Martín, J. M. and Fierro, J. L. G. (2007), Fischer-Tropsch synthesis on mono- and bimetallic Co and Fe catalysts in fixed-bed and slurry reactors, Applied Catalysis A: General, 326 ,65–73.

[5] Schulz, H. (2007), Comparing Fischer-Tropsch synthesis on iron- and cobalt catalysts: The dynamics of structure and function, Fischer-Tropsch Synthesis, Catalysts and Catalysis, Davis, B. H. and Occelli, M. L. (Editors), Elsevier B.V., Burlington, 163, 177–199.

[6] O'Brien, R. J., Xu, L., Spicer, R. L., Bao, S., Milburn, D. R. and Davis, B. H. (1997), Activity and selectivity of precipitated iron Fischer-Tropsch catalysts, Catalysis Today, 36, 325–334.

[7] Rao, V. U. S., Stiegel, G. J., Cinquegrane, G. J., and Srivastava, R. D. (1992), Iron-based catalysts for slurry-phase Fischer-Tropsch process: Technology review, Fuel Processing Technology, 30, 83–107.

[8] Luo, M., Hamdeh, H. and Davis, B. H. (2009), Fischer-Tropsch synthesis catalyst activation of low alpha iron catalyst, Catalysis Today, 140, 127–134.

[9] Dry, M. E. (2002), The Fischer-Tropsch process: 1950–2000, Catalysis Today, 71, 227–241.

[10] Davis, B. H. (2003), Fischer-Tropsch synthesis: relationship between iron catalyst composition and process variables, Catalysis Today, 84, 83–98.

[11] Zhou, W., Chen, J., Fang, K. and Sun, Y. (2006), The deactivation of Co/SiO_2 catalyst for Fischer-Tropsch synthesis at different ratios of H_2 to CO, Fuel Processing Technology, 87, 609–616.

[12] Li, J. (1999), The preparation, characterization and evaluation of boron-modified Co/TiO_2 Fischer-Tropsch catalysts, PhD thesis, University of the Witwatersrand, Johannesburg, South Africa.

[13] Wilhelm, D. J., Simbeck, D. R., Karp, A. D. and Dickenson, R. L. (2001), Syngas production for gas-to-liquids applications: technologies, issues and outlook, Fuel Processing Technology, 71, 139–148.

[14] Riedel, T. and Schaub, G. (2003), Low-temperature Fischer-Tropsch synthesis on cobalt catalysts-effects of CO_2, Topics in Catalysis, 26, 145–156.

[15] Perez-Alonso, F. J., Ojeda, M., Herranz, T., Rojas, S., Gonzalez-Carballo, J. M., Terreros, P. and Fierro, J. L. G. (2008), Carbon dioxide hydrogenation over Fe-Ce catalysts, Catalysis Communications, 9 , 1945–1948.

[16] van Der Laan, G.P. and Beenachers, A.A.C.M. (2000), Intrinsic kinetics of the gas-solid Fischer-Tropsch and water gas shift reactions over a precipitated iron catalyst, Applied Catalysis A: General, 193, 39–53.

[17] Dry, M.E. (1996), Practical and theoretical aspects of the catalytic Fischer-Tropsch process, Applied Catalysis A: General, 138, 319–344.

[18] Xu, L., Bao, S., Houpt, D. J., Lambert, S. H., Davis, B. H. (1997), Role of CO_2 in the initiation of chain growth and alcohol formation during the Fischer-Tropsch synthesis, Catalysis Today, 36, 347–355.

[19] Riedel, T., Schaub, G., Jun, K-W. and Lee, K-W. (2001), Kinetics of CO_2 hydrogenation on a K-promoted Fe catalyst, Industrial and Engineering Chemistry Research, 40, 1355–1363.

[20] Weatherbee, G.D. and Bartholomew, C.H. (1984), Hydrogenation of CO_2 on Group VIII Metals. Journal of Catalysis, 77, 352–362.

[21] Herranz, T., Rojas, S., Perez-Alonso, F. J., Ojeda, M., Terreros, P. and Fierro, J. L. G. (2006), Hydrogenation of carbon oxides over promoted Fe-Mn catalysts prepared by the microemulsion methodology, Applied Catalysis A: General , 311, 66–75.

[22] Zhang, Y., Jacobs, G., Sparks, D. E., Dry, M. E. and Davis, B. H. (2002), CO and CO_2 hydrogenation study on supported cobalt Fischer-Tropsch synthesis catalysts, Catalysis Today, 71, 411–418.

[23] Riedel, T., Claeys, M., Schulz, H., Schaub, G., Nam, S-S., Jun, K-W., Choi, M-J., Kishan, G., and Lee, K-W. (1999), Comparative study of Fischer–Tropsch synthesis with H_2/CO and H_2/CO_2 syngas using Fe- and Co-based catalysts, Applied Catalysis A: General, 186, 201–213.

[24] Visconti, C. G., Lietti, L., Tronconi, E., Forzatti, P., Zennaro, R., and Finocchio, E. (2009), Fischer-Tropsch synthesis on a Co/Al_2O_3 catalyst with CO_2 containing syngas, Applied Catalysis A: General, 355, 61–68.

[25] Yao, Y., Hildebrandt, D., Glasser, D. and Liu, X. (2010), Fischer−Tropsch synthesis using $H_2/CO/CO_2$ syngas mixtures over a cobalt catalyst, Industrial and Engineering Chemistry Research, 49, 11061–11066.

[26] Cheng, J., Song, T., Hua, P., Lok, C.M., Ellis, P., and French, S. (2008), A density functional theory study of the α-olefin selectivity in Fischer-Tropsch synthesis, Journal of Catalysis, 255, 20–28.

[27] Kuipers, E. W., Vinkenburg, I. H., and Oosterbeek, H. (1995), Chain length dependence of α-olefin readsorption in Fischer-Tropsch synthesis, Journal of Catalysis, 152, 137–146.

[28] Shi, B. and Davis, B. H. (2005), Fischer-Tropsch synthesis: the paraffin to olefin ratio as a function of carbon number, Catalysis Today, 106, 129–131.

[29] Kapteijn, F. de Deugd, R. M., and Moulijn, J. A. (2005), Fischer-Tropsch synthesis using monolithic catalysts, Catalysis Today, 105, 350–356.

[30] van Der Laan, G. P. and Beenachers, A. A. C. M. (1999), Hydrocarbon selectivity model for the gas-solid Fischer-Tropsch synthesis on precipitated iron catalysts, Industrial and Engineering Chemistry Research, 38, 1277–1290.

[31] van Der Laan, G. P. and Beenachers, A. A. C. M. (1999), Kinetics and selectivity of the Fischer-Tropsch synthesis: a literature review, Catalysis Reviews, Science and Engineering, 4, 255–318.

[32] Iglesia, E., Reyes, S. C., Madon, R. J., and Soled, S. L. (1993), Selectivity control and catalyst design in the Fischer-Tropsch synthesis: sites, pellets and reactions, in: Eley, E. E., Pines, H. and Weisz, P. B. (Edtors.), Advances in Catalysis, 39, 221–301.

[33] Botes, F. G. (2007), Proposal of a new product characterization model for the

iron-based low temperature Fischer-Tropsch synthesis, Energy & Fuels, 21, 1379–1389.

[34] van der Laan, G. P. (1999), Kinetics, selectivity and scale up of the Fischer-Tropsch synthesis, PhD Thesis, University of Groningen, Appendixes A-B, 215–223.

[35] Egiebor, N. O. and Cooper, W. C. (1985), The polyfunctionality of iron catalysts during CO hydrogenation: I. occurrence of dual chain propagation sites, Applied Catalysis, 14, 323–332.

[36] Satterfield, C. N. and Stenger, H. G. (1984), Fischer-Tropsch synthesis on a precipitated Mn/Fe catalyst in a well-mixed slurry reactor, Industrial and Engineering Chemistry Process Design and Development, 23, 26–29.

[37] Dry, M. E. (1981), The Fischer-Tropsch Synthesis, Catalysis science and etchnology, J. R. Anderson and M. E. Boudart (Edtors), Springer, New York, 1, 159–255.

[38] Patzlaff, J., Liu, Y., Graffmann, C. and Gaube, J. (1999), Studies on product distributions of iron and cobalt catalyzed Fischer-Tropsch synthesis, Applied Catalysis A: General, 186, 109–119.

[39] Madod, R. J. and Taylor, W. F. (1981), Fischer-Tropsch synthesis on a precipitated iron catalyst, Journal of Catalysis, 69, 32–43.

[40] Huff Jr, G. A. and Satterfield, C. N. (1984), Evidence for two chain growth probabilities on iron catalysts in the Fischer-Tropsch synthesis, Journal of Catalysis, 85, 370–379.

[41] Iglesia, E., Reyes, S. C., and Madon, R. J. (1991), Transport-enhanced a-olefin readsorption pathways in Ru-catalyzed hydrocarbon synthesis, Journal of Catalysis,

129, 238–256.

[42] Snel, R. and Espinoza, R. L. (1987), Secondary reactions of primary products of the Fischer-Tropsch synthesis: part 1. the role of ethene, Journal of Molecular Catalysis, 43, 237–247.

[43] Schulz, H. and Claeys, M. (1999), Kinetic modelling of Fischer-Tropsch product distributions, Applied Catalysis A: General, 186, 91–107.

[44] Tau, L. M., Dabbagh, H. A. and Davis, B. H. (1990), Fischer-Tropsch synthesis: carbon-14 tracer study of alkene incorporation, Energy Fuels, 4, 94–99.

[45] Schulz, H., Beck, K., and Erich, E. (1988), Mechanism of the Fischer Tropsch Process, Studies in Surface, Science and Catalysis, 36, 457–471.

[46] Dry, M. E. (2002), The Fischer-Tropsch process: 1950–2000, Catalysis Today, 71, 227–241.

[47] Marano, J. J. and Holder, G. D. (2007), Characterization of Fischer-Tropsch liquids for vapor-liquid equilibria calculations, Fluid Phase Equilibria , 138, 1–21.

[48] Caldwell, L. and van Vuuren, D. S. (1986), On the formation and composition of the liquid phase in Fischer-Tropsch reactors, Chemical Engineering Science, 41, 89–96.

[49] Bukur, D. B., Lang, X., Akgerman, A., and Feng, Z. (1997), Effect of process conditions on olefin selectivity during conventional and supercritical Fischer-Tropsch synthesis, Industrial and Engineering Chemistry Research, 36, 2580–2587.

[50] Dictor, R. A. and Bell, A. T. (1986), Fischer-Tropsch synthesis over reduced and unreduced iron oxide catalysts, Journal of Catalysis, 97, 121–136.

[51] Zheng, S., Liu, Y., Li, J., and Shi, B. (2007), Deuterium tracer study of pressure effect on product distribution in the cobalt-catalyzed Fischer–Tropsch Synthesis, Applied Catalysis A: General, 330, 63–68.

[52] van Dijk, H. A J., Hoebink, J. H. B. J. and Schouten, J. C. (2001), Steady-state isotopic transient kinetic analysis of the Fischer-Tropsch synthesis reaction over cobalt-based catalysts, Chemical Engineering Science, 56, 1211–1219.

[53] Cox, J. D., Wagman, D. D., Medvedev, V. A. (1989), CODATA key values for thermodynamics, New York: Hemisphere Puplishing Corporation.

[54] Rossini, F. D., Pitzer, K. S., Arnett, R. L., Braun, R. M., and Pimentel, G. C. (1953), Selected values of physical and thermodynamic properties of hydrocarbons and related compounds, Carnegie Press, Pittsburgh.

[55] Lange, N. A. (1992), Lange's handbook of chemistry, John A. Dean (Editor), New York: McGraw-Hill.

[56] Poling, B. E., Prausnitz, J. M., and O'Connell, J. P. (2001), Properties of gases and liquids (5th Edition), New York: McGraw-Hill.

[57] Sandler, S. I. (2006), Chemical, biochemical and engineering thermodynamics (4th Edition), New York: John Wiley & Sons. Inc.

[58] Stull, D. R., Westrum Jr, E. F., and Sinke. G. C. (1969), The chemical htermodynamics of organic compounds, New York: John Wiley & Sons, Inc.

9

OVERALL CONCLUSIONS

The major objective of this thesis was to investigate the effect of CO_2 on cobalt- and iron-based catalysts during FTS, and in particular its influence on catalyst activity and product selectivity. We had two secondary aims. First, we postulated that a comparison of the product distribution and paraffin to olefin ratios obtained from FTS fed by CO/H_2, CO_2/H_2 and $CO/CO_2/H_2$ syngas mixtures would help to explain the deviations from the ASF distribution model that many scientists have noted. Second, we postulated that the information gained from the comparison might reveal novel generic rules applicable to FTS products.

Accordingly, we conducted four groups of FTS experiments for CO/H_2, CO_2/H_2 and $CO/CO_2/H_2$ mixtures under different reaction conditions over both cobalt- and iron-based catalysts, which are:

- **Group A:** In this series of FTS experiments we repeatedly switched between the CO ($CO:H_2:N_2$=30%:60%:10%) and CO_2($CO_2/H_2/N_2$ = 23%:67%:10%) feeds introduced into a plug flow reactor over a cobalt-based catalyst at 180–220 ℃, 20 bar gauge and 30 ml(NTP)/(min gcat). (This series is covered in Chapter 3.)
- **Group B:** In these FTS experiments we used a wide range of $H_2/CO/CO_2$ syngas mixtures (with a ratio of $H_2/(2CO+3CO_2)$ equal to 1) over a cobalt-based catalyst at 200 ℃, 20 bar gauge and 60 ml(NTP)/(min gcat). (These are described in Chapters 4 and 6–8.)
- **Group C:** In the third group of FTS experiments we used a wide range of $H_2/CO/CO_2$ syngas mixtures (with a ratio of $H_2/(2CO+3CO_2)$ equal to 1) over an iron-based catalyst at 250 ℃, 20 bar gauge and 60 ml(NTP)/(min gcat). (The results are presented in Chapters 5–8.)

- **Group D:** For the final series of FTS experiments, we used a wide range of $H_2/CO/CO_2$ syngas mixtures (with a ratio of $H_2/(CO+CO_2)$ equal to 1) over an iron-based catalyst at 250 ℃, 20 bar gauge and 60 ml(NTP)/(min gcat). (These are discussed in Chapter 5.)

The experimental data were calculated, analyzed, compared and simulated, not only within each group of experiments but among the different groups. The major conclusions we arrived at, and the suggestions for further research we based on our findings, are summarized below.

9.1 Conclusions

9.1.1 Catalyst activity

9.1.1.1 Cobalt-based catalyst

The data show that both CO and CO_2 are readily hydrogenated over a cobalt-based catalyst (Chapters 3 and 4). The CO_2/H_2 feed mixture produced a conversion rate two times higher than that of the CO/H_2 feed when we used a fresh cobalt-based catalyst. However, when we followed this with CO hydrogenation over the same catalyst, and then went back to CO_2 hydrogenation, we found the conversion of CO_2 dropped dramatically (Chapter 3). We concluded that $CO/CO_2/H_2$ mixtures can be used as a feed to a cobalt catalyst. Also, when the feed gas is CO_2 -rich and correspondingly CO-lean ($CO_2/(CO+CO_2)$> 50%), CO_2 is not an inert or diluent gas, but can be converted to hydrocarbon products. However, CO is converted faster than CO_2 in the FT reaction when $CO/CO_2/H_2$ mixtures are used (Chapter 4).

It is worth noting that the long term effect of the CO_2 on the properties of a cobalt-based catalyst was very small under the reaction conditions described for

Group A. When we continually alternated between the CO and CO_2 feeds, we were unable to observe any catalyst deactivation for either the CO or CO_2 reaction at reaction temperatures of 180 ℃ and 200 ℃. A mild catalyst deactivation was observed at the operating temperatures of 210 ℃ and 220 ℃ , respectively. A comparison of the feed gases in terms of CO and CO_2 hydrogenation and a discussion of the possible side reactions led to our postulation that the catalyst deactivation we observed is caused by the re-oxidation of the cobalt catalyst by water rather than by CO_2 (Chapter 3).

Although cobalt catalysts are not active for water–gas shift (WGS), the results of the experiments show that the rate of hydrocarbon production is maximized when the $CO/CO_2/H_2$ mixture has an intermediate composition. This might prove to be valuable information for the design of FT processes using cobalt catalysts, in that it demonstrates the advantage of keeping some CO_2 in the syngas feed.

9.1.1.2 Iron-based catalyst

Applying the operation conditions for the experiments described as Groups C and D, we found that both CO and CO_2 were readily hydrogenated when the feeds contained either H_2/CO or H_2/CO_2 over an iron-based catalyst. However, the reactivity for CO_2 hydrogenation was lower than that for CO under the same reaction conditions. The data showed that, even with a high CO_2 mole fraction in the $H_2/CO/CO_2$ mixture feed, the conversion of CO_2 was negative, which indicated that CO_2 was formed rather than consumed. It also showed that CO_2 could be converted to hydrocarbons only when there was a very high proportion of CO_2 and a correspondingly low percentage of CO in the feed gas. The experimental results showed that when the conversion of CO_2 achieved negative values, both the FT and the WGS reaction rates were fairly constant, independent of the ratio of $CO_2/(CO+CO_2)$ when the feed gases were $CO/CO_2/H_2$ mixtures (Chapter 5).

Our findings in the FTS experiments using an iron-based catalyst and wide ranges of $H_2/CO/CO_2$ mixtures for the feed were that the hydrocarbon product formation rate achieved fairly constant values that were similar to those for typical FT CO hydrogenation. These results justify the inclusion of CO_2 in the syngas feed for FTS processes over an iron-based catalyst.

9.1.2 Product selectivity

When we compared the FTS products formed by using different syngas mixtures (CO_2/H_2, $CO_2/CO/H_2$, and CO/H_2), we were able to see that the products of CO_2 hydrogenation over a cobalt-based catalyst were methane-rich short chain saturated hydrocarbons. No olefin product could be detected for CO_2 FTS when the catalyst was cobalt-based. Although the methane selectivity remained higher than that typically obtained by FTS, the selectivity for the long chain hydrocarbon products was dramatically increased with the CO_2 rich syngas ($CO/CO_2/H_2$) in comparison with the corresponding selectivity of the CO_2/H_2 feed (Chapters 3 and 4).

Over an iron-based catalyst, both CO_2- or CO_2-rich feed gases produced more CH_4-rich short chain paraffins than was the case with CO hydrogenation, which is quite similar to the result we obtained from a cobalt-based catalyst. However, during CO_2 FTS over the iron catalyst we were able to find a small amount of olefin product (Chapter 5).

9.1.3 Product distribution

To summarize the experimental results of FTS using $H_2/CO/CO_2$ syngas mixtures over both cobalt- andiron-based catalysts (Groups 2 and 3 of the experiments) in terms of product distribution, we made the following findings.

- For CO_2-rich feeds, the products followed a typical one-alpha ASF

distribution pattern with low alpha values when the carbon number was greater than 2. In this case the point representing C_2 on the graph lay on or near the ASF distribution line, and a high yield of CH_4 was obtained.

- For CO-rich feeds, the product followed a two-alpha ASF distribution model with high alpha values when the carbon number was greater than 2. The low yield of C_2 and high yield of CH_4 that were obtained were typical.
- The growth factor for paraffin was higher than that for olefin under the same reaction conditions.

To explain the distribution of olefin and paraffin products, we introduced thermodynamic assumptions, postulating that there was quasi equilibrium among each of three adjacent olefins ($O_{(n-1)}$, $O_{(n)}$ and $O_{(n+1)}$) and paraffins ($P_{r,(n-1)}$, $P_{r,(n)}$ and $P_{r,(n+1)}$). When we compared the thermodynamic equilibrium calculations we derived from this assumption with our experimental results, we found that most of the latter were quite close to the thermodynamic calculations for the short chain hydrocarbons. We thereafter postulate that both paraffin and olefin products may achieve a quasi-equilibrium during FTS. We therefore developed a new simple model, the "quasi-equilibrium product distribution model", to enable us to predict the olefin and paraffin product distributions. The new model is in many ways consistent with those obtained experimentally. Furthermore, it offered a successful explanation for the deviations of the C_1 and C_2 components. This led to our deducing that the olefin and paraffin product distributions in FTS can be described in terms of thermodynamic equilibrium. The drawbacks of this model are that it assumes all the products are in the gas phase, and that it cannot explain why the growth factors for paraffin and olefin differ (Chapter 6).

We also introduced a new product distribution tool named the "combined paraffin and olefin growth factors distribution model", to explain the observed two-alpha ASF distribution of FTS. This was an attempt to address the phenomenon that the

product distribution changed from a one-alpha to a two-alpha ASF distribution when the CO_2-rich feeds were replaced by CO-rich feeds during FTS. This model shows that the two-alpha product distribution is probably caused by the combination of different product spectrums. We also considered the effect of VLE on product distribution, and found that our experimental data supports the postulate that the double-alpha type plot often encountered in FT results is attributable to VLE. We therefore concluded that the deviations from the ASF distribution can be explained as the co-action of the different product spectrums and VLE on the product distribution during FTS (Chapter 7).

9.1.4 Paraffin to olefin (P/O) ratio

The data showed that the P/O ratio was strongly dependent on the syngas composition. CO_2-rich feeds form products that are mostly light hydrocarbons with a high P/O ratio, whereas CO-rich feeds shift the product composition to an FT type (mainly higher hydrocarbons) product with a low P/O ratio over both iron and cobalt based catalysts (Chapters 4 and 5).

We made a comparison between our own research results and those reported in the literature [1] to postulate a linear relationship between $P_{(n+1)}/O_{(n+1)}$ and $P_{(n)}/O_{(n)}$ for FTS for a large amount of data. This relationship is independent of the type of reactor used (plug flow, spinning basket or slurry), the composition of the syngas ($H_2/CO/CO_2$), the reaction conditions and the kind of the catalyst (cobalt or iron based). We identified two features of the ratio $k=[P_{(n+1)}/O_{(n+1)}]/[P_{(n)}/O_{(n)}]$ for FT products: (1) with n>2, the experimental values of $k_{n>2}$ are higher than 1, fairly constant and independent of chain length n; (2) with a chain length of n=2, the ratio of P_3/O_3 to P_2/O_2 ($k_{n=2}$) is significantly different, and shows that $k_{n=2} \ll k_{n>2}$. We attempted to explain the experimental phenomenon in terms of an equilibrium hypothesis (Chapter 8).

The use of a simple vapour-liquid equilibrium (VLE) model indicated that the ratio of $P_{(n+1)}/O_{(n+1)}$ to $P_{(n)}/O_{(n)}$ changes in a range of (1, $1/\beta$), where β is the variation of the vapour pressure coefficient. Our experimental results supported that expression when the chain length was n>2. But with a chain length of n=2, this expression is unable to explain the relationship between P_3/O_3 and P_2/O_2. We therefore developed another model, in terms of which we assumed that the reaction of $C_{n+1}H_{2n+2}+C_nH_{2n+2}=C_{n+1}H_{2n+4}+C_nH_{2n}$ reaches quasi-equilibrium, to explain the linear relationship between $P_{(n+1)}/O_{(n+1)}$ and $P_{(n)}/O_{(n)}$. We found that the experimental results were quite close to those predicted by the equilibrium calculations, and so we postulated that product distribution might be determined by reaction equilibrium considerations (Chapter 8).

9.2 Epilogue

The use of CO_2 as a raw material is of interest to scientists because not only is it a source of carbon, but its conversion to useful products reduces the negative impact carbon dioxide emissions have on the environment through the green house effect. Recently, the synthesis of valuable chemicals and fuels by means of CO_2 hydrogenation as a technology to solve the CO_2 problem has received much attention [2–6]. The hydrogenation of CO_2 to hydrocarbons over FTS catalysts is one of the most promising of the various methods of obtaining chemicals and fuels from CO_2 [2–3]. In particular, the hydrogenation of CO_2 to methanol over methanol synthesis catalysts with high WGS reaction activity has been the subject of a great deal of research because of its minimum hydrogen requirement and the heavy demand for methanol as a bulk chemical [4–6].

During our experimental work it became apparent that because cobalt catalysts have low water gas shift and high hydrogenation activity, the products of FT CO_2 hydrogenation are CH_4-rich short chain hydrocarbons, which are not in great

demand commercially. Fortunately, we also found that even a small amount of CO in the CO_2-rich feedgas ($CO/CO_2/H_2$) mixtures changed the product distribution over a cobalt-based catalyst significantly (Chapters 4 and 7). It would therefore be very interesting to use a series of reactor configurations that combined the methanol synthesis, reverse-WGS and FTS reactions for the hydrogenation of CO_2 or CO_2-rich syngas to methanol and hydrocarbon fuels.

As we mentioned in Chapter 1, the production of syngas from biomass and coal forms CO_2-rich syngas. Using such syngas feeds in FTS to improve carbon utilization is desirable, not only for process economy but also for its contribution to sustainable development [7]. The results discussed in this thesis could lead to improvements in the design of FT processes that use cobalt- and iron-based catalysts, for example in the proof they give that keeping some CO_2 in the syngas feed to the FTS process (instead of removing it, which until recently has been the conventional wisdom) is advantageous.

However, efficient carbon utilization of CO_2 containing syngas feeds has not been given the required attention at the present time, even though developing an FT process with low CO_2 emissions will be a prerequisite for its commercialization in the future [8]. In such a project it would be necessary to find a way for the FT catalyst to convert CO_2 into hydrocarbons instead of discharging it into the atmosphere.

References

[1] van der Laan, G. P. (1999), Kinetics, selectivity and scale up of the Fischer-Tropsch Synthesis, PhD thesis, University of Groningen, Appendixes A-B, 215–223.

[2] Riedel, T., Schaub, G., on Jun, K-W., and Lee, K-W. (2001), Kinetics of CO_2 hydrogenation on a K-promoted Fe catalyst, Industrial and Engineering Chemistry Research, 40, 1355–1363.

[3] Zhang, Y., Jacobs, G., Sparks, D. E., Dry, M. E. and Davis, B. H. (2002), CO and CO_2 hydrogenation study on supported cobalt, Catalysis Today, 71, 411–418.

[4] Centi, G. and Perathoner, S. (2009), Opportunities and prospects in the chemical recycling of carbon dioxide to fuels, Catalysis Today, 148, 191–205.

[5] Guo, X., Mao, D., Wang, S., Wu, G. and Lu, G. (2009), Combustion synthesis of CuO–ZnO–ZrO_2 catalysts for the hydrogenation of carbon dioxide to methanol, Catalysis Communications, 10, 1661–1664.

[6] Joo, O., Jung, M., Moon, I., Rozovskii, A. Y., Lin, G. I., Han, S. and Uhm, S. (1999), Carbon dioxide hydrogenation to form methanol via a reverse-water-gas-shift reaction (the CAMERE Process), Industrial and Engineering Chemistry Research, 38, 1808–1812.

[7] James, O. O., Mesubi, A. M., Ako, T. C. and Maity, S. (2010), Increasing carbon utilization in Fischer-Tropsch synthesis using H_2-deficient or CO_2-rich syngas feeds, Fuel Processing Technology, 91, 136–144.

[8] Ning, W., Koizumi, N. and Yamada, M. (2009), Researching Fe catalyst suitable for CO_2-containing syngas for Fischer-Tropsch Synthesis, Energy Fuels, 23, 4696–4700.

Appendix A

The Brunauer-Emmett-Teller (BET) experimental procedure for 10 wt.% Co/TiO_2 and 10 wt.% Fe/TiO_2 catalysts:

The specific surface areas and the texture of the catalysts were determined by nitrogen physisorption according to the BET method: The N_2 adsorption-desorption experiment was conducted at -193 ℃ using a Micromeritics TriStar surface area and porosity analyzer. Prior to the experiment, the sample was outgassed at 200 ℃ for 6 h. The BET surface areas were obtained in a relative pressure range from 0.05 to 0.30. The total pore volume was calculated from the amount of N_2 vapor adsorbed at a relative pressure of 0.99.

Table 1: Texture of the catalysts (BET)

	Co/TiO_2	Fe/TiO_2
BET surface area (m^2/g)	41.43	38.07
Total Pore volume (cm^3/g)	0.355	0.349
Average pore size (nm)	34	36.6

Appendix B

The Temperature programmed reduction (TPR) experimental procedure for 10 wt.% Co/TiO_2 and 10 wt.% Fe/TiO_2 catalysts:

TPR was used to assess the reducibility of the catalysts. The same TPR experimental procedure was used for both of the catalysts.

The TPR experiment was carried out with a Micromeritics Auto Chem Ⅱ unit. The catalyst (ca. 0.1 g) was placed in a quartz tubular reactor, fitted with a thermocouple for continuous temperature measurement. The reactor was heated in a furnace. Prior to the temperature programmed reduction measurement, the calcined catalysts were flushed with high purity argon at 150 ℃ for 1 hour, to drive off water or impurities, and then cooled down to 50 ℃. Then 5% H_2/Ar was switched on and the temperature was raised at a rate of 10 ℃ /min from 50 to 800 ℃ (held for 10 min). The gas flow rate through the reactor was controlled by three Brooks mass flow controllers and was always 50 ml(NTP)/min. The H_2 consumption (TCD signal) was recorded automatically by a PC. Figure 1 shows the TPR profiles for the calcined and unreduced catalysts: (a) 10 wt.% Co/TiO_2; (b) 10 wt.% Fe/TiO_2.

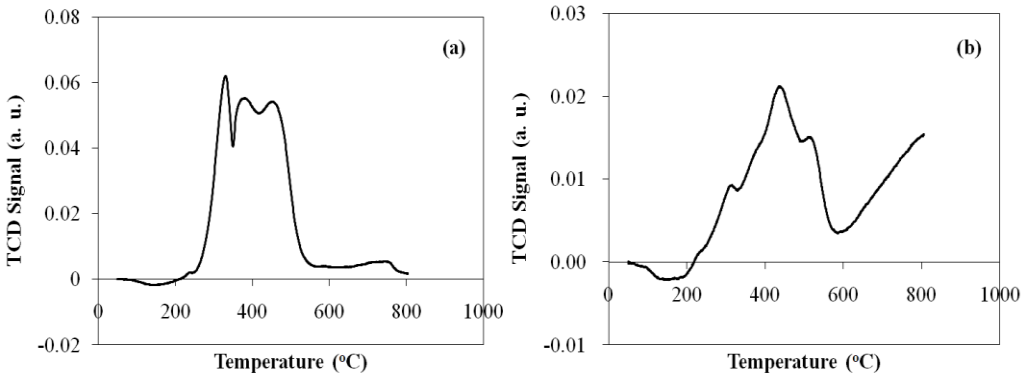

Figure 1: TPR profiles for the calcined and unreduced catalysts: (a) 10 wt.% Co/TiO_2; (b) 10 wt.% Fe/TiO_2.

Appendix C

The X-ray Powder Diffraction (XPD) experimental procedure for 10 wt.% Co/TiO_2 and 10 wt.% Fe/TiO_2 catalysts:

X-ray powder diffraction (XRD) patterns for the calcined 10 wt.% Co/TiO_2 and 10 wt.% Fe/TiO_2 catalysts were recorded with a Bruker D8 diffractometer using Cu Kα radiation and a Ni filter. The scan range was 20-90 °with 0.002 °steps. The XRD patterns for the calcined and unreduced catalysts are given in Figure 2: (a) 10 wt.% Co/TiO_2; (b) 10 wt.% Fe/TiO_2.

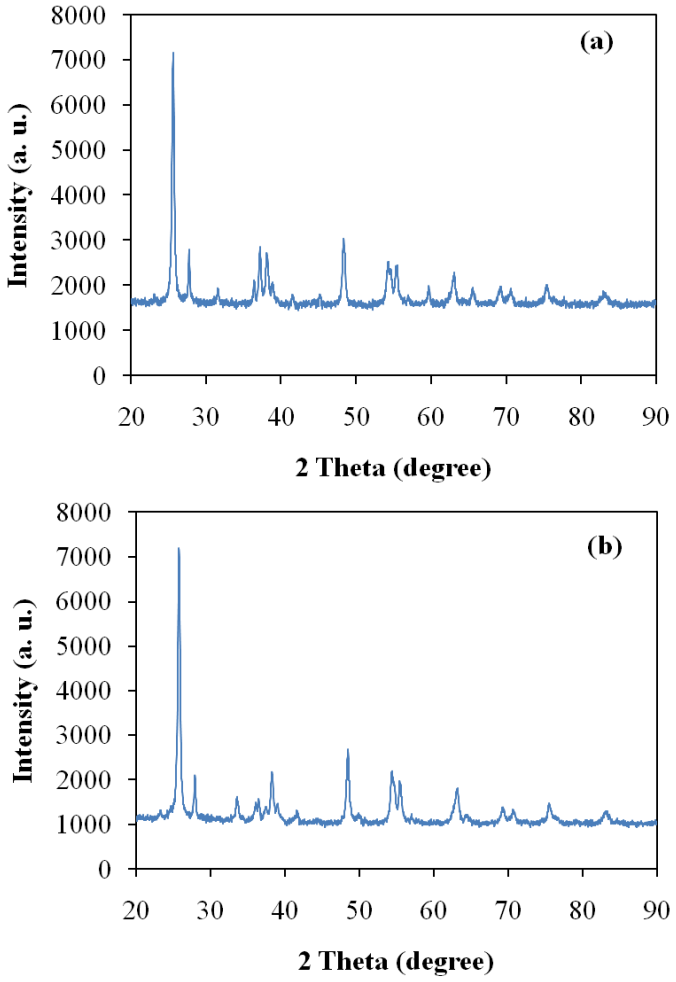

Figure 1: XRD patterns for the calcined and unreduced catalysts: (a) 10 wt.% Co/TiO_2; (b) 10 wt.% Fe/TiO_2.